

**Quantitative Classification and Assessment of Modification in
Hypoeutectic Aluminum-Silicon Alloys**

Dissertation

zur Erlangung des Grades

des Doktors der Ingenieurwissenschaften

der Naturwissenschaftlich-Technischen Fakultät III

Chemie, Pharmazie, Bio- und Werkstoffwissenschaften

der Universität des Saarlandes

von

Paulo Eliseo Rossi

Saarbrücken

10.09.2015

Tag des Kolloquiums: 02.12.2015

Dekan: Prof. Dr.-Ing. Dirk Bähre

Berichterstatter: Prof. Dr.-Ing. Frank Mücklich
Prof. Dr. mont. Christian Motz

Vorsitz: Prof. Dr.-Ing. Stefan Diebels

Akad. Mitarbeiter: Dr.-Ing. Frank Aubertin

“I found that I could say things with color and shapes that I couldn’t say in any other way.”

Georgia O’Keeffe

Acknowledgments

First of all, I want to express an enormous gratitude to my supervisor and main advisor, Prof. Dr.-Ing. Frank Mücklich, for his encouragement, guidance and support.

I am very thankful to Prof. Dr. mont. Christian Motz for co-refereeing this dissertation. I acknowledge his dedication evaluating this work.

I want to thank my group leader, Michael Engstler, for his efficient guidance and support. I owe special thanks to Kai Rochlus, Adrian Thome and Nils Harste for their collaboration in preparing and imaging samples and acquiring and computing data. I am very thankful to Dr. Flavio Soldera, Dr. Sebastián Suarez, Nicolás Souza, Mathias Linz, Federico Miguel, Federico Lasserre, Jenifer Barrirero, Simon Staudacher, Anastasia Kruglova and Dr. Dirk Schnubel (Fa. Nematik) for the contributions in several aspects of this work including proofreading, discussions and advice. I thank all my colleges and friends from the Chair of Functional Materials for the wonderful work atmosphere and support.

The present work has been performed within the framework of a project about the influence of trace elements on Al-Si-Mg alloys (Project AiF-no. 17204 N). The project was carried out together with researchers from companies or research centers specialized in aluminum casting alloys. I am very grateful for the disposition to open discussion and efficient collaboration of the project partners. I owe special thanks to those partners who took a round robin test, which was an essential part of this work. I acknowledge the efficient collaboration of the Institute of Casting Technology in Düsseldorf, Germany (Institut für Gießereitechnik, IfG) and the Foundry Institute (Gießerei-Institut, GI) at the RWTH Aachen University (Rheinisch-Westfälische Technische Hochschule Aachen, RWTH Aachen) in Aachen, Germany, for the cooperation. In particular, I thank Thomas Herfurth, from the IfG, for providing samples, micrographs and measurement of mechanical properties and Veronika Groten, from the GI, for contributing with samples and micrographs.

I acknowledge the financial support of said project (Project AiF-no. 17204 N) from the German Research Foundation (Deutsche Forschungsgemeinschaft, DFG) and the German Federation of Industrial Research Associations (Arbeitsgemeinschaft industrieller Forschungs-vereinigungen, AiF).

Part of this work was carried out in cooperation with the Metals Division at the Bariloche Atomic Centre, Bariloche, Argentina (Centro Atómico Bariloche, CAB). I gratefully acknowledge Dr. Mario Moreno from the CAB for providing measurements of mechanical properties.

I am very grateful to the German Academic Exchange Service (Deutscher Akademischer Austauschdienst, DAAD) and the Roberto Rocca Education Program for scholarships.

I am very thankful to Jessica Hilschmann, my family and friends for the constant support, love and company.

And thank you, dear reader, for your interest. Feel free to contact me.

Paulo Rossi

Abstract

Aluminum-silicon cast alloys, as those considered in this study (Al-7%Si and Al-7%Si-0.3%Mg alloys), are widely used to manufacture technical cast products, e.g. in the automotive industry. The mechanical properties of the castings depend on the eutectic microstructure which, in turn, depends on the chemical composition and manufacturing processes. A transition from a coarse eutectic structure to a finer one is called modification. The modification can be induced, for instance, by increasing the solidification cooling rate, by adding strontium and/or by increasing the alloy purity. The assessment of the modification relies usually on visual comparison, thus being ambiguous. This work suggests innovative tools to evaluate the microstructure based on quantitative image data and it develops an objective method to assess the modification. To ensure the representativeness of this method, it has been developed in collaboration with thirteen experts from different research institutions and companies. The assessment tools are applied to study the quantitative correlation between process settings, microstructures and casting properties, which are of major importance for the research and development of the studied alloys.

Kurzfassung

Aluminium-Silizium-Gusslegierungen, wie Al-7%Si und Al-7%Si-0.3%Mg Legierungen, die in dieser Arbeit untersucht werden, finden häufig Anwendung bei der Herstellung von technischen Gussprodukten, z. B., für die Automobilindustrie. Die mechanischen Eigenschaften des Gussteils hängen von der eutektischen Mikrostruktur ab, die wiederum abhängig von der chemischen Zusammensetzung und den Herstellungsverfahren ist. Eine Gefügeveränderung der eutektischen Struktur von einer groben hin zu einer feineren, wird Veredelung genannt. Die Veredelung kann hervorgerufen werden, z. B., durch die Erhöhung der Abkühlgeschwindigkeit bei der Erstarrung, durch Zusatz von Strontium und/oder durch zunehmende Reinheit der Legierung. Üblicherweise wird die Auswertung der Veredelung durch visuellen Vergleich vorgenommen und ist dadurch subjektiv. Der vorliegende Beitrag schlägt eine innovative Lösung vor, um die Mikrostruktur auf der Grundlage quantitativer Bilddaten auszuwerten, und somit die Veredelung objektiv zu beurteilen. Um Repräsentanz gewährleisten zu können, wurde die Studie unter Einbeziehung von dreizehn Experten aus verschiedenen Forschungsinstitutionen und Industrieunternehmen entwickelt. Die objektive Beurteilung wurde eingesetzt, um den quantitativen Zusammenhang zwischen Prozesseinstellungen, Mikrostruktur und mechanischen Eigenschaften zu studieren, welcher für die Forschung und Entwicklung der Legierungen von großer Bedeutung ist.

Contents:

Introduction.....	1
Organization of this text.....	2
Nomenclature used in this work.....	3
1. STATE OF THE ART.....	4
1.1. Aluminum-Silicon alloys	4
1.2. Modification	4
1.2.1. Introduction to modification.....	4
1.2.2. Theories explaining the modification.....	11
1.2.3. The influence of modification on the mechanical properties	15
1.2.4. Available methods to assess the modification.....	18
1.2.4.1. Subjective methods of classification.....	18
1.2.4.2. Objective methods of classification.....	19
1.3. Quantitative Microstructure Parameters.....	20
1.3.1. Dendrite parameters.....	21
1.3.2. 3D Basic particle parameters.....	21
1.3.3. Density of the particle features and stereological equations	23
1.3.4. The Euler number	24
1.3.5. Further size and shape parameters.....	26
1.4. Quantification of Homogeneity.....	27
1.5. Microstructure classification	31
1.6. 3D microstructure representation.....	32
2. ADDRESSED PROBLEM AND GOAL OF THIS WORK.....	36
2.1. Problem	36
2.2. Objective	39
2.3. Strategy	39

3. METHODOLOGY	40
3.1. Description of samples.....	40
3.2. Microstructure imaging and image data	43
3.3. Subjective Assessment: The Round Robin Test.....	44
3.4. Quantitative microstructure parameters.....	45
3.5. Quantitative data analysis.....	46
3.6. Mechanical properties	49
4. RESULTS AND DISCUSSION.....	52
4.1. Homogeneity.....	52
4.1.1. Applying the Lorenz curve and the Gini coefficient to quantify the homogeneity.....	52
4.1.2. The region homogeneity.....	54
4.1.3. The object homogeneity	56
4.1.4. Constructed homogeneities	57
4.1.5. Remarks of the section	58
4.2. Quantitative classification and assessment of modification.....	59
4.2.1. Subjective assessment: The round robin test.....	59
4.2.2. Objective data from the micrographs	65
4.2.3. Analysis	67
4.2.3.1. Particle classification and Percentage of Modification (<i>PM</i>)	67
4.2.3.2. Microstructure classification.....	75
4.2.3.3. Objective- vs. subjective microstructure classification.....	78
4.2.3.4. Degree of modification (<i>M</i>)	81
4.2.3.5. Comparison of <i>M</i> with the subjective assessment	82
4.2.3.6. Summary of results, including the Modification Level (<i>ML</i>)	83
4.2.4. Remarks of the section	86
4.3. Comparison between Sr- and quench-modification	87
4.3.1. Comparison in 2D.....	87

4.3.2. Comparison in 3D.....	88
4.3.3. Remarks of the section	90
4.4. Correlation between microstructure, process settings and mechanical properties.....	91
4.4.1. Small Punch Test (SPT)	91
4.4.2. Impact properties	93
4.4.3. Remarks of the section	100
5. CONCLUSIONS AND OUTLOOK	102
Appendix: List of micrographs.....	106
References.....	147
Curriculum Vitae.....	159

Introduction

Aluminum-silicon (Al-Si) cast alloys have a wide range of applications, especially in the automotive industry. They are diverse in their mechanical properties, which can be tailored by managing their microstructure. The study of the geometrical characteristics of the microstructure is not only important for the mechanical properties, but also for the understanding of the Si crystal growth mechanisms during solidification. The term “modification”, when related to the Al-Si system, is an established name for a particular morphology change of the eutectic microstructure. Since its discovery, about 100 years ago, the modification has been widely used in the industry to improve the mechanical properties of the alloys, and intensively researched.

The subjective (visual) analysis has been the principal tool to study the microstructures for a long time. Most of the works studying the modification in Al-Si alloys present visual representation of the microstructures and their subjective analysis, without a detailed, objective description of the microstructures. Because of the lack of a precise and objective definition of what modification is, and how it can be measured, the literature about modification is contradictory and confusing. Today it is required to work in interdisciplinary problems, with a high degree of precision; hence, the objective microstructure characterization has increasing importance.

This work include the development of innovative tools to quantify the homogeneity [1]. These tools are a fundamental contribution for the microstructure analysis in material sciences. Within the scope of this research, these tools have been successfully applied to characterize Al-Si alloys [2], as well as other materials [3]. This work applies these tools and focuses on the development of an objective method to classify and evaluate modified Al-Si alloys. To ensure representation of the method, the method was developed with the cooperation of several laboratories, which are specialized in Al-Si casting alloys.

An objective method to evaluate modification is the basis for further analyses. Within this work, samples modified through different modification methods are compared. Besides, the mechanical properties from structures displaying different modification levels are analyzed.

Organization of this text

This text is composed of five chapters, as follows:

Chapter 1 introduces the topic and challenges this work addresses and presents the used tools.

Chapter 2 defines the goal of this work.

Chapter 3 describes the methodology used.

Chapter 4 presents and discusses the results, and it is divided into four parts.

Section 4.1 analyzes how to quantify microstructure homogeneity disclosing new tools to evaluate modification.

Section 4.2 applies the results from Section 4.1 to develop an objective method to evaluate the modification.

Section 4.3 applies the results from Section 4.2 to analyze 3D structure representations achieved via Focused Ion Beam tomography (FIB-tomography).

Section 4.4 applies the results from Section 4.2 to study the relationship between the modification, the process settings and the mechanical behavior of castings.

And **Chapter 5** closes the text reviewing the main achievements and conclusions, and outlining the future perspectives.

Nomenclature used in this work

When naming an alloy, as Al-7Si, the number before the element has units of wt.%. For example: Al-7Si-0.3Mg (Al – 7 wt.% Si - 0.3 wt.% Mg). Amounts in ppm are wt. ppm. Particle parameters including “[*mean*”, as for example $P]_{mean}$ (where P stands for perimeter), represents that the value is a mean value, considering all the particles within the studied micrograph.

Symbols and abbreviations often used in this text are:

SCR	“Solidification cooling rate”
ML	“Modification level” → Details in Figure 1.12
DAS	“Secondary dendrite arm spacing” → Details in Figure 1.13
χ	“Euler number” → Details in Figure 1.16
<i>A, P, P_{Convex}, F_m, F_{min}</i>	Particle parameters → Details in Figure 1.17
<i>R, C, FAR, AAR</i>	Particle parameters → Details in Table 1.3
SD	“Standard deviation”
RSD	“Relative standard deviation”
<i>G</i>	“Gini coefficient” → Details in Figure 1.19
FIB-tomography	“Focused ion beam tomography” → Details in Figure 1.22
<i>D, FλR, AλR</i>	DAS related parameters → Details in Table 3.2
<i>PD, RGD</i>	Parameters for attribute assessment → Details in Figure 3.2
SPT	“Small punch test” → Details in Figure 3.4
H	“Homogeneity” → Details in Figure 4.1
<i>h_o</i>	“Object homogeneity” → Details in page 57
PM	“Percentage of modification” → Details in page 71
M	“Degree of modification” → Details in Figure 4.17

1. STATE OF THE ART

This chapter introduces the studied alloys and makes focus on their modification, which is the main matter of this work. Within this chapter, it will be discussed how the modification can be induced, how it influences the alloy properties and which are the available methods to evaluate it.

1.1. Aluminum-Silicon alloys

Aluminum alloys containing silicon as the major alloying element (Al-Si alloys) combine good mechanical behavior, low density, good corrosion resistance, and good casting ability. This characteristics make Al-Si alloys ideal for the manufacture of lightweight and resistant castings, with complex geometries [4].

The Al-Si system has a binary eutectic phase diagram with an eutectic at 577°C and 12.5 wt.% of Si, and the solubility of Si in Al is 1.6 wt.% at the eutectic temperature [5]. Hypoeutectic alloys are constituted by primary Al dendrites surrounded by the eutectic phase. The addition of Mg makes the alloy heat treatable, improving the strength of the castings through precipitate hardening [6].

The structure of the Si in the eutectic phase plays a key role in the mechanical properties of the casting. Alloys displaying, in two-dimensional (2D) analysis, a homogeneous distribution of small and round Si particles have usually better mechanical properties [7]. With the aim of obtaining such structure, a process so called “modification” is carried out.

This work focuses on the modification in Al-7Si and Al-7Si-0.3Mg alloys, which are important aluminum casting alloys.

1.2. Modification

1.2.1. Introduction to modification

The eutectic Si in Al-Si alloys can display different sizes and morphologies. As illustrated in Figure 1.1, modification is a technique to obtain a eutectic structure formed by an interconnected network of fine Si fibers [4].

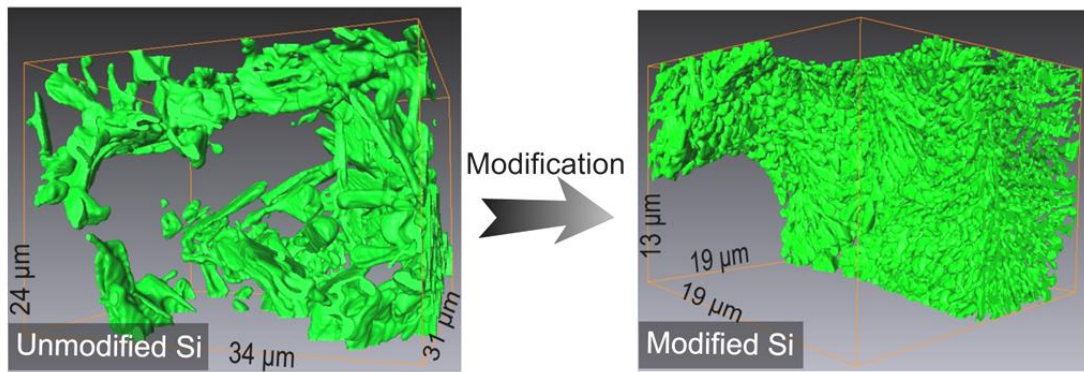


Figure 1.1: Conceptual illustration representing the modification of the eutectic Si (green).

The discovery of modification can be attributed to Frilley, who in 1911 described the modified structure [8,9]. The application of the modification for commercial purpose was introduced by Pacz, who in 1928 and in 1935 patented treatments applicable to alloys containing Al and Si, which induced the modification of the microstructure [10,11]. Pacz used the term “modification” to refer to the treatment of the alloys by adding a substance, which changes the internal physical structure in a finely divided and highly dispersed condition (considering 2D micrographs).

With the development of SEM micrography (and though a deep etching process), it was possible to recognize that those observed “finely divided and highly dispersed” particles in 2D micrographs were in fact an interconnected network in the three-dimensional space (3D) [4]. With further advance of the technology, 3D reconstructions with nano-scale resolution are today possible, which allows a precise 3D visualization of the modified structure [12]. Because of its 3D shape, the modified structure is called “coral-like” or “coralline-like” structure [12–14]. The eutectic structure of unmodified samples is coarser, but it is also interconnected [15–17].

The modification was observed to occur with the addition of very small quantities of particular chemical agents, so called *modifiers*. The most common modifiers are Sr, Na and Sb, some other modifiers are: K, Rb, Ce, Ca, Ba, La, Yb, As, Se and Cd [18]. The modification induced by chemical agents is called *chemical-modification* and if the modification can be mainly attributed to one agent, it is used to specify which was the modifier, e.g. *Sr-modification* [19,20].

It has been shown, that high cooling rates produce modification without addition of a chemical modifying agent [21,22]. The terms *chill-*, *thermal-*, or *quench-modification*,

are used to describe the modification induced through high solidification cooling rate (SCR). Beside of chemical- and quench-modification, modification can be achieved increasing the alloy purity. The addition of a chemical modifier, the increment of the alloy purity and the increment of the SCR assist each other to modify the structure as illustrated in Figure 1.2 [23].

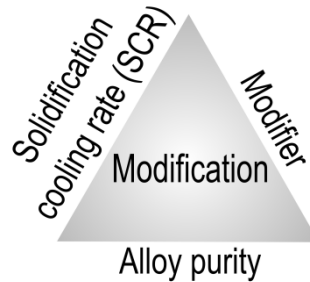


Figure 1.2: Conceptual illustration representing the principal influent parameters on the modification: The SCR, the addition of modifier and the alloy purity.

Several parameters play an important role in the resulting shape and sizes of the eutectic structure. The effects of the chemical composition interact with the effects of the process settings. Depending on how a chemical modifier is added, it can oxidize and fade, and chemical modifiers not necessarily assist each other [24,25]. Besides, there are further methods to induce modification, as the application of magnetic and/or ultrasonic fields [26].

Without addition of a chemical modifier, usually the structure is unmodified because the Al-Si alloys have impurities (e.g. P), which lead to the growth of coarse and flaky Si particles [25,27]. Besides, modification without chemical-modifier occurs under relatively high SCR and high purity, which are in commercial applications not feasible. The increase of the SCR usually scales the structure sizes down without modifying the structure morphology [23,28]. Because of these practical reasons, the chemical modification is long-established due to its effectiveness and simplicity, being the most used treatment to modify the structure [29].

Description of the unmodified and modified structures

There is no standard method to evaluate if a structure is modified or not. In most cases, the microstructure evaluation is carried out subjectively [30,31]. For microstructure assessment, researchers have suggested model micrographs with a certain given modification level or classification. These model micrographs can be used to, through

visual comparison, evaluate structures [31–34]. Particularly, the modification rating suggested by Apelian, Sigworth and Whaler in 1984 [31] is well accepted in the literature [4,28,35]. These rating classes are represented by six micrographs, as shown in Figure 1.3.

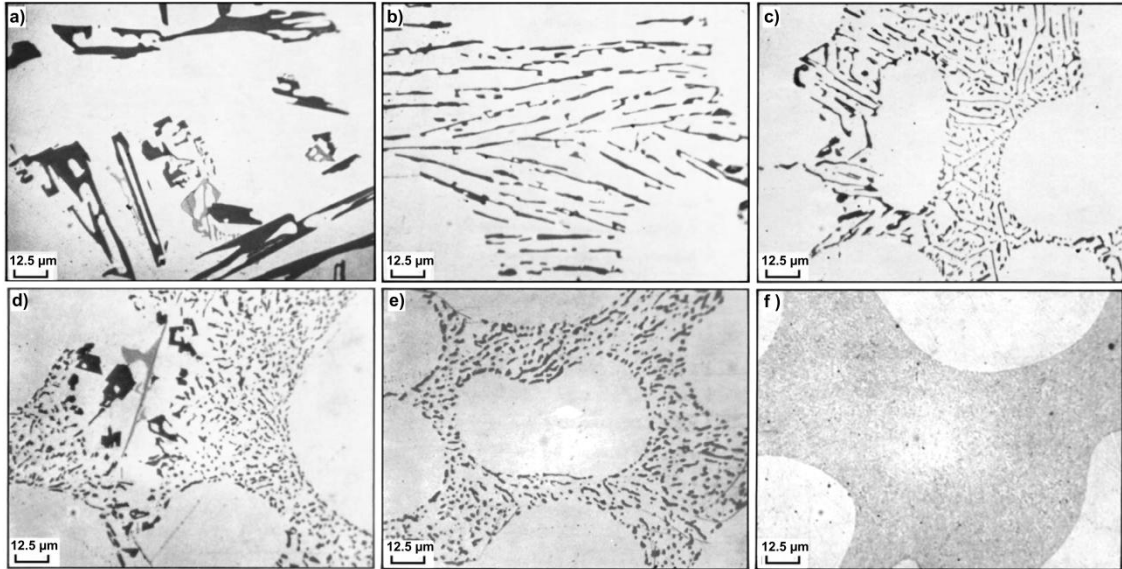


Figure 1.3: Eutectic Si structures, classified into six classes: (a) Class 1, fully unmodified structure. (b) Class 2, lamellar structure. (c) Class 3, partial modification. (d) Class 4, absence of lamellar structure. (e) Class 5, fibrous silicon eutectic. (f) Class 6, very fine structure [28,31].

The same six micrographs are shown and subjectively described in several works [4,28,30,35].

Table 1.1 summarizes typical descriptions of these six classes.

Table 1.1: Typical subjective classification and description of microstructures [18]

Class number	Structure	Description
1	Fully unmodified	Si is present in the form of large plates as well as in acicular form.
2	Lamellar	A finer lamellar structure, though some acicular Si may be present (but not large plates).
3	Partial modified	The lamellar structure starts to break up into smaller pieces.
4	Absence of lamellae	Complete disappearance of lamellar phase. Some acicular phase still may be present.
5	Fibrous Si eutectic (Fully modified)	The acicular phase is completely absent.
6	Very fine eutectic (Super modified)	The fibrous Si becomes so small, that individual particles cannot be resolved under optical microscopy.

The *fully unmodified* structure (Class 1) displays large, acicular silicon flakes (in other words, *coarse plate-like particles*) [30,31]. A treated structure (with the aim of modifying the structure, e.g., by adding a chemical-modifier) will be considered modified or not, depending on the size and shapes of the particles in the structure. If the chemical modifier is added in relatively too low amounts, only the refinement of the structure is caused, but not the modification [36,37]. A refined structure is composed by finer plate-like particles (*lamellar particles*), which are not fiber-like shaped [38,39]. Class 2 is an example of a treated alloy, which can be considered to be refined, but not modified. Structures resembling Class 1 are termed *unmodified granular* structures, while structures resembling Class 2 are termed *unmodified lamellar* structures [30,34].

Figure 1.4 shows structures being identified as unmodified in the literature, in which the 3D structure can be visualized. The class of the shown structures was not indicated. For further 3D reconstructions and 2D images of unmodified structures refer to, e.g. [12,40,41].

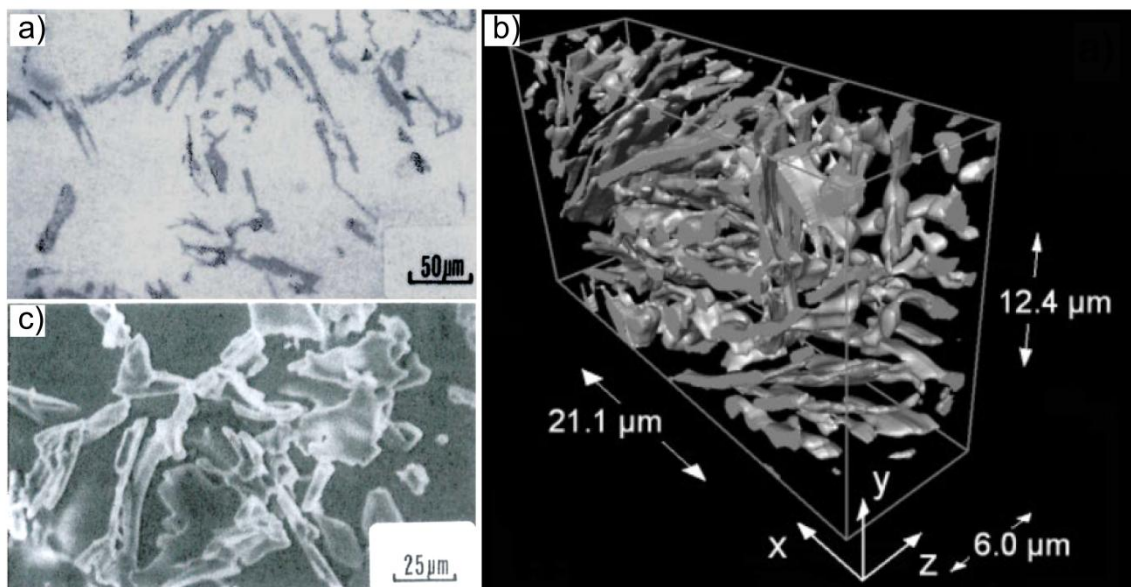


Figure 1.4: Unmodified eutectic Si structures in Al-Si alloys. (a) optical and (c) scanning electron microscopy (SEM) micrographs from the same sample [31]. (b) 3D reconstruction [12].

Regarding the chemical-modification, the modification level increases with the increasing level of added modifier [42]. A structure is *modified*, if it presents fine fiber-like particles (*modified particles*) [43–46]. Modified structures resemble the classes 3 to 6.

Figure 1.5 shows structures being identified as modified in the literature, in which the 3D structure is observable. Compound field is a modification technique that involves the combined application of power ultrasonic field and rotating electromagnetic field while the solidification occurs [26]. Further 3D reconstructions and 2D images of modified structures can be observed, e.g. in ref. [12,40,41].

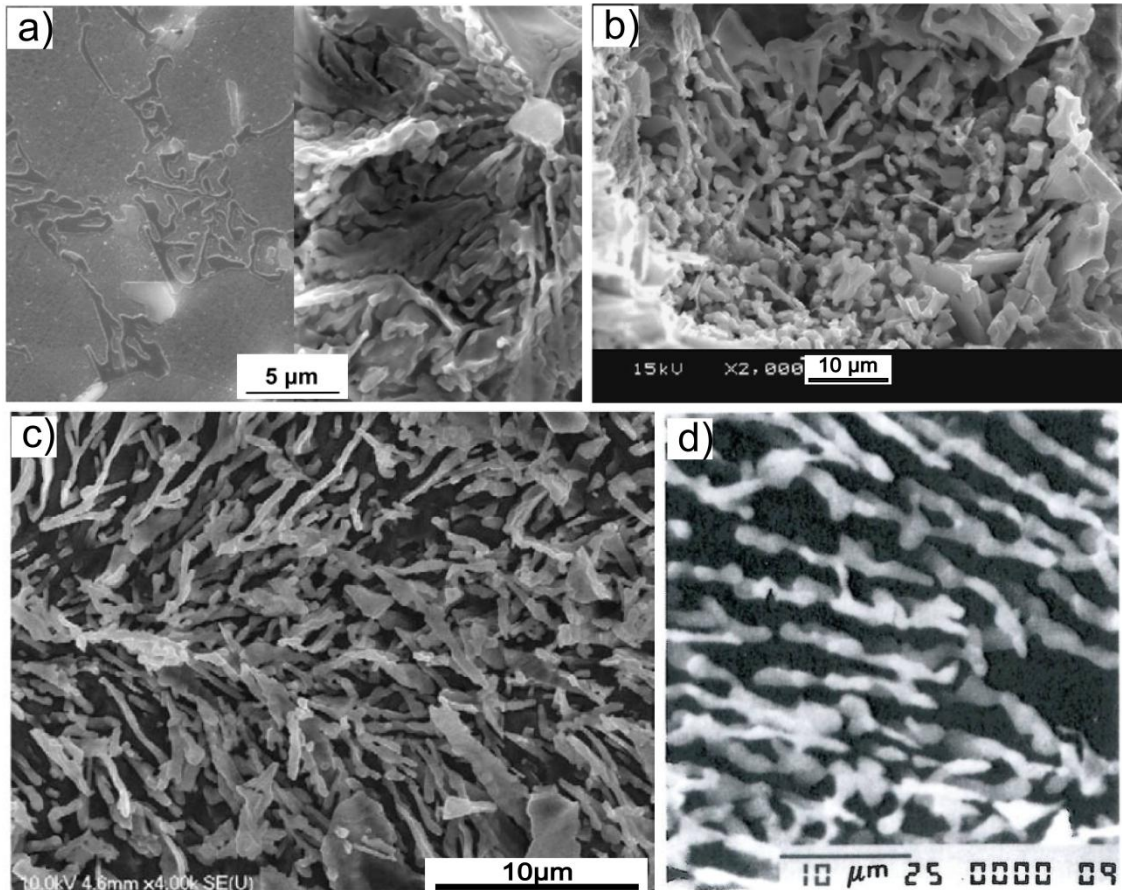


Figure 1.5: Modified structures. (a) Sb-modified (at the left hand side is the 2D micrograph, at the right hand side is the etched surface showing the 3D structure) [36], (b) Compound field modified (etched) [26], (c) Sr-modified (etched) [47], (d) Na-modified (etched) [4].

Partially modified microstructures, containing a mixture of modified and unmodified particles, are called *under-modified* [48,49]. In Classes 3 and 4, acicular phase and fine fibrous phase are visualized, thus these classes are under-modified [30]. A *fully-modified* structure is formed only by fine-fibrous, i.e. modified, particles [50–53]. The Class 5 is fully-modified, displaying only modified particles. The Class 6 is the *super-modified* structure, which is in rare occasions visualized [30].

An effect termed *over-modification* occurs, when a chemical modifier is added in an excessive amount. The over-addition of modifier causes the coarsening of coral-like

particles [43,54,55]. The coarsening caused by over-modification is accompanied by an increment of the inter-particle spacing, and in some cases segregation of compounds containing the modifier element. For example, Sr over-modification is known to segregate the $\text{Al}_2\text{Si}_2\text{Sr}$ phase [47]. Figure 1.6 shows the under-modified-, fully-modified- and over-modified structures.

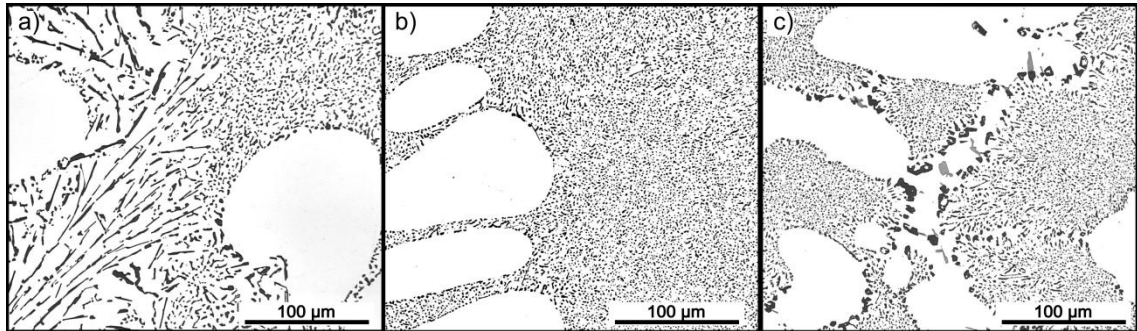


Figure 1.6: Modified Al-Si eutectic structures. (a) Under-modified, (b) fully-modified, and (c) over-modified [34].

Notice that the six classes shown in Figure 1.3 (page 7) do not have an over-modified class. Since the classification into the six classes shown in Figure 1.3, or into under-, fully-, and over-modified structures is carried out subjectively, the limits between classes depend on the considerations from the observer.

Remarks of the section

The following points can be summarized:

- The modification of the eutectic structure consists in an important reduction of the Si particles sizes and the change of their shape, towards a fibrous-like morphology.
- The shapes and sizes from the eutectic Si can be tailored by changing the process settings and chemical composition. Especially, the addition of chemical modifiers has important influence on the eutectic structure.
- To achieve a fully modified structure, an adequate amount of modifier should be added. This adequate amount will depend on the SCR and alloy purity, among other factors.
- The terms used to describe the structures are subjected to the considerations from the observer.

1.2.2. Theories explaining the modification

Although the growth mechanism of the Si has been intensively studied in the last 90 years, on-going research and several reviews addressing this topic indicate that the growth mechanisms are still not well understood [18,19].

The discussions about the growth mechanisms of the eutectic Si in Al-Si alloys have accumulated a great amount of publications. The most important suggested mechanisms are shortly introduced and discussed in this section.

“Twin plane re-entrant edge” (TPRE) theory explaining the unmodified plate-like Si growth

The “twin plane re-entrant edge” (TPRE) theory was proposed by Hamilton and Seidensticker in 1960 to explain the propagation mechanism of germanium (Ge) crystals [56]. Since Ge has diamond lattice and forms plate-like crystals, as Si; the TPRE theory was adapted to explain the growth of eutectic plate-like Si [57–59].

The TPRE theory [56] consist in the following: The equilibrium habit of a crystal is an octahedron bounded by eight $\{111\}$ planes (Figure 1.7-a), which are the planes of closest packing and of lowest free energy in the diamond lattice. The octahedron is to be twinned, as indicated by a dotted line in Figure 1.7-a. The reflection across the twin plane derives a twinned crystal, as illustrated in Figure 1.7-b. The twinned crystal emerges three reentrant corners with external angle of 141° , which alternate with “ridge structures” (the planes with external angle 219°). The theory states that the nucleation events occur likely in the reentrant corners but improvable elsewhere. Thus the crystal propagates in the $[2\bar{1}\bar{1}]$, $[\bar{1}2\bar{1}]$ and $[\bar{1}\bar{1}2]$ directions. A crystal with two twin planes generates more re-entrant corners, as shown in Figure 1.7-c, leading to six equivalent $\langle 211 \rangle$ preferred growth directions.

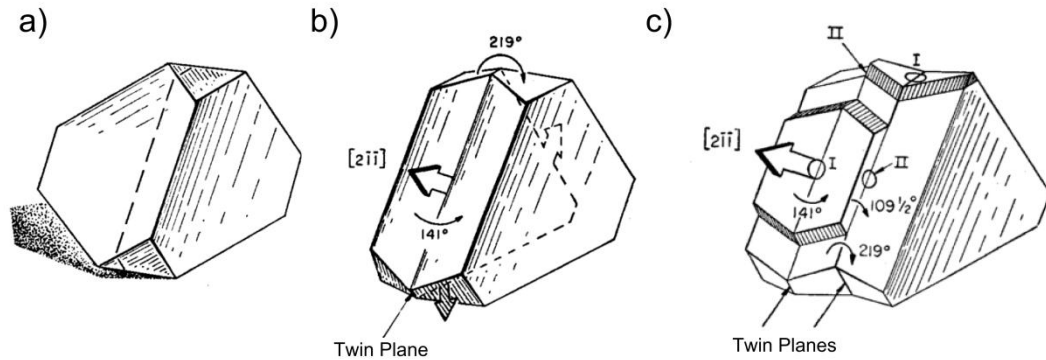


Figure 1.7: Illustration of the “twin plane re-entrant edge” (TPRE) theory. a) embryo bounded by $\{111\}$ planes, b) twinned crystal with three reentrant corners with external angle of 141° , c) creation of extra re-entrant corners and propagation in the in the $\langle 211 \rangle$ directions [56].

However, the theory of the TPRE mechanism has been questioned as mechanism explaining the growth of Si crystals [60]. It has not yet been shown, that the TPRE mechanism is the mechanism responsible for the growth of Si [19]. On the other hand, a recent work shows that the TPRE mechanism plays an important role in the growth of Si [61].

It is possible to conclude that the TPRE theory is still being discussed regarding its validity to explain the growth of plate-like (unmodified) Si particles.

Restricted Growth Theories explaining the modified fine-fibrous Si growth

Thall and Chalmers [62] suggested that Al grew at faster rate than Si, leading the solidification of the eutectic, and that for higher cooling rates, the lead of Al over Si was increased. They supported this theory with the fact that Al has a higher thermal conductivity and a lower latent heat of fusion. They claimed that the modification occurred because Al grew in front of the growing Si crystal, encasing the Si, and forcing the Si to bend and form the coral-like structure (Figure 1.8). It was determined that Na (a chemical modifier) reduces the interface energy of the interface Al/Si [63]. Because of the lower interface energy, it make more sense that Al would grow in front of the Si crystal (as illustrated in Figure 1.8-b), which is a fact towards confirming this theory. However, as it was later shown, Si, not Al, is the faster growing phase [64], which denies the theory from Thall and Chalmers.

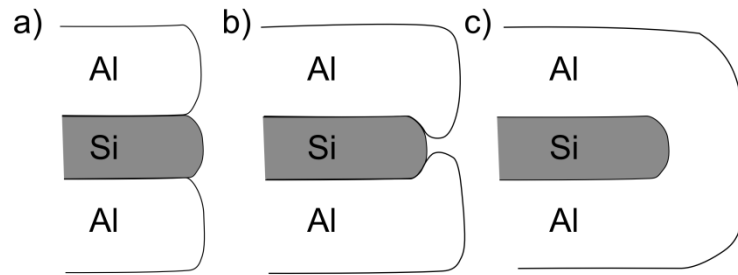


Figure 1.8: Illustration of the theory explaining the growth of the modified eutectic Si according to Thall and Chalmers [62]. a, b and c are successive in time and represent that Al grows at faster rate than Si, encasing the Si.

Tsumara [65] suggested a “diffusion theory” which states that the modifier segregate ahead of the growing plate-like Si crystal, reducing the diffusion of Si from the melt, which hinders the growth of the plate-like Si crystal. However, it has been shown that a reduced diffusion rate of Si is not responsible for the chemical modification [66], which denies the theory from Tsumara.

Lu and Hellawell theories explaining the unmodified and modified Si growth

Lu and Hellawell proposed an alternative mechanism to explain the growth of plate-like particles and fibrous-like particles.

To explain the growth of plate-like particles, they suggested a layer mechanism, which consist in the growth of atomic monolayer steps across the $\{111\}$ planes, as illustrated in Figure 1.9 [16]. To explain the growth of fibrous-like particles, they introduced the “impurity induced twining” (IIT) theory [67]. The IIT states that modifiers poison the growing monolayer step, as illustrated in Figure 1.9-a. $2 r_c$ is a critical separation between impurity atoms below which a step is prevented, by line tension, from growing between them. Since the absorbed impurity atom (modifier atom) has a radius different than the radius from the atoms in the matrix (i.e. than the radius of the Si), twinning is induced “by altering the stacking sequence of atomic layers as the newly added layers seek to grow around the adsorbed impurity atom” [19], as illustrated in Figure 1.9-b.

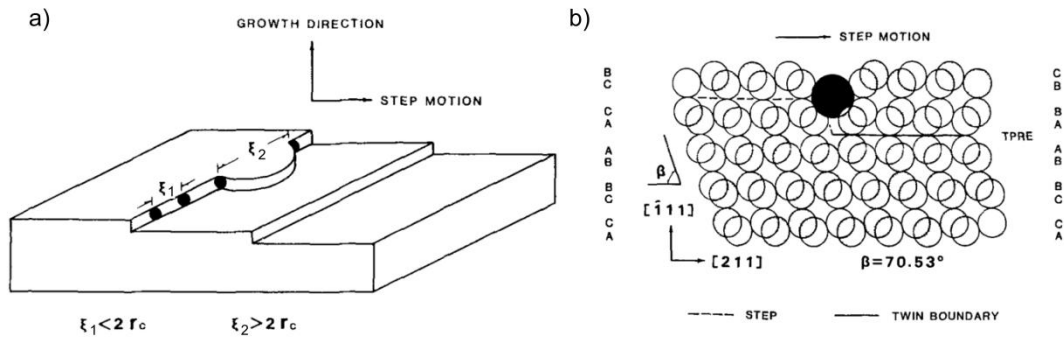


Figure 1.9 Schematic representation layer mechanism and the “impurity induced twinning” (IIT) theory. a) layer mechanism in which the impurity atoms (in black) pin the steps of the growing Si. b) plane projection of diamond cubic lattice to show how an impurity atom of certain size (in black) could promote twinning by causing a growth step to assume the alternative {111} stacking sequence [67].

The layer mechanism has been questioned, because there is strong evidence that the unmodified flake-like particles grow longitudinally (as the TPRE suggests) and not laterally on the {111} planes, as the layer growth suggests [68,69]. Since IIT mechanism is based on the layer mechanism, also the IIT mechanism is questionable. Moreover, according to the IIT, modifiers induce twinning (and so modification) if the atomic radius of the modifier is larger than 1.65 times the radius of a Si atom (r_{Si}) [67]. Nogita et al. [42] showed that there are inconsistencies between the expected modification effects of elements based on the theoretical best radius and the practical results, e.g. Na has a smaller radius than the critical radius ($r_{Na}/r_{Si} = 1.59$) and is a better modifier than Ca ($r_{Ca}/r_{Si} = 1.68$). Furthermore, since the IIT requires a modifier to explain modification, it does not explain the quench-modification.

It can be concluded that IIT definitively does not explain every case of modification. To the date, the theories from Lu and Hellawell are still under research since the modification could be caused by different mechanisms, one of these involving IIT and the other without involving it [70].

Remarks of the section

- There is on-going research and discussions regarding the mechanisms governing the eutectic Si morphology.
- Some suggested theories have been proved to be wrong; others, as the TPRE and the IIT, are still being discussed [71].

1.2.3. The influence of modification on the mechanical properties

In industrial applications, Al-Si castings contain impurities and solidify at relatively low cooling rates. Thus quench- or high purity modifications are unusual. The chemical modification is the principal tool to change the unmodified structure towards a fine-fibrous structure, which presents improved mechanical properties [49,72,73]. In this section, the tensile and impact properties of Al-Si alloys, in unmodified and modified states, are discussed.

Tensile properties

Fatahalla et al. [74] studied the dependency of the mechanical properties of Al-Si alloys with modification, in which modification was induced by different chemical modifiers. They reported that Na and Sr lead to a fine-fibrous structure, while Sb leads to a fine-flake structure. Their results show that both modified morphologies (the fine-flake and the fine-fibrous) improved the mechanical properties with respect to the unmodified alloy. Particularly, the yield stress (σ_y), ultimate tensile strength (*UTS*), elongation percent (*E%*), and the toughness (Table 1.2 and Figure 1.10). They tested samples, which were casted in metal and sand molds, promoting higher and lower cooling rates, respectively.

*Table 1.2: Effect of type of mould and Na, Sb and Sr-modification on the tensile properties of non-modified and modified Al-5.5Si alloys. In the table: 0.2% proof- (σ_{pr}) or yield stress (σ_y), ultimate tensile strength (*UTS*) and elongation percent (*E%*) [74].*

Alloy condition	Mould type	Tensile properties			
		σ_{pr} (MPa)	UTS (MPa)	<i>E%</i>	Toughness (MPa)
Non-modified	Sand mould	37	74	1.4	0.95
	Metal mould	48	96	2.5	2.0
Na-modified	Sand mould	55	114	4.3	3.9
	Metal mould	60	121	8.0	8.4
Sb-modified	Sand mould	50	109	3.7	3.7
	Metal mould	56	115	7.3	7.4
Sr-modified	Sand mould	62	124	5.0	5.2
	Metal mould	70	142	10.6	11.9

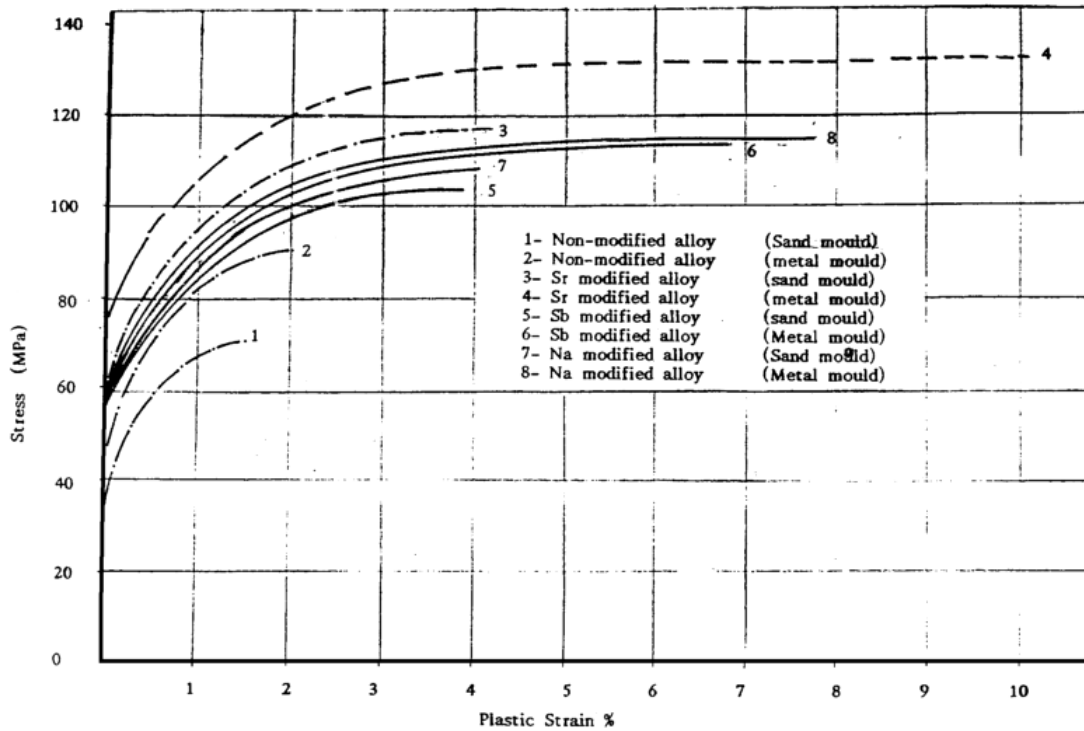


Figure 1.10: Comparison among the stress/plastic strain curves of Na, Sb and Sr modified alloys [74].

The results and analysis from Fatahalla et al. [74] indicate the following:

(1) Samples with higher solidification cooling rate (SCR) have smaller particles and better mechanical properties (with and without modifier, independent to the used modifier).

(2) Varying only the chemical composition, changes in the microstructure sizes and in the ductility and strength can be observed. Smaller microstructures have better mechanical properties. The tested samples can be ordered with increasing mechanical properties as follows: Non-modified, Sb-modified, Na-modified and Sr-modified.

Besides of these two points, Fatahalla et al. indicated that the fracture mechanism changes, from brittle to ductile, due to the change of the structure morphology, from plate-like to fibrous morphology [74]. The results from Fatahalla et al. highlight also the convenience of using Sr as modifier.

It should be pointed out that not all the mechanical properties improve always with modification. For example, Hafiz and Kobayashi [49] investigated also the tensile properties in Sr-modified Al-Si alloys, and they found that the UTS and the elongation improved with modification (equal to the work from Fatahalla et al.), while the σ_y was virtually invariant to modification (different to the work from Fatahalla et al.).

Impact behavior

Besides investigating the tensile properties, Hafiz and Kobayashi [49] practiced also Charpy tests on Sr-modified samples. The Charpy test, differing from the afore-discussed standard tensile tests, evaluates the response of a material in an impact event. The authors reported that the impact load and the impact deflection (and consequently the impact toughness) increase with both modification and SCR. They obtained the results from Figure 1.11 and concluded that the impact behavior is highly sensitive to the eutectic Si morphology. They reported that the fibrous eutectic morphology improves the crack initiation and crack propagation resistance, with a consequent enhancement of the toughness. They stated that cracks propagate in a brittle manner in unmodified samples, while they proceed ductile in modified samples.

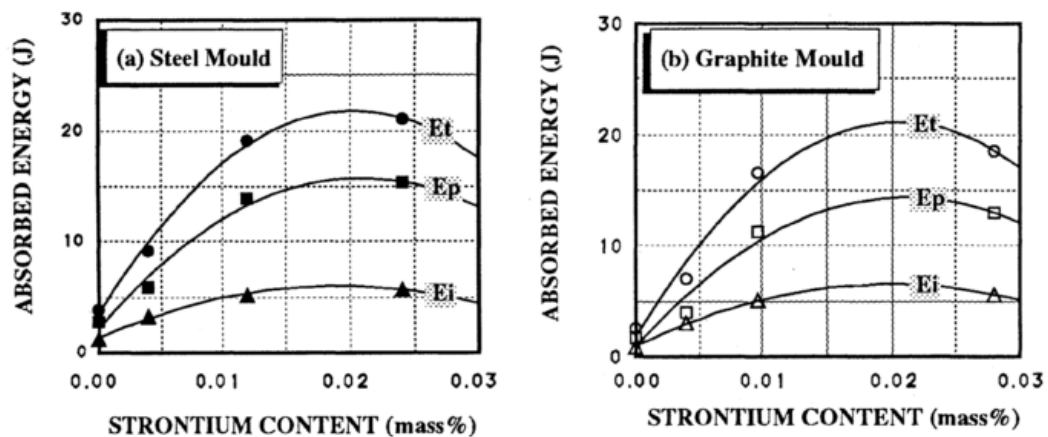


Figure 1.11: Impact toughness of eutectic alloy as a function of Sr-content for samples casted in steel and graphite moulds. E_i is the crack initiation energy. E_p is the crack propagation energy. E_t is the total absorbed energy [49].

Figure 1.11 shows that the absorbed energy is not linear with the Sr content. Considering modified structures, the absorbed energy presents a maximum for fully modified structures and decreases with under- and over-modification [75].

Remarks of the section

Regarding the dependency of the mechanical properties of the castings with modification, important remarks are:

- Modification improves the mechanical properties, as ductility, toughness, elongation and absorbed energy before failure.
- Considering modified structures, there is an optimal modification level for achieving the best mechanical properties.
- For better analysis of the relationship between the mechanical properties and the modification, an objective analysis of the modification is required.

1.2.4. Available methods to assess the modification

Considering the afore-discussed findings regarding modification, it can be summarized that the relationship between the process settings, the chemical composition, the modification and the mechanical properties of the alloy is complex and it is still being researched. One of the main challenges for researchers is the classification and description of the microstructures morphologies. The present section describes the available methods for classification of the concerning microstructures.

1.2.4.1. Subjective methods of classification

Usually, researchers, who study modification, subjectively compare the structures they work with, with each other. They simply term e.g. “modified” or “unmodified” the structures they study, based on the experience on the topic they have, without referring to a certain methodology for rating the structures or using quantitative characterization methods. The problem of this methodology is that, because of the subjectivity, interpretation issues arise.

Alternatively, researchers subjectively compare the structures they work with, with structures that other researchers subjectively classified. As discussed, for this kind of classification, the wall chart of microstructures for classification displayed in Figure 1.3 (page 7) is the most used one. [28]

Regarding the wall chart of microstructures from Figure 1.3, there are three important limitations. Firstly, it is based on a subjective comparison of structures, thus interpretation issues arise. Secondly, it is not applicable to classify over-modified

structures, because it does not have any rating for over-modified structures. Thirdly, it is difficult for the metallographer to carry out the classification if the structure is not uniform, i.e. if the structure resembles more than one class from the wall chart. The non-uniform modification, i.e. the inhomogeneous modification, is the most common case of modified structures, especially in alloys treated with Sr [4].

Regarding the difficulty on rating non-uniform structures, using the classes from Figure 1.3, Gruzleski and Closset suggested a solution, as follows: The assessment of non-uniform structures can be accomplished by examining a polished cross section of the sample under the microscope and assigning (subjectively) to each class the proportion of the sample surface. They illustrated the methodology with the following example: Considering the classes in Figure 1.3, if the a given studied area contains 20 % class 3, 50 % class 4 and 30 % class 5, its modification rating (M.R.) would then be calculated as $M.R.=(0.2*3)+(0.5*4)+(0.3*5)=4.1$ and the sample could be said to be reasonably well, but not perfectly, modified. [4]

1.2.4.2. Objective methods of classification

Djurdjevic et al. studied in 2000 the dependence of various microstructure parameters with the modification. They found that the mean value of the eutectic Si particle perimeter ($P]_{mean}$) was the fittest parameter to describe the modification. They suggested a modification level (ML), which is a function of $P]_{mean}$ [76]. Heugenhauser and Djurdjevic et al. studied in 2012 further parameters complementing the previous work from 2000. They detailed the equations to calculate ML as a function of $P]_{mean}$, as indicated in Figure 1.12-a. They also found out a linear and direct proportional relationship between $P]_{mean}$ and the mean value of the eutectic Si particle maximum Feret ($F_m]_{mean}$), as indicated in Figure 1.12-b, suggesting that ML could be quantified using $P]_{mean}$ and/or $F_m]_{mean}$ [77].

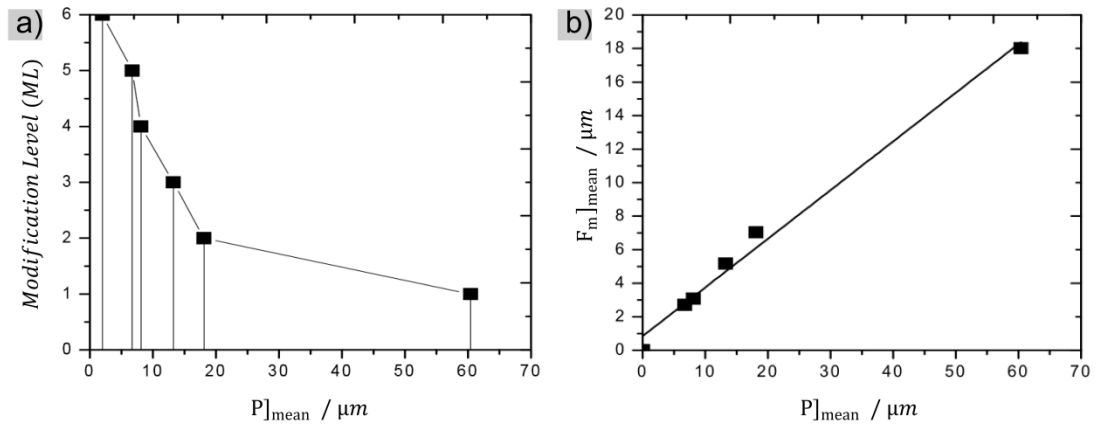


Figure 1.12: (a) Suggested dependency of the modification level (ML) with the mean value of the particle perimeter ($P]_{mean}$). (b) Linear dependency between the mean values of the particle maximum Feret ($F_m]_{mean}$) and $P]_{mean}$. The ML can be calculated knowing $P]_{mean}$ or $F_m]_{mean}$. [77]

Remarks of the section

Regarding the assessment of the modification, the following can be summarized:

- To the date, the visual inspection is the main tool to analyze and classify microstructures.
- Wall chart of microstructures for classification through visual comparison have been suggested as a method to rate the modification.
- The modification rating (M.R.) quantifies the modification based on subjective observations.
- The modification level (ML) quantifies objectively the modification based on measurements of the perimeter or maximum Feret of the eutectic Si particles.

1.3. Quantitative Microstructure Parameters

The hypoeutectic Al-Si alloys, as studied in this work, are formed by dendrites and eutectic phase. The modification alters the morphology of the eutectic phase, i.e. the morphology and sizes of the eutectic Si structure. To fully describe the structure, parameters describing the eutectic Si structure and parameters describing dendrites are required.

The objective of this section is to introduce quantitative parameters, which are used to describe dendrites and microstructural objects. In this work, these parameters will be applied to develop an improved method to characterize the modification.

1.3.1. Dendrite parameters

The *dendrite arm spacing* (DAS), the *dendrite cell interval* and the *dendrite cell size* are parameters describing the dendrites. These parameters are defined as the “*distance between developed secondary dendrite arms*”, the “*distance between centerlines of adjacent dendrite cells*” and the “*width of the individual dendrite cells*”, respectively [28]. The DAS is also called *secondary dendrite arm spacing* in the literature and the dendrite cell interval is also called *primary dendrite arm spacing*. Figure 1.13 shows dendrites and illustrates the measurement of the primary- and secondary dendrite arm spacing.

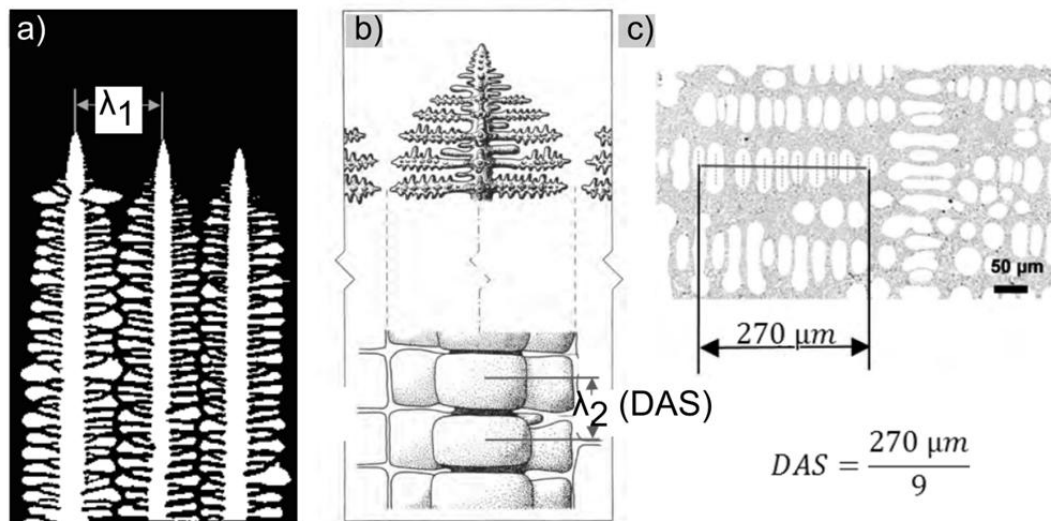


Figure 1.13: (a) Primary dendrite arm spacing (λ_1), (b) secondary dendrite arm spacing (DAS or λ_2), (c) example of DAS estimation of a dendrite [78].

1.3.2. 3D Basic particle parameters

To study objects in 3D space, all features of one object regarding size, shape, topography, etc., can be represented as linear combination of four basic parameters [79].

These parameters are: The volume (V), the surface (S), the integral of mean curvature (M_C), and the integral of the total curvature (K). M_C and K are detailed below:

The surface curvature of a particle can be described locally, at a point p , considering an infinitesimal portion of the surface ds around p as shown in Figure 1.14-a. The radii r_1 and r_2 are the radii of the largest and smallest circles which can be placed tangent to ds on two orthogonal normal planes through p . The corresponding curvatures are defined as $k_1 = 1/r_1$ and $k_2 = 1/r_2$ [80]. A radius vector is positive if, from its origin to the point p , it aims to the outside of the particle (and negative, if it aims in the opposite direction).

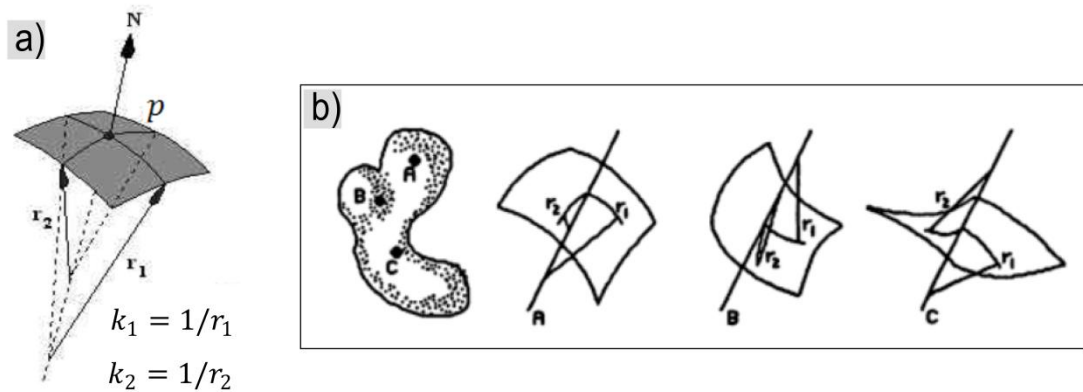


Figure 1.14: (a) The principle normal curvatures k_1 and k_2 at a point p [80]. (b) Surface of complex shapes, showing convex (A), concave (B) and saddle (C) points [81].

If $r_1 > 0$ and $r_2 > 0$, the surface is locally convex (Figure 1.14-b, A). If $r_1 < 0$ and $r_2 < 0$, the surface is locally concave (Figure 1.14-b, B). If the signs of r_1 and r_2 are opposite, the surface is locally saddle (Figure 1.14-b, C). If one radius is infinite, the surface is locally cylindrical. And, if both radii are infinite, the surface is locally flat.

Two curvatures are defined: mean curvature, which is $k_M = (k_1 + k_2)/2$, and the total (or Gaussian) curvature, which is $k_T = k_1 * k_2$ [81]. The total curvature (k_T) is positive for convex and concave points and negative for saddle points. The mean curvature (k_M) is positive for convex points, negative for concave points. Regarding the saddle shapes, two saddle shapes are distinguished, which leads to positive or negative k_M , as follows: if $|r_1| < |r_2|$, $r_1 > 0$ and $r_2 < 0$; then, $k_M < 0$, and if $|r_1| < |r_2|$, $r_1 < 0$ and $r_2 > 0$; then, $k_M > 0$ (Figure 1.15).

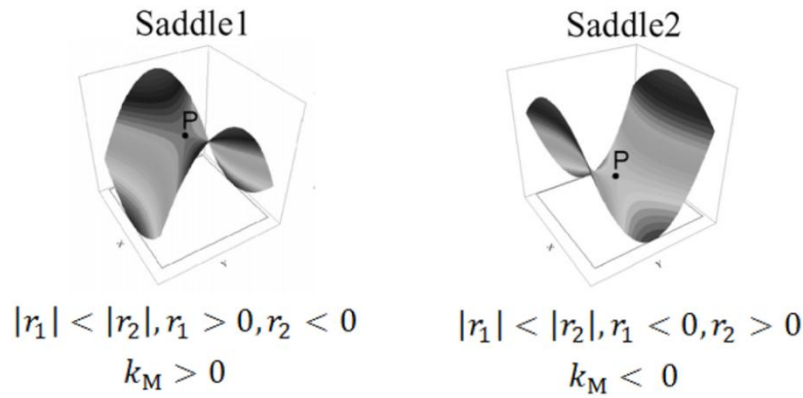


Figure 1.15: Shape of the surface elements and their local mean curvature k_M [82].

The integral of mean curvature is acquired through the integration of the mean curvature over the entire object surface, i.e. $M_C = \int k_M ds$. Similarly, the integral of the total curvature is $K = \int k_T ds$ [80,83].

In the theory, with the four basic parameters, an object can be fully described. However, the microstructure characterization is often carried out using also derivate parameters (functions of basic parameters). For example, the so called *shape parameters* or *shape descriptors*. These are derivate parameters, from which the shape of the object is easier interpreted [84]. In the following sections, stereological methods and further parameters used in the praxis are presented.

1.3.3. Density of the particle features and stereological equations

To analyze structures comparatively, the particle parameters of a given studied phase are divided by the total sample volume. The volume fraction (V_V) is the volume of the studied phase divided by the total sample volume. V_V can be estimated with 2D analysis using stereological equations [85]. The specific surface (S_V) and the specific integral of mean curvature (M_{C_V}) can be calculated through 2D analysis only for isotropic geometries, while the specific integral of total curvature (K_V) requires the 3D information to be quantified [86].

The volume fraction (V_V) can be estimated through 2D analysis using the area method, the lineal analysis or the point count method: $V_V = A_A = L_L = P_P$, where A_A is the area fraction, L_L is the lineal fraction and P_P is the point fraction. A_A is obtained dividing the area of the studied phase by the total analyzed area. Similarly, the lineal fraction and the

point fraction methods rely on tracing lines and marking points at the 2D image to calculate L_L and P_P , respectively [87–90].

The specific surface (S_V) can be estimated through 2D analysis using the area method and the lineal analysis: $S_V = \frac{4}{\pi} L_A = 2N_L$, where L_A is the length of the line per unit of surface (area method) and N_L is the point number per line length (lineal analysis) [91].

The specific integral of mean curvature (M_{C_V}) can be calculated with the area method as $M_{C_V} = 2\pi \chi_{2D}$, where χ_{2D} is the Euler number in 2D analysis. The Euler number will be introduced in the following section.

1.3.4. The Euler number

The total (or Gaussian) curvature (K) for any closed feature, such as a particle with no holes or tunnels (e.g. a potato), integrates to 4π [81]. A hole in a particle is also a closed feature, thus K evaluated for a closed particle with a hole gives $K = 2 * 4\pi$; with two holes gives $K = 3 * 4\pi$, and so on. The total curvature of a particle with a tunnel, i.e. topologically equivalent to the torus, is $K = 0$. K of a particle with two tunnel is $K = -1 * 4\pi$, and so on. The Euler number is a parameter with the same information as K , defined as $\chi = K/4\pi$, and can be interpreted to characterize the topology of the constituents of a structure. Thus, $\chi = 1$ indicates that the evaluated particle has no holes or tunnels, $\chi = 2$ indicates that the evaluated particle has one hole, and so on.

In a 3D structure, the Euler number (χ) has positive contribution from the concave and convex points (curvatures with same sign, see Figure 1.14-b, A and B) and negative contributions from saddle points (curvatures with opposite sign, see Figure 1.14-b, C). The quantification of χ is carried out using probe of the “sweeping tangent plane”. The Euler number, as evaluated with the “sweeping tangent plane”, has a 2D version, using the probe of the “sweeping tangent line”. These probes are conceptually equivalent and are carried out as follows:

As conceptually illustrated in Figure 1.16, to evaluate the Euler number in 2D (χ_{2D}), a line is visualized to sweep through the structure. The line, while sweeping through the structure, defines tangents points at the structure, which can be concave or convex. $N_{Concave}$ is the number of concave points; and N_{Convex} , the number of convex

points. The Euler number in 2D (χ_{2D}) is defined as $\chi_{2D} = \frac{1}{2}(N_{Convex} - N_{Concave})$. Regarding the 3D version of the probe, illustrations can be found, e.g., in ref. [80]. In 3D, a plane is visualized to sweep through the 3D structure and the tangent points can be concave, convex or saddle. $N_{Concave}$, N_{Convex} and N_{Saddle} are the number of 3D concave, convex and saddle tangent points at the structure surface, respectively. The Euler number in 3D is defined as $\chi = \frac{1}{2}(N_{Concave} + N_{Convex} - N_{Saddle})$ [80,92].

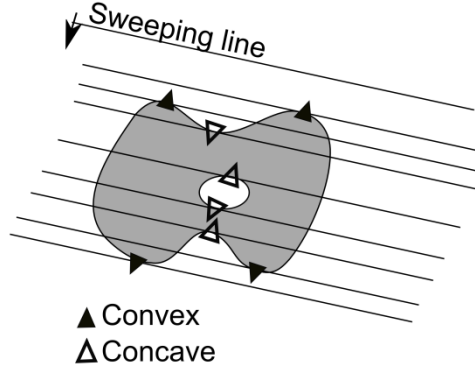


Figure 1.16: Conceptual illustration representing the quantification of the Euler number in 2D using the “sweeping tangent line” probe. Convex and concave indicate the corresponding characteristics of the tangent points on the particle. In this drawing, $\chi_{2D} = \frac{1}{2}(N_{Convex} - N_{Concave}) = \frac{1}{2}(4 - 4) = 0$.

An alternative interpretation of χ_{2D} is $\chi_{2D} = N - N_{Holes}$, where N and N_{Holes} are the number of 2D particles and holes in the studied 2D surface, respectively. Notice that, for a closed feature without holes, $\chi_{2D} = 1$; for a closed feature with one hole, $\chi_{2D} = 0$ (as in the example in Figure 1.16), and so on. Analogously, an alternative interpretation of the Euler number in 3D is $\chi = N + N_{Holes} - N_{Tunnels}$, where N , N_{Holes} and $N_{Tunnels}$ define the number of particles, of holes and of tunnels in the studied volume, respectively. Besides, χ can be used to define “connectivity” through the equation $\chi = N - C$, where C is the connectivity [82]. These equivalent equations help the researcher, depending on the case, to interpret the Euler number. E.g. (1): For a phase formed by particles with holes or tunnels, $\chi = N + N_{Holes} - N_{Tunnels}$ helps quantifying the amount of holes or tunnels. E.g. (2): In the case of sintering, in which the formation of necks (saddle shaped points) “connects” the particles, the equation $\chi = N - C$ can be employed to quantify the connectivity.

1.3.5. Further size and shape parameters

The gathered 2D particle size parameters are (see Figure 1.17) the particle area (A), the particle perimeter (P), the perimeter of the particle's convex envelope (P_{Convex}), the maximum Feret diameter (F_m) and the minimum Feret diameter (F_{min}).

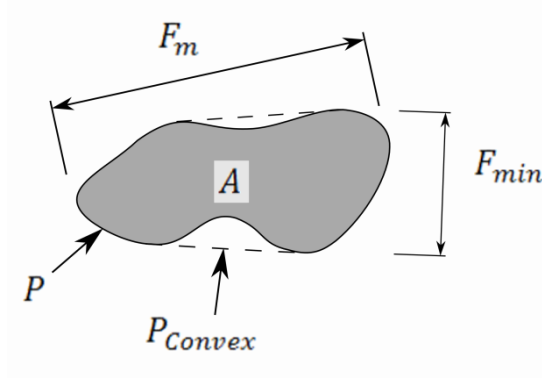


Figure 1.17: 2D size particle parameters

Shape parameters are combinations of size parameters arranged so that the dimensions cancel out. They commonly compare the particle with a circle (in 2D) or a sphere (in 3D) and they are ranged between zero and one. They are constructed so that the higher the shape parameter is, the more like a circle or sphere the particle is. [84,93,94]

In 2D analysis, the eutectic Si particles, characterized in this work, can be stretched (lamellar or plate-like) or quite compact and circular, depending on the modification level. The most relevant shape parameters to characterize these morphologies are summarized in Table 1.3 [84,93,94].

Table 1.3: Definition of 2D Shape parameters.

<i>Shape parameter</i>	<i>Definition</i>	<i>Description</i>
Roundness (R)	$R = \frac{4\pi \cdot A}{P^2}$	Ratio between A and the area of a circle with perimeter P
Convexity (C)	$C = \left(\frac{P_{convex}}{P}\right)^2$	Ratio between the area of a circle with perimeter P_{convex} and the area of a circle with perimeter P
Feret aspect ratio (FAR)	$FAR = \frac{F_{min}}{F_m}$	Particle stretching
Area aspect ratio (AAR)	$\left(AAR = \frac{4 \cdot A}{\pi \cdot F_m^2}\right)$	Ratio between A and the area of a circle with diameter F_m

In this work, the arithmetic mean of 2D particle parameters, from particles within a micrograph, is indicated with “ $]_{mean}$ ”. Parameters representing characteristics of the entire micrograph (e.g. $AAR]_{mean}$) are called “microstructure parameters”, to differentiate them from “particle parameters” (e.g. AAR).

In 3D analysis, shape parameters comparing particles with spheres were successfully used; for example, to describe the graphite in cast iron [95]. In the case of this study, the 3D structures are too different from spheres (3D networks of fibers or plates), thus shape parameters comparing the particles with a sphere are not applicable in this work.

1.4. Quantification of Homogeneity

The homogeneity is an important concept in material sciences. However, there is no standard method to evaluate the homogeneity and consequently, the use of the term varies. The Voronoi tessellation is often used in materials sciences to analyze the object distribution homogeneity. The Voronoi tessellation consist in partitioning the space into mutually congruent polygons (in 2D) or polyhedrons (in 3D) [96]. The planar Voronoi diagrams, which are also known as Thiessen, or Dirichlet polygons or cells, are the most common in material sciences. The planar Voronoi tessellation consists in dividing the space into cells. The boundaries of the cells are perpendicular bisectors between the closest neighboring points. Each cell corresponding to a given point contains the closest

regions of the plane to the point [97]. An example of the Voronoi tessellation is given in Figure 1.18, in which the cells in (b) help studying the distribution of the points in (a) [98].

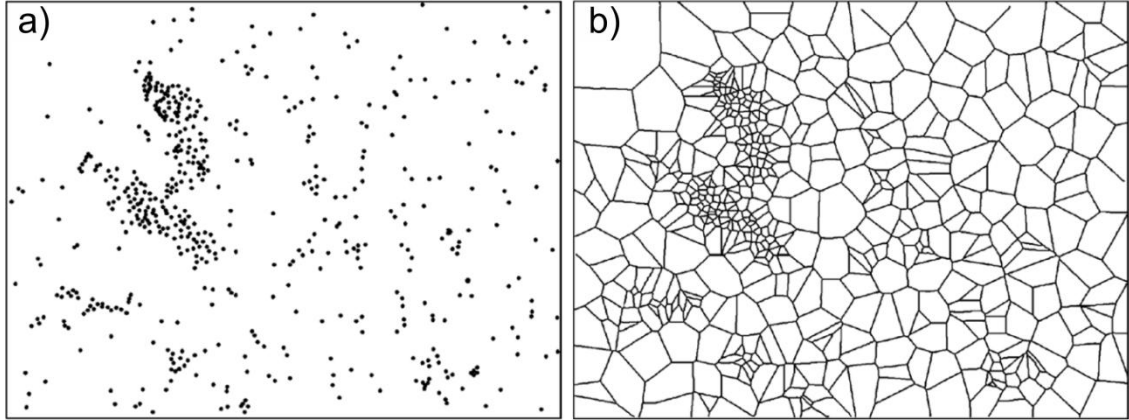


Figure 1.18: Illustration of the Voronoi tessellation: (a) Points in the plane to be analyzed, which in this example represent tetragonal zirconia (TZ) grains within a lead zirconate titanate (PZT) ceramic matrix and (b) and the Voronoi diagram representing the zirconia distribution [98]

Still with tessellation methods, the homogeneity remains without being quantified. To quantify the homogeneity, size parameters of the cells can be analyzed. In some works, the homogeneity is quantified considering the ratio between the standard deviation (SD) and the arithmetic mean (\bar{x}) of a data set. This ratio (SD/\bar{x}) is inconsistently named in the literature. [97,99–101]

The Lorenz curve and the G can be interesting tools to analyze the homogeneity in material sciences. The Lorenz curve and the G have been developed to study questions related to Economy. In addition to their use in Economy, there are vast amount of works that use these tools in diverse fields of study; e.g., Social Sciences, Agricultural and Biological Sciences, Chemistry, Medicine, Pharmacology, Physics and Astronomy [102–106]. However, in Materials Science, these tools are still not common. As part of this work, it has been shown that these tools are convenient to quantify the homogeneity in microstructures [1,3].

The Lorenz curve was introduced by Max Lorenz, in 1905, for the measurement of the concentration of wealth in a society [107]. To obtain the Lorenz curve of income, one proceeds as follows: A society of n persons is considered, where y_i is the income of a single person, with $i = 1$ to n , indexed so that $y_i \leq y_{i+1}$ (ordered from lowest to

highest income). The Lorenz curve is the function connecting the points (F_i, L_i) , $i = 0$ to n , where $F_0 = 0$, $L_0 = 0$, and for $i = 1$ to n : $F_i = i/n$ and $L_i = S_i/S_n$, where $S_i = \sum_{j=1}^i y_j$. Thus, F_i is the cumulative share of people, S_n is the total income from the whole society ($S_n = \sum_{j=1}^n y_j$) and L_i is the cumulative share of income up to the i -th person. The Lorenz curve always contains the points $(0,0)$ and $(1,1)$. A hypothetical example of a Lorenz curve of income is represented in Figure 4.1. The line of perfect distribution (the line of equality) is the straight line. The Lorenz curve is always below the line of equality or it is coincident with the line of equality. A Lorenz curve for income being the line of equality would represent that each person in the society earns the same. The more unequal the incomes from the individuals are, the farther the Lorenz curve from the line of equality is.

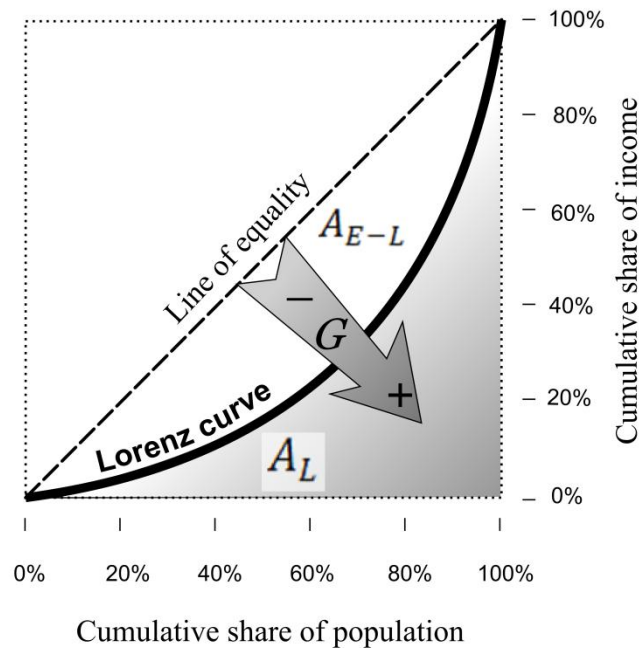


Figure 1.19: Illustration of the Lorenz curve for the income of a society and the Gini coefficient (G). G increases as the Lorenz curve gets further away from the line of equality.

The statistician Corrado Gini developed in 1912 a coefficient (today known as *Gini coefficient* or *Gini index*) to measure inequality in the distribution of income in a given society [108]. The Gini coefficient (G) can be interpreted and formulated in several ways, including the graphical approach using the Lorenz curve [109–111]. Using the Lorenz curve, the G is defined as $G = A_{E-L}/(A_{E-L} + A_L)$ where, as represented in Figure 1.19; A_{E-L} is the area between the line of equality and the Lorenz curve, and A_L is the area below the Lorenz curve (shaded area). Besides, $G = 2A_{E-L} = 1 - 2A_L$ due

to the fact that $(A_{E-L} + A_L) = 0.5$. G ranges from 0 to 1 and the closer the G is to 1, the farther the Lorenz curve is from the line of equality. G represents the “inequality”, i.e. how much the measurements differ from each other. For example, considering the distribution of wealth, G represent how dissimilar the incomes from the individuals are [109].

An innovative idea of this work is to apply these tools from Economics (the Lorenz curve and the Gini coefficient) in Materials Sciences. The conceptual illustration in the Figure 1.20 represents the quantification of a given parameter, in different regions of a microstructure. The idea is to measure the inequality, using the tools from Economics, to study microstructure homogeneity. Further details are described in the section of results.

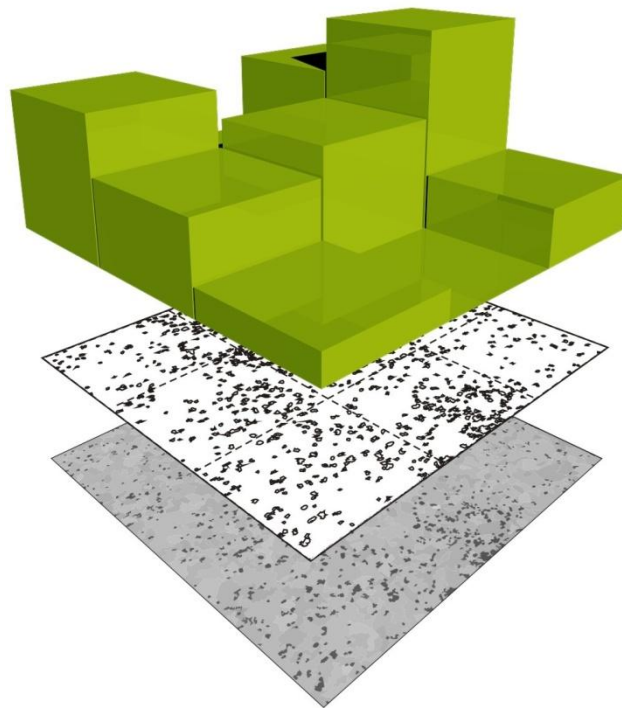


Figure 1.20: Conceptual representation of “inequality” in a microstructure. The Gini coefficient (G) can be used to analyze homogeneity in microstructures.

1.5. Microstructure classification

In this work methodologies to classify structures will be implemented, which later will be in detail described. The methodologies consist in carrying out of a round robin test and applying computed processes to classify structures. In this section, the goal is to introduce these tools and to show how they have been already successfully applied in other works, which confronted similar problems.

The round robin test:

Smirnov et al. reviewed the designations used in several publications of different structures in steels and they found over forty structural component names. They concluded that the development of a classification method was required, to standardize the terminology used to describe the structures. They indicate that a classification method would facilitate the team work in research organizations and plant laboratories. They remarked that a single classification should be carried out combining the work from several researchers. [112]

Thewlis formulated a classification scheme providing guidelines and terminology for identification of the principal structures of microstructures in steel. He suggested the use of round robin tests to evaluate the subjective assessment from different operators. [113]

From the works from Smirnov et al. [112] and from Thewlis [113] two significant ideas are pointed out. Firstly, the idea of combining the experience from several researchers to develop a well accepted classification. Secondly, the idea of carrying out a round robin test to evaluate the assessment from different operators. In this work, as later will be detailed, these ideas are adapted to identify micrographs representing the different structures in Al-Si alloys.

The computed processes:

Once micrographs representing well the different structures are identified, an objective analysis can be carried out to classify the structures based on image data. To objectively find out quantitative rules classifying the structures, computed processes and evaluating parameters are applied in this work.

Regarding the computed processes to evaluate quantitative data, such as Artificial neural networks (ANNs), offer possibilities to study problems in Material Sciences.

ANNs are adaptive learning algorithms that can be used to build prediction models. ANNs are capable of extracting the relevant features from the input data and perform a pattern recognition task by learning from examples [114]. There are several uses of computed processes in Materials Sciences and Engineering [115–117]; for example, to predict the mechanical behavior of materials [118]. Regarding the modification of Al-Si alloys, Francis and Sokolowski used ANNs to predict the Si level of modification (SiLM) based on thermal analysis data [119]. Computed processes are proved to be useful for classification of microstructures [120–122]. Computed processes can apply different algorithms, so-called learner operators [123]. In this work, as it will be detailed later, computed processes are used to analyze the microstructure data from Al-Si alloys with different modification levels.

1.6. 3D microstructure representation

Techniques to capture the 3D nature of the material's microstructure are of interest; especially, for complex, non isotropic structures, such as the ones studied in this work. 3D visualization allows better understanding of the structure and the gathering of quantitative microstructure characteristics, which cannot be estimated by means of 2D analysis. The different methodologies achieve different combination of spatial coverage and resolution, as represented in Figure 1.21 [124].

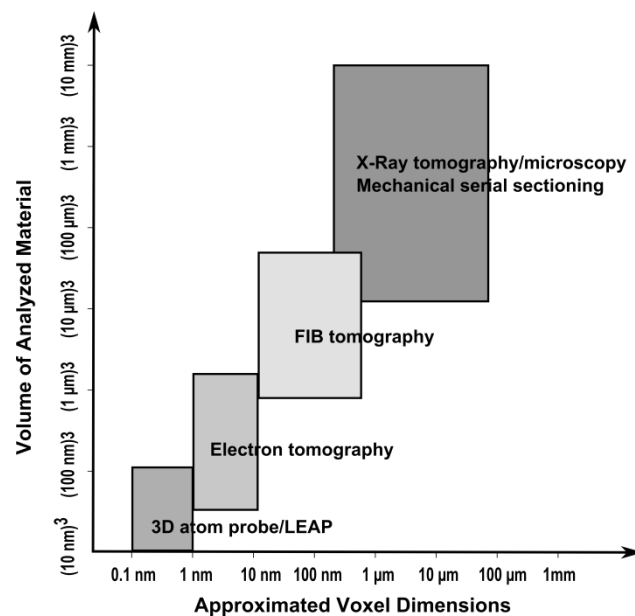


Figure 1.21: Graphical representation of the resolution and typical volume analyzed per experiment for tomographic characterization methods. LEAP is local electrode atom probe tomography; FIB, focused ion beam [124].

X-ray tomography is a nondestructive evaluation technique, which uses x-rays to produce 3D images of the sample's microstructure. A large series of 2D radiographic images are taken around an axis of rotation of the sample [125]. The series of such images allow the computed tomography (CT) of the material's microstructure [126]. The signal noise together with the fact, that the X-ray attenuation depends on the atomic numbers of the elements and the density of the materials, are important limitations of X-ray tomography. These limitations lead to low resolution of the images [127] and difficulties in interpreting the data [128]. Synchrotron based X-rays sources offer continuous energy spectra with high photon flux and with the possibility of choosing a convenient, monochromatic beam. The advantages of these sources, with respect to the conventional x-ray tomography, are that a higher spatial resolution (down to 0.5 μm) and a higher signal-noise ratio are achievable [129]. X-ray tomography has been applied successfully to study Al-Si alloys, e.g. to study the porosity in castings [130–133]. However, the eutectic structure in Al-Si alloys is too small and Al and Si have similar atomic number, thus relatively low resolution and low contrast are achievable between Al and Si using x-ray tomography. Therefore, the detailed characterization of the eutectic structure of modified Al-Si alloys, as it is the aim of this work, is not possible using these techniques.

Electron tomography employs the transmission electron microscope (TEM) to collect projections of a sample that is tilted in multiple directions for later reconstruction, similar as in x-ray tomography [134]. Atom probe tomography is a destructive technique that provides a 3D analytical mapping of materials with atomic-scale resolution. Atom probe uses needle-shaped specimens, which in the base have a diameter of about 100 nm [135]. The specimen is subjected to a standing (DC) electrostatic field combined either with high-voltage or laser pulses that trigger the evaporation of individual ions. The electrostatic field causes the ions to accelerate towards a detector. The positions of the impact and the time-of-flight, of the detected ions, are used to generate a three-dimensional reconstruction [136,137]. Electron- and Atom-probe tomography are useful to study local characteristics of the eutectic structure in Al-Si alloys [138]. However, because of the small volume under study, the characterization of the structure at the micro-scale, as it is the aim of this work, cannot be achieved with these techniques.

The serial sectioning technique and the FIB-tomography

The serial sectioning technique is a destructive technique, which consists in serially removing a thin section from the sample parallel to the surface and imaging the resulting surface [139]. This technique is usually coupled with computer-aided reconstruction techniques to obtain visualizations of the 3D structure [140]. To remove the material, there are different techniques including polishing (mechanical removal of material) and ion milling (sputtering).

Regarding the polishing technique to remove material, to measure the material removal during polishing/grinding, commonly fiducial marking by indentation (e.g. Vickers indentation) is used. To image the surfaces, light microscopy is ordinarily used. To control the material removal, variables in the polishing process, such as time of polishing, applied load and wheel speed should be managed [140]. This technique was successfully applied in Al alloys, e.g. to characterize large (of several μm in size) particles in reinforced Al composites. [141,142]. However, the resolution is not high enough to study the eutectic modification, because to control the material removal is difficult and slices thinner than 1 μm cannot be reliably achieved [143].

FIB-tomography is based on the serial sectioning technique, in which a focused ion beam (FIB) is used to serially slice the material by milling, and the slices are imaged with a SEM [128]. To perform FIB-tomography, dual-beam machines are used, which have both a FIB and a SEM [95,144]. The precise control of the material removal during milling allows the reconstruction of the spatial microstructure of materials, with a resolution down to 10 nm [13,145].

FIB-tomography has been found useful for precise representation of the eutectic morphologies in Al-Si alloys [12,40,41,144]. It can be concluded that FIB-tomography is the technique that meets the requirements of this work, regarding the studied volume and resolution achieved.

The geometrical configuration for FIB-Tomography procedure is represented in Figure 1.22. Firstly, the sample is placed with a polished surface perpendicular to the ion beam. Secondly, a layer of Platinum (Pt) is deposited over the area of investigation. This layer protects the sample and suppresses curtaining effects improving the ion polishing [12,128]. Thirdly, about 10 μm wide trenches are milled around the volume to be studied, as shown in Figure 1.22. These trenches enable access of the electron beam

(which has a tilt angle with respect to the ion beam) to the imaging plane and reduce shadowing effects [146]. After these steps, the serial sectioning technique is carried out, collecting the images for later reconstruction of the imaged structure. FIB-tomography will be applied in this work and further details will be provided later.

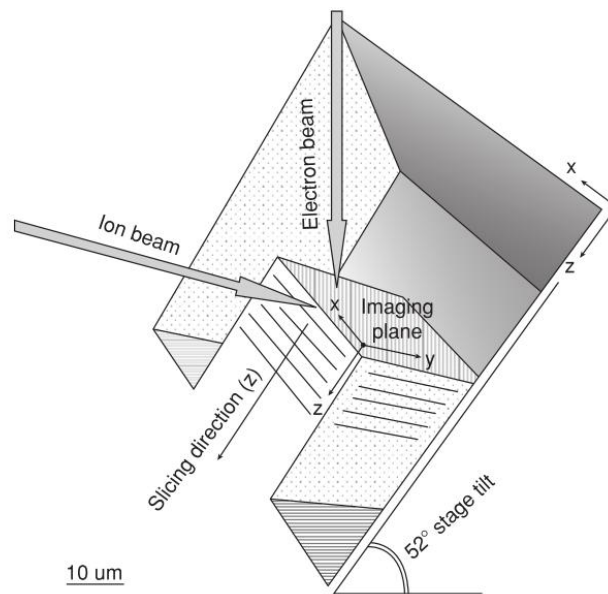


Figure 1.22: Schematic illustration of the geometrical configuration for the serial sectioning procedure in FIB-tomography (From ref. [146], in turn adapted from ref. [147]).

2. ADDRESSED PROBLEM AND GOAL OF THIS WORK

The term “modification” is well established and widely used in the context of the Al-Si casting alloys. However, the available definitions of “modification” are often imprecise and based on subjective observations. Despite the effort shown by many researchers in clarifying questions about the modification problem, several questions remain without a widely accepted answer. Not fully clarified topics regarding the modification are: how to control the modification, which are the mechanisms governing the modification and how the modification affects the mechanical properties.

The evaluation of the microstructure morphology is of major importance to propose, deny and justify hypotheses regarding the modification. Thus a precise method to evaluate the modification is required.

This chapter presents a few results, to show the limitations of the available methods, highlighting the growing concern for improvement in this regard.

2.1. Problem

The problem of the subjective methods is that these are irreproducible and lead to misinterpretation and communication issues. It has been observed that the subjective information about the phenomenon of modification is confusing and contradictory [30,58,148].

With regard to objective characterization methods, the available method discussed in page 20 (Figure 1.12) allows quantifying a modification level (*ML*). This method was tested and limitations were faced, which are detailed below.

In this work, the mean value of the perimeter and the mean value of the maximum Feret ($P]_{mean}$ and $F_m]_{mean}$) were quantified, from a total of 38 samples. The samples were Al-7Si and Al-7Si-0.3Mg alloys with different modification states. The results of these measurements (Measured Al-7Si) are represented in Figure 2.1 together with the linear function from Figure 1.12-b (“Literature” in Figure 2.1). The line $P]_{mean} = \pi * F_m]_{mean}$ (Circle) is displayed as reference. The measured data points differ from those in the literature, especially for large values of $P]_{mean}$. The relationship between $P]_{mean}$ and $F_m]_{mean}$ suggested by [77], which has been developed for Al-7Si-0.5Cu-Mg and Al-8Si-3Cu alloys, was not applicable for the alloys studied in this work.

Nevertheless, ML was estimable through $F_m]_{mean}$, using the obtained relationship between $P]_{mean}$ and $F_m]_{mean}$ (Measured Al-7Si).

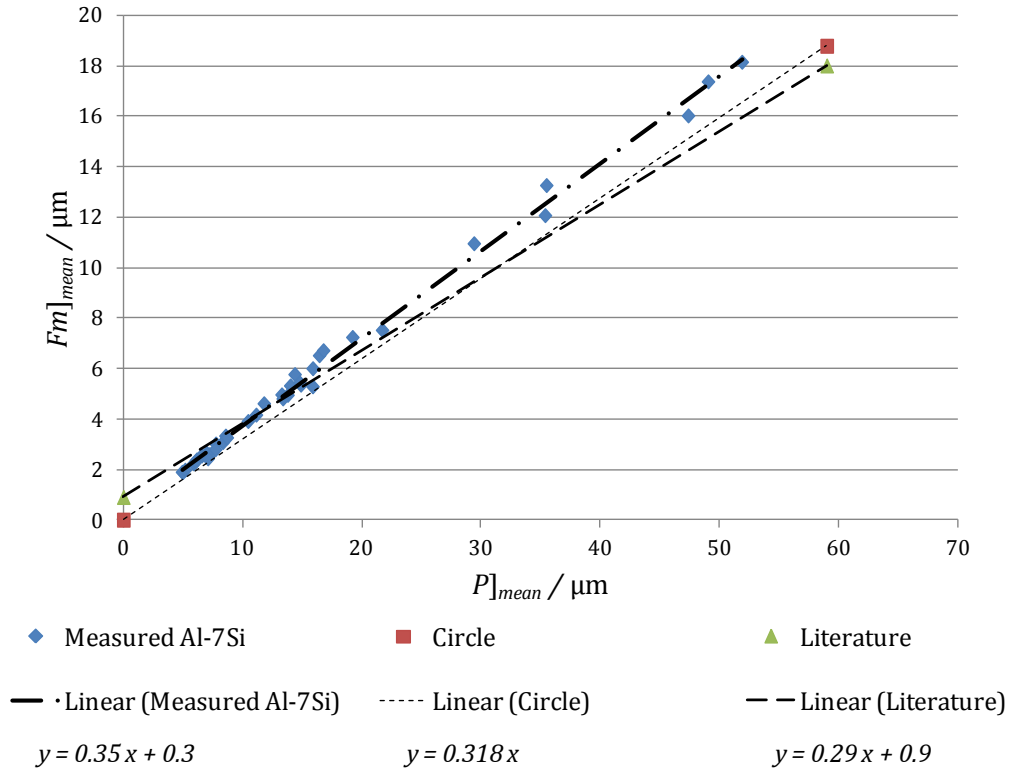


Figure 2.1: Mean values of the particle maximum Feret ($F_m]_{mean}$) as a function of the mean value of the particle perimeter ($P]_{mean}$). **Measured Al-7Si:** Measured data points for samples of Al-7Si and Al-7Si-0.3Mg alloys. **Circle:** Reference to a circle $P]_{mean} = \pi * F_m]_{mean}$. **Literature:** Data points from Al-7Si-0.5Cu-Mg and Al-8Si-3Cu from ref. [77].

However; either if ML is quantified through $P]_{mean}$ or $F_m]_{mean}$, the problem of this methodology relies on that inhomogeneously modified structures are not reliable rated. There are two arguments related to the use of the mean values of size parameters, such as $F_m]_{mean}$ or $P]_{mean}$, to evaluate modification: One is that the SCR scales the structure sizes, thus structures with equivalent modification states may present different absolute sizes [28]. The other is that no information about the microstructure homogeneity is considered, thus a smaller structure, but inhomogeneously modified, can have a better rating than a larger, but well better modified structure. To illustrate this problem, the following analysis is carried out:

In this work, ML was quantified for the micrographs displayed in Figure 2.2, using $P]_{mean}$ as suggested by Heugenhauer et al. [77]. These micrographs correspond to Micrograph No. 5 (Figure 2.2-a) and Micrograph No. 3 (Figure 2.2-b) from a round robin test carried out in this work, which will be later introduced. These micrographs were classified by experts as “homogeneously modified” and “inhomogeneously modified”, respectively. The homogeneously modified state was understood to be the better modification state.

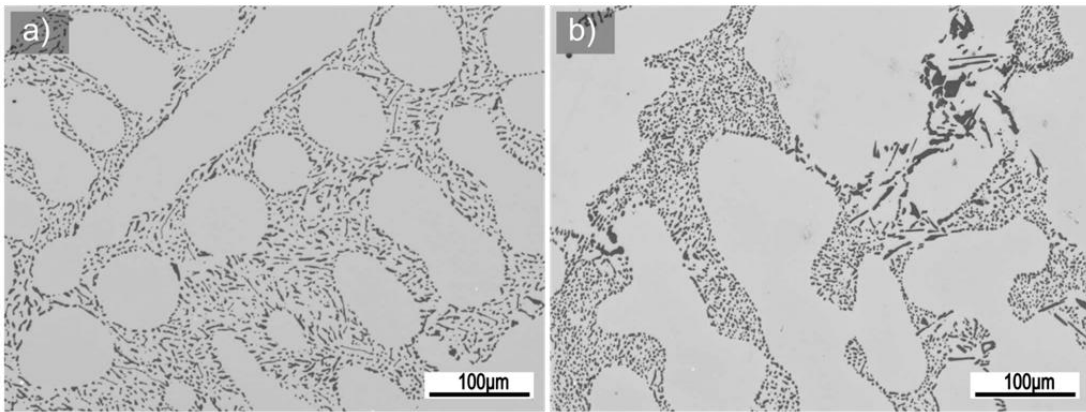


Figure 2.2: (a) Homogeneously modified sample, $ML = 2.8$. (b) Inhomogeneously modified, $ML = 3.0$. The problem is that the method of ML rates better micrograph (b) than (a), while micrograph (a) is better modified than (b).

The micrograph in Figure 2.2-a has $P]_{mean} = 14.3 \mu m$ and the micrograph in Figure 2.2-b has $P]_{mean} = 13.3 \mu m$. Thus taking into account the method of ML , in Figure 2.2-a has a lower ML ($ML = 2.8$) than Figure 2.2-b ($ML = 3.0$). The relatively small $P]_{mean}$ for Figure 2.2-b is attributable to the presence of a large amount of very small particles, despite of the few coarse particles. As a result, the inhomogeneously modified structure (Figure 2.2-b) has a better rating of ML than the homogeneously modified one (Figure 2.2-a). Thus it can be concluded that ML does not give representative values for inhomogeneous cases. This example shows clearly, that not the average sizes of a micrograph, but also its homogeneity is the key to correctly assess the modification.

The advantage of this method is that it is very simple and straightforward. Its problem is that it uses the mean values of size parameters, discarding the information from individual particles. An objective assessment is needed, especially when complex, inhomogeneous structures have to be assessed. And exactly for such cases, this method

is not reliable. Thus an improvement of the methodology to assess the modification is required.

2.2. Objective

The objectives of this work are:

- To develop an improved objective method to assess the modification in Al-7Si and Al-7Si-0.3Mg alloys with different cooling rates.
- To analyze objectively the correlation between the process settings, the microstructure and the mechanical properties.

2.3. Strategy

To develop an improved objective method to assess the modification, it will be preceded as follows:

- Because of the disadvantages of using absolute size parameters, alternative parameters will be analyzed. In addition to parameters from the literature, new parameters will be suggested in this work.
- Using the most adequate parameters to describe the microstructure, an objective methodology to assess the modification will be developed.
- To ensure that the method provides reliable results, it will be developed with the feedback from thirteen specialized laboratories in Al-Si casting alloys.
- After having developed a reliable assessment method, information regarding the process settings and mechanical properties will be objectively studied with relation to the modification.

3. METHODOLOGY

In this chapter, the applied techniques and parameters to analyze the structure are presented. In addition, further parameters are defined, which were developed to describe concerning microstructure characteristics.

The terminology to describe the microstructures had to be defined. Figure 3.1 shows the suggested classification of the microstructures. The adjectives selected to describe the particle morphologies are: lamellar, plate-like, coral-like, and coarsened coral-like. One class can have several morphologies; for example, under-modified microstructures can present lamellar, plate-like and coral-like shaped particles. Subjective descriptions of the microstructures using this terminology have been already carried out in the literature [30,34]. In this work, firstly, representative micrographs for the classes are identified with the help of the experts, and secondly, quantitative microstructure characteristics of the classes are identified.

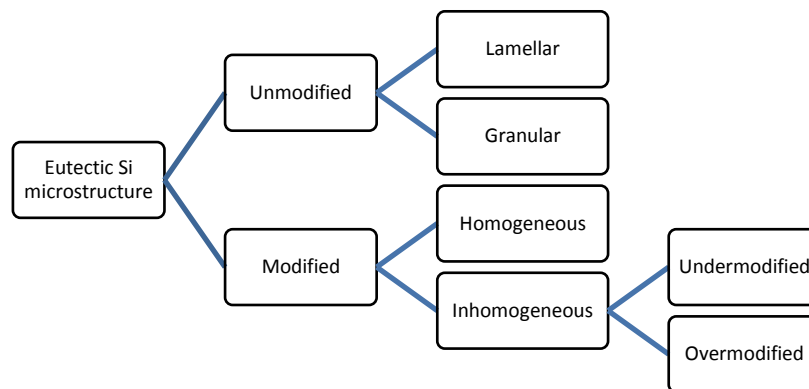


Figure 3.1: Proposed classification of the eutectic Si microstructures.

3.1. Description of samples

The castings are Al-7Si base alloys differing in the chemical composition and solidification cooling rate (SCR). The chemical composition of the alloy was varied with the addition of 0.3 wt.% of Mg and different, controlled amounts of P, Fe and Sr. P and Fe are impurities commonly present in commercial casting, which were added to analyze their effect. Sr was the chemical agent used to induce modification. The casting

processes were non-directional gravity casting and the samples were studied in as-cast condition.

The samples used are listed in Table 3.1. The samples were casted at the Institute of Casting Technology (Institut für Gießereitechnik, IfG) in Düsseldorf, Germany and the Foundry Institute (Gießerei-Institut, GI), from the RWTH Aachen University (Rheinisch-Westfälische Technische Hochschule Aachen, RWTH Aachen) in Aachen, Germany. The sample preparation, which involves cutting, mounting and polishing, was carried out at the IfG, at the GI and at the Saarland University (UdS).

At the GI, Al with 99.9995 % purity and high purity Si and Mg were used. The addition of P was performed through a SiP alloy (P amount: 940 wt. ppm); Fe, through Fe powder; and Sr, through an Al-15 wt.% Sr alloy. To vary the cooling rate, the melt was casted simultaneously into three cylindrical-shaped molds with 30 mm, 60 mm and 90 mm of diameter. The samples are called Triplex D30, -D60 and -D90, respectively (larger specimens have lower SCR).

The samples from IfG were commercial alloys casted in metal and sand molds. The metal mold causes the melt to solidify at higher rates, than the sand mold. “Ingot” indicates that the sample was taken from an aluminum ingot; and “Technical”, that the sample is from a technical casting.

Table 3.1 List of used samples with detail of the chemical composition and process setting. GI: Foundry Institute, Aachen. IfG: Institute of Casting Technology, Düsseldorf. UdS: Saarland University, Saarbrücken.

Micrograph Nr.	Sample from	Prepared and imaged by	Chemical composition: Al 7 wt. % Si and controlled amounts of				Casting process
			Mg/wt. %	Sr / wt. ppm	P / wt. ppm	Fe/ wt. ppm	
1	GI	GI	-	50	2.5	-	Triplex D30
2	GI	GI	-	50	2.5	-	Triplex D60
3	GI	GI	-	50	2.5	-	Triplex D90
4	GI	GI	-	50	5	-	Triplex D30
5	GI	GI	-	100	2.5	-	Triplex D90
6	GI	GI	0.3	-	2.5	-	Triplex D30
7	GI	GI	0.3	50	-	-	Triplex D30
8	GI	GI	0.3	50	5	800	Triplex D30
9	GI	GI	0.3	250	5	-	Triplex D30
10	GI	GI	0.3	250	-	400	Triplex D90
11	IfG	IfG	-	250	4	290	Sand mould
12	IfG	IfG	0.3	200	5	800	Technical
13	IfG	IfG	0.3	300	8	1200	Ingot
14	IfG	IfG	0.3	90	8	260	Metal mould
15	IfG	IfG	0.3	90	8	260	Sand mould
16	IfG	IfG	-	100	6	290	Sand mould
17	GI	UdS	-	50	2.5	-	Triplex D30
18	GI	UdS	-	50	-	400	Triplex D30
19	GI	UdS	-	100	2.5	-	Triplex D30
20	GI	UdS	-	100	-	400	Triplex D30
21	GI	UdS	-	100	-	800	Triplex D30
22	GI	UdS	-	100	5	-	Triplex D30
23	GI	UdS	-	250	2.5	800	Triplex D30
24	GI	UdS	-	250	-	-	Triplex D30
25	GI	UdS	-	250	5	400	Triplex D30
26	GI	UdS	0.3	-	5	-	Triplex D30
27	GI	UdS	0.3	-	2.5	-	Triplex D30
28	GI	UdS	0.3	-	-	800	Triplex D30
29	GI	UdS	0.3	50	-	-	Triplex D30
30	GI	UdS	0.3	50	5	800	Triplex D30
31	GI	UdS	0.3	100	-	-	Triplex D30
32	GI	UdS	0.3	250	2.5	-	Triplex D30
33	IfG	UdS	-	-	-	300	Metal mould
34	IfG	UdS	-	-	-	300	Sand mould
35	IfG	UdS	0.3	350	-	300	Sand mould
36	IfG	UdS	0.3	350	-	300	Metal mould
37	IfG	UdS	0.3	55	-	300	Sand mould
38	IfG	UdS	0.3	55	-	300	Metal mould
39	IfG	UdS	0.3	-	-	300	Sand mould
40	IfG	UdS	0.3	-	-	300	Metal mould

3.2. Microstructure imaging and image data

To image the structure in 2D, light microscopy was considered convenient because images with adequate contrast and resolution are achievable. To properly characterize the dendrites, commonly a lower magnification (about 200X) is required than the required to characterize the eutectic structure (about 1000X).

For 2D analysis, light microscopes (from *Leica* and *Olympus*) equipped with cameras for digital imaging were used. Using the image analysis system *a4i Analysis* of the *Aquino AG*, the images were binarized (setting a threshold value of gray value to segment the Si) and the quantitative image data gathered.

To image the structure in 3D, FIB-tomography was considered convenient because relatively large studied volumes, with adequate resolution are achievable. The dual beam platform used was the *FEI Helios NanoLab*, which employs Ga liquid metal as ion source. The angle between the ion beam and the electron beam is 52°. The methodology to carry out the FIB-tomography is as follows:

An ion current of 20 nA is utilized to deposit the Pt layer over the area of operation. The layer of Pt deposited is about 1.5 µm to 2µm thick. Also using an ion current of 20 nA, a trench around the volume to be investigated is milled. An ion current of 5 nA is utilized to mill the slices. An electron beam with 5 kV of acceleration voltage is utilized to take the (2D) SEM images. The serial sectioning procedure is performed using the software *Slice&View*. The gap between images is 150 nm and the images pixels measure 50 nm x 63 nm, thus the resolution (voxel size) of the achieved tomographies is of 50 nm x 63 nm x 150 nm.

The collected SEM images are aligned, with the help of the software package *Amira*, using as reference the Pt-layer and the trench borders, which are observable at the SEM images. The imaged volume is cropped so that only the relevant study volume is visible, i.e. the Pt-layer and the trench are cropped out. The cropped SEM image stack is improved using shadow correction operations in the software *a4i Analysis* of the *Aquino AG*. The improved and cropped SEM image stack is segmented, and the 3D structure reconstructed, using the software package *Amira*. Quantitative parameters from the 3D reconstruction are gathered using the *Modular Algorithms for Volume Images (MAVI)* software system from the Fraunhofer ITWM, Kaiserslautern, Germany.

Errors are involved throughout the image processing, segmentation and reconstruction. These errors give rise to small isolated artifacts and inaccuracies on the particle characteristics. To minimize the errors, isolated objects in the tomographies being smaller than 1 μm are discarded.

3.3. Subjective Assessment: The Round Robin Test

A round robin test was carried out to be taken by experts with experience in the subjective assessment of Al-Si alloys microstructures. The round robin test was developed with the aim of identifying micrographs representing the suggested classes and their corresponding microstructure shapes (Figure 3.1).

A micrograph from each sample (Table 3.1) was taken. The round robin test consisted in three questions related to the eutectic Si structure of each micrograph, to which the participant replied independently and subjectively. The questions/tasks were defined in collaboration with the project partners. The first and the second questions/tasks were multiple-choice. The first question/task was to identify the modification state, marking one option from the following options: unmodified granular, unmodified lamellar, under-modified, homogeneously modified, and over-modified. The second question/task was to identify the morphology, marking up to two options from the following options: lamellar, plate-like, coral-like, and coarsened coral-like. In the third question/task, the participant was asked to subjectively estimate the homogeneity with a directly proportional number from 0 to 100 %.

The micrographs, together with the questions, were handed to the project partners. A total of thirteen project partners gave feedback, which, because of privacy protection, remain anonymous and are identified with a laboratory number.

Quantification of the feedback

To quantify the overall results from the round robin test, the “percentage agreement” is defined in this work as the relative amount of marks in a given option. Considering the replies for the first question, to group the micrograph in modified or unmodified, the percentage of agreement for the option “unmodified” ($U_{\%}$) was calculated as the amount of marks in the options “Unmodified granular” (UG) and “Unmodified lamellar” (UL) divided by the total amount of marks in the first question (T_1), i.e. $U_{\%} = (UG + UL) / T_1$. Similarly, the percentage of agreement of the option “modified” ($M_{\%}$) is

$M_{\%} = 1 - U_{\%} = (OM + UM + HM)/T_1$, where OM, UM and HM are the number of marks in the options “Over-modified”, “Under-modified” and “Homogeneously modified”, respectively. For the option “unmodified granular”, the percentage agreement ($UG_{\%}$) is $UG_{\%} = UG/T_1$. The percentage of agreement of the options, under-modified lamellar, over-modified, under-modified and homogeneously modified, are calculated analogously. The percentage of agreement for the option “Inhomogeneously modified” ($IM_{\%}$) is $IM_{\%} = (OM + UM)/T_1$.

Analogously as for the first question, the percentage of agreement for each option of the second question was calculated.

3.4. Quantitative microstructure parameters

The defined 2D microstructure parameters (page 21) were calculated using the data obtained using the image analysis system *a4i*, with exception to the dendrite parameters.

Regarding the dendrite parameters, the DAS was quantified because the DAS is the most remarkable characteristic to describe the dendrites in non-directional solidified microstructures (as the ones studied in this work) [149]. In this work, the DAS of the samples was estimated as suggested in ref. [78].

As discussed earlier (page 15), the particle sizes and the DAS decrease with increasing cooling rate. With the aim of characterizing the particle sizes for a range of cooling rates, the particle sizes relative to the DAS have been calculated. In addition to the standard 2D microstructure parameters (page 21), further 2D parameters are defined in this work, which describe how relatively large are the particles in a given structure, as indicated in Table 3.2.

Table 3.2: Definition of DAS related parameters.

<i>DAS related parameter</i>	<i>Definition</i>	<i>Meaning</i>
Density of objects (D)	$D = \frac{n * DAS^2}{A_{\text{imaged}}}$	n is the total number of particles in the considered imaged area (A_{imaged}), thus D is the average number of particles in a square of sides equal to the DAS.
Feret-DAS ratio ($F\lambda R$)	$F\lambda R = \frac{F_m}{DAS}$	Ratio between the particle's F_m and the DAS
Area-DAS ratio ($A\lambda R$)	$A\lambda R = \frac{A}{DAS^2}$	Ratio between A and the surface of a square of sides equal to the DAS

3.5. Quantitative data analysis

The analysis of the data is carried out to find out which are the most suitable parameters describing a given structure. For example, if two different structures are studied which have similar particles in shape, but one structure have larger particles than the other, size parameters will help to comparatively study these structures. To find out objectively which parameter is the most suitable, mathematical functions or computed processes are used to analyze the data.

Evaluation of parameters

Particle- or microstructure parameters are evaluated to determine if they are capable of differentiating particles or microstructures (“items”), respectively. The particle- or microstructure parameters are quantitative “attributes” describing the items.

Let us suppose that it is desired to evaluate a positive attribute (x) differentiating items, which are classified into two classes. A given number of items belongs to class A, and a given number of other items belongs to class B. The value of x is quantified for all the items and the minimum, the maximum and the mean for each class is calculated. The variables x_{\min_A} , x_{\max_A} and \bar{x}_A are the minimum, the maximum and arithmetic mean of the items in class A. Similarly, x_{\min_B} , x_{\max_B} and \bar{x}_B are the corresponding values of the items in class B. Figure 3.2 represents graphically an attribute x quantified for two classes.

The percentage difference is defined as $PD = \frac{2|\bar{x}_A - \bar{x}_B|}{(\bar{x}_A + \bar{x}_B)}$ and represents how relatively different are the mean values [150].

The intervals of values of x for class A and B are $[x_{\min_A}, x_{\max_A}]$ and $[x_{\min_B}, x_{\max_B}]$, respectively. In this work, the relative gap size (*RGS*) is defined, in Equation 3.1, which can be calculated if there is no interval intersection, i.e. if there is a “gap” (α in Figure 3.2) between the intervals.

$$RGS \begin{cases} = \frac{x_{min_A} - x_{max_B}}{x_{max_A} - x_{min_B}} & \text{for } x_{min_A} > x_{max_B} \\ = \frac{x_{min_B} - x_{max_A}}{x_{max_B} - x_{min_A}} & \text{for } x_{min_B} > x_{max_A} \end{cases}$$

Equation 3.1: Definition of the relative gap size (RGS).

The RGS represents, in the range of variation, how relatively large is the gap between the intervals $[x_{min_A}, x_{max_A}]$ and $[x_{min_B}, x_{max_B}]$. PD and RGS are represented in Figure 3.2.

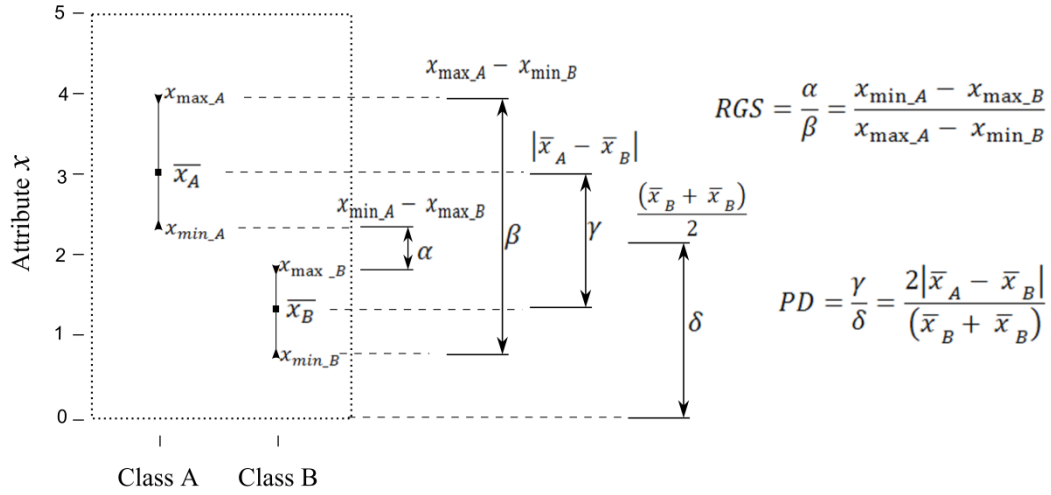


Figure 3.2: Definition of the relative gap size (RGS) and the percentage difference (PD) of a given parameter x quantifying two classes (class A and class B).

PD and RGS are quantitative parameters evaluating the attributes, i.e. evaluating the particle or microstructure parameters. The interpretation of PD and RGS is that they quantify the discriminatory efficiency of the attribute x , differentiating two classes. The higher these values are, the more suitable the attribute to differentiate the classes is.

Analysis of data using computed processes

In this work, computed processes were used to classify particles and microstructures based on the microstructure data. The computed processes were carried out with the data mining software *Rapid Miner*. In the computed processes, rules defining a classification model are performed by a so called learner operator. The learner operator used in this work was the “Decision Tree”. This operator needs as input a labeled data

set, which is for example, a group of classified particles or microstructures (“labeled items”). Each item is labeled, and described by means of attributes. The learner operator “learns” from these examples how to classify the items. As a result, a classification model is obtained, which is composed by rules applicable to the attributes. Figure 3.3 illustrates the process with a hypothetical example. The classification model can be used to predict the label of unlabeled items.

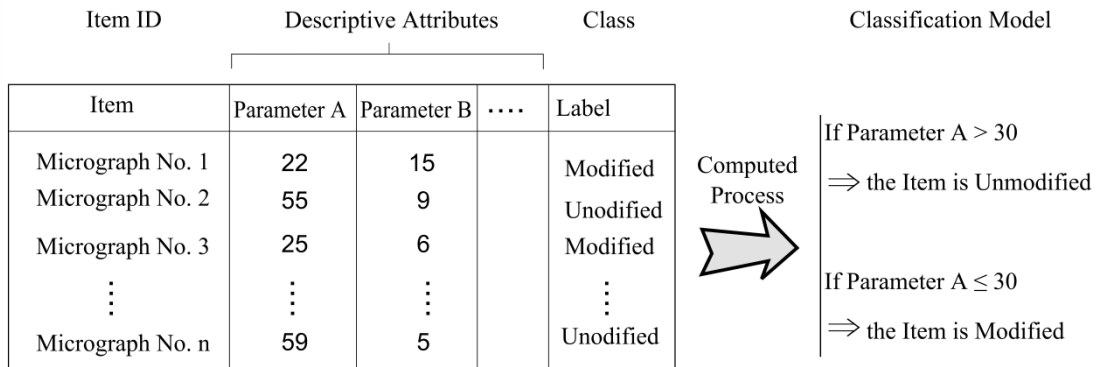


Figure 3.3: Conceptual illustration of the use of a computed process to generate a classification model. A data set of described and labeled items is the input to the computed process. The result is a classification model, which is applicable to label unclassified items.

The learner operator “Decision Tree” is an algorithm based on recursive partitioning. In every recursion, the algorithm selects an attribute and split the data set into subsets, which are formed by disjoint ranges of the selected attribute. In the hypothetical example in Figure 3.3, the selected attribute is the “Parameter A” and the disjoint ranges for the attribute are $(-\infty, 30]$ and $(30, \infty)$. For these subsets, the same algorithm is recursively applied. The recursion stops at the latest when all the items of the subset have the same label. As a results, a series of rules conforming a classification model is obtained, which can be represented graphically in a tree-like graph (a decision tree).

To achieve a meaningful classification model, options in the software should be adjusted, as the criterion to select the attribute and the minimal number of items in a subset for splitting. If the classification model has too many rules, the rules may overfit the example data, increasing the risk of misclassification; and if it has insufficient amount of rules, it will be robust but too generalized, thus not descriptive.

To evaluate the classification model, a validation system was built implementing the cross-validation process in the software. This technique consists in splitting the input data set into two sub-processes: a training sub-process and a testing sub-process. In the

training sub-process, the learner operator generates the model; in the testing sub-process, the performance of the model is measured. The “class recall” and “class precision” are results from the validation, which will be later detailed. The computed process has been run repeatedly using different settings. The classification models have been optimized using the results from the validation, the parameters *PD* and *RGS* and the physical interpretation.

3.6. Mechanical properties

Small Punch Test

Small punch test (SPT) [151,152] was carried out to evaluate the mechanical behavior of Al-Si alloys. The tests were performed at the Metals Division, at the Bariloche Atomic Centre, in Bariloche, Argentina (Centro Atómico Bariloche, CAB).

The SPT was conducted under constant displacement, at room temperature. A schematic diagram of the experiment is shown in Figure 3.4-a. Disks specimens of 10 mm in diameter were tested, with thicknesses $t = 0.50 \text{ mm}$ and $t = 0.55 \text{ mm}$. To control the thickness, the samples were polished. A universal testing machine Instron 5567, was used to apply a displacement rate of 0.1 mm/min. A hard steel puncher, pushing a silicon nitride ball (with a diameter of 2.5 mm), was used to deform the clamped specimen. During the test, the load and the displacement are measured until the maximum load is reached. The displacement is measured at the bottom side of the specimen by a linear variable differential transducer (LVDT) HBM W1T3 linked by a silica push rod. SEM images from the specimens, after the test, were taken using the electron microscope Philips SEM 515.

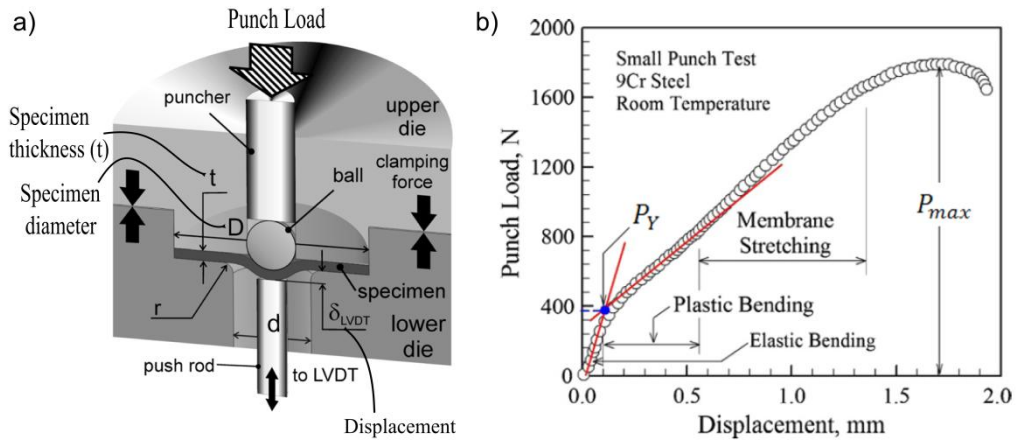


Figure 3.4: (a) Schematic diagram of the Small Punch Test (SPT). (b) Typical punch load–displacement curve generated from a SPT for a ductile material and the definition of P_Y and P_{max} [153]

The curve of punch load vs. displacement for ductile materials presents different stages separated by changes in the slope of the curve, as illustrated in Figure 3.4-b. The stages are: (1) initial elastic bending, (2) plastic bending, (3) membrane stretching, and (4) appearance of the maximum load (P_{max}). P_Y is the load, where initial non-linearity is observed. The maximum displacement is related to the ductility of the material and the area below the curve, from zero displacement up to the displacement at P_{max} , is related to the toughness of the material. P_Y/t^2 , where t is the initial thickness of the tested specimen, is proportional to the yield stress of the material (σ_{YS}), according to the equation $\sigma_{YS} = \alpha \frac{P_Y}{t^2}$. [154]

Charpy impact test

Instrumented Charpy impact test [155] was carried out to evaluate the impact behavior of Al-Si alloys. The tested samples through Charpy test are apart from the list of samples shown in Table 3.1 (page 42). The samples for Charpy test were casted at the IfG. Besides, the IfG provided the results from the Charpy tests and the micrograph from the tested samples.

The results regarding impact properties present in this work were carried out using computer-aided instrumented Charpy impact testing, at room temperature. The tests were carried out on an impact pendulum tester, with pendulum energy of 300 J. To conduct the tests, specimens of dimensions $55 * 10 * 10 \text{ mm}^3$ were used, without

notch, according to ISO 148-1. The force (load) as a function of the time is measured. The force and the energy, as functions of the displacement during the impact event, are computed according to DIN EN ISO 14556.

4. RESULTS AND DISCUSSION

In this chapter, the results are shown and discussed, and it is divided into four sections. The Section 4.1 studies how to quantify homogeneity. The Section 4.2 develops an objective method for evaluation of the modification. Section 4.3 compares the morphologies of quench- and Sr-modified microstructures, thereby using FIB-Tomography. Section 4.4 is about the correlation between the modification, the process settings and the mechanical behavior of castings.

4.1. Homogeneity

This work presents a new method to evaluate homogeneity, which is the result of analyzing the homogeneity and how its quantification can be improved.

With the available tools in the literature, difficulties to describe accurately the homogeneity were found. Tessellations, as the Voronoi tessellations, results in a new image, but the homogeneity still remains without being quantified. As mentioned (page 28), the ratio (SD/\bar{x}) has been used in some works to quantify the homogeneity. This ratio was developed in statistics to measure the dispersion of frequency distribution and it is commonly called “relative standard deviation” (*RSD*), $RSD = (SD/|\bar{x}|) * 100 \%$ [156,157]. The following section explains why the Gini coefficient (*G*) is more appropriated than the *RSD*, to describe the homogeneity. Afterwards, different kinds of homogeneities are defined and it is pointed out, which is the most appropriate to study the modification of Al-Si alloys.

4.1.1. Applying the Lorenz curve and the Gini coefficient to quantify the homogeneity

In statistics, the relative standard deviation *RSD* is used to quantify the data dispersion resulting from repeating the same experiment several times, as in the following example:

- Example 1: The area of one particle is measured several times.

In the example 1, the area values are expected to be one “real value”, but they differ because of measurement or statistical errors. In contrast, to evaluate the homogeneity, measurements from physically different elements are considered, as in the following example:

- Example 2: The areas of different particles are measured (each particle is measured once).

In the example 2, unlike to the example 1, the differing values come from physically different particles and the data points are not expected to be equal. In statistics, there are different tools to study dispersion of data points, depending on whether the data points are expected to be equal or not.

- The question applicable in example 1 is “how much the measurements differ from the real value” and the *RSD* is the appropriate tool to analyze this question.
- The question applicable in example 2 is “how much the measurements differ from each other” and the *G* is the appropriate tool to analyze this question [109].

The homogeneity (*H*) can be evaluated applying the Lorenz curve, with an analogous procedure to the described earlier using people and income (page 29). As illustrated in Figure 4.1, instead of people from a society, items, such as particles or regions from a microstructure, are considered. Instead of income, a given parameter *x*, as for instance the maximum Feret (F_m), is considered. The values of the parameter *x* are indexed in non-decreasing order. The Lorenz curve is obtained by plotting the cumulative share of the *x* values versus the cumulative share of analyzed items. The *H* is defined as the area below the Lorenz curve (A_L) divided by the area below the Line of equality (which is 0.5). This means that $H = 2A_L = 1 - G$. *H* represents “how similar are the data points”

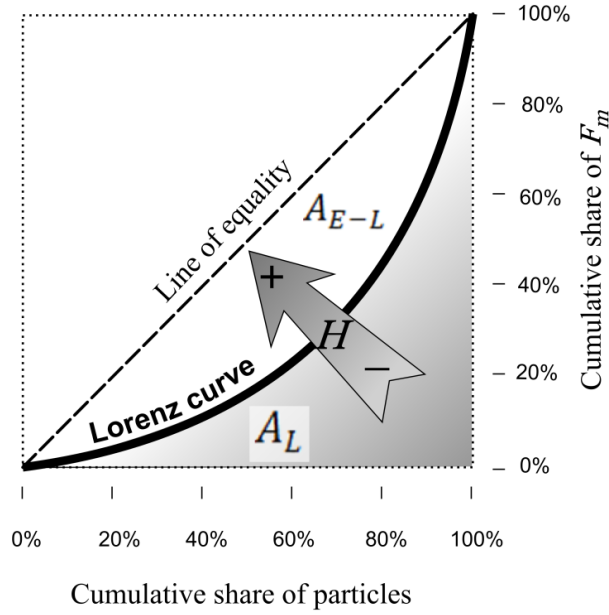


Figure 4.1: Illustration of the Lorenz curve for the maximum Feret (F_m) of the particles in a micrograph and the homogeneity (H). H increases as the Lorenz curve gets closer the line of equality.

It can be shown that H can be expressed as in Equation 4.1 [1]. The interpretation is: the more similar are the data points are, the closer the Lorenz curve to the line of equality is, and the more homogeneous the system is. A Lorenz curve coincident with the line of equality ($H = 100\%$) means that all the data points are equal.

$$H_{(x)} = \frac{2}{n^2 \bar{x}} \left(\sum_{i=1}^n (n+1-i) x_{(i)} \right) - \frac{1}{n}$$

Equation 4.1: Definition of the homogeneity. n is the number of studied items. The x values are indexed in non-decreasing order, and \bar{x} is their arithmetic mean value [1].

4.1.2. The region homogeneity

To quantify how homogeneous is the distribution of objects, different regions of an analyzed area can be compared. These regions are micrographs from a given studied area, which can be adjacent, taken with a regular periodicity or from random spots. We termed this kind of homogeneity *region homogeneity* [1]. The example in Figure 4.2, shows how analyzed areas are partitioned in four regions. The area fraction and/or the amount of particles in each region can be used to evaluate the homogeneity. The interpretation of the region homogeneity is: The more similar the regions are, the more homogeneous the system is.

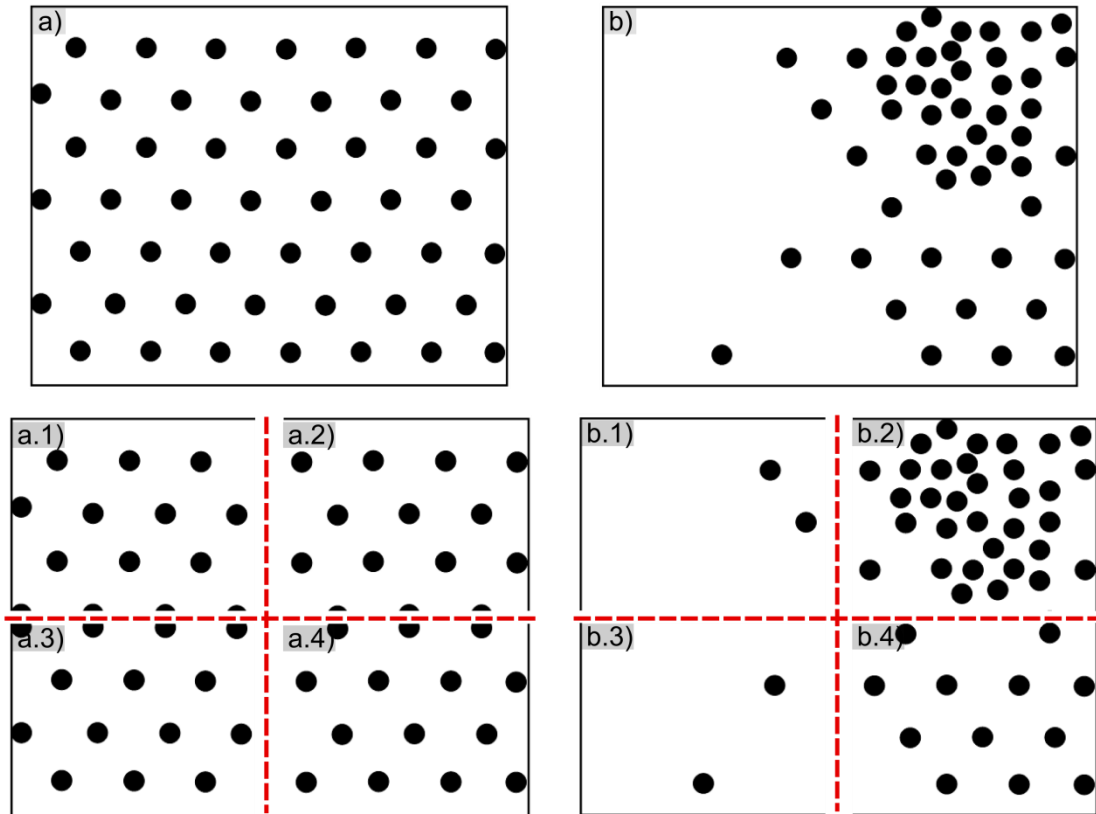


Figure 4.2: Illustration of the region homogeneity: **a** and **b** represent different cases of object distribution. The images at the bottom represent the partitioning of the images **a** and **b** into four regions. Since the individual regions for case **a** are more similar than for **b**, the distribution of objects in **a** is more homogeneous than in **b** [1].

Considering the Figure 4.2 and for illustration purpose, the region homogeneity of the particle number is quantified. The studied items for each micrograph are the four regions ($n = 4$), and the parameter x is the particle number. The Table 4.1 and the Figure 4.3 show the results. The results indicate that the case **a** of Figure 4.2 is more homogeneous than **b**.

Table 4.1: Quantitative data corresponding to Figure 4.2. The homogeneity results indicate that case **a** is more homogeneous than **b**.

Index i	Parameter x_i (in this example: the number of particles in each region)		Cumulative share of items F_i (in this example: the cumulative share of regions)		S_i (cumulative x)		L_i (cumulative share of x)		Homogeneity	
	Case a	Case b	Case a	Case b	Case a	Case b	Case a	Case b	Case a	Case b
1	12.0	2.0	0.25	0.25	12.0	2.0	0.24	0.04	0.99	0.47
2	12.0	2.0	0.50	0.50	24.00	4.00	0.49	0.08		
3	12.5	12.0	0.75	0.75	36.50	16.00	0.74	0.33		
4	12.5	33.0	1.00	1.00	49.00	49.00	1.00	1.00		

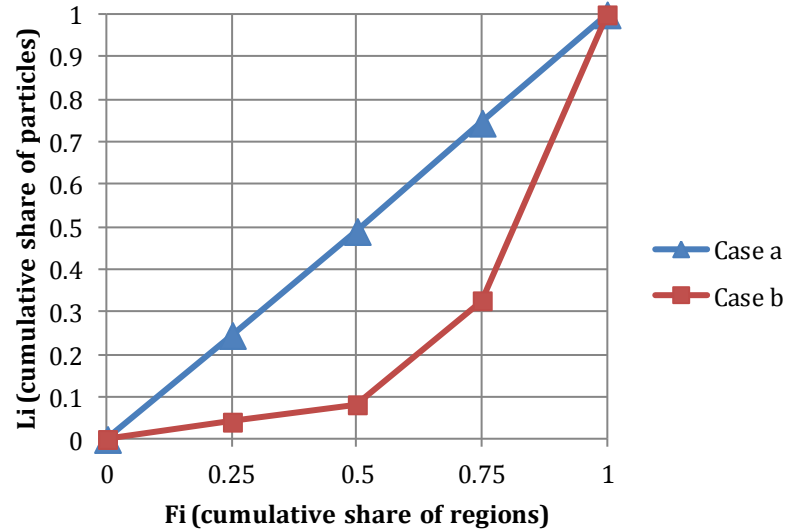


Figure 4.3: Lorenz curve corresponding to Figure 4.2. Case **a** is closer to the line of equality than **b**, thus **a** is more homogeneous than **b**.

4.1.3. The object homogeneity

Other kind of homogeneity can be defined, representing the similarity of particles, regardless to their physical position in the structure. To quantify the similarity of particles, the homogeneity of particle parameters is analyzed. We termed this kind of homogeneity *object homogeneity* [1] and is illustrated in the Figure 4.4. The Figure 4.5 shows the Lorenz curves of the object area (A) and the maximum Feret (F_m). Since the objects in case **a** are equal, the resulting Lorenz curves are lines of equality (straight lines). In case **b**, different objects are observable, and the resulting Lorenz curves are below the line of equality. The homogeneity results are: $H_{(A)} = 100\%$ and $H_{(F_m)} = 100\%$ for case **a**, and $H_{(A)} = 58\%$ and $H_{(F_m)} = 75\%$ for case **b**.

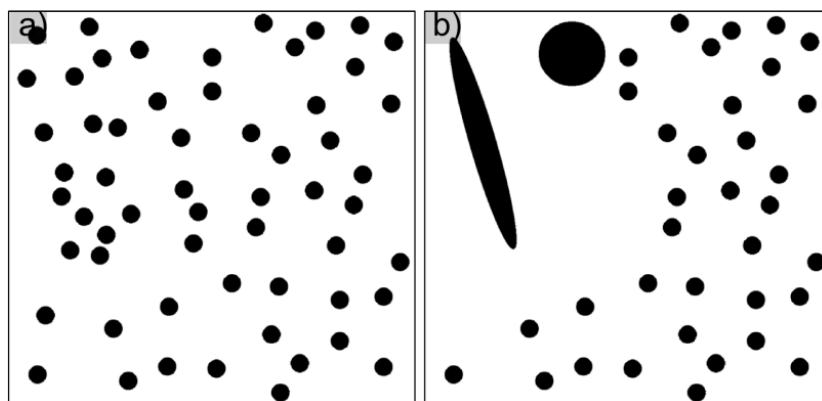


Figure 4.4: Illustration of the object homogeneity. **a** presents equal objects and **b** presents different objects, thus **a** is more homogeneous than **b** [1].

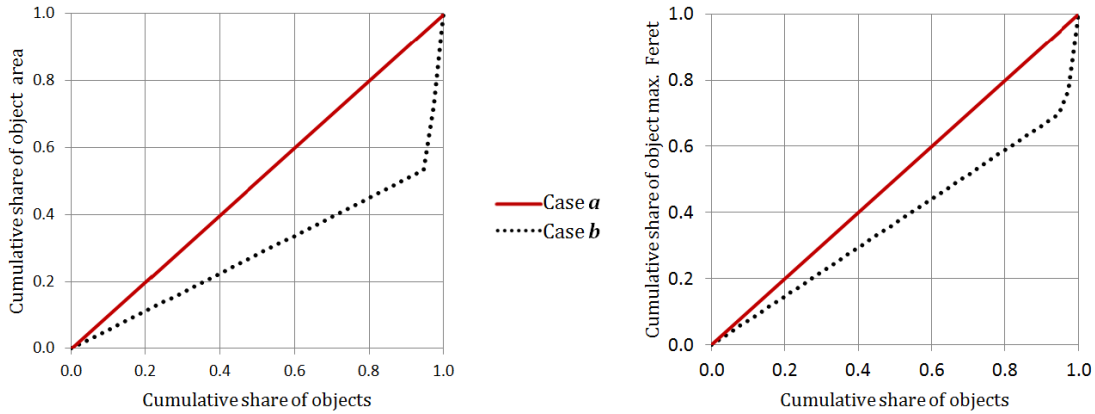


Figure 4.5: Lorenz curves of the area and of the maximum Feret, corresponding to Figure 4.4. Case **a** presents Lorenz curves coincident with lines of equality (all objects are equal) and **b** has an inhomogeneous distribution.

4.1.4. Constructed homogeneities

Homogeneities $H_{(x)}$ as defined in Equation 4.1 are “basic homogeneities”, because they depend on only one parameter. Functions of basic homogeneities are called “constructed homogeneities”. The object homogeneity (h_o), defined as $h_o = H_{(Fm)} * H_{(A)}$, is an example of a constructed homogeneity [1]. A raising question is why the basic homogeneities are multiplied instead averaged. It is in fact a matter of definition and a discussion follows.

Figure 4.6 shows the average and the product of variables between zero and one (x and y). x and y represent basic homogeneities, thus the average $((x + y)/2)$ and the product $(x y)$ represent the results of averaging and multiplying basic homogeneities. $z = (x + y)/2$ can have relatively high values, also if one variable is very low; instead, $z = x y$ has high values, only if both variables have high values. Therefore, the meaning of $h_o = H_{(Fm)} * H_{(A)}$ is that h_o will have high values only if the studied objects are similar (to each other) considering both, Fm and A .

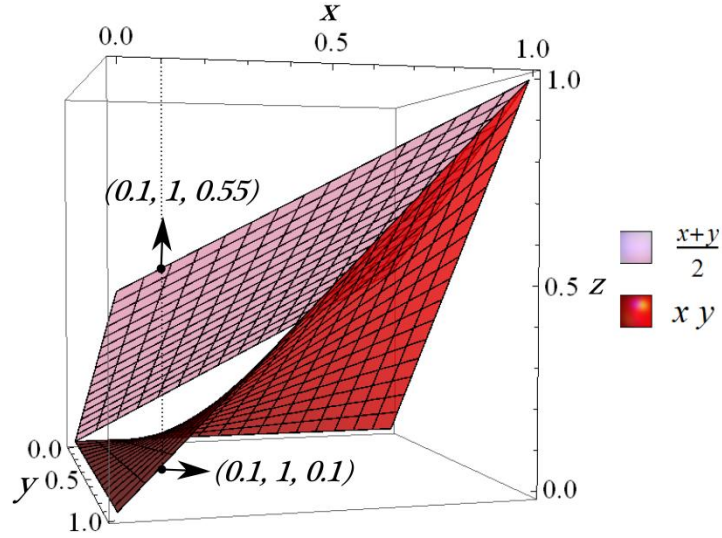


Figure 4.6: Graphical representation of the product ($z = x y$) and the average ($z = (x + y)/2$) of two variables, x and y , $0 \leq x \leq 1, 0 \leq y \leq 1$. If either x or y is small, the product is small (e.g. $P(0.1, 1, 0.1)$), while the average can take relatively large values (e.g. $P(0.1, 1, 0.55)$).

Going back to the example from Figure 4.4, the results of the object homogeneity are $h_o = H_{(A)} * H_{(Fm)} = 1 * 1 = 100\%$ for case **a** and $h_o = H_{(A)} * H_{(Fm)} = 0.58 * 0.75 = 44\%$ for case **b**. In real cases, the differences between basic homogeneities can be slight. Thus the h_o is helpful, because it combines the results of $H_{(A)}$ and $H_{(Fm)}$, and it makes the differences between cases more explicit.

4.1.5. Remarks of the section

In 2D analysis, (see Figure 1.3 in page 7, and Figure 1.6 in page 10) the difference between fully modified structures and other modified structures, is that fully modified structures have only fine-fibrous particles, which are alike to each other. Instead, non-fully modified structures (such as under- or overmodified) have a mixture of particles, with different sizes and morphologies. Under-modified structures have fine fibrous and coarse and stretched particles; and over-modified structures have fine fibrous and coarse particles. Therefore, it makes sense to evaluate the object homogeneity to evaluate the modification. Instead, the region homogeneity is not applicable to study hypoeutectic Al-Si alloys, because the particles are concentrated in the eutectic regions. The region homogeneity is relevant to study other materials, for example, the distribution of carbon nanotubes (CNT) in reinforced composites [3].

In Al-Si alloys, the object homogeneity h_o represents how similar the eutectic Si particles are. If a microstructure is fully modified, h_o will be relatively large, because the particles have similar A and Fm . If the structure is modified with most particles being fine-fibrous, but it has coarse particles (particles with relatively large A , e.g. granular or over-modified particles) or stretched particles (particles with relatively large Fm , e.g. plate-like particles), h_o will be relatively low. Thus it is expected that, among modified samples, h_o has a direct relationship with the modification level.

It is worth to point out, that also fully unmodified structures may present also high homogeneity values. Thus the homogeneity is useful to evaluate modification among modified samples, but not to distinguish modified from unmodified samples. Therefore, further parameters, e.g. relative size parameters, will be required to fully characterize the modification.

4.2. Quantitative classification and assessment of modification

The following section is focused on the discussion and analysis of 2D micrographs used in the round robin test. These micrographs are listed in the Appendix.

4.2.1. Subjective assessment: The round robin test

In the Appendix, together with each micrograph, the graphical representation of the results from the round robin test is displayed.

For better visualization of the results, a scale represented by color and symbols was developed. Table 4.2 shows these scales and the results are summarized in Table 4.3. Using this data, the list of samples (Table 3.1, page 42) was ordered from homogeneously modified to unmodified. Taking into account the percentage of agreement, model micrographs representing the classes were identified in Table 4.3.

Table 4.2: Color and symbolic scale for classifying the microstructures based on the subjective results from the round robin test. This scale is used in Table 4.3

Question	%	Symbol	Meaning: The microstructure...
State (Question 1)	90 - 100		... belongs to this group
	75 - 89		... belongs most likely to this group
	60 - 74		
	50 - 59		
	0 - 49		... does not belong to this group
Morphology (Question 2)	90 - 100		... is a good model for this shape
	60 - 89		... presents mainly this shape
	40 - 59		... may present this shape
	20 - 39		
	0 - 19		... does not present this shape
Homogeneity (Question 3)	95 - 100		... has a subjective homogeneity within the corresponding range
	85 - 94		
	70-84		
	50 - 69		
	0 - 49		

Table 4.3: Results from the round robin test. Images ordered from homogeneously modified to unmodified. The best models microstructures are considered to represent very well the corresponding class.

Micrograph No.	Percentage agreement / %													Question 3: Homogeneity Homogeneity Average / %	Best models for each class	
	Question 1: State							Question 2: Morphology								
	Unmodified	Modified	Unmodified, granular	Unmodified, lamellar	Homogeneously modified	Inhomogeneously modified	Undermodified	Overmodified	Lamellar	Plate-like	Coral-like	Coarsened coral-like				
24	0	100	0	0	100	0	0	0	0	0	0	100	0	96	Homogeneous	Homogeneously modified
20	0	100	0	0	100	0	0	0	7	0	93	0	95			
2	0	100	0	0	92	8	0	8	0	0	87	13	96			
33	0	100	0	0	92	8	8	0	7	0	87	7	95			
5	0	100	0	0	85	15	15	0	16	0	58	26	94			
38	0	100	0	0	77	23	0	23	0	0	80	20	93			
23	0	100	0	0	77	23	0	23	0	0	65	35	91			
22	0	100	0	0	69	31	15	15	15	0	85	0	95			
17	0	100	0	0	69	31	15	15	12	0	76	12	89			
11	0	100	0	0	62	38	0	38	0	5	63	32	89			
18	0	100	0	0	62	38	38	0	10	10	62	19	84			
21	0	100	0	0	62	38	38	0	15	0	60	25	92			
12	0	100	0	0	62	38	15	23	0	11	58	32	78			
37	0	100	0	0	54	46	15	31	0	5	68	26	86			
14	0	100	0	0	54	46	15	31	5	15	55	25	79			
32	0	100	0	0	46	54	31	23	4	21	54	21	76			
19	0	100	0	0	42	58	17	42	30	0	55	15	75			
36	0	100	0	0	38	62	0	62	0	5	55	41	89			
35	0	100	0	0	38	62	38	23	4	29	42	25	70			
31	0	100	0	0	38	62	54	8	8	36	28	28	62			
3	0	100	0	0	31	69	62	8	4	39	52	4	71			
13	0	100	0	0	31	69	62	8	4	26	43	26	69			
29	0	100	0	0	100	92	8	17	13	42	29	29	69			
25	8	92	8	0	77	15	0	15	6	0	76	18	97			
9	8	92	0	8	46	46	23	23	5	19	57	19	82			
30	8	92	0	8	23	69	69	0	20	12	44	24	73			
1	8	92	0	8	23	69	69	0	20	20	40	20	75			
8	8	92	8	0	8	85	77	8	8	32	40	20	60			
4	8	92	0	8	0	92	92	0	24	36	36	4	27			
7	15	85	8	8	0	85	85	0	21	38	21	21	58			
15	15	85	8	8	0	85	77	8	17	46	13	25	60			
34	46	54	0	46	0	54	54	0	61	22	11	6	85			
10	62	38	38	23	0	38	38	0	14	59	18	9	58			
16	69	31	15	54	0	31	31	0	41	41	6	12	93			
40	85	15	15	69	0	15	15	0	50	44	0	6	82			
6	92	8	62	31	0	8	8	0	7	93	0	0	95			
39	92	8	15	77	0	8	8	0	50	50	0	0	73			
26	100	0	75	25	0	0	0	0	7	93	0	0	96			
27	100	0	62	38	0	0	0	0	7	93	0	0	93			
28	100	0	21	79	0	0	0	0	52	48	0	0	66			
															Unmodified	Unmodified, granular
																Unmodified, lamellar

It can be observed that experts agree when they classify fully unmodified and homogeneously modified micrographs. On the other hand, for those inhomogeneously

modified, ample variation among the replies is noticeable. Analyzing the assessment from the experts (Table 4.3 and the Appendix), the following summary is made:

Modified microstructures have coral-like shapes as common characteristic. Most micrographs (29 out of the 40) have over 90 % of agreement for the modified option and therefore, they can be considered as good models for modified microstructures.

Unmodified microstructures are mostly plate-like shaped and they may present also lamellar shaped particles. They may present homogeneous aspect and they do not present coral-like shaped particles. Good models for unmodified granular and lamellar are micrographs no. 26 and 28, respectively.

Modified microstructures can be homogeneous or inhomogeneous. Homogeneously modified can be considered the first four micrographs of Table 4.3; especially, the micrographs No. 20 and 24. Homogeneously modified structures have coral-like particles and high subjective homogeneity.

Inhomogeneously modified microstructures present a mixture of coral-like and coarse particles. In the list there are several samples displaying an inhomogeneously modified microstructure. Micrographs No. 29 and 4 have an agreement of over 90 % in this class.

The micrograph No. 4 is considered a good model for an under-modified microstructure with coral-like and plate-like eutectic regions. The micrograph No. 36 is the best model of an over-modified microstructure, which has coral-like and coarsened coral-like particles.

Figure 4.7 represents the arithmetic average of the subjective homogeneity for each micrograph. The error bars (standard deviation (*SD*)) allow appreciating the remarkable data variation. Figure 4.8 represents the *SD* and the relative standard deviation (*RSD*) of the subjective homogeneities, as a function of the average subjective homogeneity. The *RSD*, is quantified as the *SD* divided by the average subjective homogeneity (page 52).

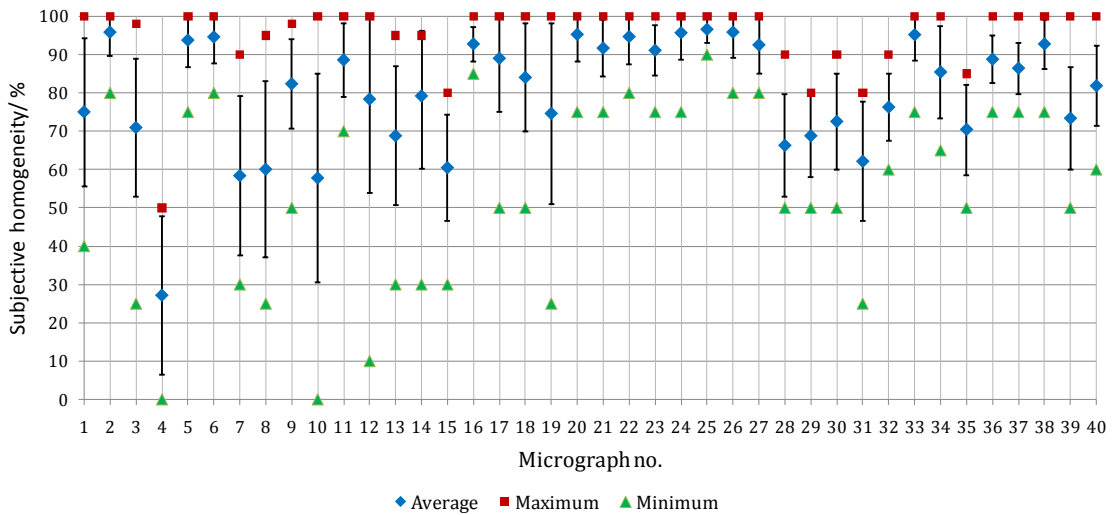


Figure 4.7: Subjective homogeneity reported by the experts for each micrograph. The data variation is remarkable [2].

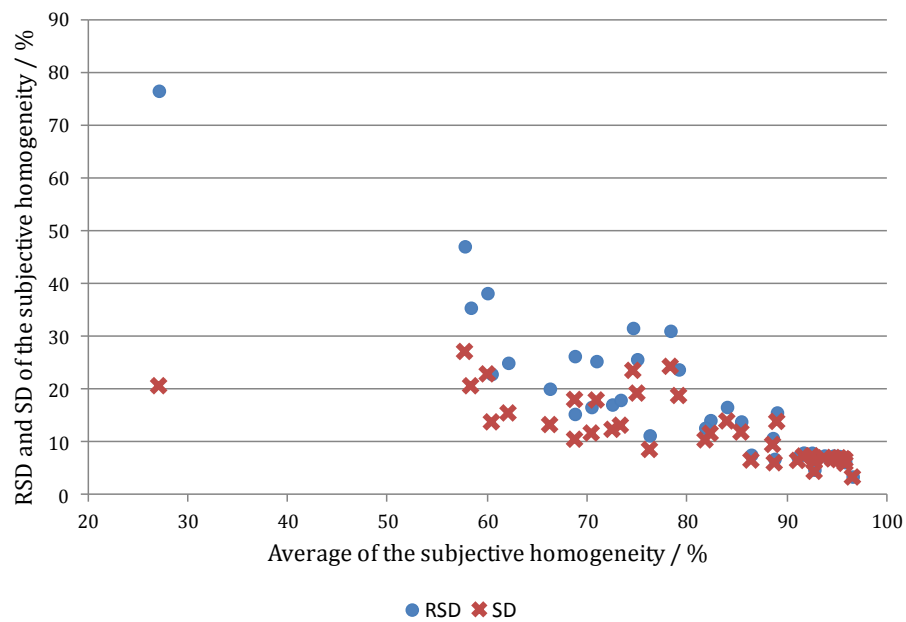


Figure 4.8: Standard deviation (SD) and relative standard deviation (RSD) of the subjective homogeneity, as a function of the average of the subjective homogeneity. The data variation is especially important for inhomogeneous structures. [2]

Figure 4.9 shows the subjective homogeneity from the different laboratories for each micrograph. Laboratory 12 and some other data points are not present because not all laboratories replied all the questions for all micrographs, thus some data points were not available.

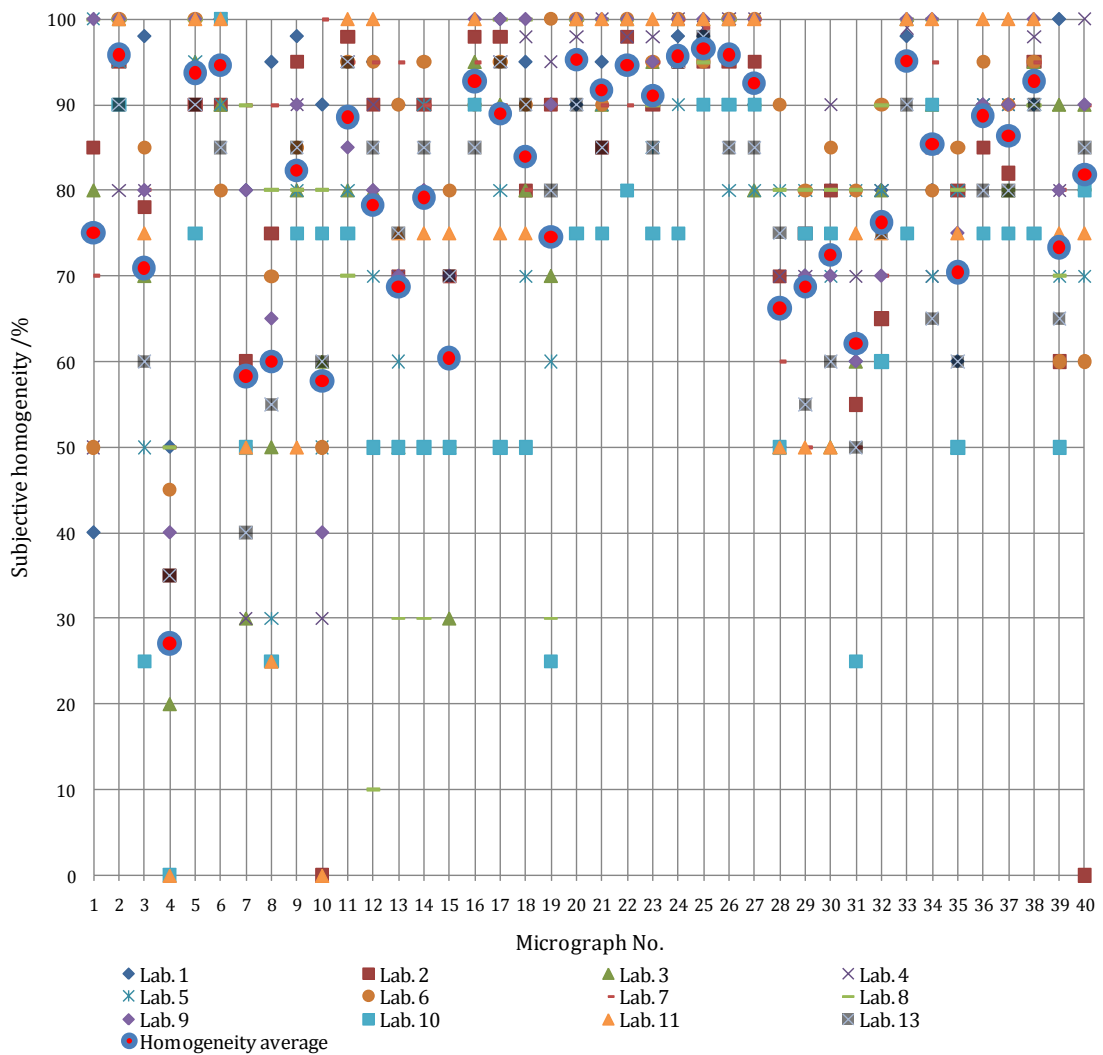


Figure 4.9: Feedback from the round robin test. Subjectively rated homogeneity from each laboratory (Lab.) and their average value (Homogeneity average), for each micrograph.

The difference between the reported homogeneity of the one laboratory and the average value from all the laboratories was calculated. Those differences, being positive, are called “overestimation”; those being negative, “underestimation”. Figure 4.10 shows the average results for each laboratory.

Figure 4.9 and Figure 4.10 show that the variation on the subjective homogeneity is due to an overall variation on the subjective ratings from all the laboratories. In general, there are no laboratories always rating high values or always rating low values; hence, the variation cannot be attributed to systematic differences in the individual ratings.

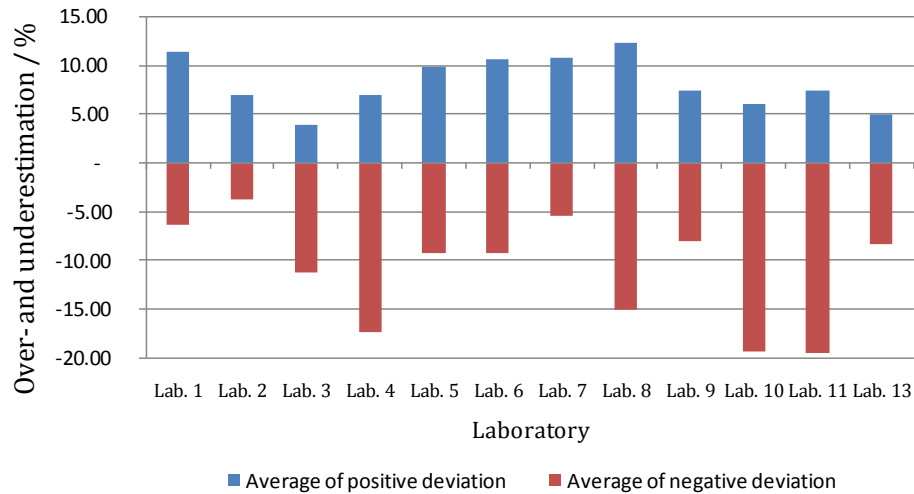


Figure 4.10: Average over- and underestimation with respect to the average for each laboratory.

Partial remarks

- Through visual evaluation, experts agree when classifying fully modified and fully unmodified structures. However, the subjective evaluations of inhomogeneously modified samples have important variation.
- It is important to emphasize that the Sr-modification results often in an inhomogeneous structure, and Sr is the most important modifier in the industry. This highlights the importance of developing an objective evaluation method, especially for inhomogeneously modified samples.

4.2.2. Objective data from the micrographs

Micrographs No. 12 and 14 were appropriate for visual evaluation. However, because of their low data resolution, the eutectic region could not be properly segmented. Thus the objective data from these micrographs was no possible to be gathered.

With the particle area (A), maximum Feret (F_m) and roundness (R); the corresponding homogeneities ($H_{(A)}$, $H_{(F_m)}$ and $H_{(R)}$) were calculated using the Equation 4.1 (page 54). The 2D microstructure parameters are summarized in Table 4.4.

Table 4.4: 2D microstructure parameters, for each micrograph. Micrographs No. 12 and 14 are missing because of low resolution issues.

Micrograph Nr.	DAS / μm	A] _{mean} / μm^2	P] _{mean} / μm	Pconvex] _{mean} / μm	Fmin] _{mean}	Fm] _{mean}	Euler no.] _{mean}	R] _{mean}	C] _{mean}	FAR] _{mean}	AAR] _{mean}	AAR] _{mean} / 10^{-3}	FAR] _{mean} / 10^{-3}	D	H (Fm)	H (A)	H (R)
1	45	2.1	6.6	6.1	1.2	2.5	1.0	0.7	1.0	0.56	0.43	1.0	57	116	0.60	0.47	0.83
2	59	2.5	7.2	6.4	1.4	2.6	1.0	0.7	0.9	0.60	0.48	0.7	44	303	0.66	0.51	0.83
3	72	10.5	13.3	12.4	2.8	5.0	1.0	0.7	1.0	0.62	0.51	2.0	69	59	0.65	0.47	0.88
4	46	9.1	14.0	12.5	2.3	5.3	1.0	0.6	0.9	0.53	0.41	4.3	116	26	0.52	0.33	0.82
5	79	10.6	14.4	13.8	2.7	5.8	1.0	0.7	1.0	0.56	0.45	1.7	73	57	0.64	0.53	0.85
6	45	53.2	49.0	39.2	5.7	17.4	0.9	0.4	0.8	0.41	0.27	26.3	386	3	0.51	0.40	0.67
7	39	15.3	21.7	17.9	3.4	7.5	0.9	0.5	0.9	0.50	0.35	10.1	193	11	0.56	0.39	0.74
8	42	9.2	14.9	12.7	2.5	5.4	1.0	0.6	0.9	0.52	0.38	5.2	127	21	0.56	0.35	0.78
9	41	5.6	10.4	9.5	2.0	3.9	1.0	0.6	0.9	0.55	0.43	3.3	95	32	0.63	0.43	0.84
10	90	43.7	35.4	28.7	5.2	12.1	0.9	0.5	0.9	0.52	0.38	5.4	134	17	0.50	0.33	0.74
11	58	4.1	8.6	8.2	1.8	3.3	1.0	0.7	1.0	0.55	0.45	1.2	57	102	0.71	0.53	0.88
13	45	9.5	13.8	12.0	2.5	4.9	1.0	0.6	0.9	0.54	0.41	4.7	110	24	0.60	0.36	0.82
15	58	14.6	19.2	17.0	3.1	7.2	1.0	0.6	0.9	0.48	0.36	4.4	125	22	0.57	0.38	0.77
16	58	10.8	16.4	15.2	2.7	6.5	1.0	0.6	0.9	0.50	0.38	3.2	112	28	0.58	0.46	0.79
17	43	1.2	4.9	4.6	1.0	1.9	1.0	0.6	0.9	0.56	0.42	0.6	44	219	0.69	0.56	0.84
18	42	3.2	7.7	7.4	1.5	3.0	1.0	0.7	1.0	0.58	0.46	1.8	72	62	0.67	0.54	0.86
19	41	1.2	5.0	4.6	1.0	1.9	1.0	0.7	1.0	0.56	0.43	0.7	46	238	0.67	0.52	0.84
20	40	1.6	5.9	5.4	1.1	2.2	1.0	0.6	0.9	0.56	0.43	1.0	56	121	0.67	0.53	0.83
21	41	6.1	11.8	11.0	2.1	4.6	1.0	0.6	0.9	0.54	0.41	3.6	113	29	0.62	0.52	0.81
22	38	1.3	5.2	4.8	1.0	2.0	1.0	0.7	0.9	0.57	0.44	0.9	52	123	0.68	0.55	0.85
23	36	2.5	7.0	6.5	1.4	2.6	1.0	0.6	0.9	0.57	0.44	1.9	74	53	0.65	0.48	0.84
24	38	2.0	6.1	5.8	1.3	2.4	1.0	0.7	1.0	0.58	0.45	1.4	63	85	0.69	0.56	0.86
25	41	1.8	6.0	5.7	1.2	2.3	1.0	0.7	0.9	0.58	0.45	1.1	57	98	0.69	0.57	0.85
26	38	52.8	47.4	37.0	5.8	16.0	0.7	0.4	0.8	0.43	0.28	36.6	422	2	0.55	0.41	0.68
27	43	56.3	51.9	40.9	5.9	18.1	0.8	0.4	0.8	0.41	0.28	30.4	422	3	0.57	0.47	0.67
28	38	21.0	29.4	24.4	3.2	11.0	0.9	0.4	0.9	0.39	0.27	14.5	288	9	0.51	0.36	0.68
29	36	5.2	11.1	9.9	1.9	4.2	0.9	0.6	0.9	0.54	0.40	4.0	116	29	0.59	0.44	0.80
30	39	2.8	8.3	7.3	1.4	3.1	1.0	0.6	0.9	0.54	0.40	1.8	79	55	0.58	0.42	0.80
31	36	9.3	15.9	12.7	2.5	5.3	0.9	0.5	0.9	0.54	0.38	7.2	147	11	0.56	0.34	0.76
32	38	3.6	8.7	7.8	1.5	3.3	0.9	0.6	0.9	0.53	0.39	2.5	86	23	0.59	0.38	0.81
33	24	2.2	6.6	6.2	1.3	2.6	1.0	0.7	1.0	0.57	0.45	3.8	106	28	0.68	0.56	0.85
34	59	10.8	16.8	15.5	2.6	6.7	1.0	0.6	0.9	0.48	0.36	3.1	114	36	0.60	0.49	0.78
35	57	12.7	15.9	14.4	2.9	6.0	1.0	0.6	0.9	0.55	0.42	3.9	105	27	0.61	0.41	0.82
36	22	2.5	7.7	6.8	1.4	2.8	1.0	0.6	0.9	0.56	0.40	5.2	127	24	0.64	0.47	0.80
37	55	8.1	13.4	11.7	2.5	4.8	0.9	0.6	0.9	0.56	0.42	2.7	87	42	0.64	0.44	0.81
38	18	2.0	7.1	6.0	1.3	2.4	0.9	0.6	0.9	0.57	0.41	6.3	135	17	0.62	0.43	0.79
39	59	35.4	35.5	29.9	4.4	13.3	0.8	0.5	0.9	0.42	0.30	10.2	225	9	0.55	0.40	0.70
40	21	6.7	14.8	12.5	2.1	5.4	0.9	0.5	0.9	0.46	0.32	15.1	259	7	0.58	0.44	0.73

4.2.3. Analysis

The goal of this section is to find out the most adequate parameters, which describe the best the different kinds of particles and microstructures. The analysis is carried out combining the imaged data with results from the round robin test, i.e. with the results from Table 4.3 (page 61). Groups of classified particles or micrographs were achieved considering the results from the round robin test and these were analyzed with help of the software *Rapid Miner*.

4.2.3.1. Particle classification and Percentage of Modification (PM)

In this section, particles are analyzed. The goal is to find out which are the characteristics from well modified particles. Particles from homogeneously modified micrographs (Micrographs No. 24, 20, 2 and 33) were compared with those from fully unmodified micrographs (Micrographs No. 6, 39, 26, 27 and 28). The former were considered as true modified particles; the latter, as true unmodified. All these classified particles (labeled items) are analyzed with help the computed processes in the software *Rapid Miner*.

Particle classification

Since the absolute size parameters depend on the modification level but also on the SCR, the first attempt was to use only particle shape parameters (R , C , χ_{2D} , FAR and AAR) to build a classification model. Using only particle shape parameters as attributes, the following classification model was obtained:

Classification rules: (Modified/Unmodified)

- if $AAR > 0.233$ then Modified (20861 / 1342)
- if $AAR \leq 0.233$ and $AAR > 0.125$ and $FAR > 0.240$ then Modified (1425 / 558)
- if $AAR \leq 0.233$ and $SAR > 0.125$ and $FAR \leq 0.240$ and $R > 0.385$ then Modified (19 / 2)
- if $AAR \leq 0.233$ and $AAR > 0.125$ and $FAR \leq 0.240$ and $R \leq 0.385$ then Unmodified (113 / 179)
- if $AAR \leq 0.233$ and $AAR \leq 0.125$ then Unmodified (102 / 443)

Correct: 22927 out of 25044 training examples.

After the classification rules, the numbers between parentheses represent the results of the validation. These are the number of particles satisfying the given rule, and being modified or unmodified, respectively (Modified/Unmodified). A particle classified as modified is correctly classified, if the particle is true modified, i.e. if it was from one of

the homogeneously modified structures. Similarly, a particle classified as unmodified is correctly classified, if the particle was from one of the fully unmodified structures.

In this case, a total of 25044 particles (training examples) were used to create this classification model. The validation indicates that applying the model, 22927 out of the 25044 particles are correctly classified. To illustrate: the first rule is “if $AAR > 0.233$ then Modified” and $20861+1342=22203$ particles satisfy “ $AAR > 0.233$ ”. Thus these particles are classified as “modified”. From these particle, 20861 are true modified (i.e. from homogeneously modified microstructures) and 1342 are true unmodified (i.e. from unmodified microstructures). This information is graphically represented in Figure 4.11. The blue/white bar in the end-nodes represents the amount of particles satisfying the rules for the corresponding end-node. The proportion of particles being true modified is represented in blue color; and the proportion of true unmodified, in white color.

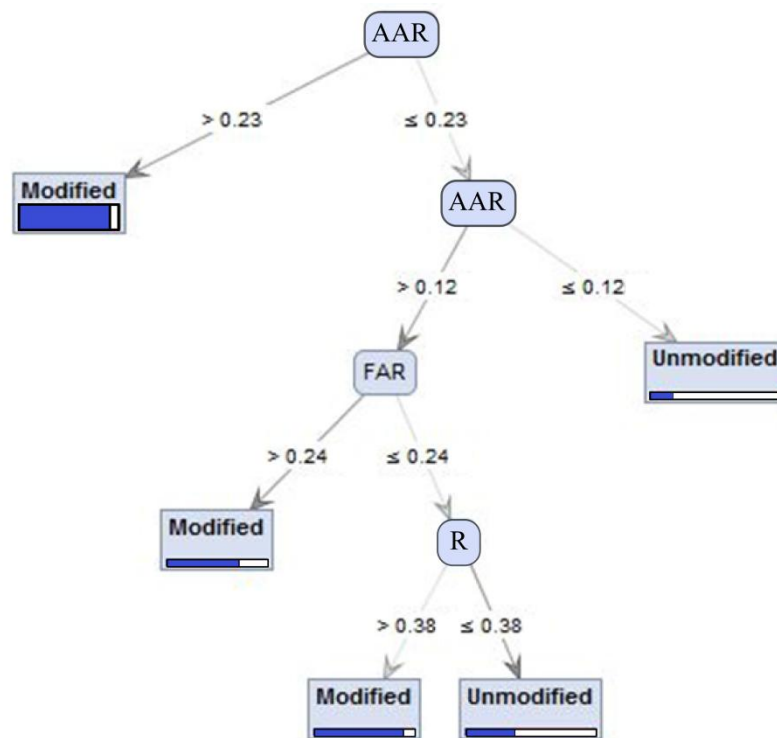


Figure 4.11: Obtained particle classification model considering only shape parameters. The model represents that modified particles have higher shape parameters than unmodified ones. In the end nodes, the blue/white bars represent the proportional amount of true modified/unmodified particles, respectively.

The validation results are shown in Table 4.5. In this table, “class recall” represents the percentage of particles correctly classified. To illustrate: the “class recall” of 99%, for the true modified means, that 22300 particles, from a total of $22300+220=22520$ true

modified particles, were correctly (as modified) classified (notice that $22300/22520=99\%$). The “class precision” represents, from all the particles with a given prediction class, the percentage being, in fact, from that class, e.g. the class precision of the prediction modified is $(22300/(22300+1920))=92\%$.

Table 4.5 Validation results of the model shown in Figure 4.11. Color scale red to green indicates relatively low to high values, respectively.

	<i>true Modified</i>	<i>true Unmodified</i>	<i>class precision</i>
pred. Modified	22300	1920	92%
pred. Unmodified	220	604	73%
class recall	99%	24%	

The color scale red to green in Table 4.5 indicates lower to higher values, respectively. This color scale will be often used in this work, when searching for relatively high or low values. In this case, the colors help identifying where the model has good or bad performance. Only 24 % of the unmodified particles are correctly classified.

To build the classification model of Figure 4.11, only shape parameters (and not size parameters) were considered. Most of the unmodified particles ($100\% - 24\% = 76\%$) cannot be differentiated, using shape parameters, from the modified ones. This fact indicates that unmodified particles can have similar shapes to modified ones. Therefore, a particle classification using only shape parameters is inadequate.

To improve the particle classification, size parameters should be involved. However, the absolute size parameters depend on the modification but also on the solidification cooling rate (SCR). Increasing the SCR, the eutectic particles and the dendrites decrease in size. The developed relative size parameters describe the particle sizes, with respect to the DAS. Thus these parameters are a good approach to characterize the particle sizes with respect to the modification, and regardless to the SCR. In the following analysis, shape parameters and the relative size parameters are considered.

Table 4.6 shows all the particle parameters, including the relative size parameters $A\lambda R$ and $F\lambda R$, quantified for the modified and the unmodified particles. In this case, the evaluation parameter RGS could not be quantified because of interval intersection. Based on the PD values, $A\lambda R$ and $F\lambda R$ are the fittest parameters to classify the particles.

Table 4.6: Results of comparing modified with unmodified particles. The percentage difference (PD) evaluates the difference between the classes considering the corresponding parameter.

Class	Value	R	C	Euler no.	FAR	AAR	AAR / 10 ⁻³	FAR / 10 ⁻³
Modified particles	Min	0.03	0.15	-3.00	0.11	0.05	0.03	8
	Max	0.96	1.00	1.00	0.92	0.79	44.26	711
	Average	0.66	0.94	0.98	0.58	0.45	1.68	67
	SD	0.19	0.12	0.16	0.15	0.14	2.31	51
Unmodified particles	Min	0.03	0.18	-6.00	0.06	0.02	0.14	19
	Max	0.94	1.00	1.00	0.90	0.81	388	3125
	Average	0.42	0.85	0.84	0.41	0.28	26.03	373
	SD	0.24	0.20	0.57	0.19	0.16	38.37	365
Evaluating parameters (dimensionless)	PD	22%	5%	8%	17%	23%	88%	70%
	RGS	Interval intersection						

The relatively low *PD* values in the shape parameters indicate that modified and unmodified 2D particles can have similar shapes. The results indicate that the most pronounced differences between modified and unmodified particles are the sizes, and not the shapes. This is because, on the one hand, well modified, fine and fiber-like particles can be round (transversal intersected by the observation plane) or stretched (longitudinal intersected). For example, the Micrograph no. 29 from the Appendix is modified and presents several stretched particles. On the other hand, unmodified particles can be plate-like (stretched) or quite compact and round. For example, the Micrograph no. 40 from the Appendix is unmodified and presents several compact particles. Thus through shape parameters, modified and unmodified particles are not adequately differentiable.

The Euler number (χ_{2D}), which indicates the amount of holes that a particle has, does not help differentiating modified from unmodified particles. This is because most of the particles, modified and unmodified, have Euler number equal to one ($\chi_{2D} = 1$), which indicates that the particle have no holes. Only a few particles, usually unmodified, have holes; however, this is not a remarkable characteristic.

The results from *Rapid Miner* (Figure 4.12 and Table 4.7) indicate that the size related parameters are the most convenient to distinguish modified from unmodified particles. Using these parameters, the amount of true unmodified particles correctly classified improved (from 24 % to 44 %).

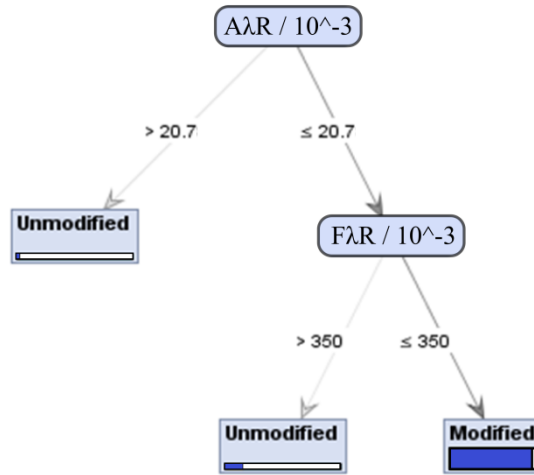


Figure 4.12: Particle classification model. The model represents that modified particles are relatively smaller than unmodified ones. In the end nodes, the blue/white bars represent the proportional amount of true modified/unmodified particles, respectively.

Table 4.7: Validation results of the model shown in Figure 4.12.

	true Modified	true Unmodified	class precision
pred. Modified	22450	1424	94%
pred. Unmodified	70	1100	94%
class recall	100%	44%	

It can be concluded that the main difference between modified and unmodified particles is the relative size. Implementing the developed relative size parameters, the results improved. However, still most of the unmodified particles are misclassified (100 % - 44 % = 56 %). To improve the classification model, further models were tested, which were obtained by changing settings in the software. More complex decision trees, which include a higher number of decision nodes, presented over-fitting and did not improve the classification results. Those unmodified particles, which are misclassified using the model in Figure 4.12, are small and not distinguishable from modified particles.

The Percentage of modification (PM)

Making use of the particle classification model in Figure 4.12, a “percentage of modification” (PM) is defined. For a micrograph with a number n of Si particles, $n = m + u$, where m is the number of modified particles and u the number of unmodified particles, the PM ($0 \leq PM \leq 1$) is defined as $PM = \sum_{i=1}^m A_{m i} / \sum_{i=1}^n A_i$, where $\sum_{i=1}^m A_{m i}$ is the summation of the areas of modified particles (A_m) and $\sum_{i=1}^n A_i$ is the total area of Si particles.

Table 4.8 shows the values of PM and the subjective classification from the round robin test. Considering the results from the round robin test, for most cases, structures with PM over 40 % are modified; and with PM under 40 %, unmodified. Figure 4.13 illustrates the result of applying the particle classification model from Figure 4.12 and calculating PM . The original micrographs, the Micrographs No. 3, 4, 27 and 28, are in the Appendix.

Table 4.8: Quantitative percentage of modification (PM) compared with the subjective results from the round robin test.

Micrograph no.	Objective percentage of modification (PM)	Subjective percentage of agreement	
		Unmodified	Modified
2	100%	0	100
24	100%	0	100
17	99%	0	100
22	99%	0	100
20	99%	0	100
25	98%	8	92
5	98%	0	100
18	96%	0	100
11	96%	0	100
1	96%	8	92
19	95%	0	100
33	93%	0	100
23	92%	0	100
3	87%	0	100
21	86%	0	100
37	85%	0	100
9	84%	8	92
34	83%	46	54
30	83%	8	92
16	81%	69	31
29	74%	0	100
36	73%	0	100
32	73%	0	100
35	68%	0	100
38	66%	0	100
15	64%	15	85
13	63%	0	100
8	57%	8	92
4	54%	8	92
10	51%	62	38
31	49%	0	100
7	43%	15	85
39	39%	92	8
40	32%	85	15
28	21%	100	0
27	13%	100	0
6	13%	92	8
26	8%	100	0

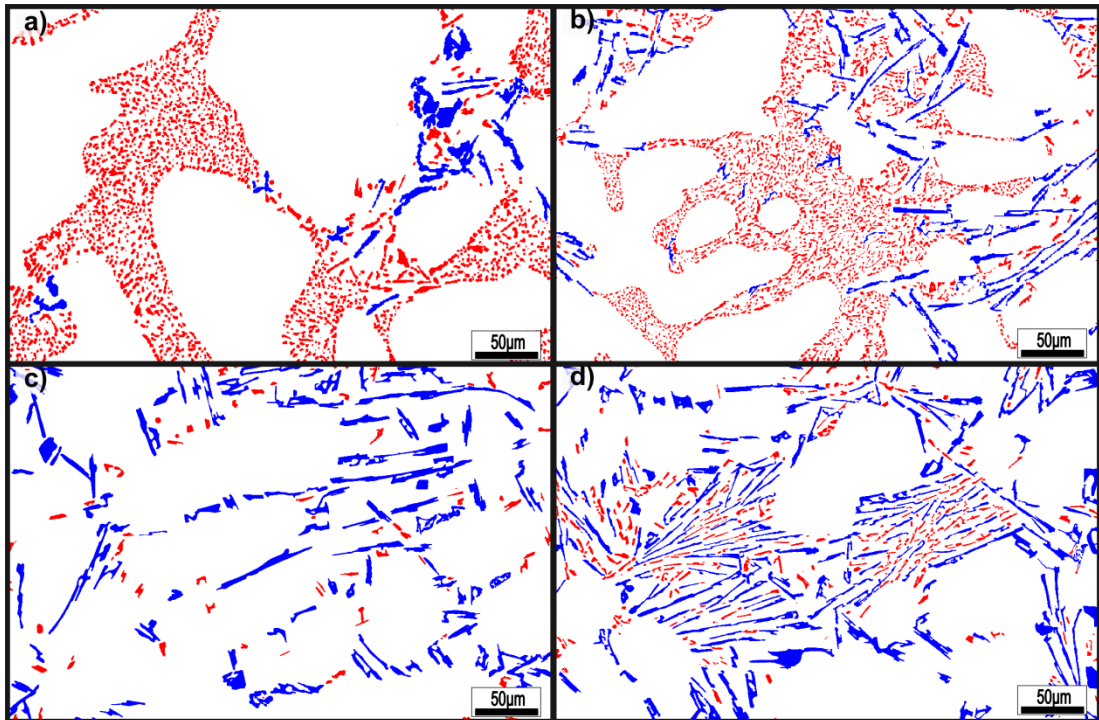


Figure 4.13: Particle classification model (Figure 4.12) applied to the Micrographs No. 3 (a), No. 4 (b), No. 27 (c) and No. 28 (d). Particles in red are modified; in blue, unmodified. The percentages of modification (PM) are, respectively: (a) 87 %, (b) 54 %, (c) 13 % and (d) 21 %.

Partial remarks

To distinguish modified from unmodified particles, the most remarkable parameters are the relative size parameters $A\lambda R$ and $F\lambda R$ (as defined in Table 3.2).

The particle classification method allows identifying which are the modified and the unmodified particles in a structure. The method to evaluate the modification using the PM , in comparison to the model based on ML (discussed in page 38), has the advantage of considering relative parameters to the DAS values (though the particle classification model of Figure 4.12). However, similarly to the model based on $P]_{mean}$, the PM does not involve the homogeneity. Hence, either ML or PM is recommendable to evaluate the modification.

To assess the overall structure, the homogeneity and further microstructure parameters should be considered. Following, a study of microstructure parameters to assess the modification is carried out.

4.2.3.2. Microstructure classification

In this section, the goal is to analyze micrographs and not individual particles (as in the prior section). Considering the results from the round robin test, the microstructure parameters for the different classes are calculated. A total of 38 micrographs are available for the analysis, which is a relatively low amount of items for the use of computed processes. Therefore, the physical interpretation and the parameters *PD* and *RGS* (page 47) take importance for building a classification model.

Taking as reference the graph from Figure 3.1 (page 40), the first step is to find out the difference between modified and unmodified structures. The data to be analyzed is summarized in Table 4.9. The microstructure shape parameters and homogeneities are shown graphically in Figure 4.14.

Table 4.9: Comparison between modified and unmodified microstructures. *PD* and *RGS* help identifying the fittest parameters distinguishing the classes.

Class	Value / Parameter	H (Fm)	H (A)	H (R)	R] _{mean}	C] _{mean}	Euler no.] _{mean}	FAR] _{mean}	AAR] _{mean}	AAR] _{mean} / 10 ⁻³	FAR] _{mean} / 10 ⁻³	D
Modified	Min	0.52	0.33	0.74	0.52	0.87	0.91	0.48	0.35	0.6	44	11.2
	Max	0.71	0.57	0.88	0.72	0.97	1.00	0.62	0.51	10.1	193	303
	Average	0.63	0.47	0.82	0.63	0.93	0.97	0.55	0.42	3.1	91	70.9
	SD	0.05	0.08	0.03	0.05	0.02	0.02	0.03	0.03	2.2	36	72.0
Unmodified	Min	0.51	0.36	0.67	0.38	0.77	0.67	0.39	0.27	10.2	225	2.2
	Max	0.57	0.47	0.70	0.45	0.87	0.88	0.43	0.30	36.6	422	9.5
	Average	0.54	0.41	0.68	0.41	0.82	0.81	0.41	0.28	23.6	349	5.5
	SD	0.03	0.04	0.01	0.03	0.05	0.08	0.02	0.01	11.0	88	3.5
	PD	8%	7%	10%	21%	6%	9%	15%	20%	77%	59%	86%
	RGS	-	-	21%	20%	-	8%	21%	24%	0%	8%	1%

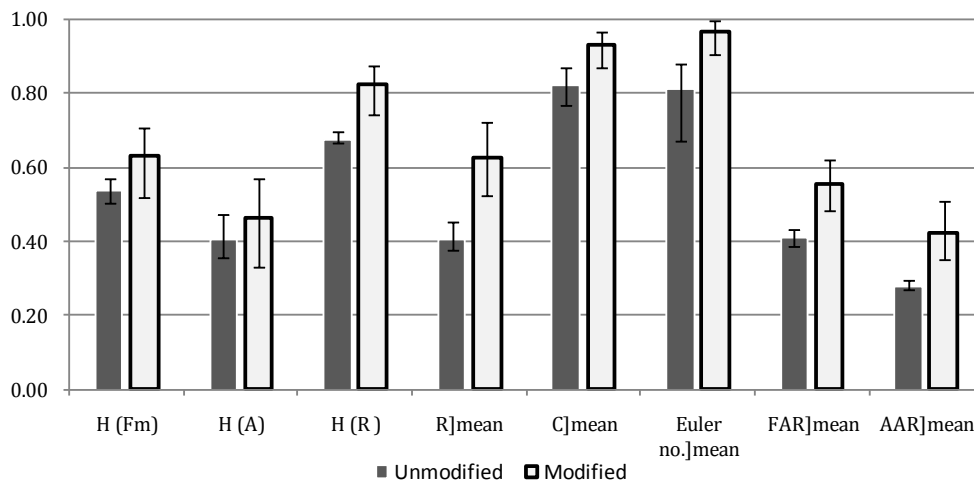


Figure 4.14: Comparison between modified and unmodified microstructures considering the homogeneities and shape parameters.

The results show that generally, although for some parameters the difference is marginal, modified micrographs have higher shape parameters and homogeneities. This indicates that modified structures have particles which are compact, round (relatively high particle shape parameters), without holes ($\chi_{2D} = 1$) and similar to each other (relatively high homogeneities).

Modified micrographs, in comparison to unmodified micrographs, have relatively small particles, presenting lower $A\lambda R]_{mean}$ and $F\lambda R]_{mean}$ and a much higher density of particles (higher D). This can be understood from the physical point of view as follows: For alloys with the same content of Si and dendrite sizes (and eutectic region size), if the Si particles are smaller, consequently, a larger amount of Si particles should be present.

In the following analysis, only modified structures are considered and the homogeneous and the inhomogeneous structures are compared. The results are summarized in Table 4.10. The homogeneities $H_{(A)}$ and $H_{(Fm)}$ do not present interval intersection, thus the calculation of the RGS is possible. The fact that $H_{(A)}$ and $H_{(Fm)}$ do not present interval intersection indicates, that they are the most suitable parameters to distinguish these subgroups of microstructures (homogeneously- vs. inhomogeneously modified).

The homogeneously modified structures, which were identified by experts, have higher quantitative homogeneity. Thus the developed quantitative homogeneity represents well the subjective judgment from experts.

The large values of PD for the parameters $A\lambda R]_{mean}$ and D indicate that homogeneous modified microstructures have smaller and more particles, than inhomogeneously modified. However, the classes share large ranges of values of these parameters. For example, for D , the interval for homogeneously modified structures is (28, 303) and for inhomogeneously modified is (11, 116), thus the classes share the range (28, 116). Because of the extensive intersection (despite of the relatively large PD) $A\lambda R]_{mean}$ and D are not convenient for classification.

Table 4.10: Comparison between homogeneous and inhomogeneous modified microstructures.

Modified subgroups	Value / Parameter	H (Fm)	H (A)	H (R)	R] _{mean}	C] _{mean}	Euler no.] _{mean}	FAR] _{mean}	AAR] _{mean}	AAR] _{mean} / 10 ⁻³	FAR] _{mean} / 10 ⁻³	D
Homogeneous	Min	0.66	0.51	0.83	0.64	0.92	0.98	0.56	0.43	0.73	44	28
	Max	0.69	0.56	0.86	0.67	0.96	0.99	0.60	0.48	3.85	106	303
	Average	0.68	0.54	0.84	0.66	0.94	0.98	0.58	0.45	1.74	67	134
	SD	0.01	0.02	0.01	0.01	0.02	0.00	0.02	0.02	1.43	27	119
Inhomogeneous	Min	0.52	0.33	0.74	0.52	0.87	0.91	0.48	0.35	1.02	57	11
	Max	0.65	0.47	0.88	0.72	0.96	0.99	0.62	0.51	10.05	193	116
	Average	0.59	0.40	0.80	0.60	0.92	0.96	0.54	0.41	4.48	114	35
	SD	0.04	0.05	0.04	0.06	0.03	0.02	0.03	0.04	2.43	36	29
	PD	0.07	0.15	0.04	0.05	0.01	0.01	0.03	0.05	0.44	0.26	0.58
	RGS	3%	16%									

Considering the analyses carried out, the microstructure classification model shown in Figure 4.15 is suggested. This tree-like graph represents that modified microstructures, in comparison to unmodified microstructures, have more round and smaller particles. Homogeneous modified microstructures have round particles, similar to each other.

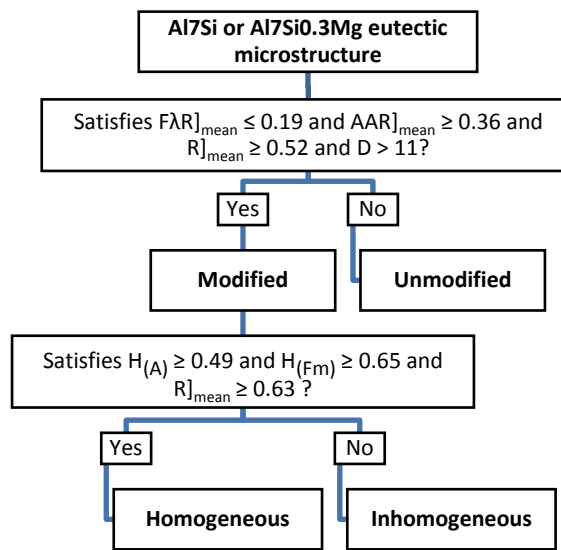


Figure 4.15: Micrograph classification model [2].

The model shown in Figure 4.15 is applicable to Al-7Si and Al-7Si-0.3Mg base alloys with a DAS of 20 μm to 90 μm. Micrographs with a number of 400 to 500 particles should be analyzed to ensure representation of the result. Alloys with other alloying elements or different quantities of Si or Mg, or other DASs, were not tested and these may require adjustment of the classifying rules.

Classification of unmodified lamellar vs. granular and over- vs. under-modified

Among the available classified samples based on the round robin test (Table 4.3, page 61), there are only a few microstructures classified in the remaining subclasses, namely the unmodified lamellar, unmodified granular, over-modified and under-modified. Because of the low amount of microstructures with these classes in the round robin test, reliable rules for classification of these sub-classes were not possible to be defined.

4.2.3.3. Objective- vs. subjective microstructure classification

In this section, the developed method for microstructure classification (Figure 4.15) is applied, and the objective results are compared with the subjective classification from the experts (Table 4.3, page 61).

Table 4.11 and Table 4.12 show the objective classification for the micrographs (in the table, the columns with title “Objective”). Figure 4.16 exhibits examples of differently classified structures.

In some cases, due to the variation in the results from the round robin test, the assignment is too ambiguous. A subjective assignment is considered unambiguous if the percentage of agreement for a class is above 50%, and the percentage of agreement for the opposite class is, at least 25% lower. The objective classification is compared with the unambiguous replies from experts and it is determined if the objective classification match the replies (“fit”) or not (“not fit”). These results are also shown in Table 4.11 and Table 4.12.

For the case of modified vs. unmodified (Table 4.11), there is a correspondence of 94 % between the subjective and the objective classification. The Micrographs No. 7 presents a mismatch. For this micrograph, the subjective assessment indicates that it is undermodified and the objective classification indicates that it is unmodified. In favor of the objective classification, most experts indicate that the structure does not present the coral like morphology. Micrographs 10 and 16 present also mismatches. It should be pointed out that, for these two micrographs, the subjective opinions are particularly wide spread (see Appendix).

Table 4.11: Objective and subjective microstructure classification for the classes Modified and Unmodified. The objective classification coincides, in 94 % of the cases, with the expert unambiguous classification.

Micrograph no.	Objective Modified / Unmodified	Subjective (RRT)			Comparison	
		Unmodified	Modified	Assignment		
2	Modified	0	100	Unambiguous	Fit	✓
3	Modified	0	100	Unambiguous	Fit	✓
5	Modified	0	100	Unambiguous	Fit	✓
11	Modified	0	100	Unambiguous	Fit	✓
13	Modified	0	100	Unambiguous	Fit	✓
17	Modified	0	100	Unambiguous	Fit	✓
18	Modified	0	100	Unambiguous	Fit	✓
19	Modified	0	100	Unambiguous	Fit	✓
20	Modified	0	100	Unambiguous	Fit	✓
21	Modified	0	100	Unambiguous	Fit	✓
22	Modified	0	100	Unambiguous	Fit	✓
23	Modified	0	100	Unambiguous	Fit	✓
24	Modified	0	100	Unambiguous	Fit	✓
29	Modified	0	100	Unambiguous	Fit	✓
31	Modified	0	100	Unambiguous	Fit	✓
32	Modified	0	100	Unambiguous	Fit	✓
33	Modified	0	100	Unambiguous	Fit	✓
35	Modified	0	100	Unambiguous	Fit	✓
36	Modified	0	100	Unambiguous	Fit	✓
37	Modified	0	100	Unambiguous	Fit	✓
38	Modified	0	100	Unambiguous	Fit	✓
1	Modified	8	92	Unambiguous	Fit	✓
4	Modified	8	92	Unambiguous	Fit	✓
8	Modified	8	92	Unambiguous	Fit	✓
9	Modified	8	92	Unambiguous	Fit	✓
25	Modified	8	92	Unambiguous	Fit	✓
30	Modified	8	92	Unambiguous	Fit	✓
15	Modified	15	85	Unambiguous	Fit	✓
34	Modified	46	54	Ambiguous	-	⚠
10	Modified	62	38	Ambiguous	-	⚠
16	Modified	69	31	Unambiguous	Not fit	✗
7	Unmodified	15	85	Unambiguous	Not fit	✗
40	Unmodified	85	15	Unambiguous	Fit	✓
6	Unmodified	92	8	Unambiguous	Fit	✓
39	Unmodified	92	8	Unambiguous	Fit	✓
26	Unmodified	100	0	Unambiguous	Fit	✓
27	Unmodified	100	0	Unambiguous	Fit	✓
28	Unmodified	100	0	Unambiguous	Fit	✓
Fit/(Fit+Not fit) = 94 %						

Table 4.12 indicates that the objective classification “homogeneously modified” vs. “inhomogeneously modified” matches, in 89 % of the cases, the unambiguous subjective classification. As discussed before, the Micrographs No. 10 and 16 are subjectively classified rather as unmodified, than as modified. Those experts, who classified these structures as modified, classified these structures as inhomogeneously

modified. The objective method classify these structures also as inhomogeneously modified. The Micrographs No. 23 and 38 are objectively classified as inhomogeneously modified, but is homogeneously modified when considering the round robin test (not fit). Nevertheless, considering the displayed shapes in these structures (see Appendix), they have coarsened particles; hence, the objective classification (inhomogeneously modified) is also reasonable.

Table 4.12: Objective and subjective microstructure classification for the classes homogeneously modified and inhomogeneously modified. The objective classification coincides, in 89 % of the cases, with the expert unambiguous classification.

Micrograph no.	Objective Modified: Homogeneous or inhomogeneous	Subjective (RRT)			Comparison	
		Homogeneously modified	Inhomogeneously modified	Assignment		
20	Homogeneous	100	0	Unambiguous	Fit	✓
24	Homogeneous	100	0	Unambiguous	Fit	✓
2	Homogeneous	92	8	Unambiguous	Fit	✓
33	Homogeneous	92	8	Unambiguous	Fit	✓
5	Homogeneous	85	15	Unambiguous	Fit	✓
25	Homogeneous	77	15	Unambiguous	Fit	✓
17	Homogeneous	69	31	Unambiguous	Fit	✓
22	Homogeneous	69	31	Unambiguous	Fit	✓
11	Homogeneous	62	38	Ambiguous	-	⚠
18	Homogeneous	62	38	Ambiguous	-	⚠
19	Homogeneous	42	58	Ambiguous	-	⚠
23	Inhomogeneous	77	23	Unambiguous	Not fit	✗
38	Inhomogeneous	77	23	Unambiguous	Not fit	✗
21	Inhomogeneous	62	38	Ambiguous	-	⚠
37	Inhomogeneous	54	46	Ambiguous	-	⚠
9	Inhomogeneous	46	46	Ambiguous	-	⚠
32	Inhomogeneous	46	54	Ambiguous	-	⚠
31	Inhomogeneous	38	62	Ambiguous	-	⚠
35	Inhomogeneous	38	62	Ambiguous	-	⚠
36	Inhomogeneous	38	62	Ambiguous	-	⚠
3	Inhomogeneous	31	69	Unambiguous	Fit	✓
13	Inhomogeneous	31	69	Unambiguous	Fit	✓
1	Inhomogeneous	23	69	Unambiguous	Fit	✓
30	Inhomogeneous	23	69	Unambiguous	Fit	✓
8	Inhomogeneous	8	85	Unambiguous	Fit	✓
16	Inhomogeneous	0	31	-	-	⚠
10	Inhomogeneous	0	38	-	-	⚠
34	Inhomogeneous	0	54	Unambiguous	Fit	✓
15	Inhomogeneous	0	85	Unambiguous	Fit	✓
4	Inhomogeneous	0	92	Unambiguous	Fit	✓
29	Inhomogeneous	0	100	Unambiguous	Fit	✓
Fit/(Fit+Not fit) = 89 %						

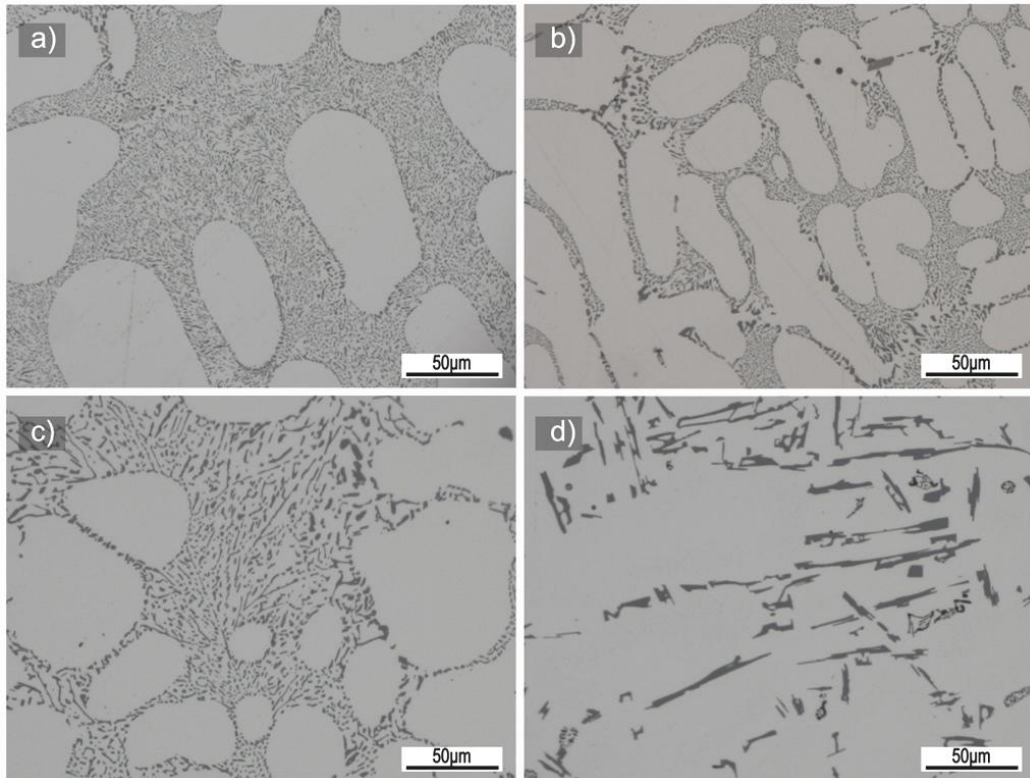


Figure 4.16: Example of classified micrographs. (a) Micrograph No. 20: Homogeneous modified. (b) Micrograph No. 36 and (c) Micrograph No. 29: Inhomogeneous modified. (d) Micrograph No. 28: Unmodified.

4.2.3.4. Degree of modification (M)

In this section, an alternative objective parameter is developed, that describes the modification level. As discussed in the Chapter 1 (page 20), “modification level” (ML , $SiML$) and “modification rating” ($M.R.$) were already used in the literature to define other parameters. Besides, in this work a “percentage of modification” (PM) was suggested. Thus now, this new alternative parameter is called “degree of modification” (M). It should be said, that the terminology “degree of modification” has been already used as synonym of the modification rating [28]. As a matter of fact, all these parameters are different approaches describing the same characteristic.

To develop the degree of modification, four micrographs were selected, which represent different levels of modification. For the selection, the results from the round robin test and further assistance from the experts has been considered. Using these micrographs as reference, a function of the object homogeneity ($\varphi = f(h_o)$) was created fitting the reference values so that φ represents the modification level as shown in Figure 4.17.

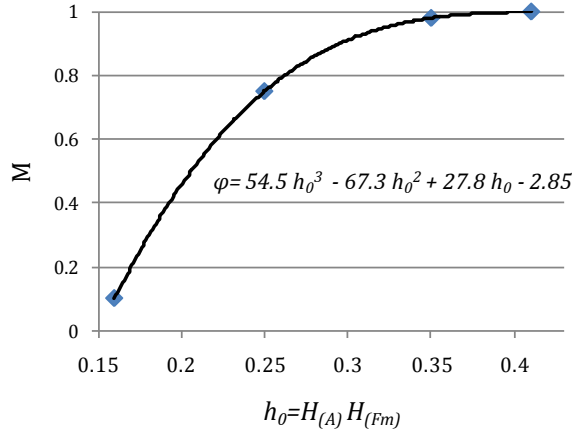


Figure 4.17: The degree of modification (M) as function of the object homogeneity h_0 . $h_0 \geq 0.35$ indicates very good modification; $h_0 \leq 0.2$ indicates poor modification.

M is the function φ in the representative interval, as defined in Equation 4.2, and is applicable to modified microstructures.

$$M \begin{cases} = \varphi & \text{for } 0 \leq \varphi \leq 1 \\ = 0 \% & \text{for } \varphi < 0 \\ = 100 \% & \text{for } \varphi > 1 \end{cases}$$

Where $\varphi = 54.5 h_0^3 - 67,3 h_0^2 + 27,8 h_0 - 2,85$, and $h_0 = H_{(A)} * H_{(Fm)}$

Equation 4.2: Definition of the degree of modification (M) to evaluate modified microstructures.

Homogeneities are representative for any microstructure, whereas M was developed only to evaluate modified microstructures. Hence, the evaluation of M is valid for micrographs, that were previously classified as modified. M should be quantified in micrographs with a number of 400 to 500 particles to ensure representative results. For the assessment of a sample, it is recommended considering various calculations of M in random spots of the sample.

4.2.3.5. Comparison of M with the subjective assessment

For those micrographs classified as modified by the experts and the quantitative method (29 micrographs from the total of 40 analyzed micrographs), M is compared with the subjective homogeneity. The results of M are displayed in Figure 4.18. M is always between the minimum and maximum subjective homogeneities. In 23 micrographs out of the 29 modified micrographs (79%), M is within the standard deviation interval of the subjective homogeneity (error bars).

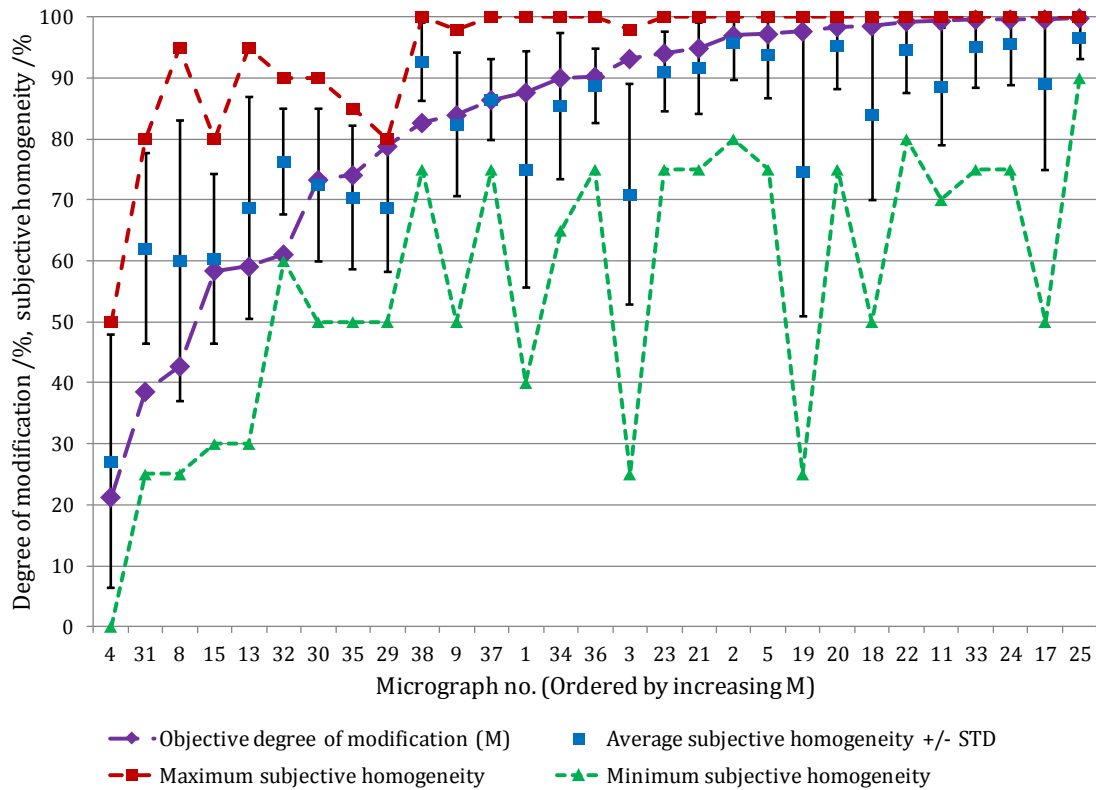


Figure 4.18: Objective degree of modification and subjective homogeneity of modified micrographs. Micrographs are ordered with increasing M . The lines connecting points are only for visualization purpose.

4.2.3.6. Summary of results, including the Modification Level (ML)

The most important results are summarized in Table 4.13. Beside of the results from the objective methods developed in this work (M and PM), the results of ML (objective method from the literature detailed in ref [77], discussed in this work in page 20) are shown. The corresponding micrographs, together with further information, are in the Appendix.

The ML represents the six classes from Figure 1.3 (page 7). The problem with regards to ML has been already discussed and illustrated in this work (page 38). Further examples of misclassification through ML are, for instance, Micrographs No. 21 ($ML = 3.3$, which is too low for such structure) and Micrographs No. 40 ($ML = 2.7$, which is too high for such structure).

It can be concluded that the method of the degree of modification (M) developed in this work is robust, accurate and reliable. M considers the object homogeneity and it is the recommended parameter to evaluate modification.

Table 4.13: Summary of objective and subjective results. Objective results from Micrographs No. 12 and 14 are missing because of low resolution issues. M is the degree of modification. PM is the percentage of modification. ML is the modification level.

Micrograph no.	Objective method developed in this work				Objective method from the literature		Subjective results from experts					
	Modified (Mod)/ Unmodified (Unmod)	Modified: Homogeneous or Inhomogeneous	M	PM	Classification	ML	Unmodified	Modified	Homogeneously modified	Inhomogeneously modified	Homogeneity Average [%]	Homogeneity STD
1	Mod	Inhomogeneous	88%	96%	Modified Fibrous	5.0	8	92	23	69	75	19
2	Mod	Homogeneous	97%	100%	Modified Fibrous	4.7	0	100	92	8	96	6
3	Mod	Inhomogeneous	93%	87%	Partial modified	3.0	0	100	31	69	71	18
4	Mod	Inhomogeneous	21%	54%	Partial modified	2.8	8	92	0	92	27	21
5	Mod	Homogeneous	97%	98%	Partial modified	2.8	0	100	85	15	94	7
6	Unmod	-	-	13%	Fully unmodified	1.3	92	8	0	8	95	7
7	Unmod	-	-	43%	Lamellar	1.9	15	85	0	85	58	21
8	Mod	Inhomogeneous	43%	57%	Partial modified	2.7	8	92	8	85	60	23
9	Mod	Inhomogeneous	84%	84%	Absence of lamellae	3.6	8	92	46	46	82	12
10	Mod	Inhomogeneous	13%	51%	Lamellar	1.6	62	38	0	38	58	27
11	Mod	Homogeneous	99%	96%	Absence of lamellae	3.9	0	100	62	38	89	10
12	-	-	-	-	-	-	0	100	62	38	78	24
13	Mod	Inhomogeneous	59%	63%	Partial modified	2.9	0	100	31	69	69	18
14	-	-	-	-	-	-	0	100	54	46	79	19
15	Mod	Inhomogeneous	58%	64%	Lamellar	2.0	15	85	0	85	60	14
16	Mod	Inhomogeneous	81%	81%	Lamellar	2.3	69	31	0	31	93	5
17	Mod	Homogeneous	100%	99%	Modified Fibrous	5.4	0	100	69	31	89	14
18	Mod	Homogeneous	99%	96%	Absence of lamellae	4.3	0	100	62	38	84	14
19	Mod	Homogeneous	98%	95%	Modified Fibrous	5.4	0	100	42	58	75	24
20	Mod	Homogeneous	98%	99%	Modified Fibrous	5.2	0	100	100	0	95	7
21	Mod	Inhomogeneous	95%	86%	Partial modified	3.3	0	100	62	38	92	7
22	Mod	Homogeneous	99%	99%	Modified Fibrous	5.3	0	100	69	31	95	7
23	Mod	Inhomogeneous	94%	92%	Modified Fibrous	4.8	0	100	77	23	91	7
24	Mod	Homogeneous	100%	100%	Modified Fibrous	5.1	0	100	100	0	96	7
25	Mod	Homogeneous	100%	98%	Modified Fibrous	5.1	8	92	77	15	97	3
26	Unmod	-	-	8%	Fully unmodified	1.3	100	0	0	0	96	7
27	Unmod	-	-	13%	Fully unmodified	1.2	100	0	0	0	93	8
28	Unmod	-	-	21%	Lamellar	1.7	100	0	0	0	66	13
29	Mod	Inhomogeneous	79%	74%	Partial modified	3.5	0	100	0	100	69	11
30	Mod	Inhomogeneous	73%	83%	Absence of lamellae	4.0	8	92	23	69	73	13
31	Mod	Inhomogeneous	39%	49%	Lamellar	2.5	0	100	38	62	62	16
32	Mod	Inhomogeneous	61%	73%	Absence of lamellae	3.9	0	100	46	54	76	9
33	Mod	Homogeneous	100%	93%	Modified Fibrous	5.0	0	100	92	8	95	7
34	Mod	Inhomogeneous	90%	83%	Lamellar	2.3	46	54	0	54	85	12
35	Mod	Inhomogeneous	74%	68%	Lamellar	2.5	0	100	38	62	70	12
36	Mod	Inhomogeneous	90%	73%	Absence of lamellae	4.3	0	100	38	62	89	6
37	Mod	Inhomogeneous	86%	85%	Partial modified	3.0	0	100	54	46	86	7
38	Mod	Inhomogeneous	83%	66%	Modified Fibrous	4.8	0	100	77	23	93	6
39	Unmod	-	-	39%	Lamellar	1.6	92	8	0	8	73	13
40	Unmod	-	-	32%	Partial modified	2.7	85	15	0	15	82	11

4.2.4. Remarks of the section

The broad variation in the subjective assessment indicates that the subjective evaluation from one observer may not be representative for the others. Subjective evaluations give rise to interpretation and communication issues, limiting the potential advantages of one laboratory using the results from others. Thus it is important to rely on objective methods to analyze microstructures.

An objective method for evaluation of the modification was achieved. The homogeneities and the relative size parameters are remarkable characteristics of the studied structures. Representative microstructural features were quantitatively defined. The main characteristic of well-modified structures is their high homogeneity and small particles. Inhomogeneously modified structures present coexistence of small and large particles, thus lower quantitative homogeneities. Unmodified structures have large, often stretched particles.

The advantages of the suggested method are that it gives objective, reasonable, precise and descriptive results for a variety of structures in a wide range of DAS (i.e. wide range of SCR). In comparison to the available objective methods (Figure 1.12, page 20), important improvements were achieved. Notice that the Micrographs No. 5 and No. 3 from the round robin test, which were discussed in Figure 2.2 (page 38), are classified matching the classification from the experts using the suggested method, i.e. the Micrograph No. 5 is homogeneously modified with higher M and the No. 3 is inhomogeneously modified with lower M.

4.3. Comparison between Sr- and quench-modification

As discussed in page 5, there are different methods to achieve modification, including the chemical- and the quench modification. There are contradictory statements in the literature regarding the differences between quench- and chemical-modification. Generally, it is considered that both kinds of modification can induce the transformation towards the fine-fibrous structure [39]. If rapidly freezing the alloy modifies the structure as the chemical-modification, both kinds of modifications could have the same growth mechanisms. Consistently, a workable explanation of the modification should deal with the fact that modification can be produced by adding chemical modifiers or by very rapid solidification. In favor of this theory are, for instance, Gruzleski and Closset [4]. However, if the chemical- and the quench-modification are different, they could be studied as different phenomena. In favor of this theory are, for instance, Shamsuzzoha and Hogan [50].

With help of the developed objective methods for evaluation and FIB tomography, this section compares the quench- and the Sr-modification. Sr- and quench-modified structures have been identified before, as shown in Table 4.11 (page 79) and Table 4.13 (page 85). The compared microstructures are the Micrograph No. 33 (quench-modified) and the Micrograph No. 36 (Sr-modified).

4.3.1. Comparison in 2D

Considering the results from the round robin test (Table 4.3, page 61), the micrograph No. 33 (quench-modified) is homogeneous modified, comparable to Sr modified microstructures with the same classification. The subjective assessment from the experts indicate that there is no difference between quench- and Sr- modified samples. An analysis of the microstructure parameters is carried out, to disclose if there is an observable difference considering the microstructure data. Figure 4.19 shows 2D parameters from the micrograph No. 33 and Sr-modified structures. The objective microstructure parameters from 2D analysis also indicate that there is no difference between the chemical- and the quench- modified structures.

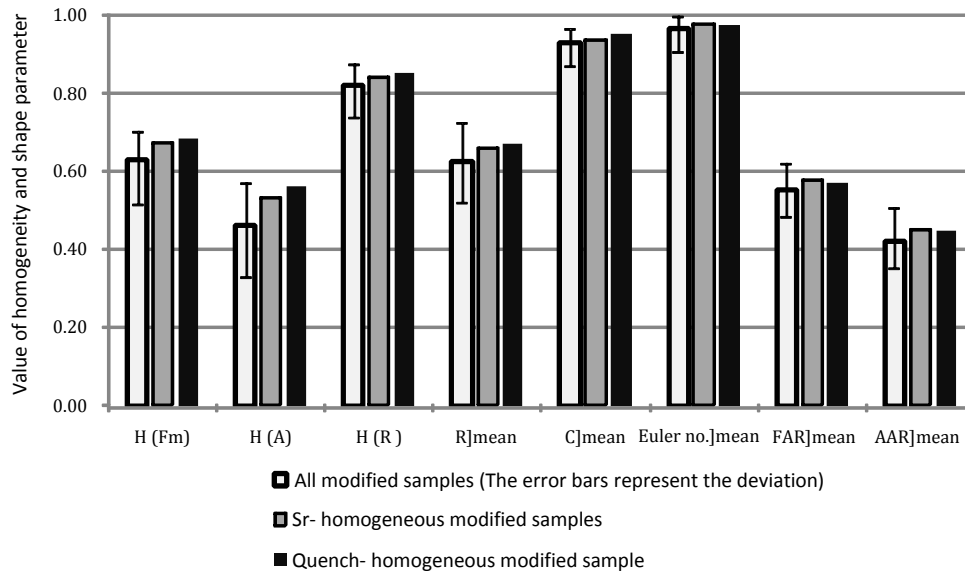


Figure 4.19: 2D parameters comparing quench- and Sr-modified structures. There is no difference between quench- and Sr- modified structures. “Model” refers to the model microstructures as defined in Table 4.3 (page 61)

Figure 4.20 shows the Micrograph No. 33 (quench-modified) next to the Micrograph No. 36 (Sr-modified). Further information and larger images of these structures can be found in the Appendix. From these samples, the eutectic Si will be next analyzed in 3D space.

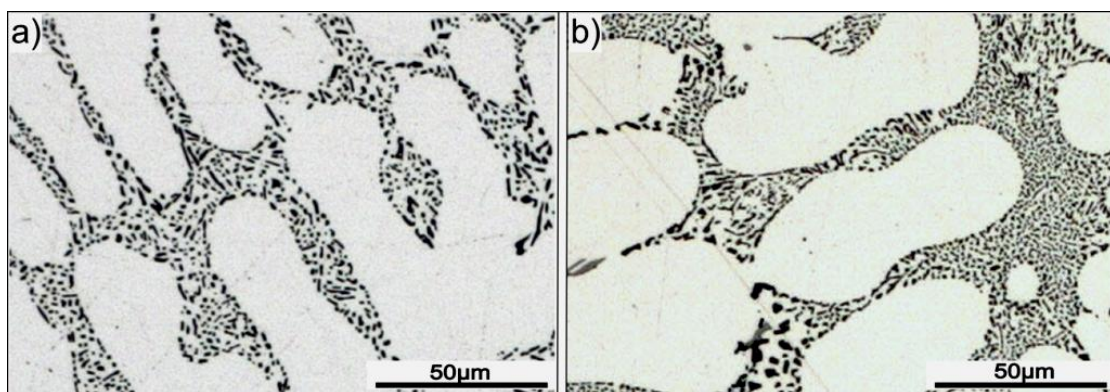


Figure 4.20: (a) Quench modified structure (Micrograph No. 33, Al-7Si) and (b), Sr-modified structure (Micrograph No. 36, Al-7Si-0.3Mg-0.035Sr)

4.3.2. Comparison in 3D

Figure 4.21 shows 3D reconstruction of the modified structures obtained via FIB-Tomography. Through subjective observations, a clear difference between the morphologies was not identified; both are coral-like structures.

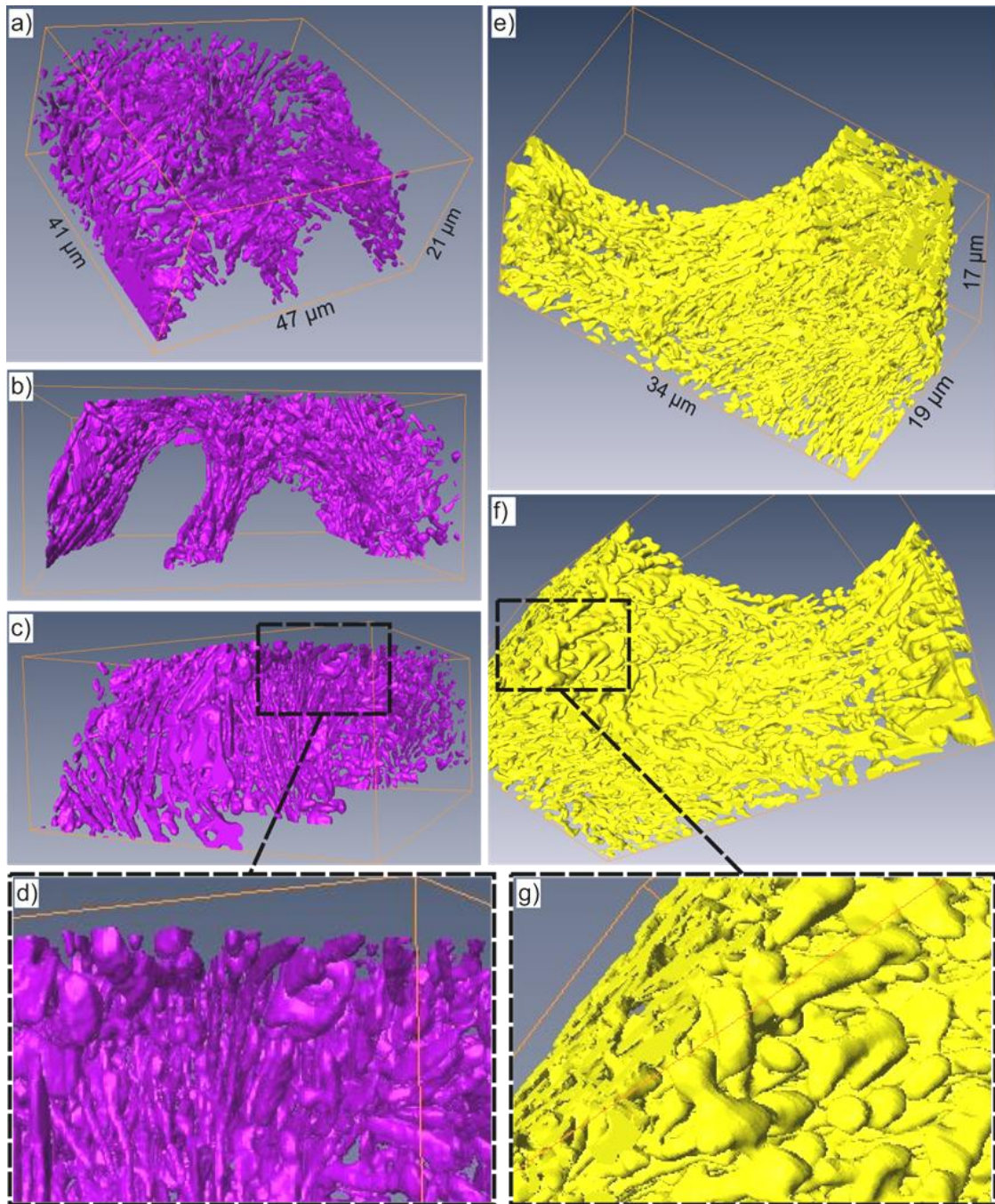


Figure 4.21: (a), (b), (c) and (d): Quench modified structure (Micrograph No. 33, Al-7Si). (e), (f) and (g): Sr-modified structure (Micrograph No. 36, Al-7Si-0.3Mg-0.035Sr). The observed curved interfaces of the eutectic phase (e.g. in images b and e) are given by the α -Al dendrites.

Quantitative parameters of these tomographies, including the four basic parameters, are listed in Table 4.14. The total studied volume of the quench modified sample is about four times larger than the volume of the chemical modified sample. The quench modified sample has less eutectic Si volume fraction (8.1%) than the chemical modified sample (10.2%). A problem of the FIB-tomography is that the studied volumes are relatively small so that the amount of eutectic Si depends on the particular portion of

material studied. Notice that in fact, both samples contain the same percentage amount of Si (7%). It is possible to subjectively analyze from the images, that the Sr modified sample has finer particles more connected to each other. This can be noticed through the quantitative analysis since the Sr modified particles have in average a higher ratio of surface/volume ($0.93/10.2 \mu\text{m}^{-1}$) than the quench modified particles ($0.40/8.1 \mu\text{m}^{-1}$). Both structure present negative Euler number indicating connectivity between particles.

Table 4.14: 3D parameters comparing quench- and Sr-modified structures.

Sample	Total studied volume	Si volume fraction	Specific surface	Specific integral of mean curvature	Specific integral of total curvature	Euler number
	$V/\mu\text{m}^3$	$V_V/\%$	$S_V/\mu\text{m}^{-1}$	$M_V/\mu\text{m}^{-2}$	$K_V/\mu\text{m}^{-3}$	χ
Al7Si (Quench modified)	40500	8.1	0.40	0.41	-0.22	-700
Al7Si0.3Mg0.035Sr (Sr modified)	11000	10.2	0.93	2.44	-1.57	-1400

4.3.3. Remarks of the section

The 2D analysis indicates that the chemical- and the quench modification are similar. Regarding the 3D analysis, an objective method for evaluation was neither developed in this work nor found in the literature. The evaluation in 3D of the modification and of the structure shapes, such as fine-fibrous or fine-flake, are subjected to the observer's opinion. Further studies of the 3D structures, involving larger volumes and more samples, would be required to improve the 3D characterization of the modification. The main limitation of 3D analysis is the small study volumes, which are achievable for the required resolution. For industrial applications, 3D techniques have still poor possibilities and 2D analysis is the main tool for characterization.

It is possible to conclude that chemical- and quench modified structures present similar characteristics. Still, different growth mechanisms could result in similar morphologies. Therefore, if the growth mechanisms from chemical- and quench-modification are the same, remains as open question.

4.4. Correlation between microstructure, process settings and mechanical properties

As discussed before, in the literature it has been shown, that the modification can improve the mechanical properties. However, those microstructures identified as modified in the literature, were subjectively evaluated, thus an objective correlation between the modification and the mechanical properties has not been yet carried out. In this section, the developed method for objective microstructure assessment is applied to analyze the correlation between the microstructure, process settings and mechanical properties.

Firstly, an analysis using SPT tests is carried out to compare the behavior of the two extremes microstructures, namely the fully unmodified structure, with plate-like shapes, and the fully modified, with coral-like shape. Secondly, an analysis using Charpy tests is carried out to analyze several samples in different states of modification.

4.4.1. Small Punch Test (SPT)

SPT tests were carried out to evaluate comparatively the elastoplastic behavior of fully-unmodified and fully-modified samples with same DAS. The studied specimens are the Micrographs/Samples No. 24, 25, 26 and 28 from the round robin test. These micrographs are in the Appendix, and listed in Table 3.1 (page 42). Micrographs/Sample No. 24 and 25 are homogeneously modified (H.M.), with $M = 100\%$; and the No. 26 and 28 are unmodified (see Table 4.11, Table 4.12 and Table 4.13, in page 79). The results are summarized in Figure 4.22.

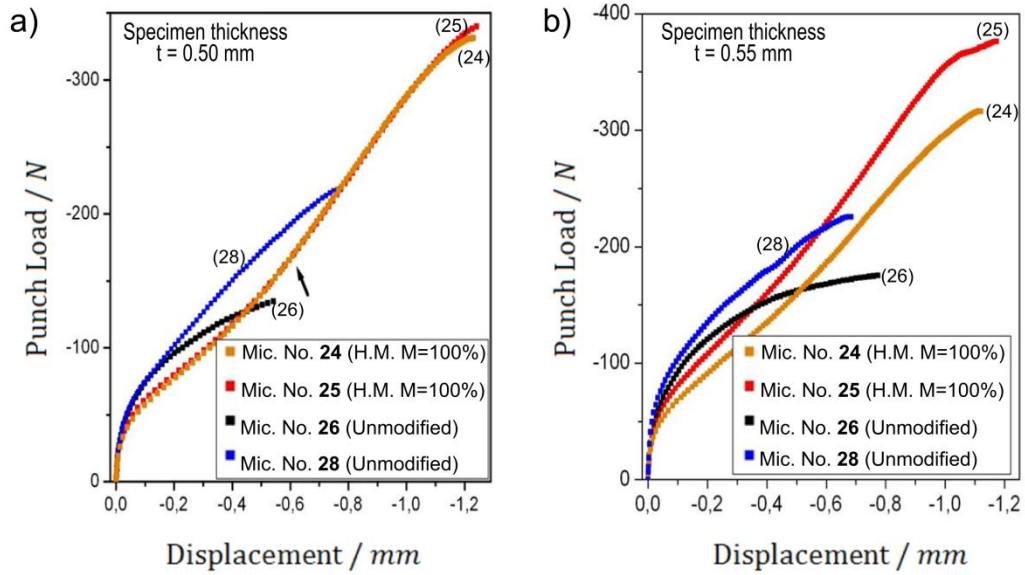


Figure 4.22: (a) and (b) SPT curves for specimens of thickness (a) 0.50 mm and (b) 0.55 mm. The row in (a) indicates the second change in the slope present in ductile materials. See the micrographs (Mic.) in the Appendix. H.M. stands for homogeneously modified and M is the degree of modification.

The H.M. samples present the membrane stretching stage, which is the stage after the second change of slope in the punch load-displacement. Such change of slope is indicated in Figure 4.22-b by an arrow. The unmodified samples, unlike, do not present the membrane stretching regime, indicating that cracking occurs during plastic bending. The load in which non-linearity of the curve load-displacement is initiated (P_Y) is virtually unaffected with modification. For $t = 0.50$ mm, $P_Y \approx 30$ and for $t = 0.55$ mm, $P_Y \approx 40$. This represents that a difference between the yield strength (σ_{YS}) of fully unmodified and fully modified samples is marginal (according to $\sigma_{YS} = \alpha \frac{P_Y}{t^2}$). The maximum load and the maximum displacement are about twice larger for H.M. samples, as for the unmodified samples.

Figure 4.23 shows that the H.M. samples developed circumferential cracks at the specimen surface after relative high plastic deformation. Unmodified samples developed cracks in circumferential and radial directions at the specimen surface, and showed a smaller deformed region than H.M.. The detail of the fracture shows a typical ductile fracture for the modified sample, while for the unmodified sample, the fracture mechanism is a mixture of ductile and brittle. In Figure 4.23, the imaged modified sample is the Sample No. 25; and the imaged unmodified sample is the Sample No. 26.

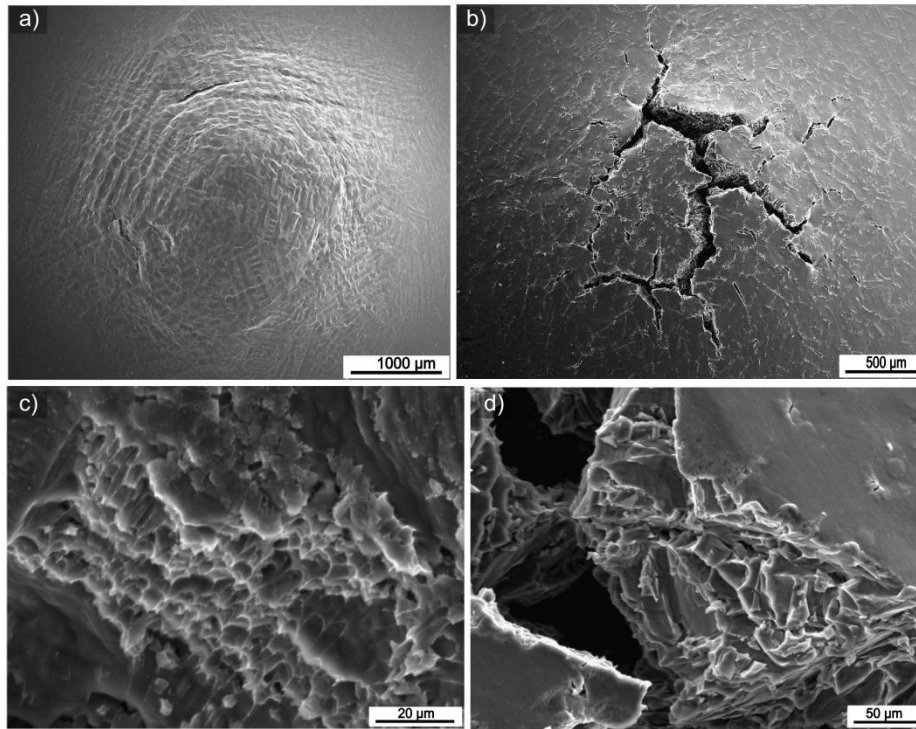


Figure 4.23: (a) and (b) Specimen surfaces after SPT. (c) and (d) Detail of the inner surfaces of cracks. (a) and (c) Homogeneously modified specimen. (b) and (d) Unmodified specimen.

It can be concluded that the modified samples have higher ductility and toughness. They can absorb more energy while deforming plastically, hindering the crack growth.

4.4.2. Impact properties

Charpy impact tests were carried out to estimate the impact properties of samples. The tested samples were Al-7Si and Al-7Si-0.3Mg alloys with different content of Sr, casted in metal and sand molds. The Fe and P contents are about 300 ppm and 5 ppm, respectively. The samples are sorted in four groups according to the used mold and the amount of Mg, as shown in Table 4.15. From each one of the twelve listed alloys, four samples were obtained, i.e. a total of 48 specimens were tested. Table 4.15 summarizes the mean values of the results. Samples casted in the metal mold have higher solidification cooling rate (SCR) than those casted in sand molds. The DAS of samples casted in metal mold is $(21 \pm 3) \mu\text{m}$; and in sand mold, $(58 \pm 4) \mu\text{m}$.

The measurements corresponding to the mechanical properties are: S_y : Displacement at general yield, P_y : Load at general yield, S_m : Displacement at peak load, P_m : Peak load, W_m : Energy at peak load, S_t : Displacement at fracture, W_t : Total impact energy.

“Modified (H)” represents the homogeneously modified class; “Modified (I)”, the inhomogeneously modified.

Table 4.15: Analyzed samples. The casting process and the estimation of the mechanical properties were carried out by the IfG. The quantification of the class and *M* (columns with title “Microstructure”) was carried out as part of this work. *: IfG reported that the specimen slid out of the specimen support without breaking through, but the fracture initiation was clearly observable.

Group	Mold	Composition		Mechanical properties							Microstructure	
		Mg / wt.%	Sr / wt.ppm	Sy / mm	Py / kN	Sm / mm	Pm / kN	Wm / J	St / mm	Wt / J	Class	<i>M</i> / %
Metal 0Mg	Metal	0	0	0.26	1.7	7	5.3	29	12	40	Unmodified	-
	Metal	0	250	0.30	1.8	12	5.3	55*	*	*	Modified (I)	86
	Metal	0	100	0.25	1.7	12	5.3	56*	*	*	Modified (H)	98
Metal 0.3Mg	Metal	0.3	0	0.18	2.1	2	6.0	10	3	12	Unmodified	-
	Metal	0.3	350	0.19	2.3	5	7.1	31	7	35	Modified (I)	80
	Metal	0.3	55	0.20	2.3	7	7.3	40	9	48	Modified (I)	85
Sand 0Mg	Sand	0	0	0.26	1.6	5	4.9	21	9	29	Unmodified	-
	Sand	0	100	0.26	1.6	7	4.7	29	17	47	Modified (I)	95
	Sand	0	250	0.34	1.8	8	4.8	33	19	52	Modified (H)	97
Sand 0.3Mg	Sand	0.3	0	0.20	2.2	2	4.9	6	3	8	Unmodified	-
	Sand	0.3	350	0.22	2.1	2	4.7	7	4	10	Modified (I)	67
	Sand	0.3	55	0.23	2.1	2	4.9	8	4	11	Modified (I)	83

The next four figures (Figure 4.24, Figure 4.25, Figure 4.26 and Figure 4.27) present two micrographs for each group; one unmodified, the other, modified. For the alloy without Mg, the modified sample with 250 ppm Sr is displayed; for the alloy with Mg, the modified sample with 55 ppm Sr.

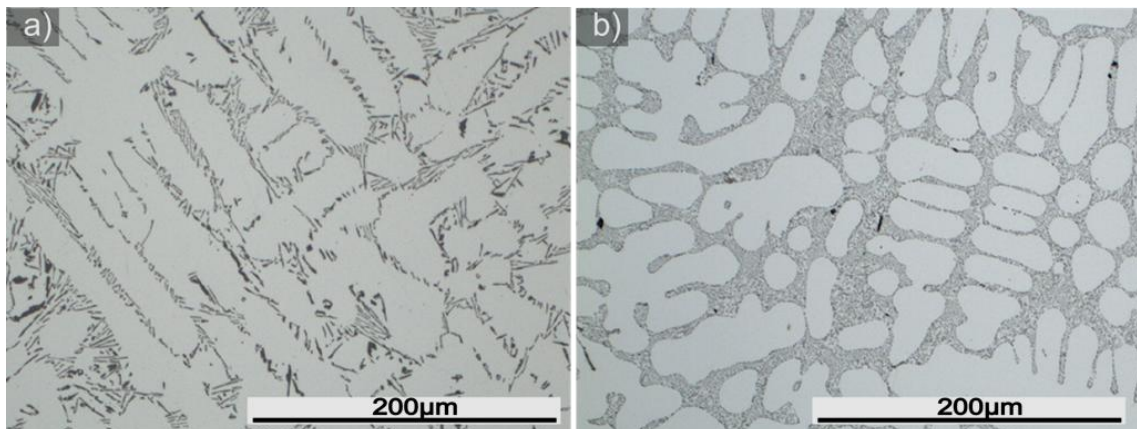


Figure 4.24: Micrographs from the group “Metal 0Mg”, (a) unmodified, (b) modified.

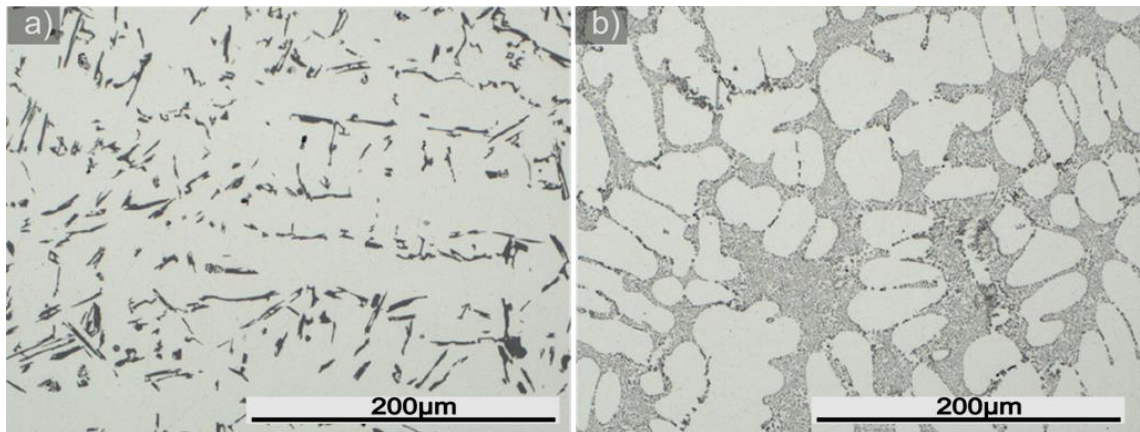


Figure 4.25: Micrographs from the group “Metal 0.3Mg”, (a) unmodified, (b) modified.

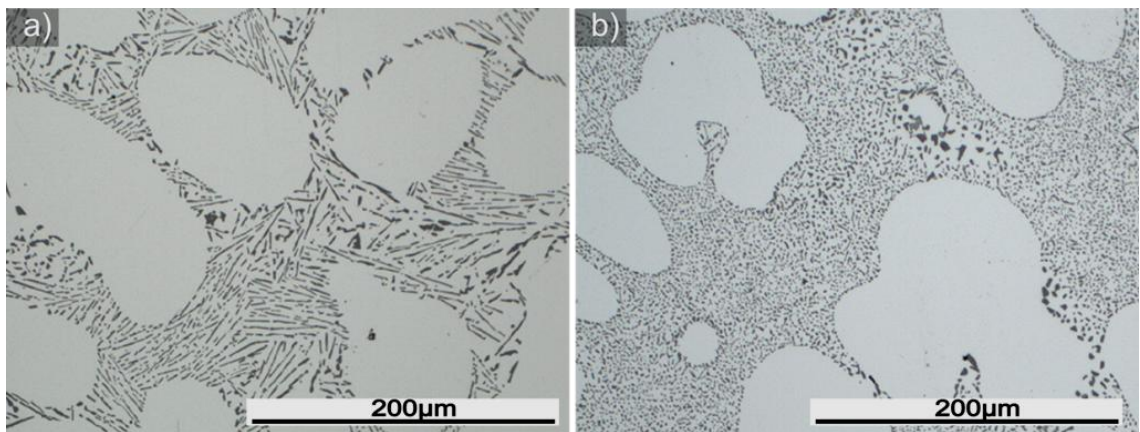


Figure 4.26: Micrographs from the group “Sand 0Mg”, (a) unmodified, (b) modified.

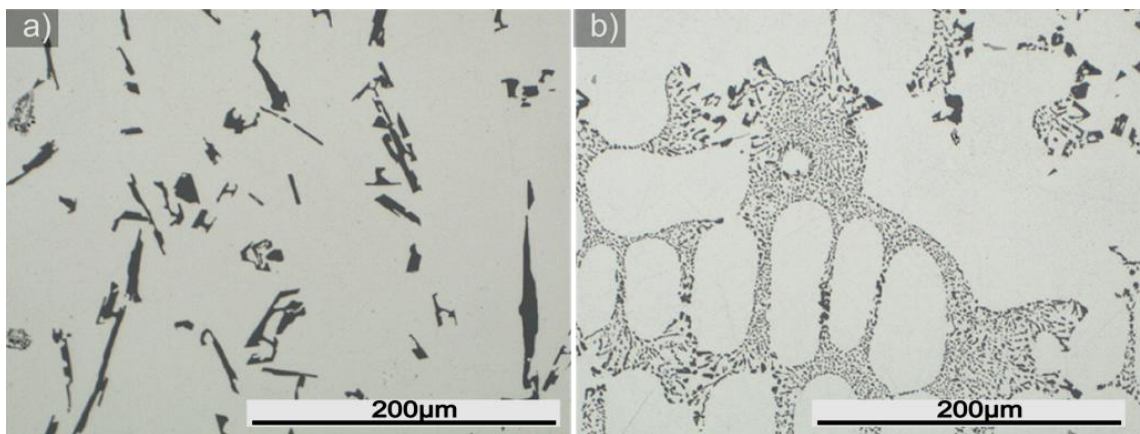


Figure 4.27: Micrographs from the group “Sand 0.3Mg”, (a) unmodified, (b) modified.

Relationship between Sr content, SCR and M

In Figure 4.28, M is plotted as a function of the Sr content. M , of samples with 55 ppm of Sr, is close to or slightly above 80 %. M increases to close to 100 %, by 100 ppm Sr and decreases with Sr content above 300 ppm. The lower values of M , for too low or too high content of Sr, are attributable to under- and over-modification, respectively. The results indicate that samples casted in metal mold have a maximum M close to 100 ppm Sr, while the samples casted in sand have their maximum displaced towards higher content of Sr, between 100 ppm Sr and 250 ppm Sr. This effect can be related to the assistance of the SCR in the modification process.

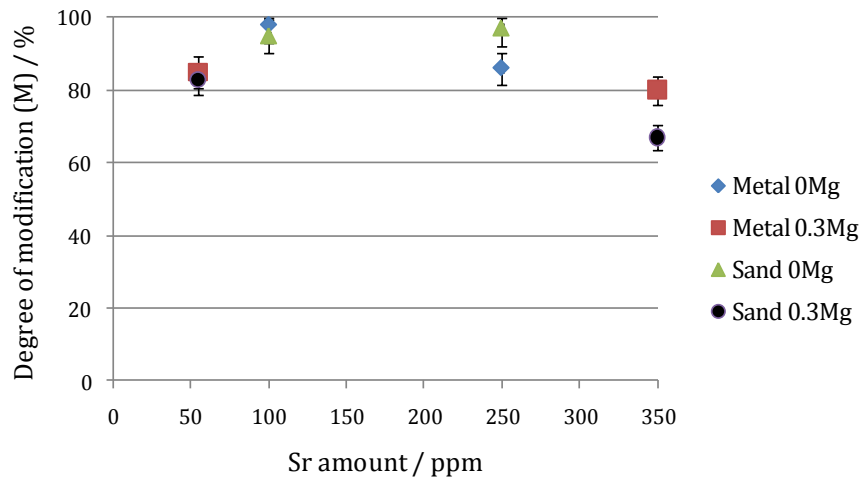


Figure 4.28: M as a function of the Sr content for modified alloys. Group of samples as indicated in Table 4.15.

Mechanical properties as a function of M and SCR

As listed in Table 4.15, the samples in each group have different states: firstly the unmodified; secondly, the modified one with the lower M available; and thirdly, the modified one with the higher M available. The maximum displacement, load and absorbed energy (Sm , Pm and Wm) are graphically represented in Figure 4.29, for each group. The columns, for each represented quantity, represent comparatively the results for each state: unmodified (left hand side column), modified with the lower M (middle column) and modified with the higher M (right hand side column). For each displayed quantity, the results are presented relatively to the unmodified state, i.e. 100 % represent the unmodified state.

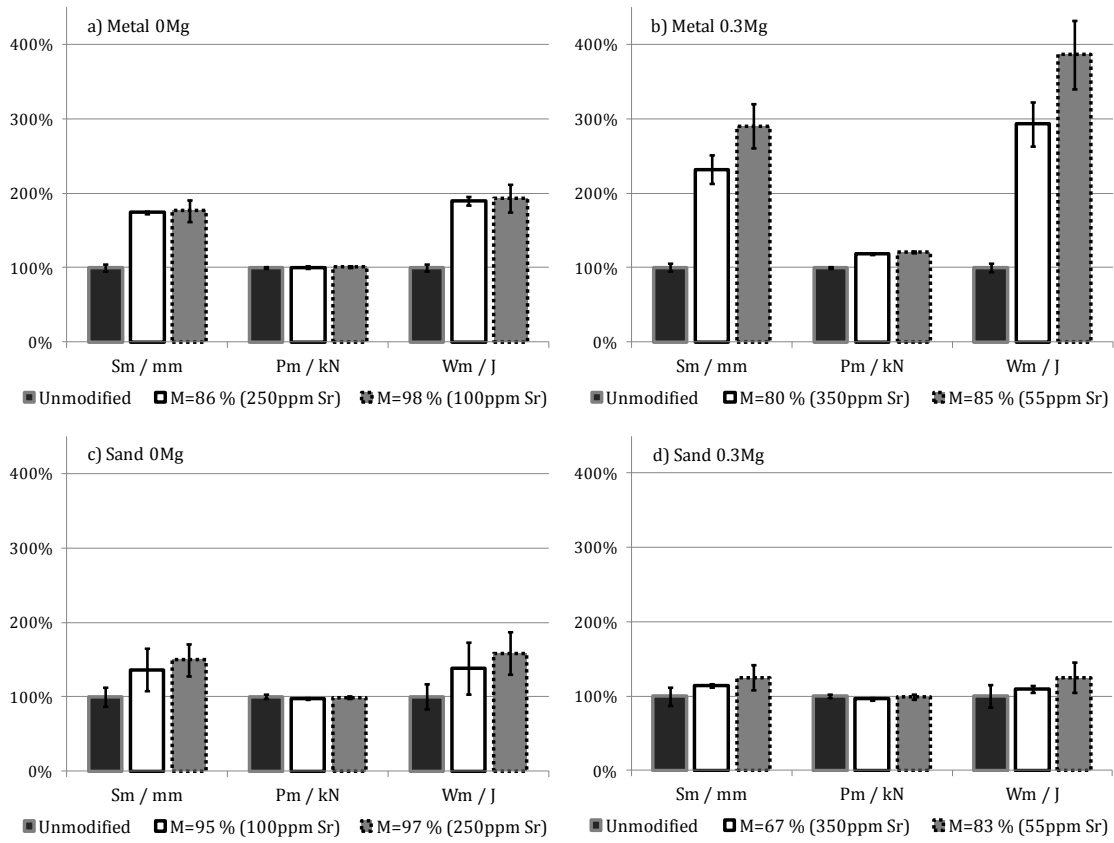


Figure 4.29: Mechanical properties of modified alloys with respect to the unmodified state (Unmodified state = 100 %). For each displayed quantity (Sm , Pm and Wm), the three columns represent: unmodified (left hand side column), modified with the lower M (middle column), and modified with the higher M (right hand side column). Group of samples as indicated in Table 4.15.

In general, if an increase in the mechanical properties was measured, modification and a rise in M was quantified. However, modification or an increment in M does not imply an improvement of the mechanical properties. A clear improvement of the mechanical properties with modification is observed for the samples casted in metal molds. For the samples casted in sand molds, an improvement can be observed; however, it is in some cases marginal. In general, the deformation and the absorbed energy are the variables that show the most remarkable response with modification. Pm improved with modification, only for the group “Metal 0.3Mg”, in about 16 %. This group (Metal 0.3Mg) displayed also the maximum percentage improvement for the adsorbed energy and deformation capability before rupture. For this group of samples, the values of Sm and Wm improved about three to four times with modification.

Analysis of 1% largest particles

Figure 4.29 shows that, among different samples, it is not possible only through studying the modification to understand the change in the mechanical properties. A hypothesis is that the largest objects, such as particles, defects or pores dominate the behavior of the material if they are able to reach a given size. Relatively large objects are more likely to be found in samples with lower SCR, since they have more time to grow. In this way it could be explained why the modifications is not that effective in samples with large DAS, as the results indicate. To study this hypothesis, an analysis of the particle parameters of the 1% largest particles with regards to the particle area (*Largest 1%*) was conducted. The arithmetic mean values of relevant particle parameters, describing the “*Largest 1 %*” and all the particles (*All*) in the micrograph, are listed in Table 4.16. The listed samples correspond to the micrographs shown in Figure 4.24 to Figure 4.27.

Table 4.16: Arithmetic mean value of the 1% largest particles with regard to the particle area (*Largest 1 %*) and of all the particles (*All*) in a micrograph. Group of samples as indicated in Table 4.15.

Group	State	Particles	A / μm^2	P / μm	Fm / μm	R	FAR	AAR
Metal 0Mg	Unmodified	All	17	23	8	0.5	0.5	0.4
		Largest 1 %	163	157	41	0.1	0.4	0.1
	Modified	All	3.7	9	3.4	0.6	0.6	0.4
		Largest 1 %	31	62	16	0.1	0.5	0.2
Metal 0.3Mg	Unmodified	All	28	30	11	0.5	0.5	0.3
		Largest 1 %	236	192	45	0.1	0.5	0.2
	Modified	All	3.6	9	3.3	0.6	0.6	0.4
		Largest 1 %	37	64	16	0.1	0.5	0.2
Sand 0Mg	Unmodified	All	13	19	8	0.6	0.5	0.4
		Largest 1 %	122	125	39	0.1	0.3	0.1
	Modified	All	3.3	7	2.8	0.7	0.6	0.5
		Largest 1 %	40	43	13	0.4	0.5	0.3
Sand 0.3Mg	Unmodified	All	111	63	22	0.5	0.5	0.3
		Largest 1 %	733	321	103	0.1	0.2	0.1
	Modified	All	3.7	8	3.0	0.7	0.6	0.5
		Largest 1 %	77	70	19	0.2	0.6	0.3

Figure 4.30 summarizes graphically the information including mechanical properties, *M* and the size parameters of the “*Largest 1 %*” particles. In this figure, the graphs *a*, *b* and *c* compare the mechanical properties of modified and unmodified samples. The graph *d*, *e* and *f* compare modified samples from the different alloy groups. The graph *d* shows the degree of modification, and *e* and *f*, the size of the largest particles.

In Figure 4.30, the graphs *a*, *b* and *c* show that the sample “Sand 0.3Mg” shows marginal change of the mechanical properties with modification. In the other hand, the sample “Metal 0.3 Mg” shows strong change of the mechanical properties with modification. The graphs *d*, *e* and *f* show that, the main difference between the modified samples of the different alloys is the area of the largest particles.

Therefore it is possible to say that the modification signifies an improvement of the mechanical properties only in absence of relatively large objects such as particles or defects. The results indicate that, if there are particles with area of about $A = 80 \mu m^2$, the modification does not cause any improvement.

Regarding the effects of Mg in as-cast samples, Mg acts declining the toughness and slightly improving *Pm*. In both unmodified and modified samples, the increase in *Pm* with Mg is the best in metal mould (see change in Figure 4.30-c, from “Metal 0Mg” to “Metal 0.3Mg”).

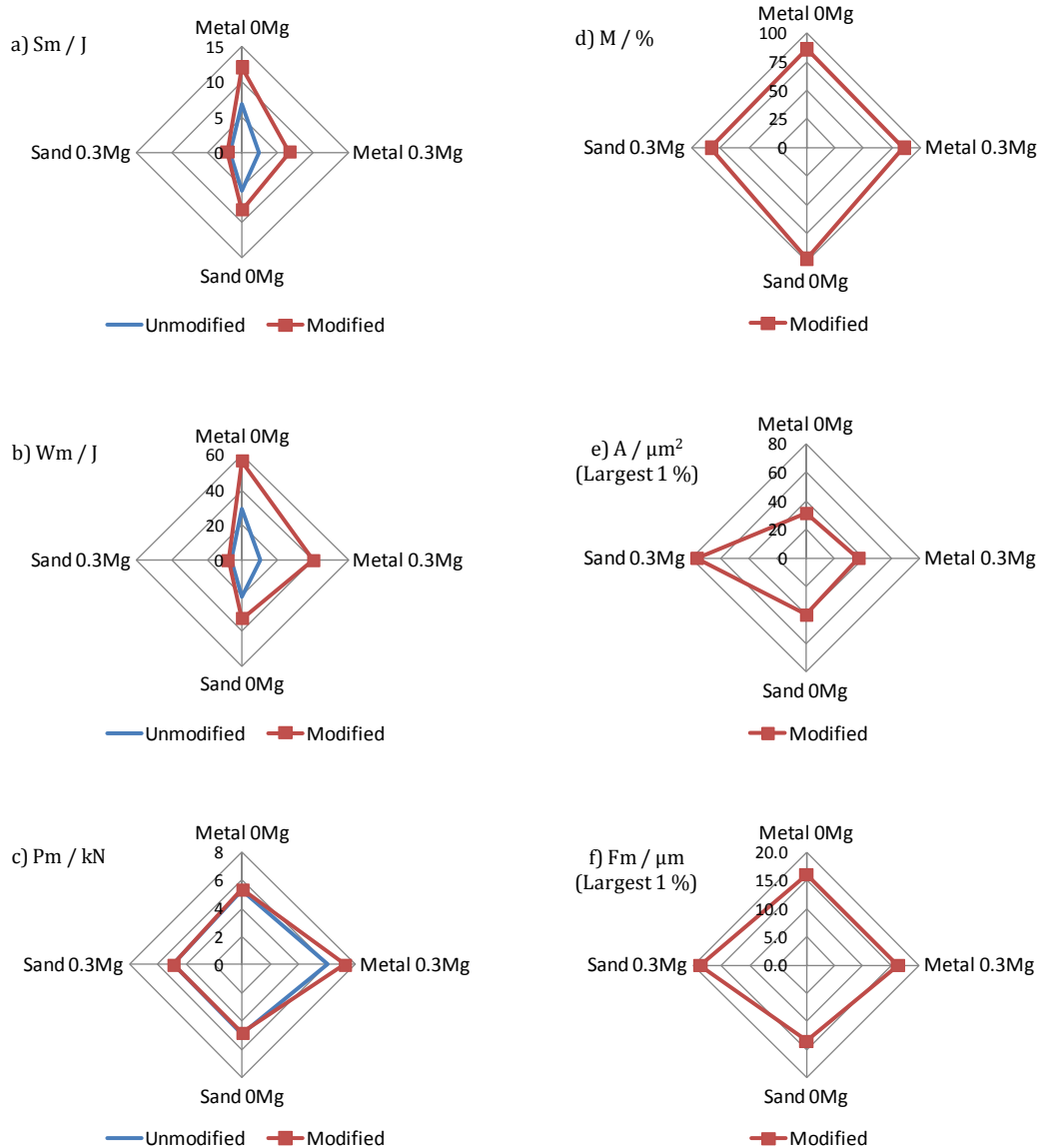


Figure 4.30: (a), (b) and (c) show the change on the impact behavior between unmodified and modified samples. (d), (e) and (f) compare modified samples. (d): Degree of modification M . (e) and (f): Average value of A and F_m of the 1 % largest particles (Largest 1%) of modified samples. Group of samples as indicated in Table 4.15.

4.4.3. Remarks of the section

The method to assess modification is sensitive enough to quantify the contributions of the chemical- and the thermal-modification so as to identify under- and over-modification. Interpretations of the M , as a function of the Sr content, help identifying the adequate amount of Sr to achieve an optimal modification.

In the literature, it is reported that both load and deflection (and consequently the toughness) are observed to improve with the modification. The objective analysis in this work shows that the impact behavior can improve with modification, but not implicitly. The mechanical properties can improve with the modification, especially the toughness. The positive influence of the modification on the mechanical properties is more appreciable in samples with higher solidification cooling rate (SCR). The modification does not cause any improvement if the microstructure presents large particles or defects such as particles with an area $A \geq 80 \mu m^2$.

Regarding the small punch test (SPT), it was observed that homogeneously modified Al-7Si samples are more ductile and have lower strength than unmodified Al-7Si-0.3Mg samples. Further samples would be required to evaluate the effect of Mg separately.

Regarding the Charpy test, the improvement in the mechanical properties cannot be only adjudicate to M ; then, for similar values of M , the improvement, in samples cast in metal mold, was much better than in those cast in sand mold.

Although the modified and unmodified structures in Figure 4.27 are quite different, the difference regarding the mechanical properties of the corresponding specimens is marginal. An attempt, trying to explain this, was conducted with the analysis of the 1 % largest particles. A possible explanation is that the absolute sizes of the largest particles have a dominant effect on the impact behavior of modified samples.

For the alloy with Mg and high SCR (group “Metal 0.3Mg”), the improvement in the impact behavior with the modification is remarkable. For this sample, the maximum impact load and capability of deformation improved with modification. This was the only group of alloys, which presented improvement of the maximum impact load with modification.

5. CONCLUSIONS AND OUTLOOK

Conclusions

It is of increasing importance to study objectively the modification in Al-Si alloys. Fully modified structures are homogeneous whereas under- and over modified structures displays a mixture of fine and coarse particles. To evaluate the modification level of Al-Si alloys, the homogeneity of the eutectic Si should be considered. The innovative application of the Gini coefficient (G) was the key to develop the microstructure homogeneity characterization. The homogeneity is applicable to study different problems in material sciences and required to objectively describe the modification in Al-Si alloys.

The sizes of eutectic particles were described with respect to the secondary dendrite arm spacing (DAS). These relative particle sizes are the most important characteristic to distinguish modified particles from unmodified ones. A particle classification model was obtained for Al-7Si and Al-7Si-0.3Mg alloys.

With the feedback from thirteen laboratories, specialized in aluminum casting alloys, representative structures have been identified. A quantitative analysis was carried out considering parameters from the literature and parameters developed in this work. A microstructure classification model was obtained for Al-7Si and Al-7Si-0.3Mg alloys, which objectively define the “modified”, “unmodified” and “homogeneous modified” microstructures. Besides, an alternative parameter describing the modification for these alloys was suggested, the “degree of modification” (M). With respect to other evaluations methods available in the literature, M has advantages of being objective and considering the homogeneity.

The study of the structure morphologies is important to build or deny theories explaining the modification. A comparison of Sr- and quench-modified structures was carried out, using 2D and 3D analysis. The observed differences between these structures were marginal. It is still not clear if the chemical- and the quench-modified Si have the same growth mechanism.

Through small punch tests (SPT) it was shown that fully modified samples have higher ductility and toughness than the unmodified samples. Through Charpy tests, it was found that the impact behavior of the castings can improve with modification, especially

regarding the ductility and toughness; however, not implicitly. Besides of the degree of modification, the DAS and the absolute sizes of the largest particles or defects play an important role in the impact behavior of the castings.

Outlook

The tools developed in this work to evaluate homogeneity are a fundamental contribution for the microstructure analysis in material sciences. For example, the homogeneity of the reinforcement distribution in carbon nanotube (CNT) composites has influence on the mechanical properties. This effect can be studied applying the developed tools. As shown in Figure 5.1, the region homogeneity was quantified for the CNT composites, considering the number of objects and the phase amount of CNT clusters (black objects in the images). [3]

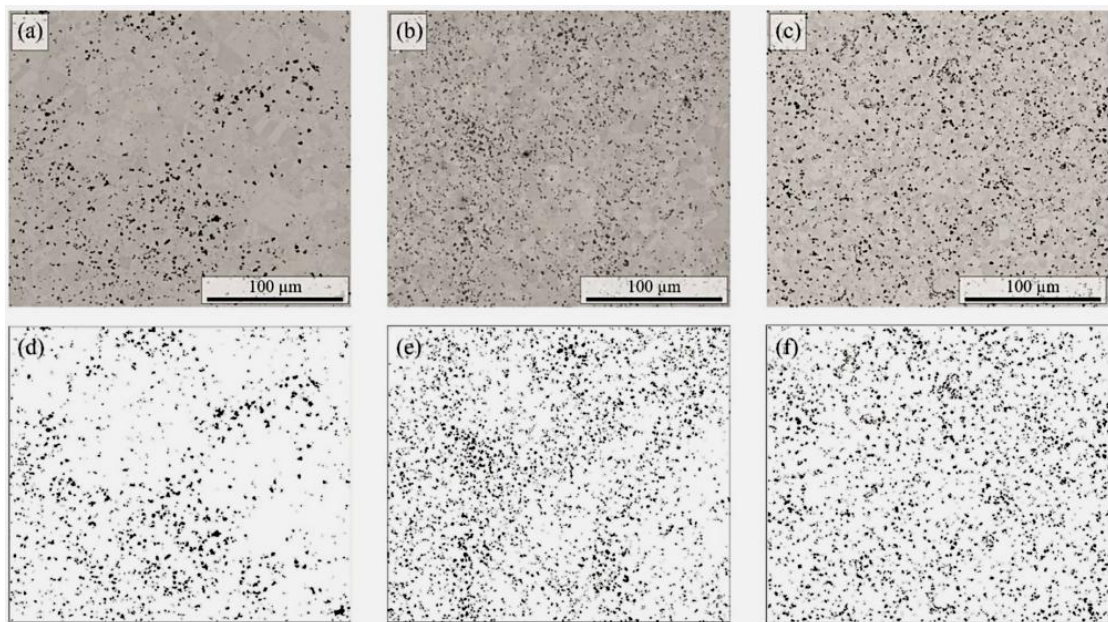


Figure 5.1: (a), (b) and (c) are electron micrographs of CNT reinforced Ni composites and (d), (e) and (f) are the corresponding binarized images, respectively. The region homogeneity (h_R) values are $(58 \pm 3)\%$, $(73 \pm 3)\%$ and $(85 \pm 4)\%$, respectively[3].

The application of the homogeneity concepts can be used in other systems besides of microstructures, for instance, to evaluate the topography of laser structured surfaces, as shown in Figure 5.2.

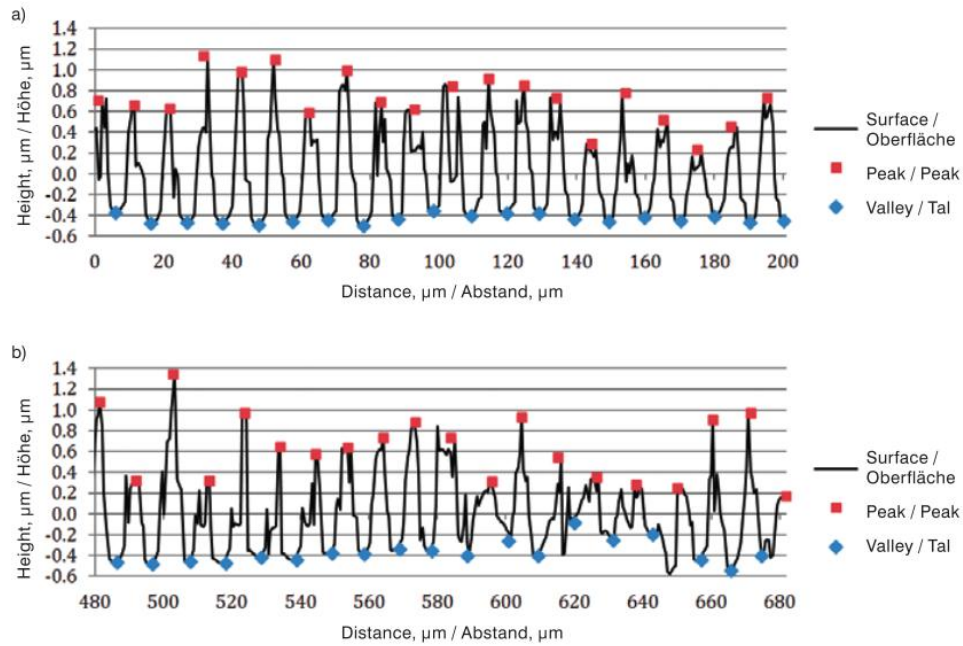


Figure 5.2: (a) and (b) are topography of laser structured surfaces. The homogeneity values considering the height of the peaks are 82% and 72% for images (a) and (b), respectively [1].

Regarding the modification of Al-Si alloys, further activities of interest are:

- (1) To automatize the classification models and the quantification of M

There are software products including built-in functions to calculate the Gini coefficient, e.g. *NumXL* for *Excel*. To quantify the DAS, automatic methods could be applied, e.g. ref. [158] and the software solution *Leica Dendrite Expert*. The optimal solution would be to incorporate the classification, the DAS as well as the developed parameters, including M , to an image software analysis.

- (2) To further research the concerning structures in 3D space

It is required to define the “plate-like” and “coral-like” shapes in 3D space to improve the characterization. This would allow distinguishing the microstructure refinement and the modification.

- (3) To extend the suggested method

It would be interesting to adapt the method for alloys with different compositions and to add further classes, as the over- and under-modified classes. There are several challenges, for example: In alloys with grain refinement, it is more difficult to measure

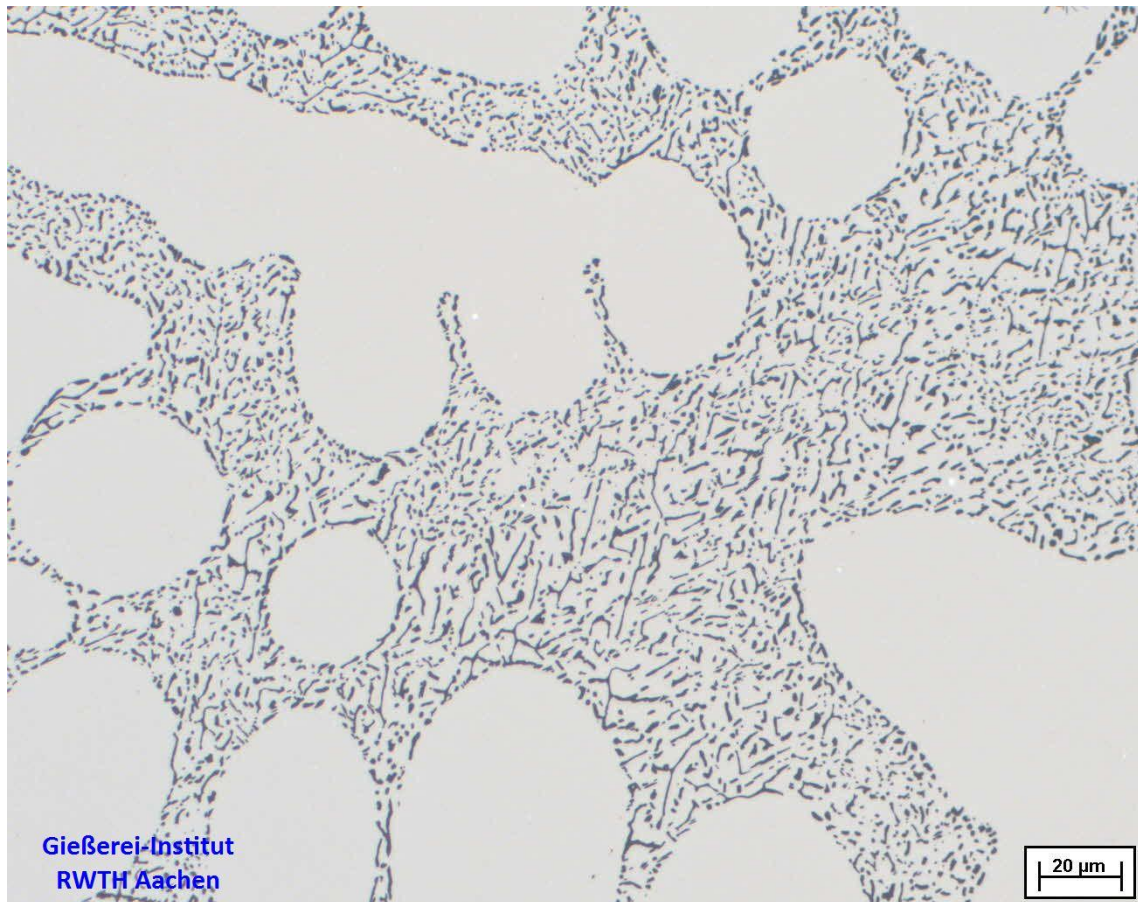
the DAS. In alloys with several intermetallic phases, it is more difficult to segment the eutectic Si particles.

(4) To further study the correlation between the structure and the mechanical properties

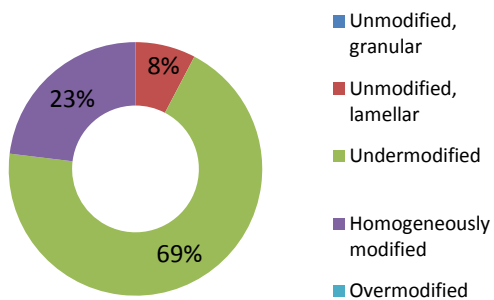
This work gives useful, innovative tools to objectively analyze the microstructure. This makes possible the quantitative correlation between the structure and the mechanical properties.

Appendix: List of micrographs

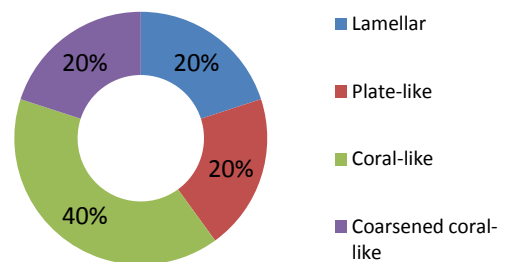
Micrograph No. 1:



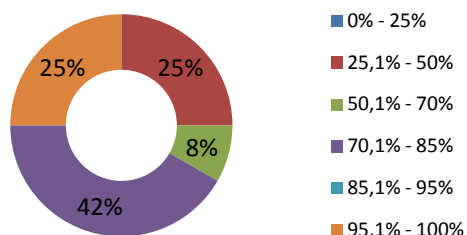
Question 1: State



Question 2: Morphology



Question 3: Distribution of the subjective homogeneity



Chemical composition:

Al - 7 wt.% Si - 50 ppm Sr - 2.5 ppm P

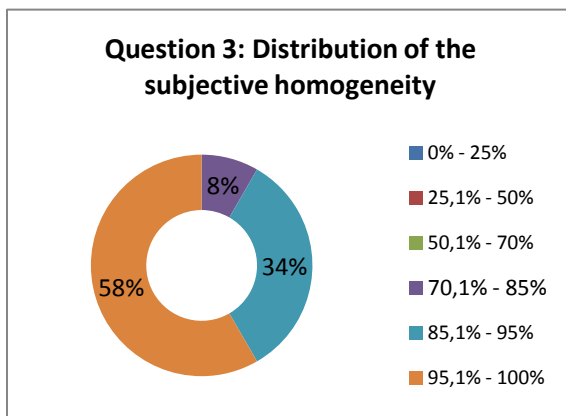
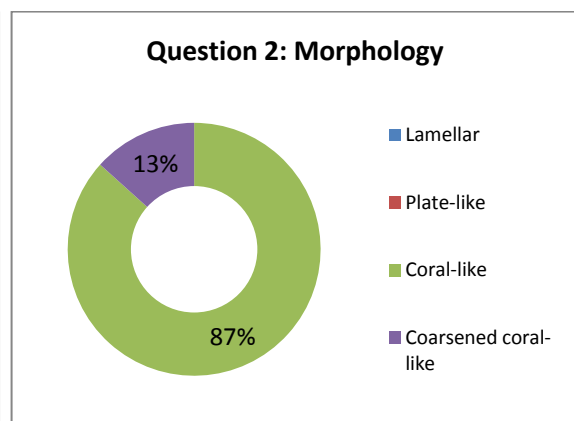
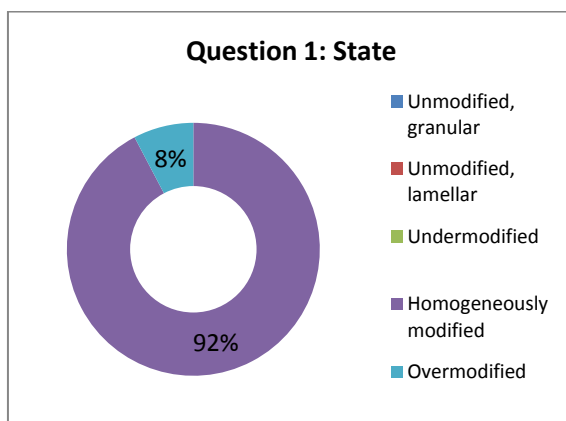
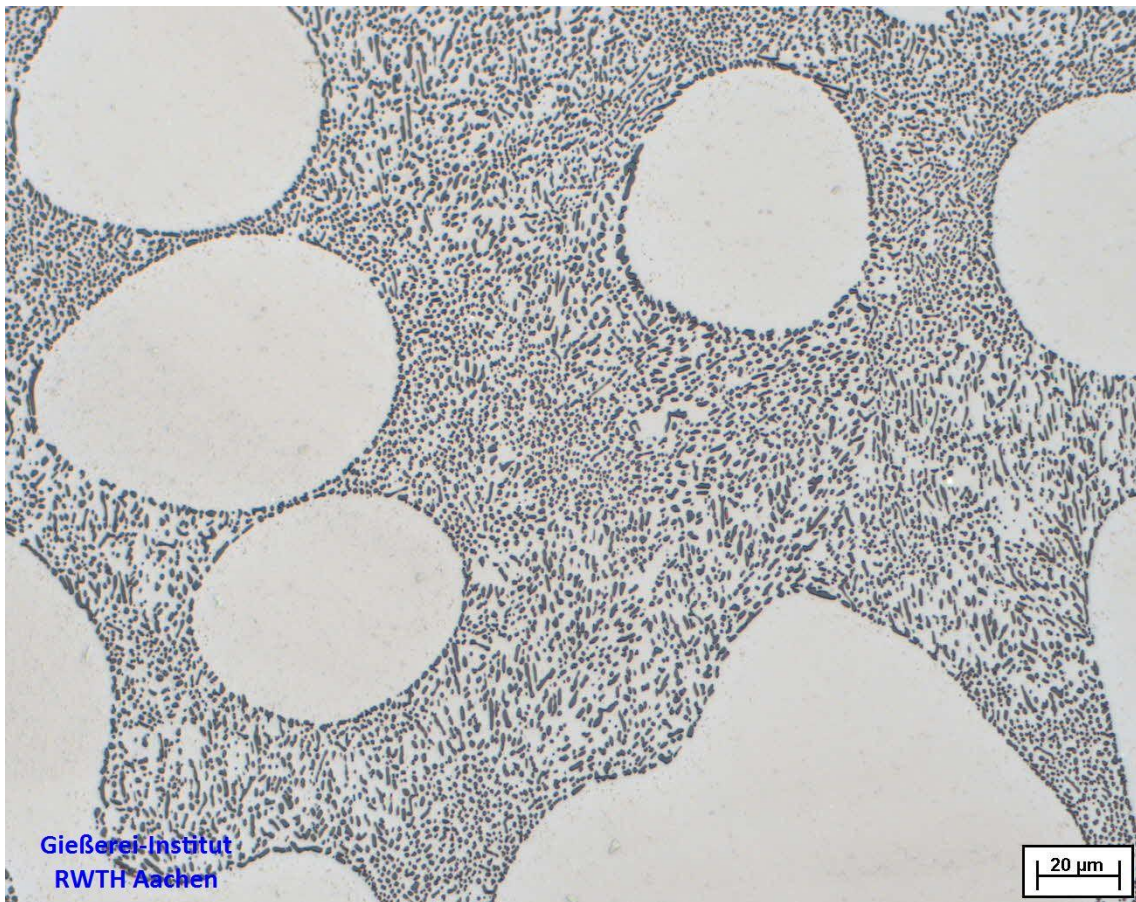
Casting process: **Triplex D30**

Subjective homogeneity: **(75 ± 19) %**

Objective classification, degree of mod. (*M*):

Modified, Inhomogeneous, *M* = 88 %

Micrograph No. 2:



Chemical composition:

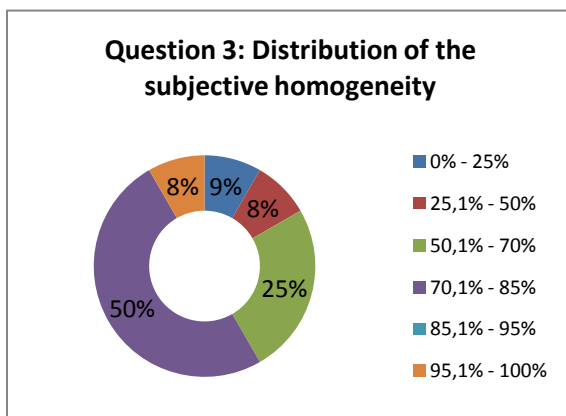
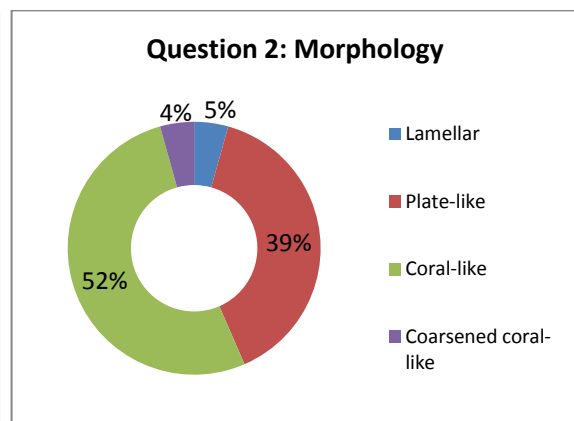
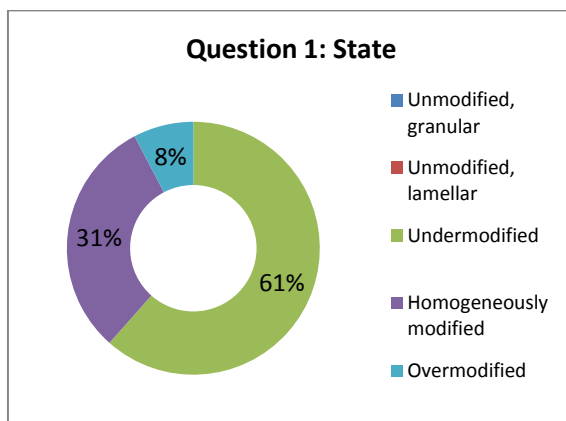
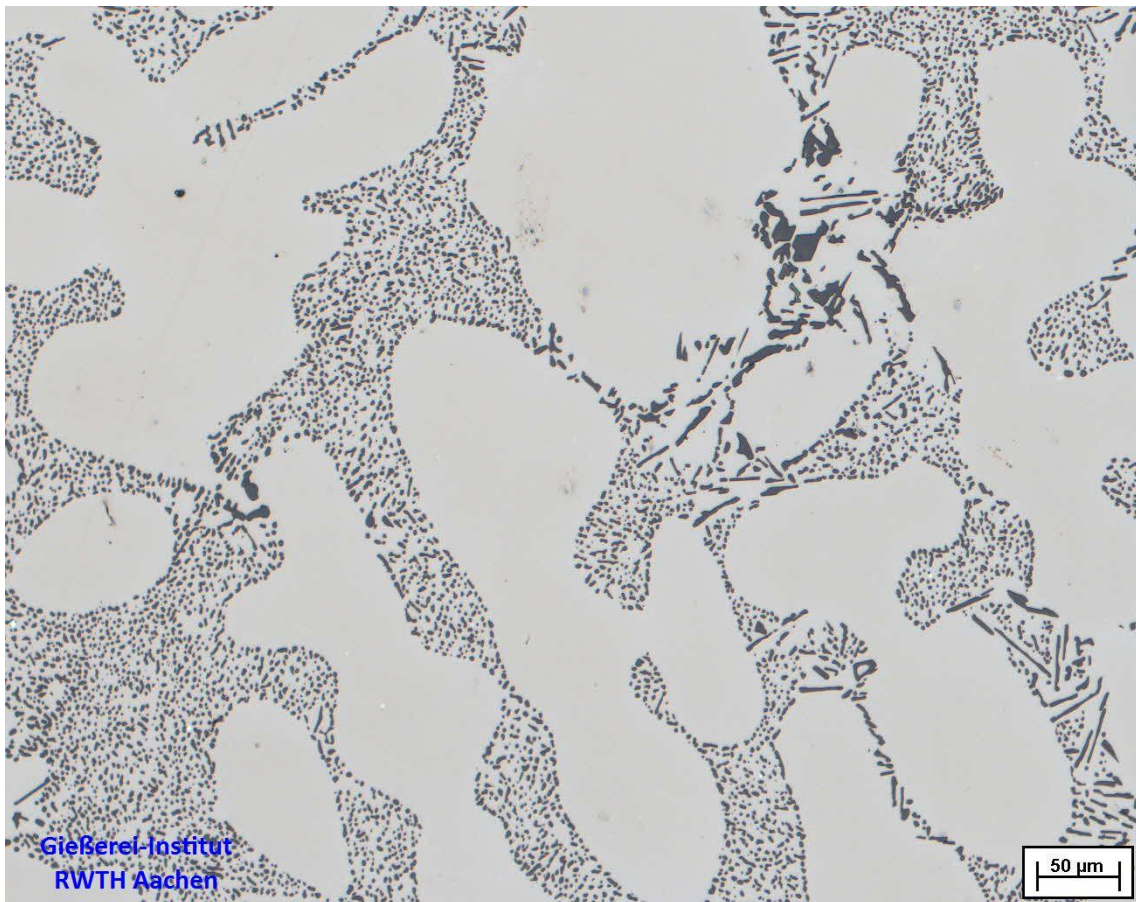
Al - 7 wt.% Si - 50 ppm Sr - 2.5 ppm P

Casting process: **Triplex D60**

Subjective homogeneity: **(96 ± 6) %**

Objective classification, degree of mod. (*M*):

Modified, Homogeneous, *M* = 97 %



Chemical composition:

Al - 7 wt.% Si - 50 ppm Sr - 2.5 ppm P

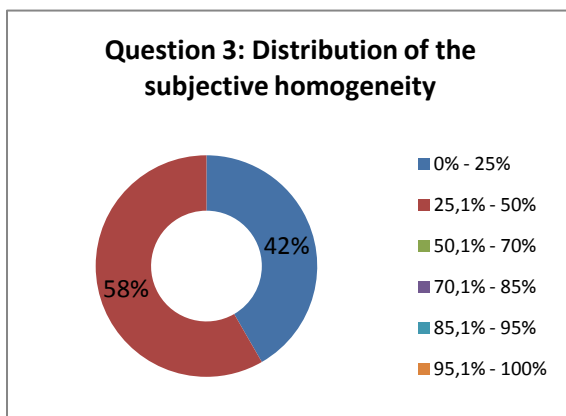
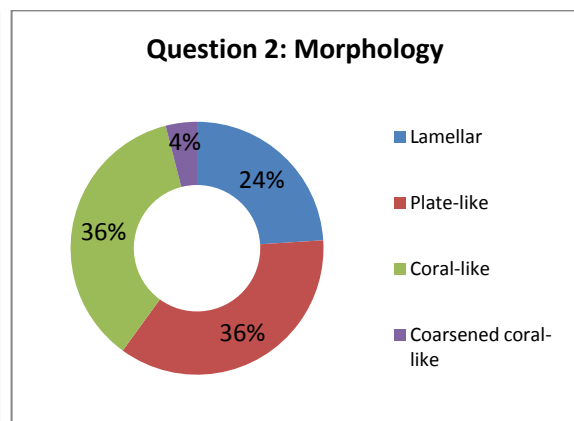
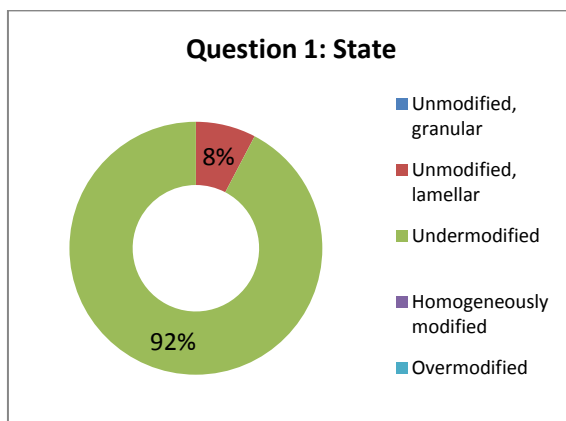
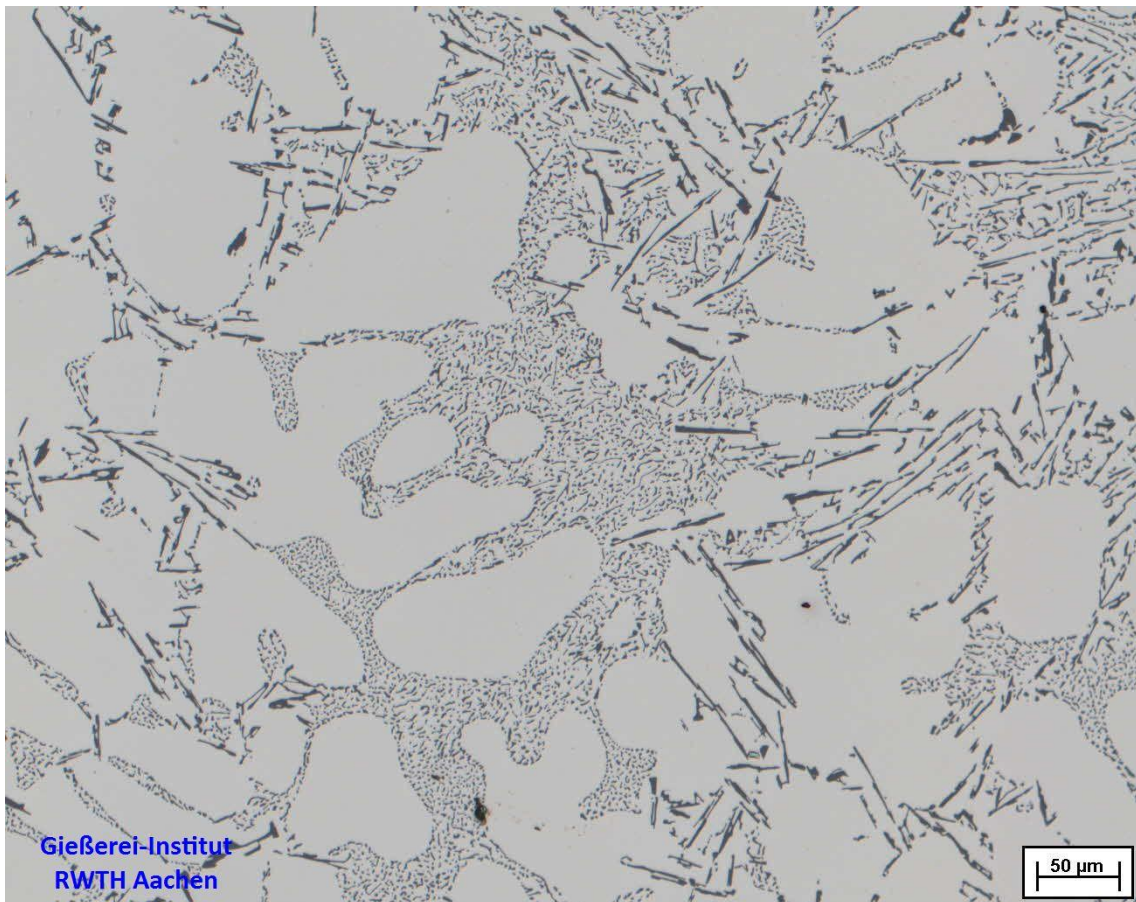
Casting process: **Triplex D90**

Subjective homogeneity: **(71 ± 18) %**

Objective classification, degree of mod. (*M*):

Modified, Inhomogeneous, *M* = 93 %

Micrograph No. 4:



Chemical composition:

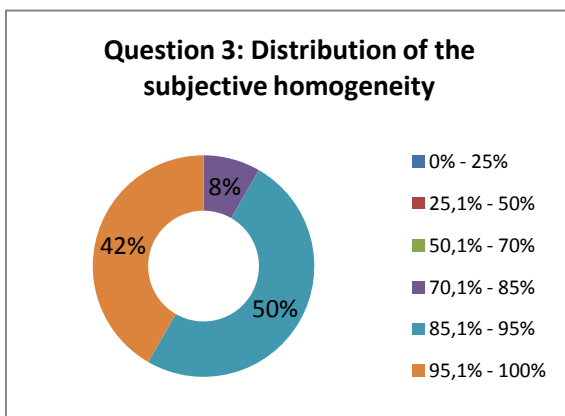
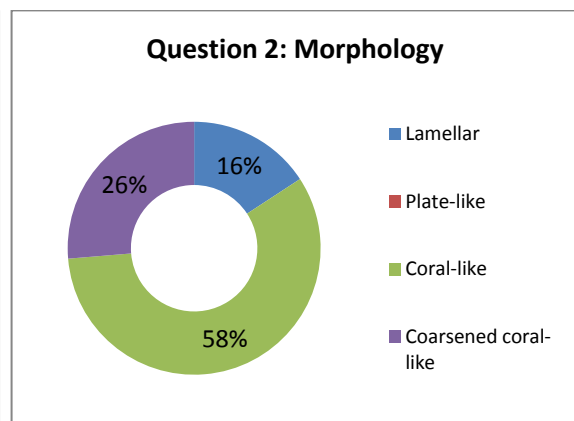
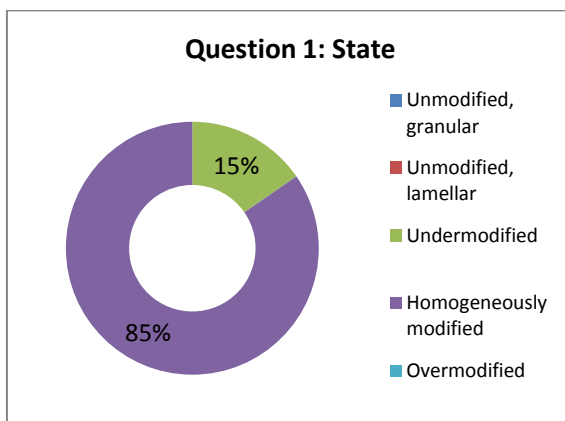
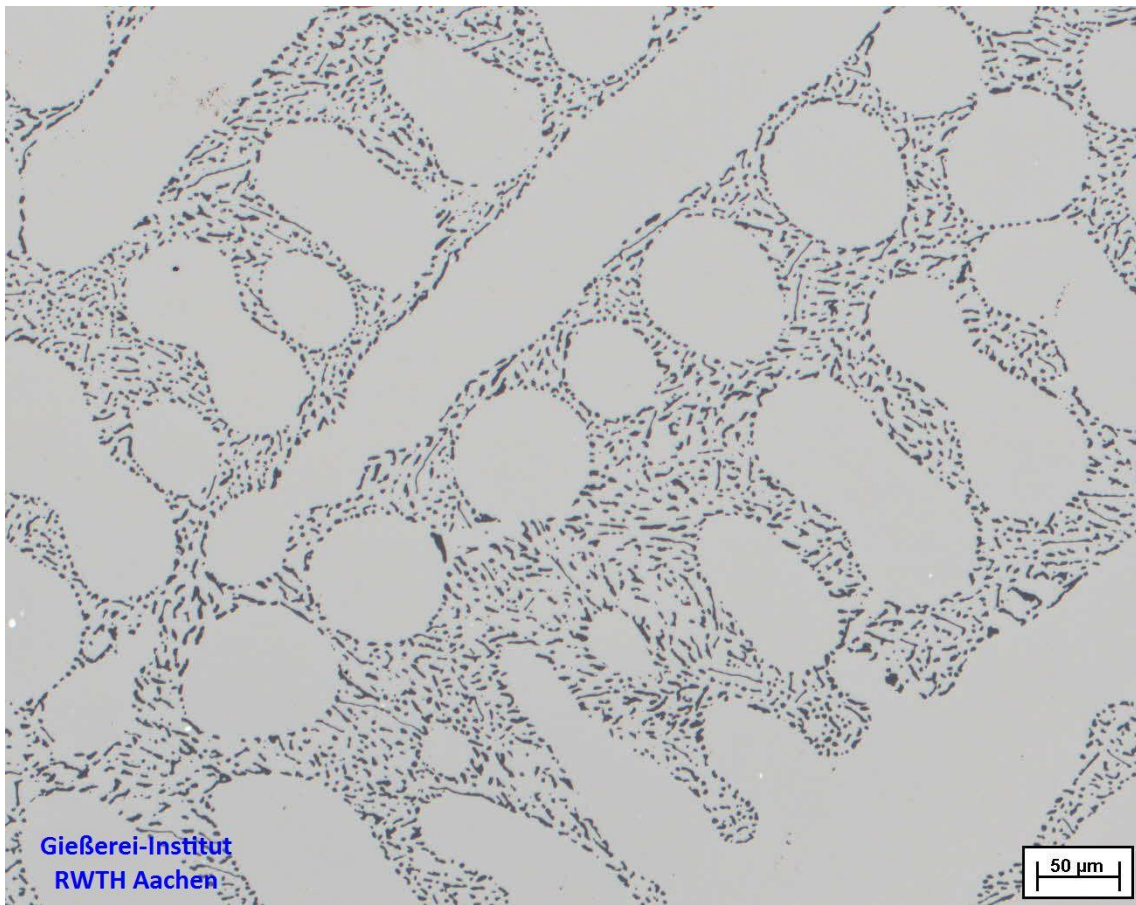
Al - 7 wt.% Si - 50 ppm Sr - 5 ppm P

Casting process: **Triplex D30**

Subjective homogeneity: **(27 ± 21) %**

Objective classification, degree of mod. (*M*):

Modified, Inhomogeneous, *M* = 21 %



Chemical composition:

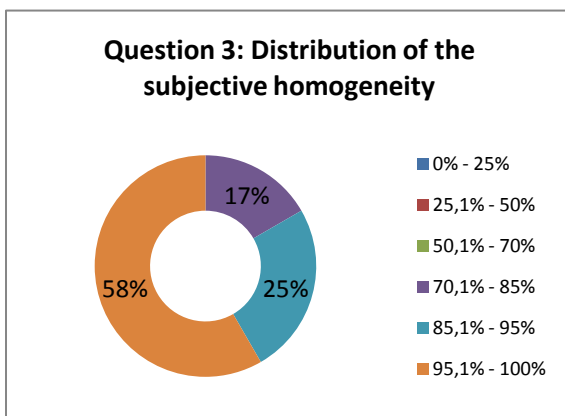
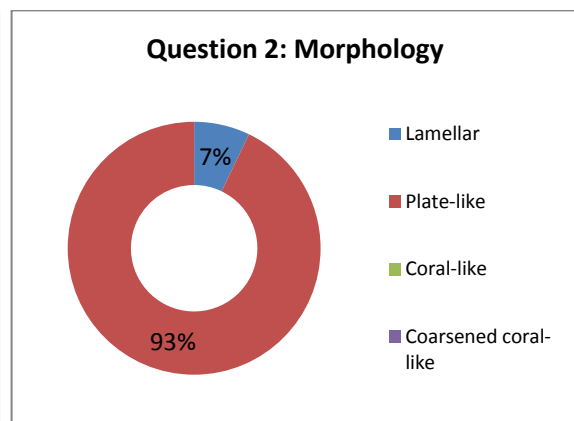
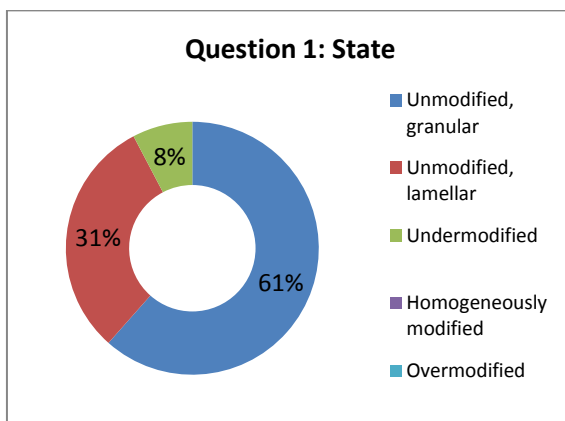
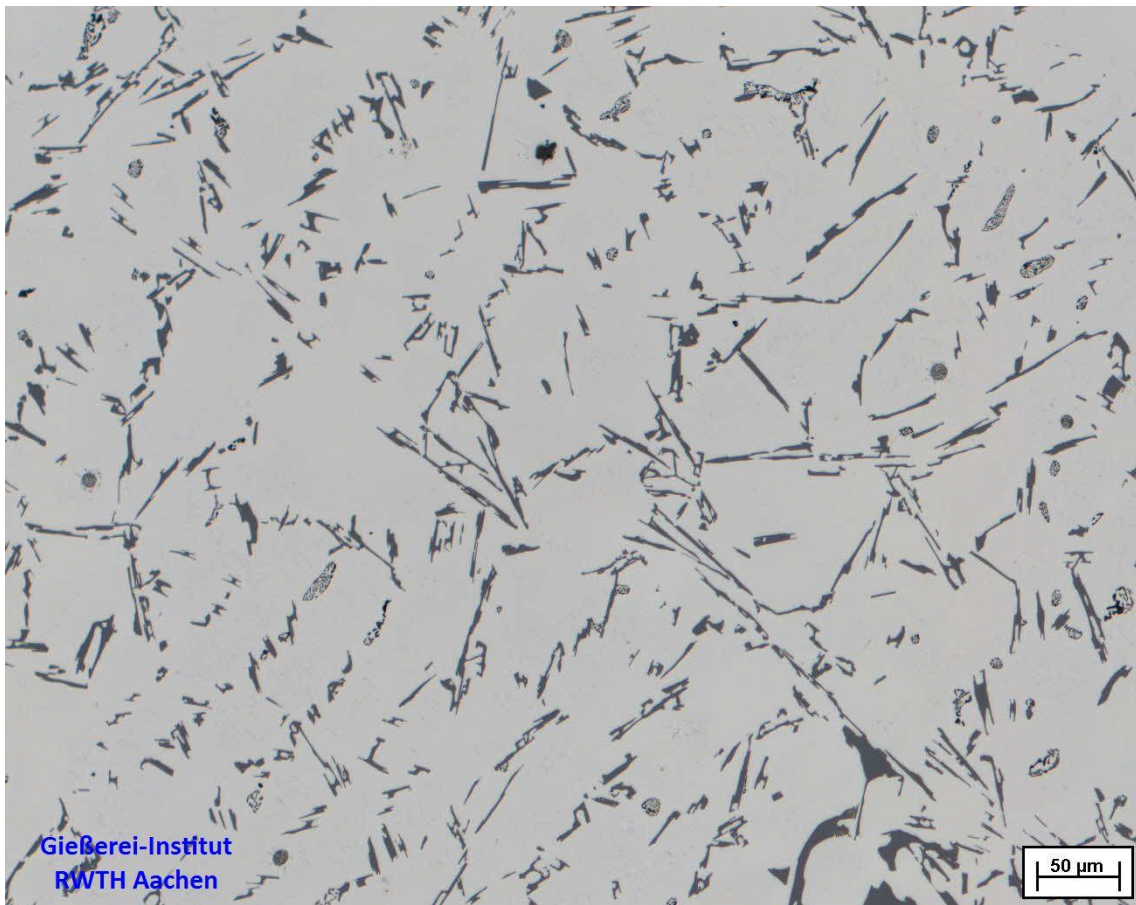
Al - 7 wt.% Si - 100 ppm Sr - 2.5 ppm P

Casting process: **Triplex D90**

Subjective homogeneity: **(94 ± 7) %**

Objective classification, degree of mod. (*M*):

Modified, Homogeneous, *M* = 97 %



Chemical composition:

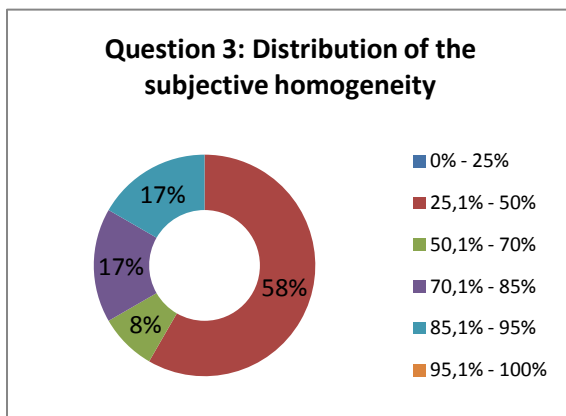
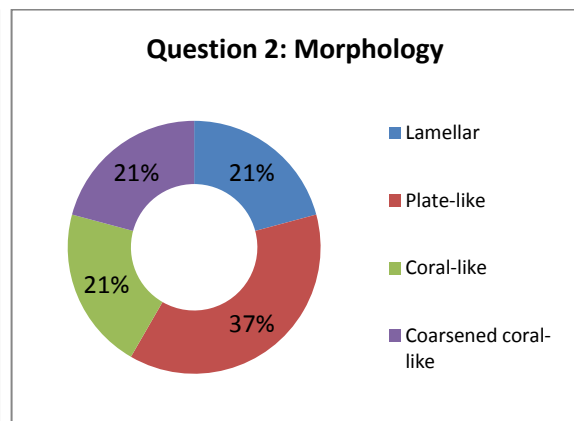
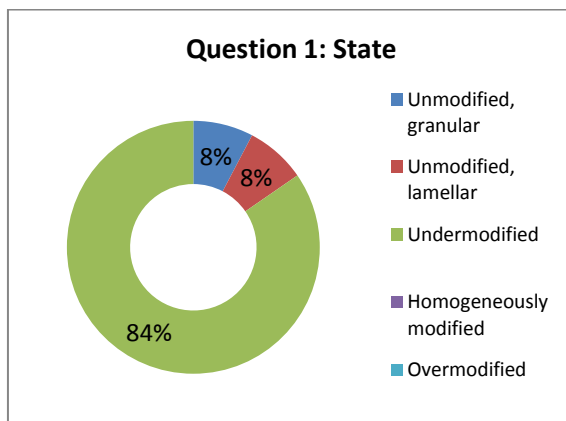
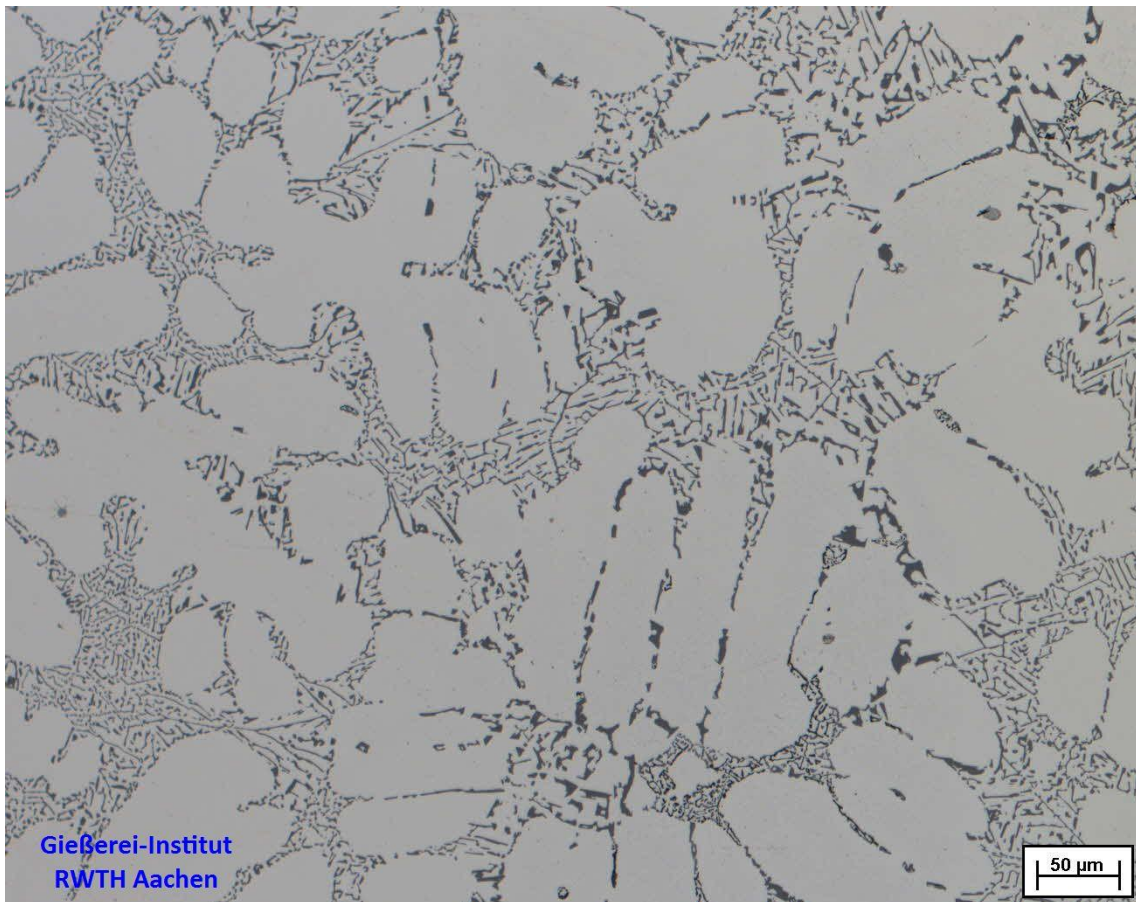
Al - 7 wt.% Si - 0.3 wt.% Mg - 2.5 ppm P

Casting process: **Triplex D30**

Subjective homogeneity: **(95 ± 7) %**

Objective classification, degree of mod. (*M*):

Unmodified, *M* = n.a.



Chemical composition:

Al - 7 wt.% Si - 0.3 wt.% Mg – 50 ppm Sr

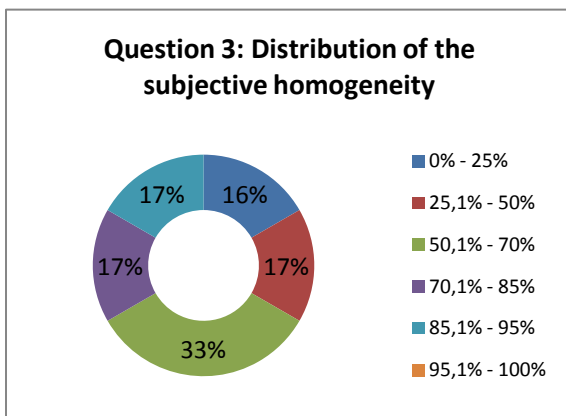
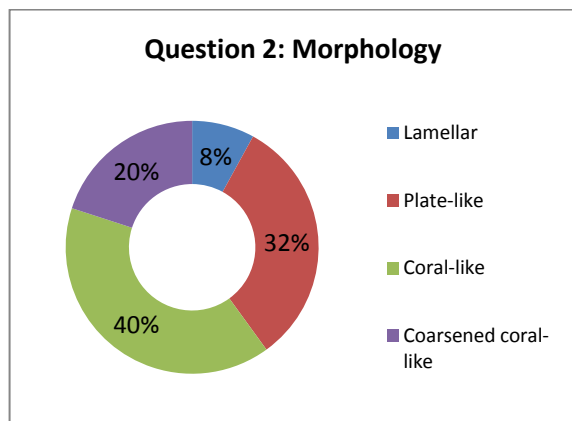
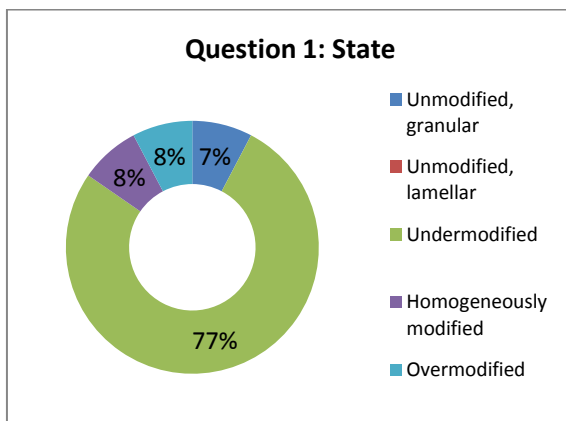
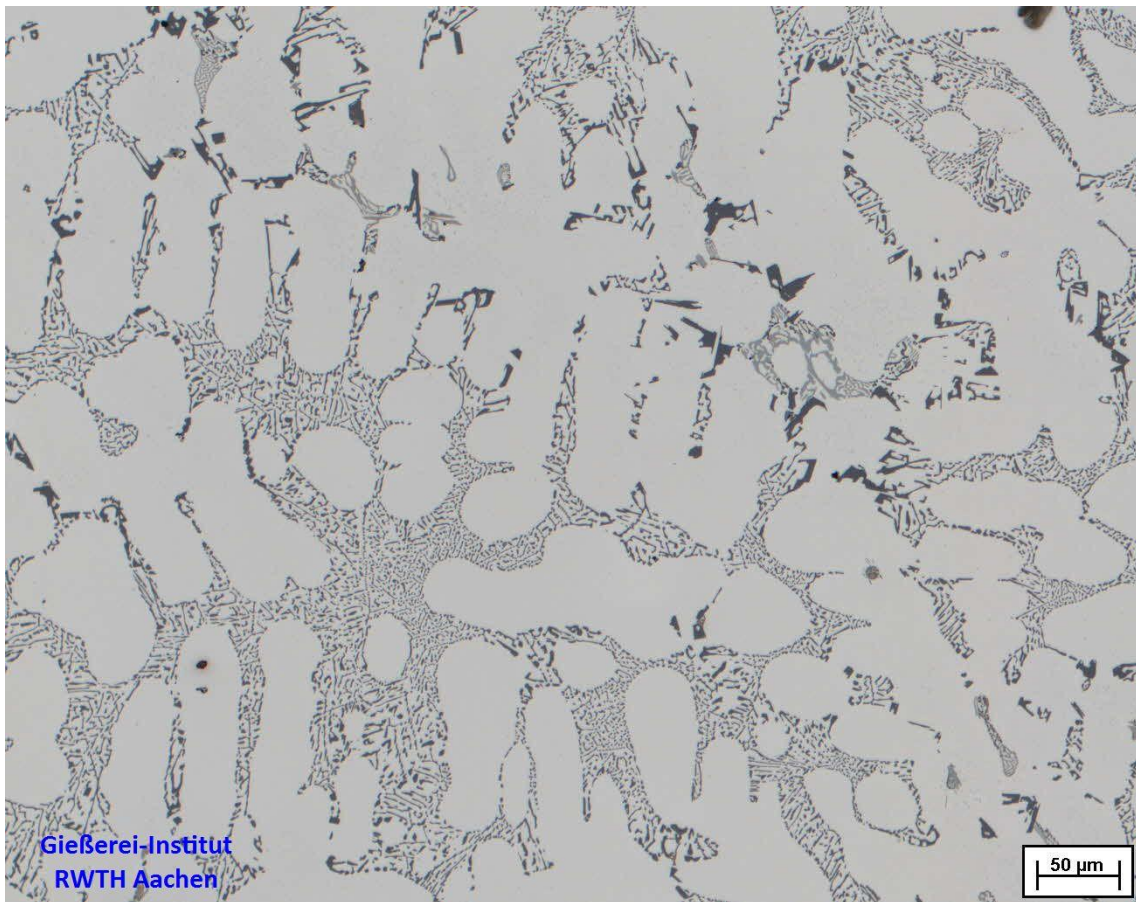
Casting process: **Triplex D30**

Subjective homogeneity: **(58 ± 21) %**

Objective classification, degree of mod. (*M*):

Unmodified, *M* = n.a.

Micrograph No. 8:



Chemical composition:

**Al - 7 wt.% Si - 0.3wt.% Mg - 50 ppm Sr
- 5 ppm P - 800 ppm Fe**

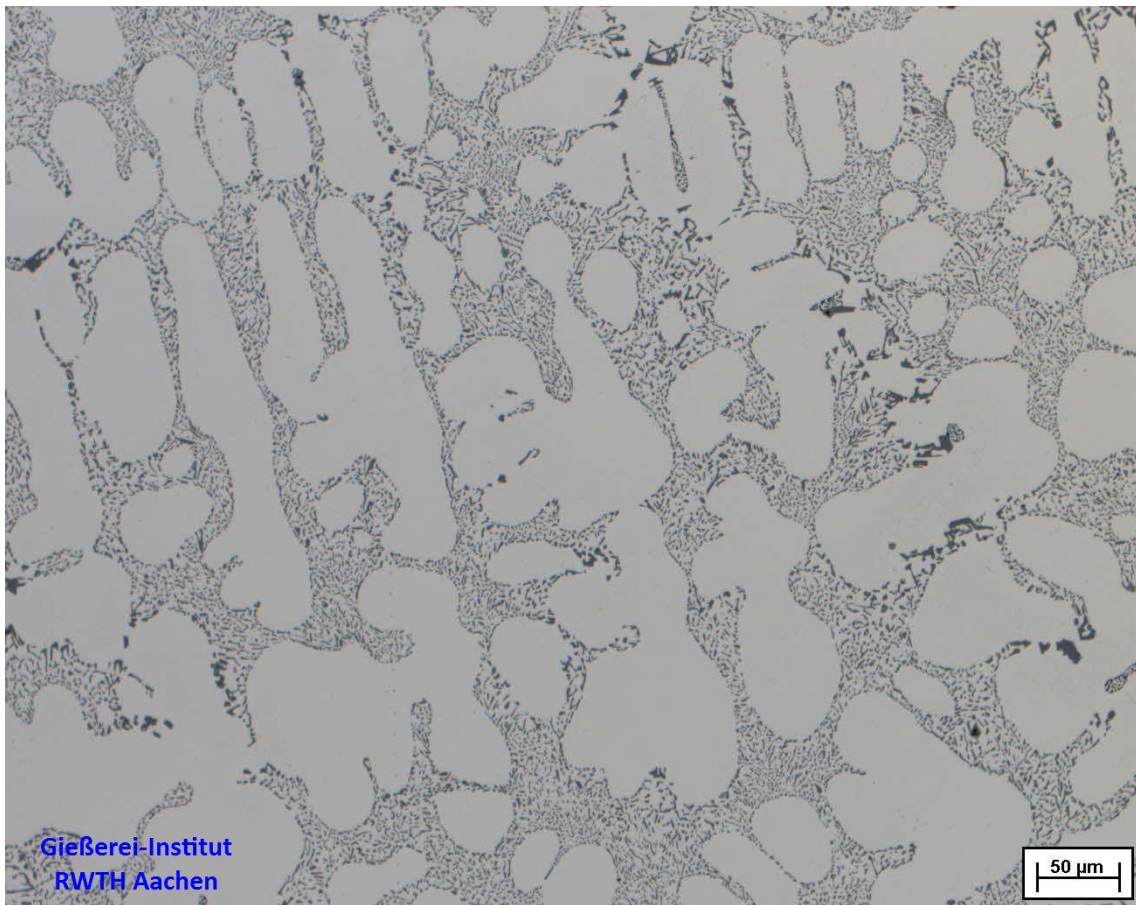
Casting process: **Triplex D30**

Subjective homogeneity: **(60 ± 23) %**

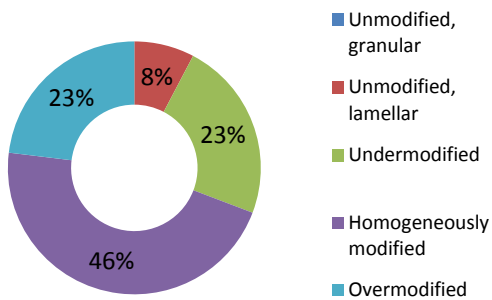
Objective classification, degree of mod. (*M*):

Modified, Inhomogeneous, *M* = 43 %

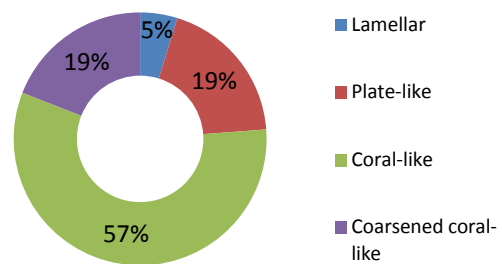
Micrograph No. 9:



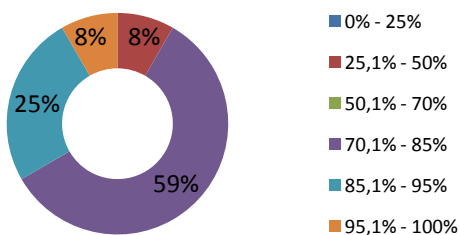
Question 1: State



Question 2: Morphology



Question 3: Distribution of the subjective homogeneity



Chemical composition:

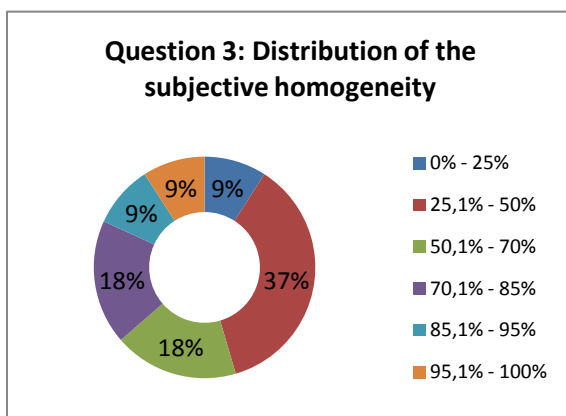
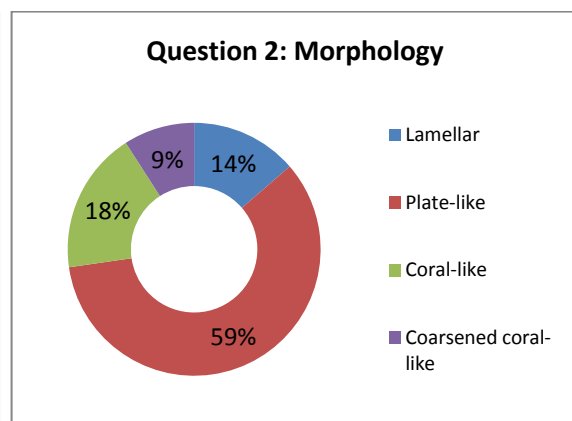
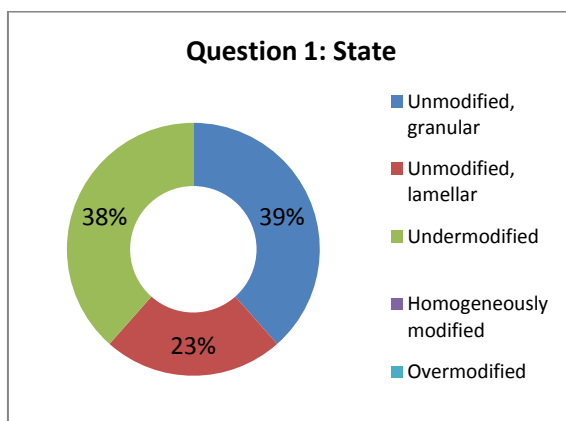
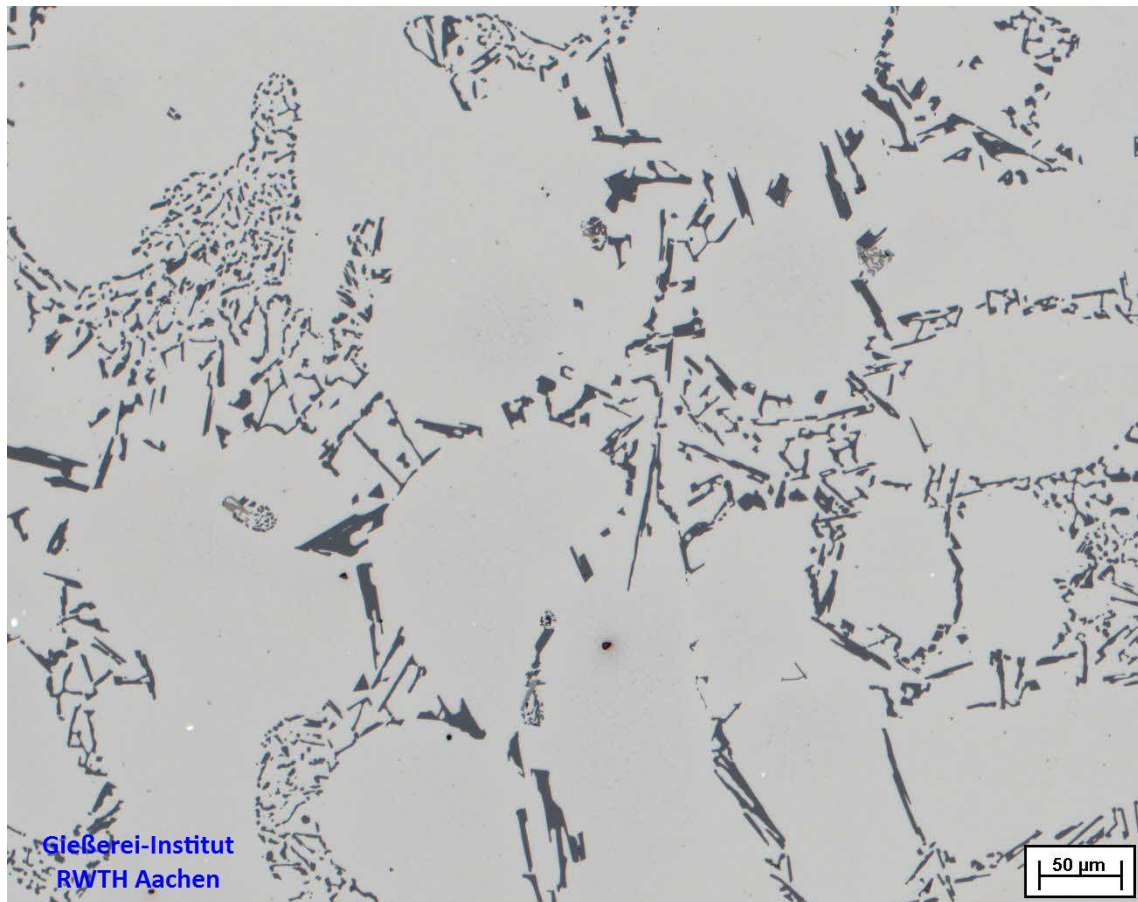
Al - 7 wt.% Si - 0.3wt.% Mg - 250 ppm Sr - 5 ppm P

Casting process: **Triplex D30**

Subjective homogeneity: **(82 ± 12) %**

Objective classification, degree of mod. (*M*):

Modified, Inhomogeneous, *M* = 84 %



Chemical composition:

Al - 7 wt.% Si - 0.3wt.% Mg - 250 ppm Sr - 400 ppm Fe

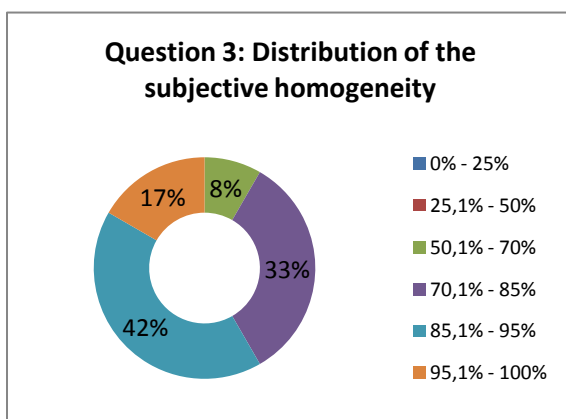
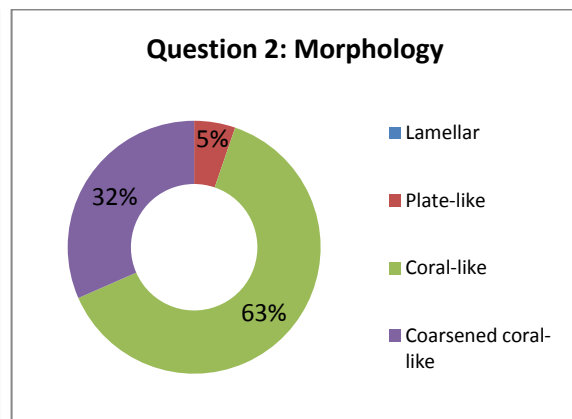
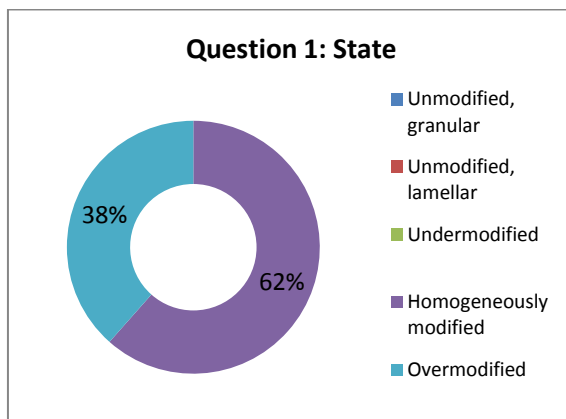
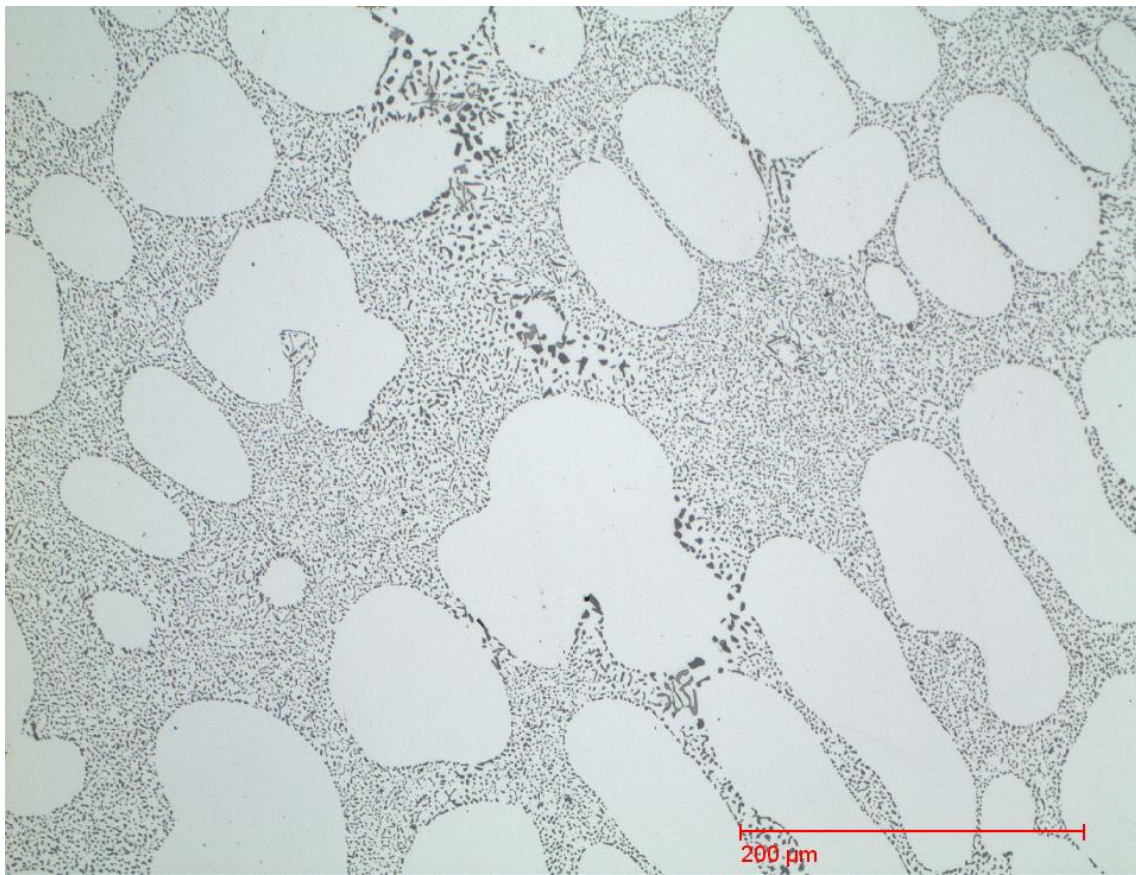
Casting process: **Triplex D90**

Subjective homogeneity: **(58 ± 27) %**

Objective classification, degree of mod. (*M*):

Modified, Inhomogeneous, *M* = 13 %

Micrograph No. 11:



Chemical composition:

Al - 7 wt.% Si - 250 ppm Sr - 4 ppm P -290 ppm Fe

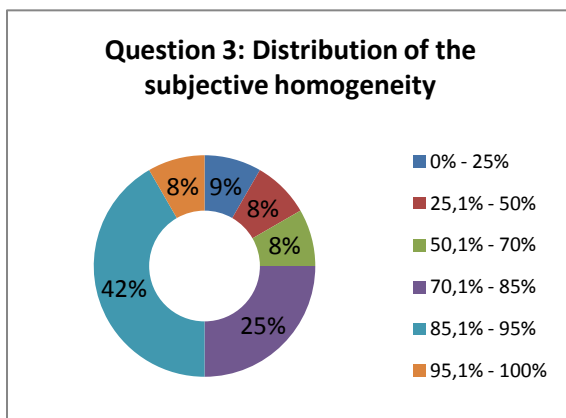
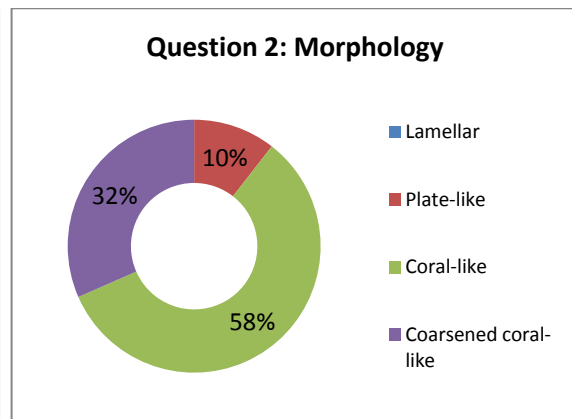
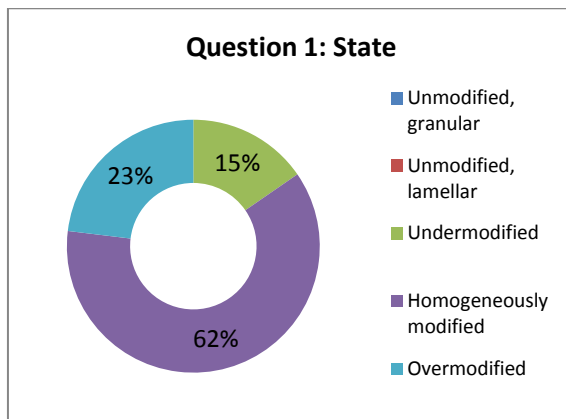
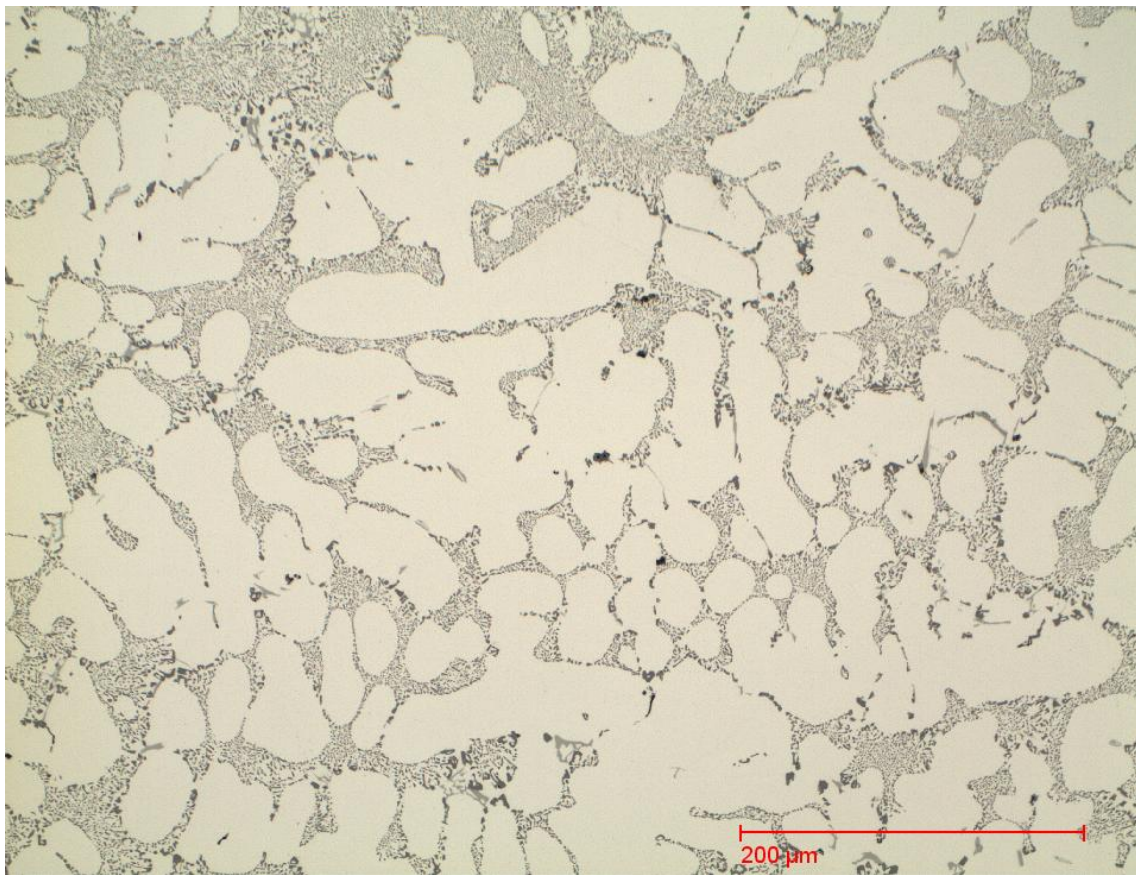
Casting process: **Sand mould**

Subjective homogeneity: **(89 ± 10) %**

Objective classification, degree of mod. (*M*):

Modified, Homogeneous, *M* = 99 %

Micrograph No. 12:



Chemical composition:

Al - 7 wt.% Si - 0.3wt.% Mg - 200 ppm Sr - 5 ppm P - 800 ppm Fe

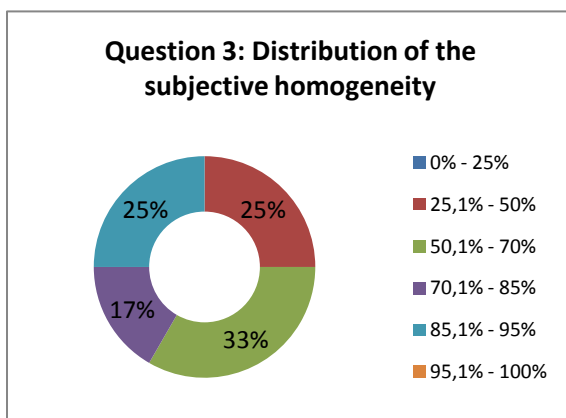
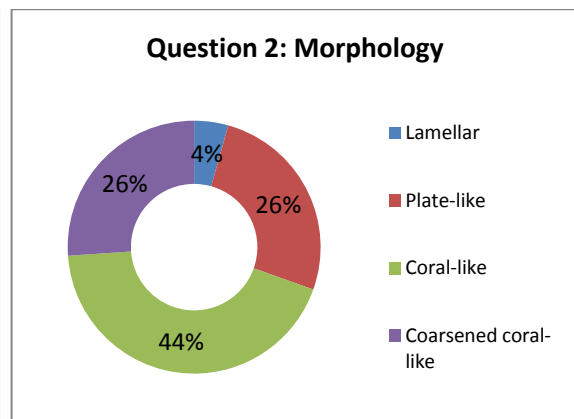
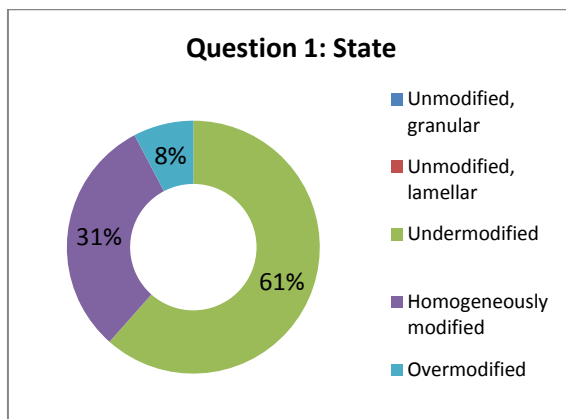
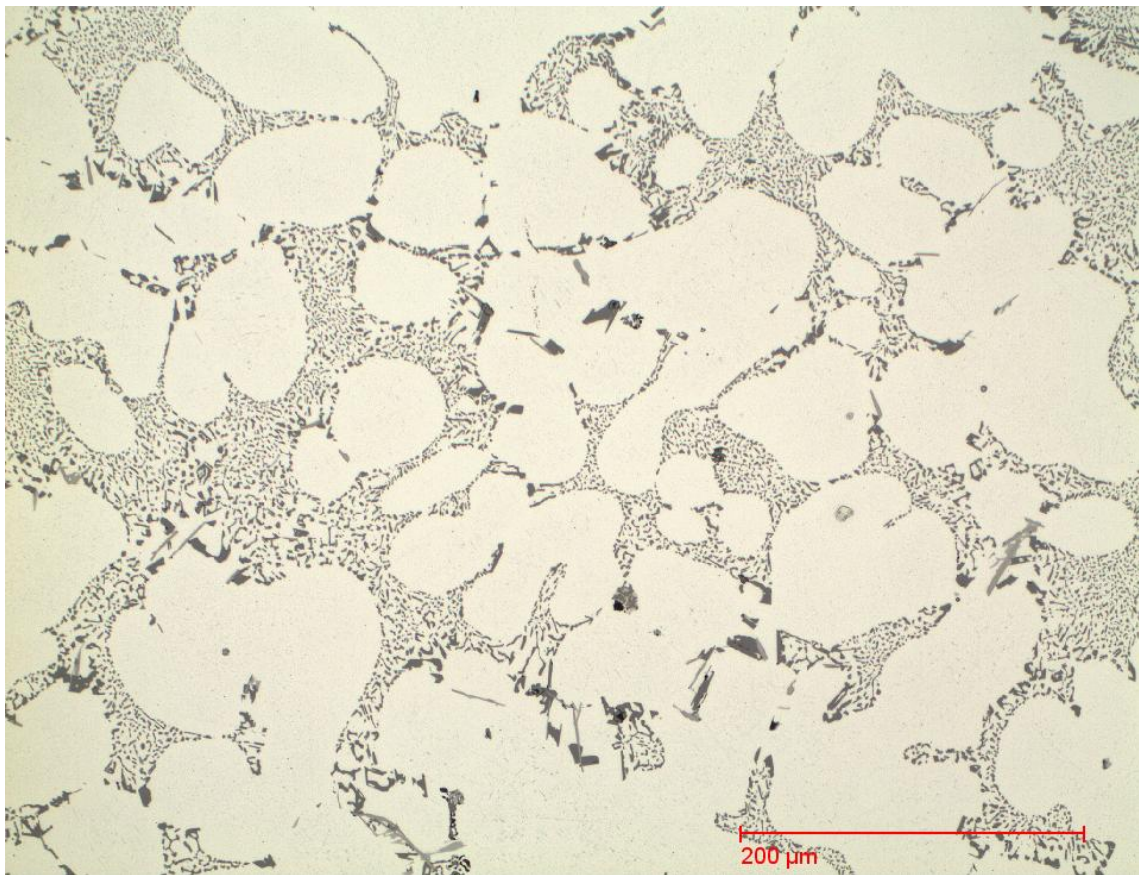
Casting process: **Technical**

Subjective homogeneity: **(78 ± 24) %**

Objective classification, degree of mod. (*M*):

Resolution too low for quantitative analysis

Micrograph No. 13:



Chemical composition:

Al - 7 wt.% Si - 0.3wt.% Mg - 300 ppm Sr - 8 ppm P - 1200 ppm Fe

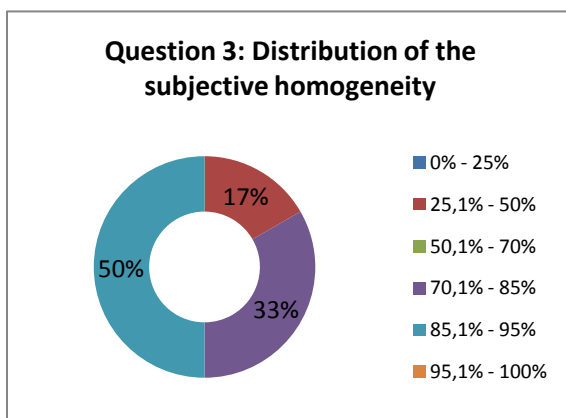
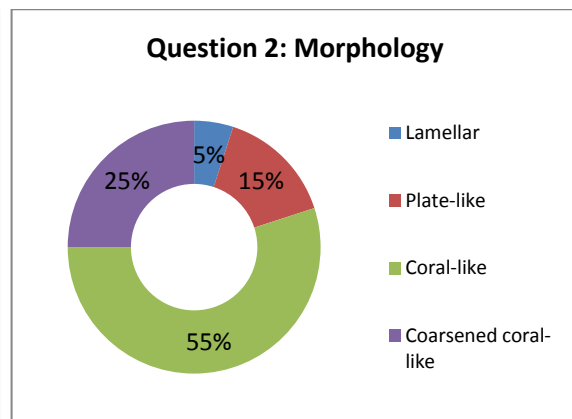
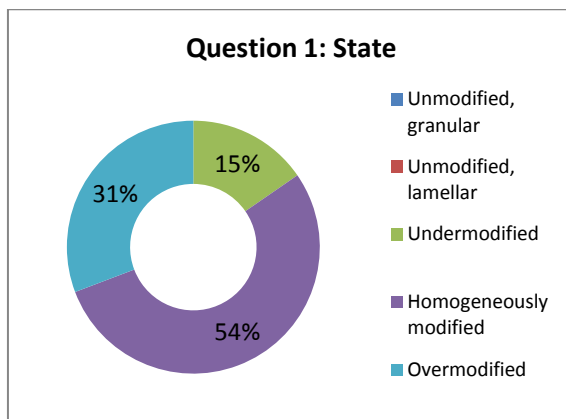
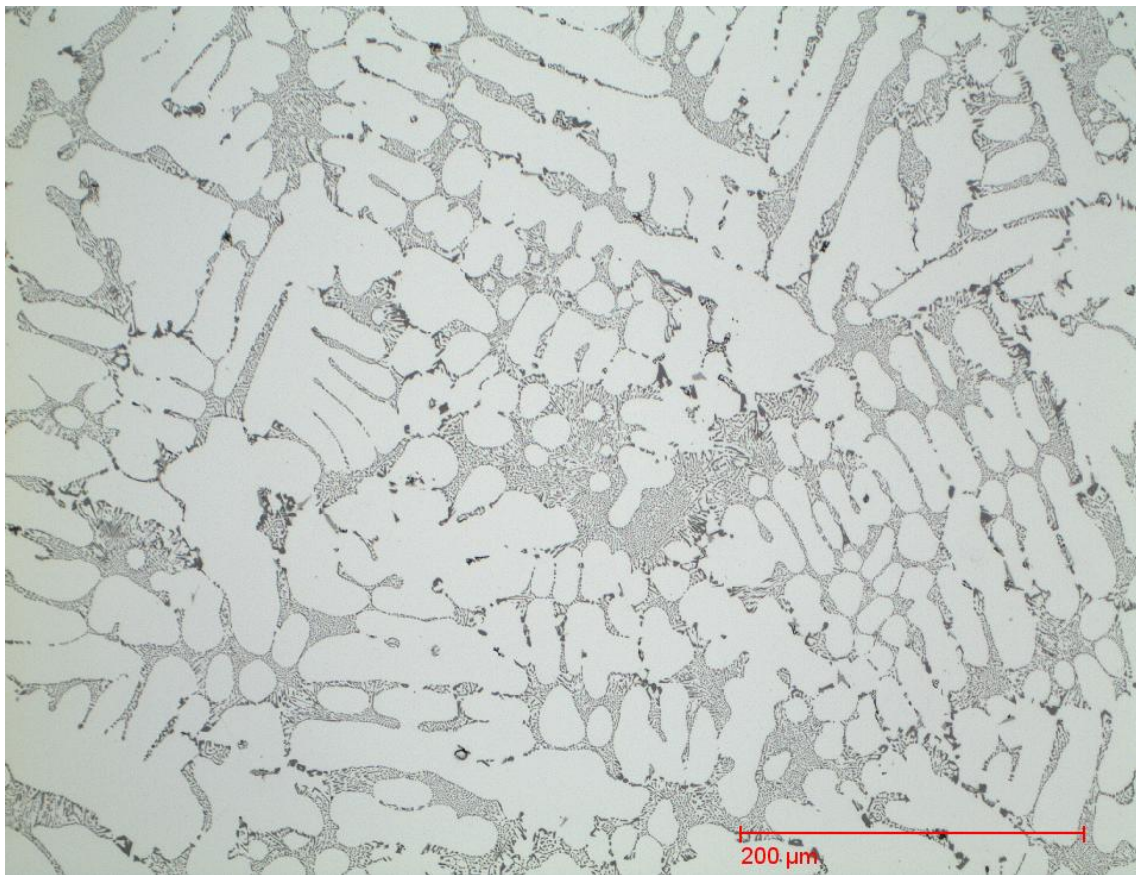
Casting process: **Ingot**

Subjective homogeneity: **(69 ± 18) %**

Objective classification, degree of mod. (*M*):

Modified, Inhomogeneous, *M* = 59 %

Micrograph No. 14:



Chemical composition:

Al - 7 wt.% Si - 0.3wt.% Mg - 90 ppm Sr - 8 ppm P - 260 ppm Fe

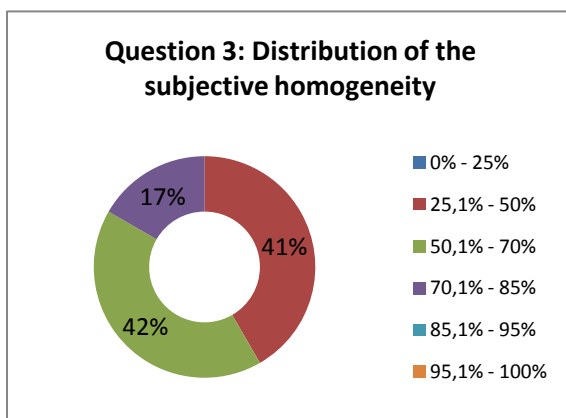
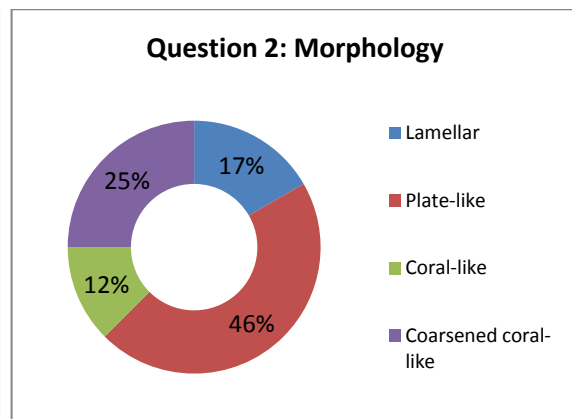
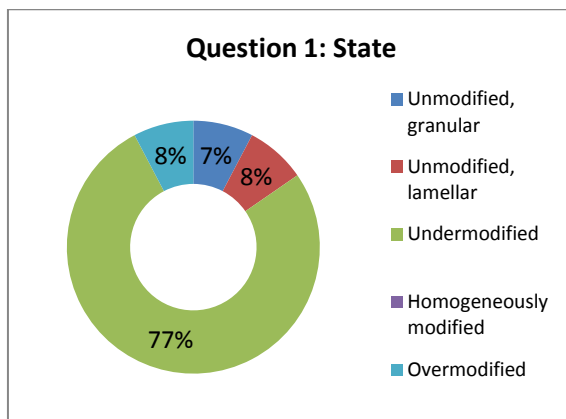
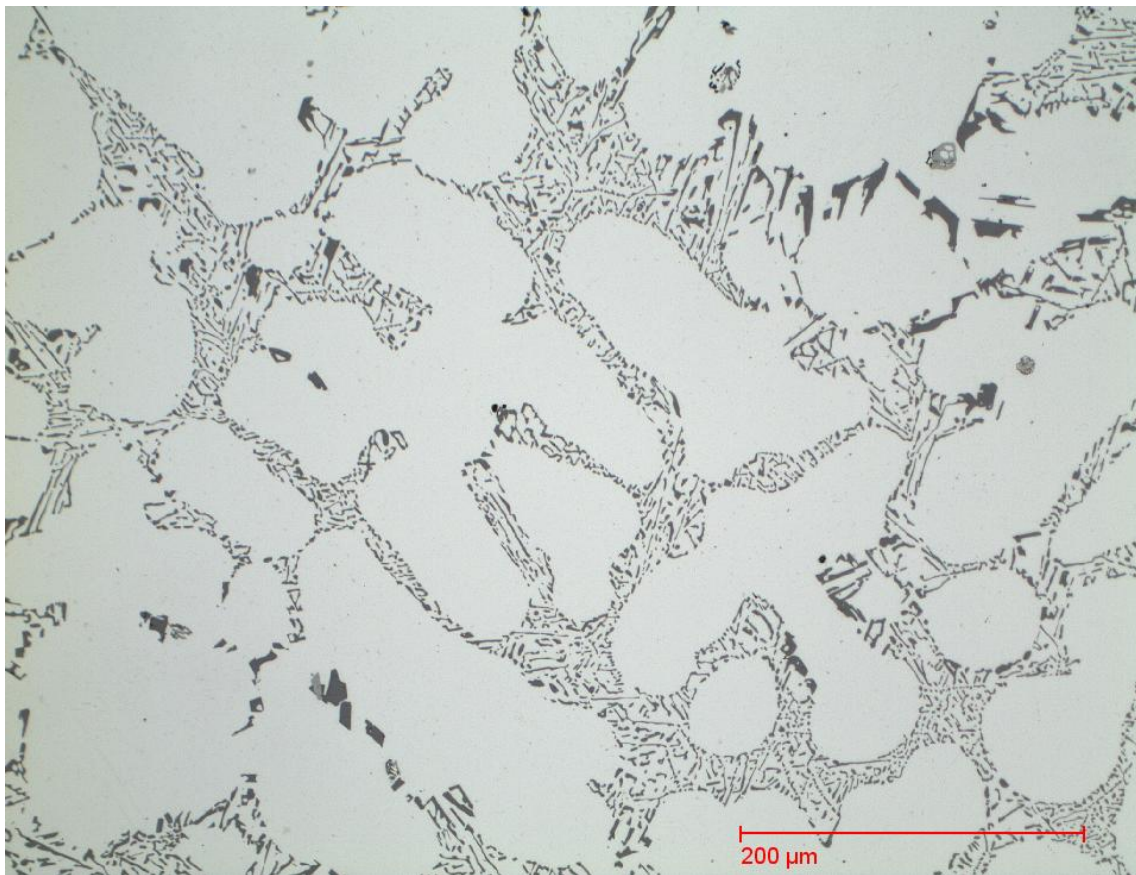
Casting process: **Metal mould**

Subjective homogeneity: **(79 ± 19) %**

Objective classification, degree of mod. (*M*):

Resolution too low for quantitative analysis

Micrograph No. 15:



Chemical composition:

Al - 7 wt.% Si - 0.3wt.% Mg - 90 ppm Sr - 8 ppm P - 260 ppm Fe

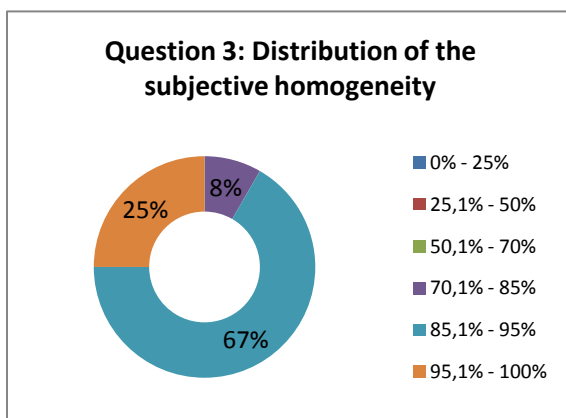
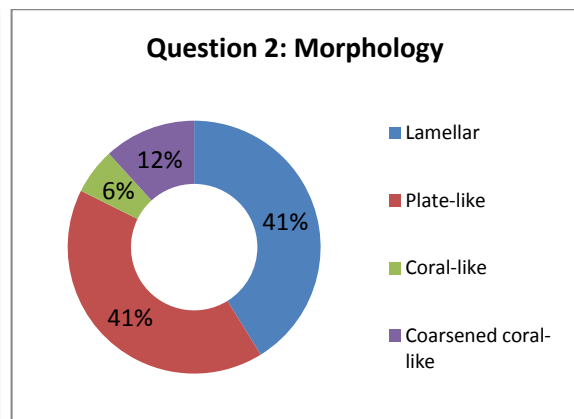
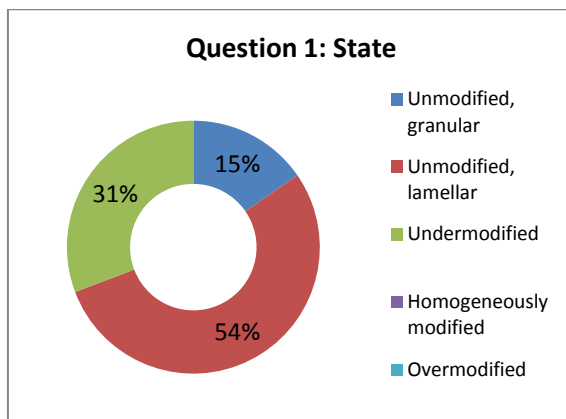
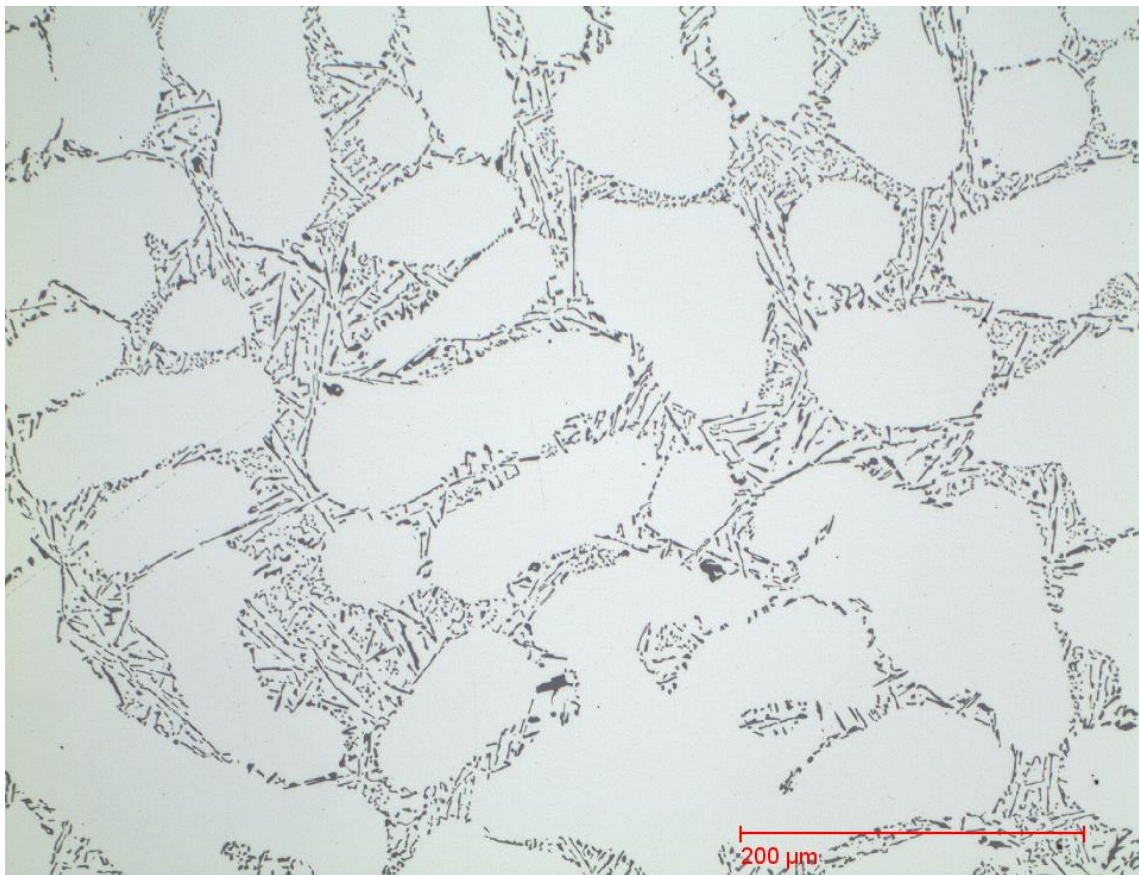
Casting process: **Sand mould**

Subjective homogeneity: **(60 ± 14) %**

Objective classification, degree of mod. (*M*):

Modified, Inhomogeneous, *M* = 58 %

Micrograph No. 16:



Chemical composition:

Al - 7 wt.% Si - 100 ppm Sr - 6 ppm P - 290 ppm Fe

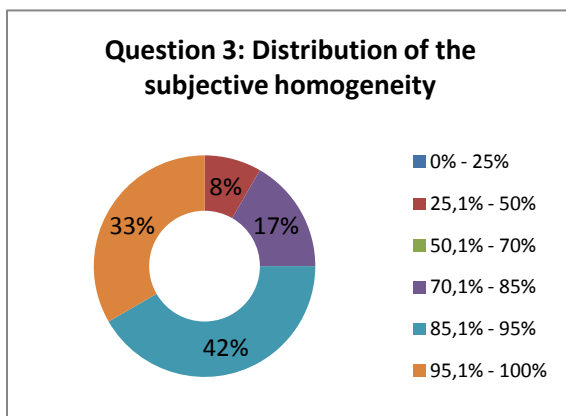
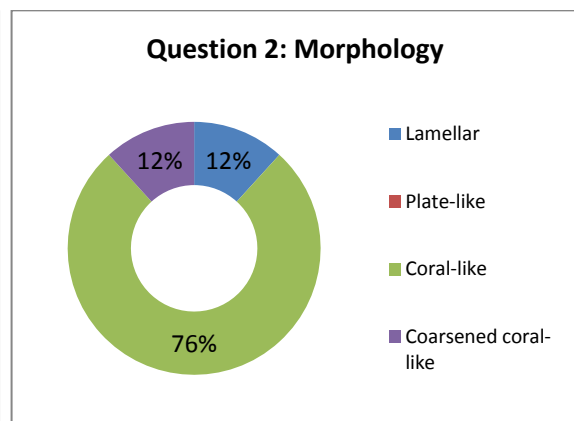
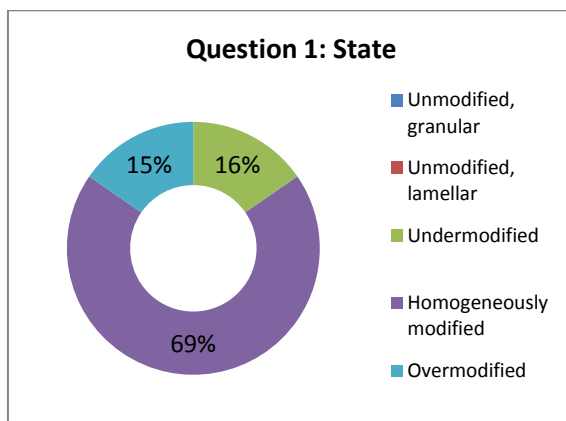
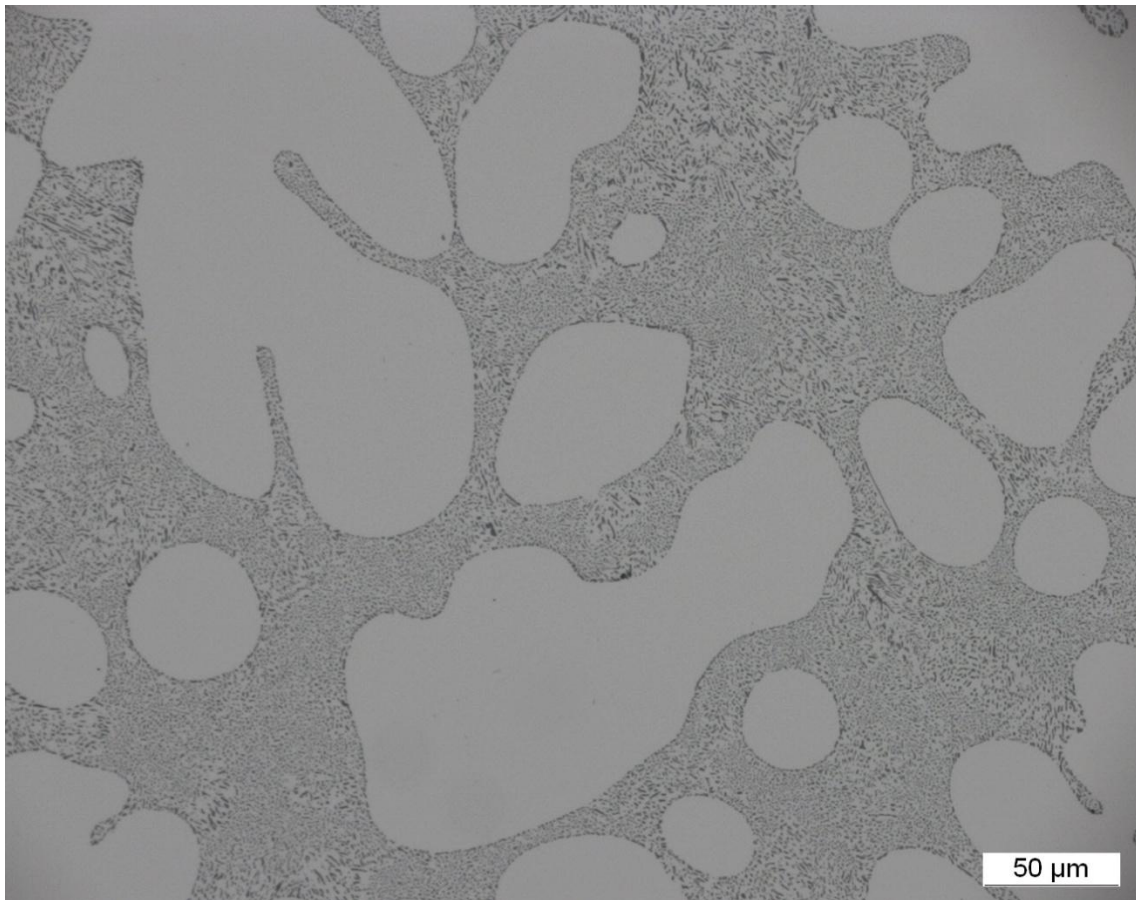
Casting process: **Sand mould**

Subjective homogeneity: **(93 ± 5) %**

Objective classification, degree of mod. (*M*):

Modified, Inhomogeneous, *M* = 81 %

Micrograph No. 17:



Chemical composition:

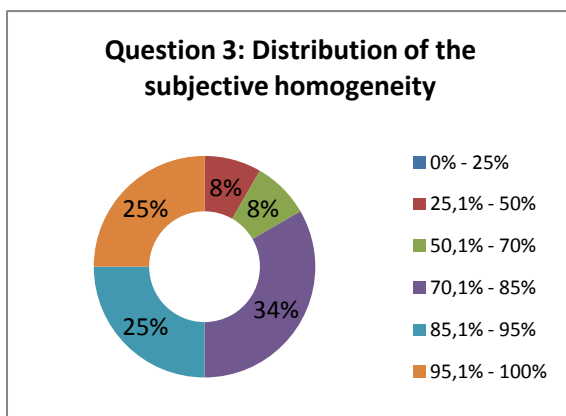
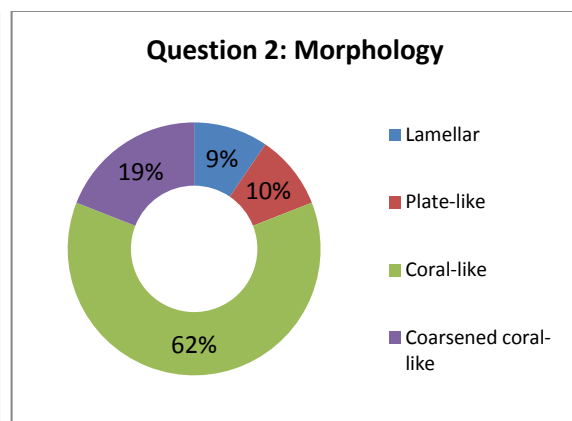
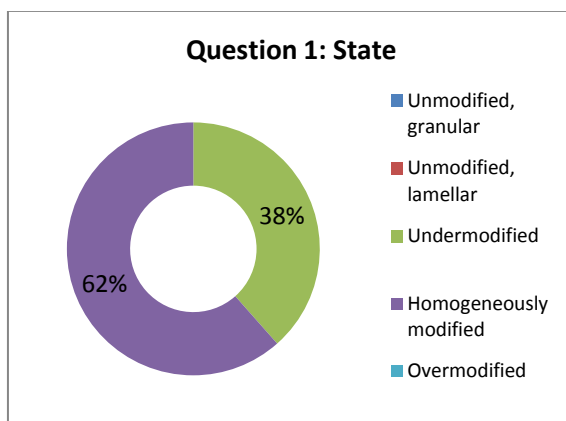
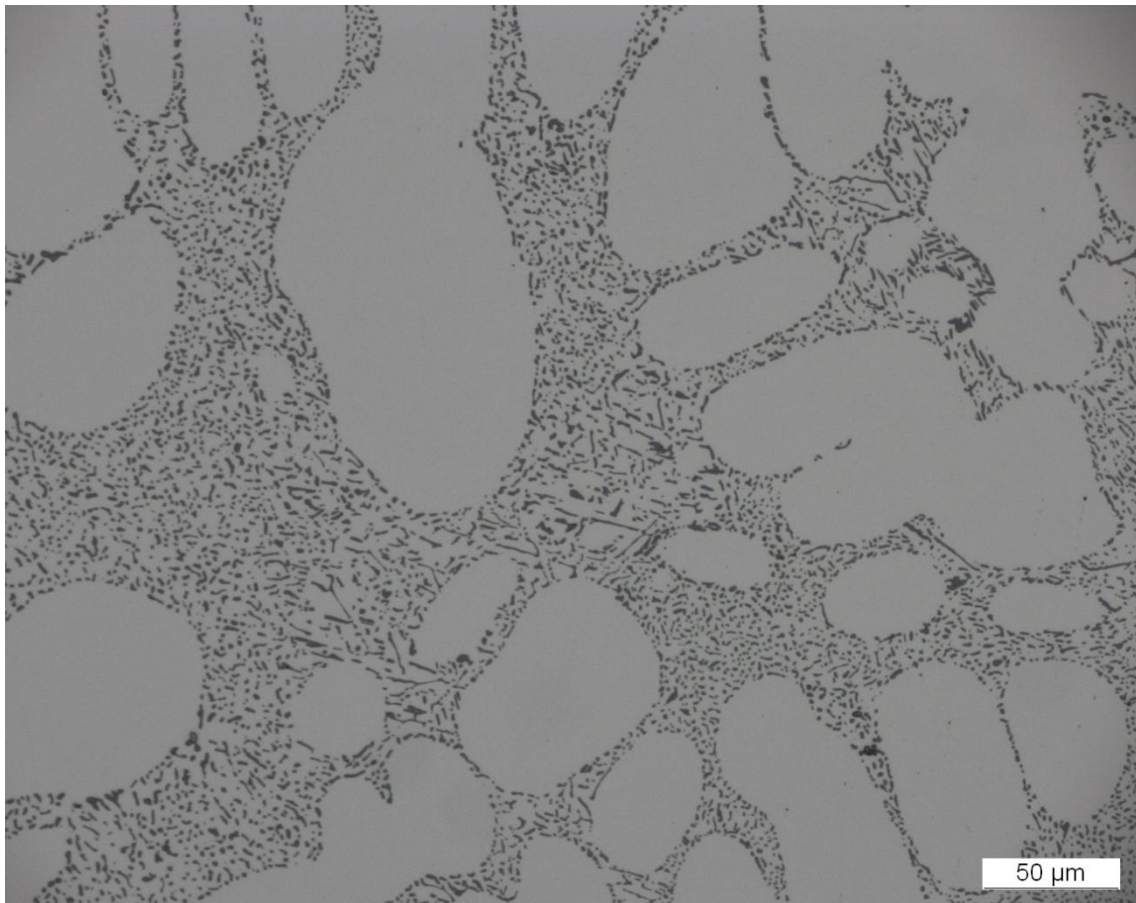
Al - 7 wt.% Si - 50 ppm Sr - 2.5 ppm P

Casting process: **Triplex D30**

Subjective homogeneity: **(89 ± 14) %**

Objective classification, degree of mod. (*M*):

Modified, Homogeneous, *M* = 100 %



Chemical composition:

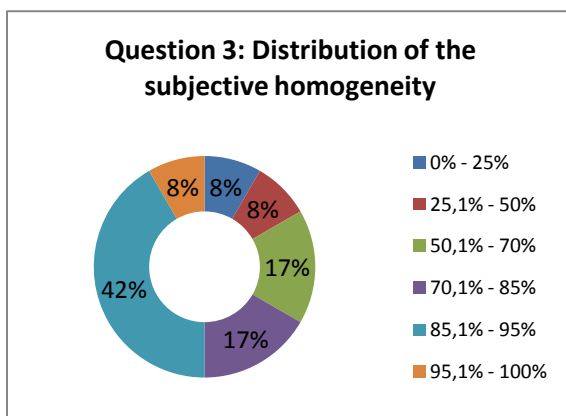
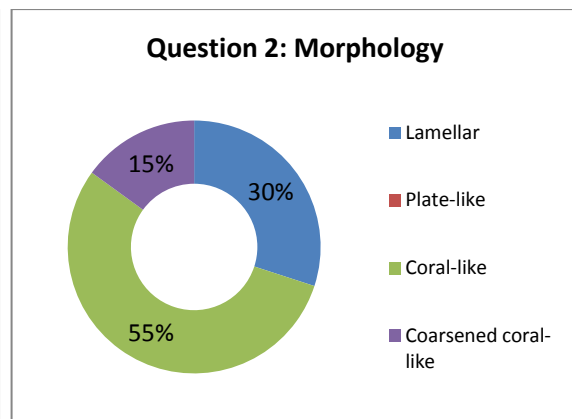
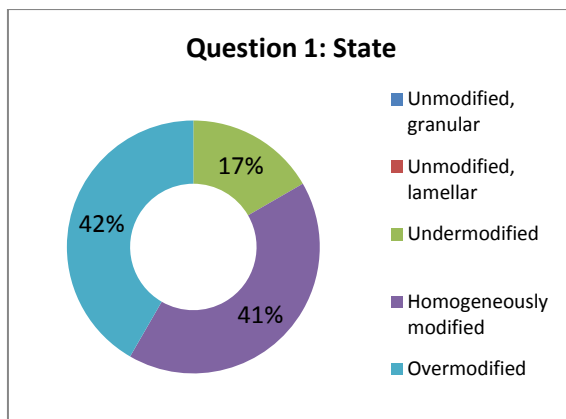
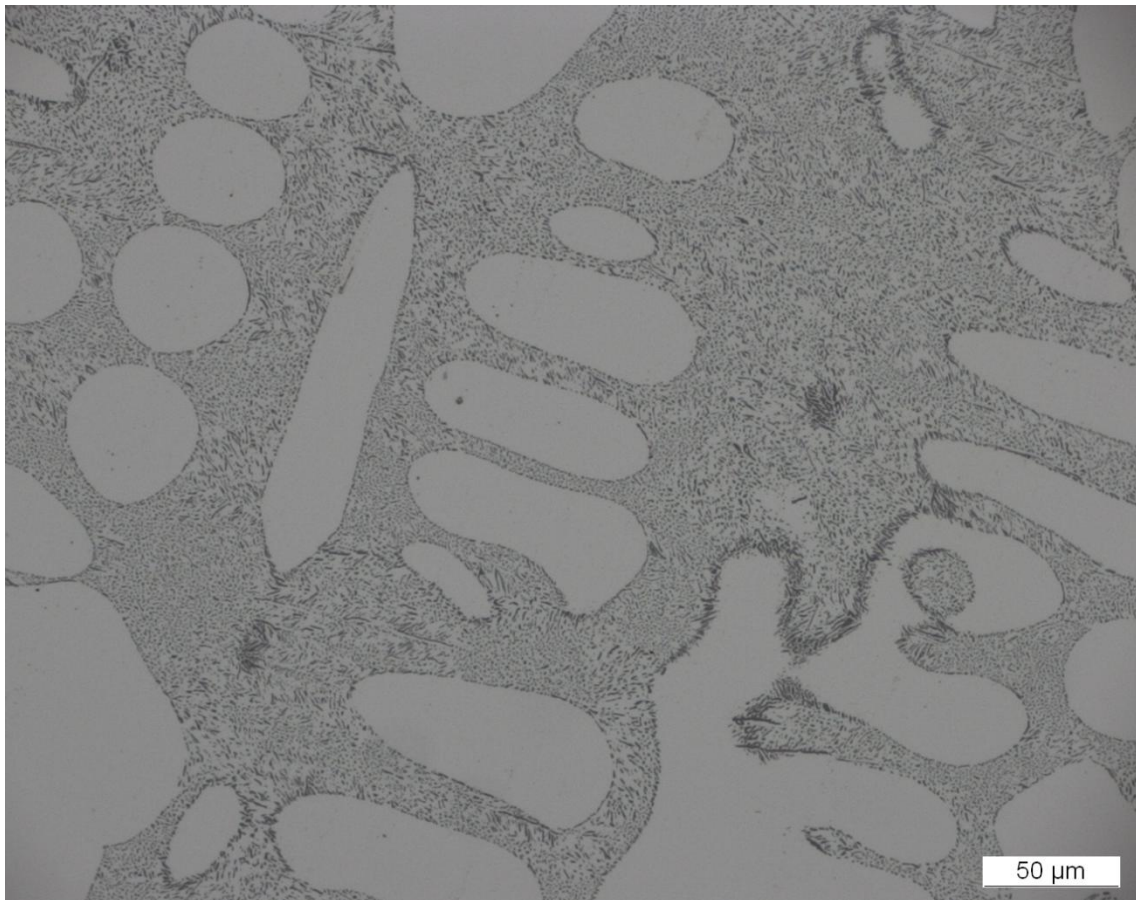
Al - 7 wt.% Si - 50 ppm Sr - 400 ppm Fe

Casting process: **Triplex D30**

Subjective homogeneity: **(84 ± 14) %**

Objective classification, degree of mod. (*M*):

Modified, Homogeneous, *M* = 99 %



Chemical composition:

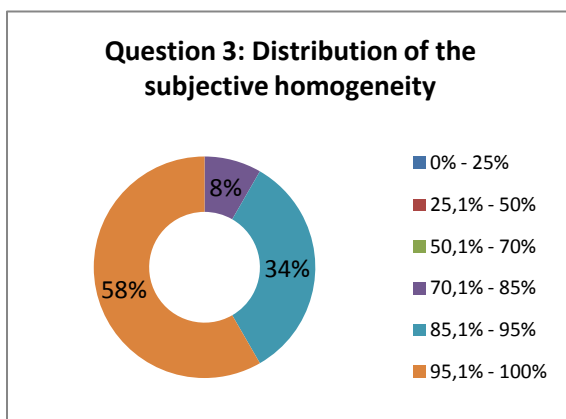
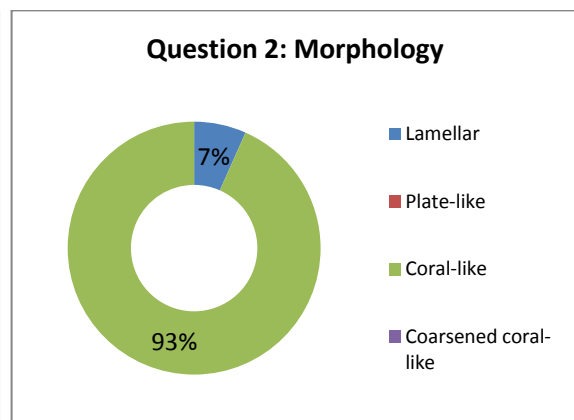
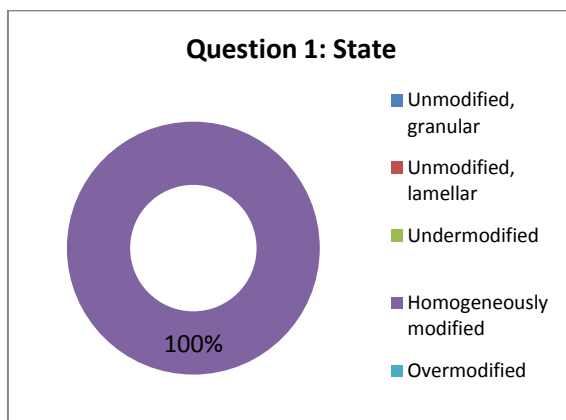
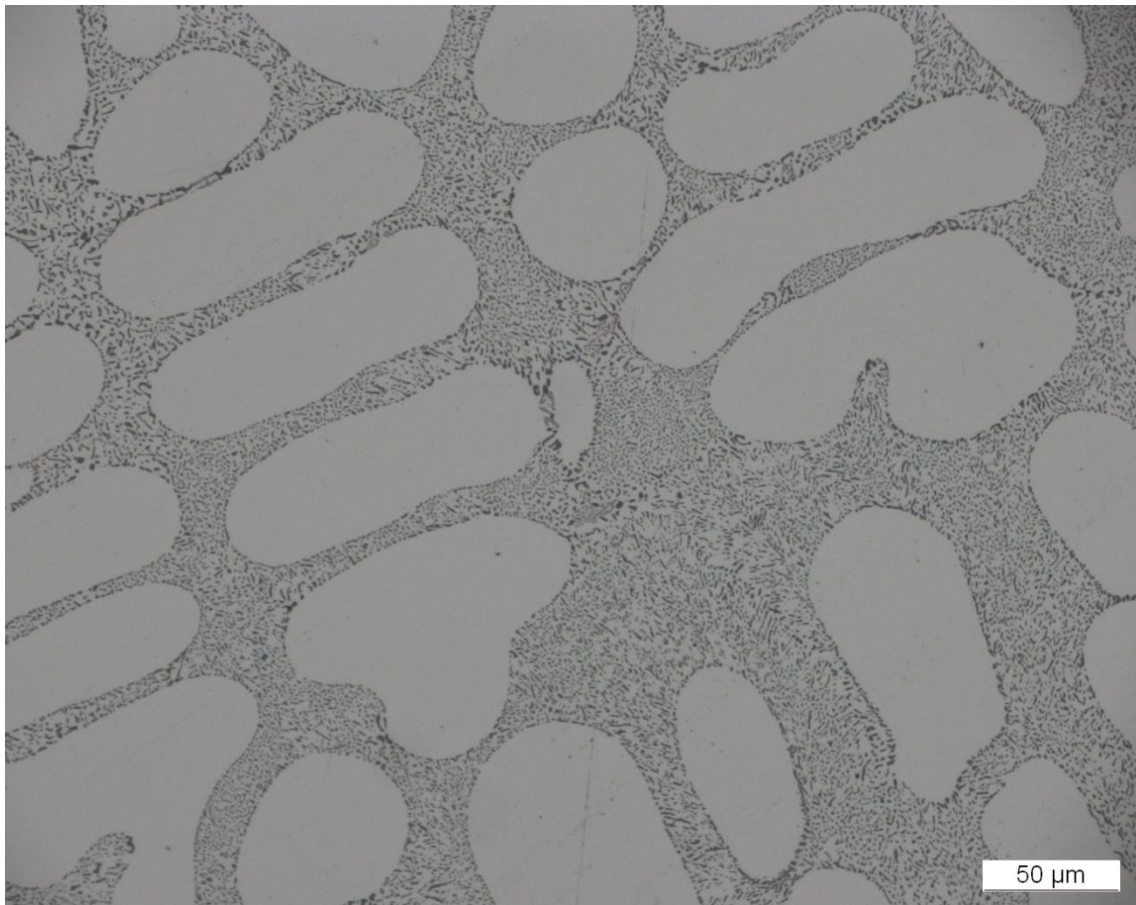
Al - 7 wt.% Si - 100 ppm Sr - 2.5 ppm P

Casting process: **Triplex D30**

Subjective homogeneity: **(75 ± 24) %**

Objective classification, degree of mod. (*M*):

Modified, Homogeneous, *M* = 98 %



Chemical composition:

Al - 7 wt.% Si – 100 ppm Sr – 400 ppm Fe

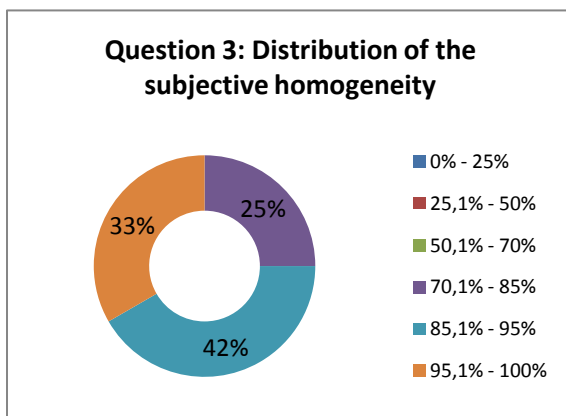
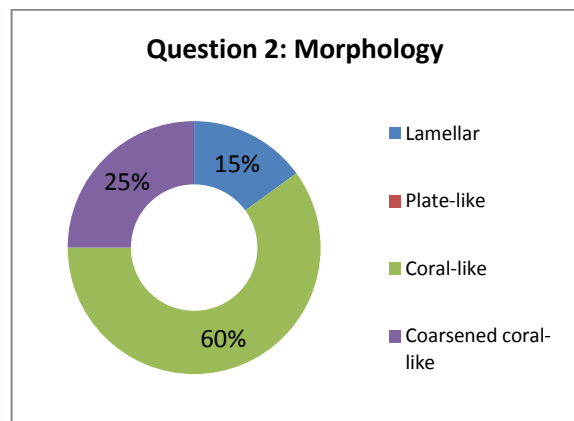
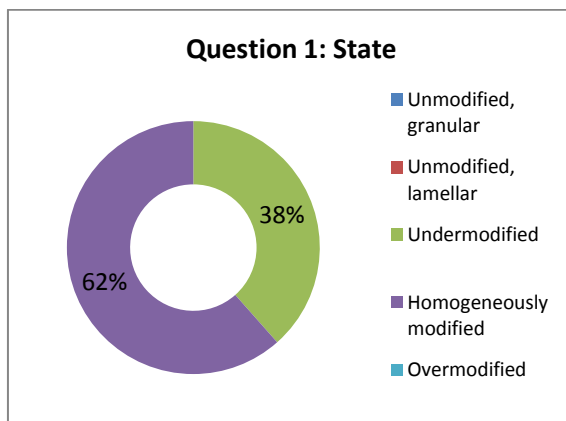
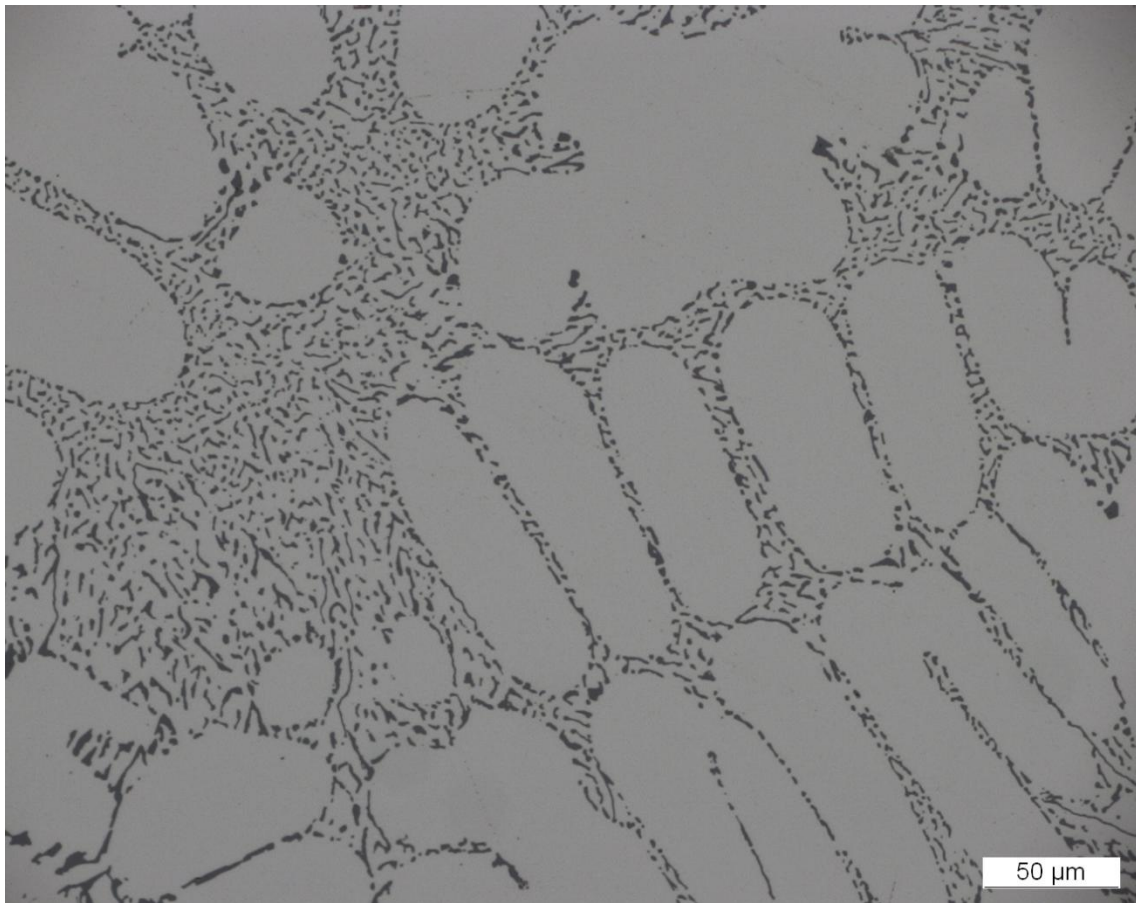
Casting process: **Triplex D30**

Subjective homogeneity: **(95 ± 7) %**

Objective classification, degree of mod. (*M*):

Modified, Homogeneous, *M* = 98 %

Micrograph No. 21:



Chemical composition:

Al - 7 wt.% Si – 100 ppm Sr – 800 ppm Fe

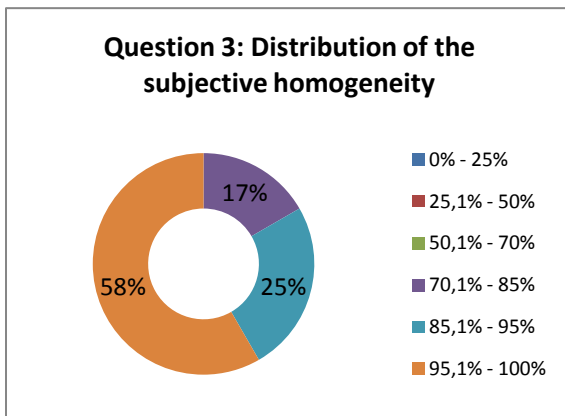
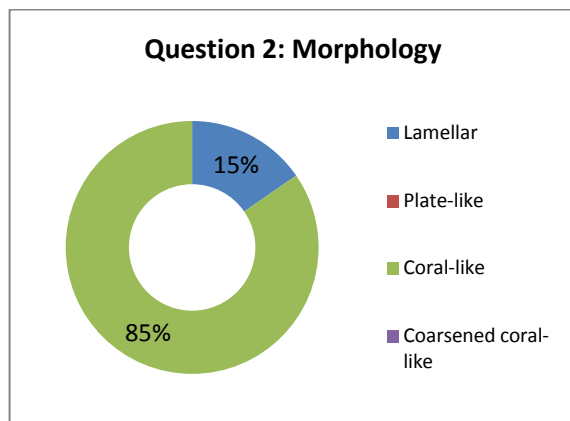
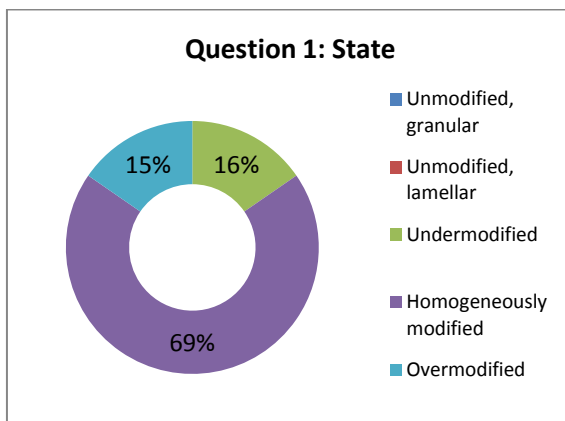
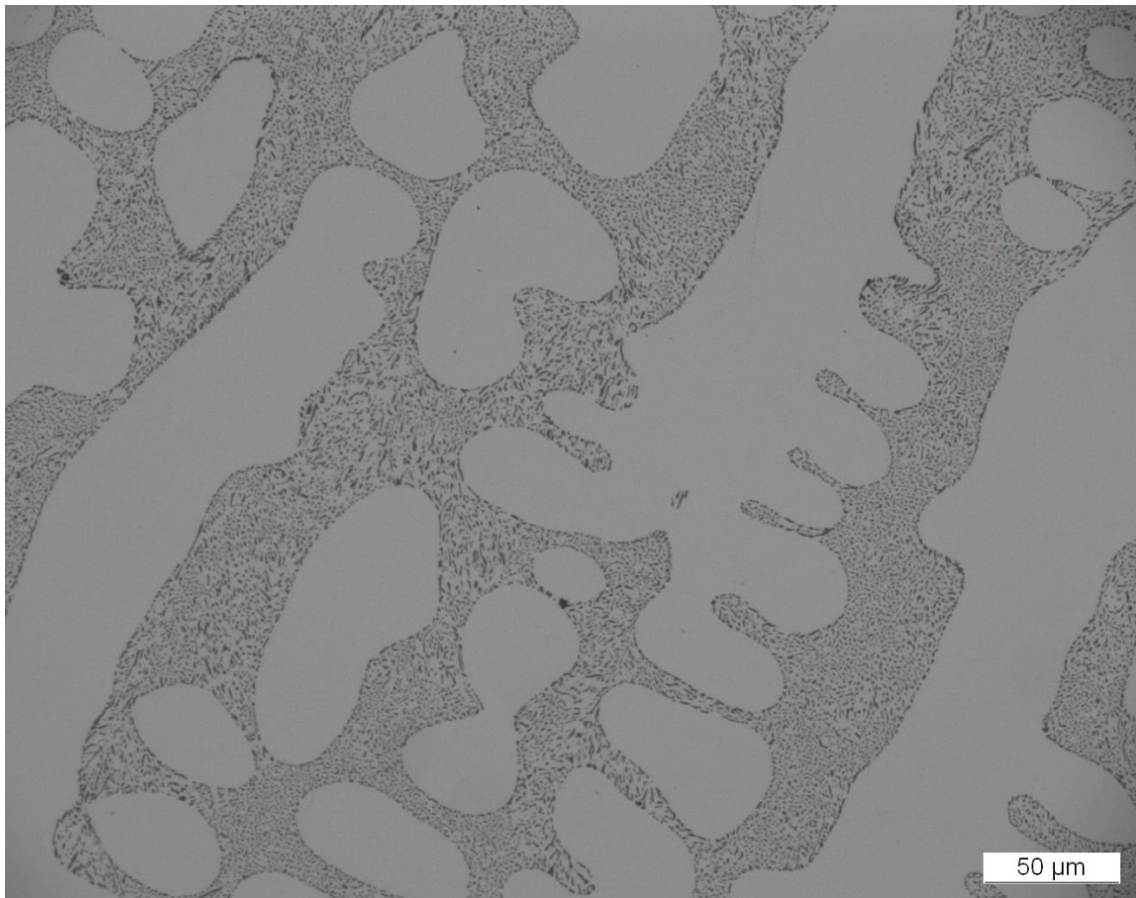
Casting process: **Triplex D30**

Subjective homogeneity: **(92 ± 7) %**

Objective classification, degree of mod. (*M*):

Modified, Inhomogeneous, *M* = 95 %

Micrograph No. 22:



Chemical composition:

Al - 7 wt.% Si - 100 ppm Sr - 5 ppm P

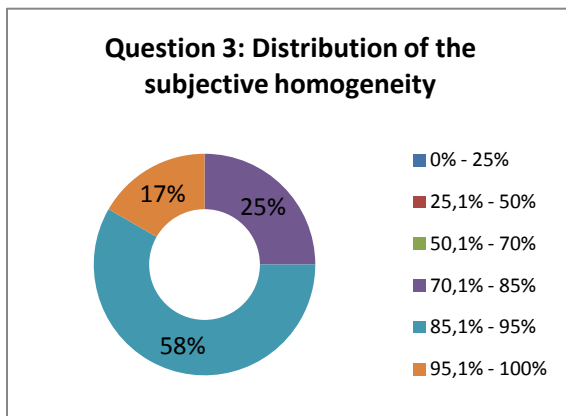
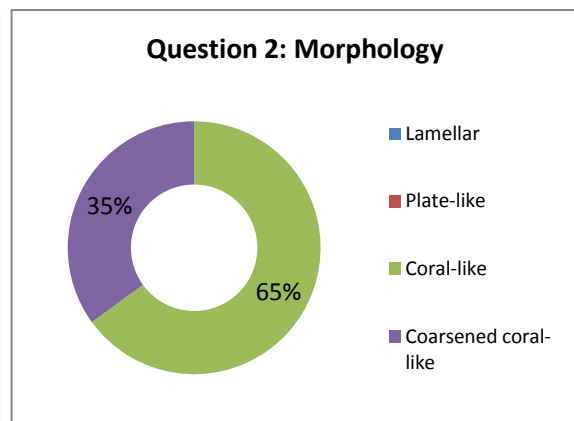
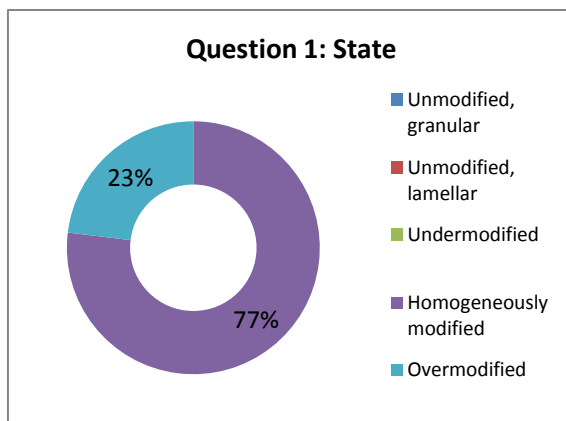
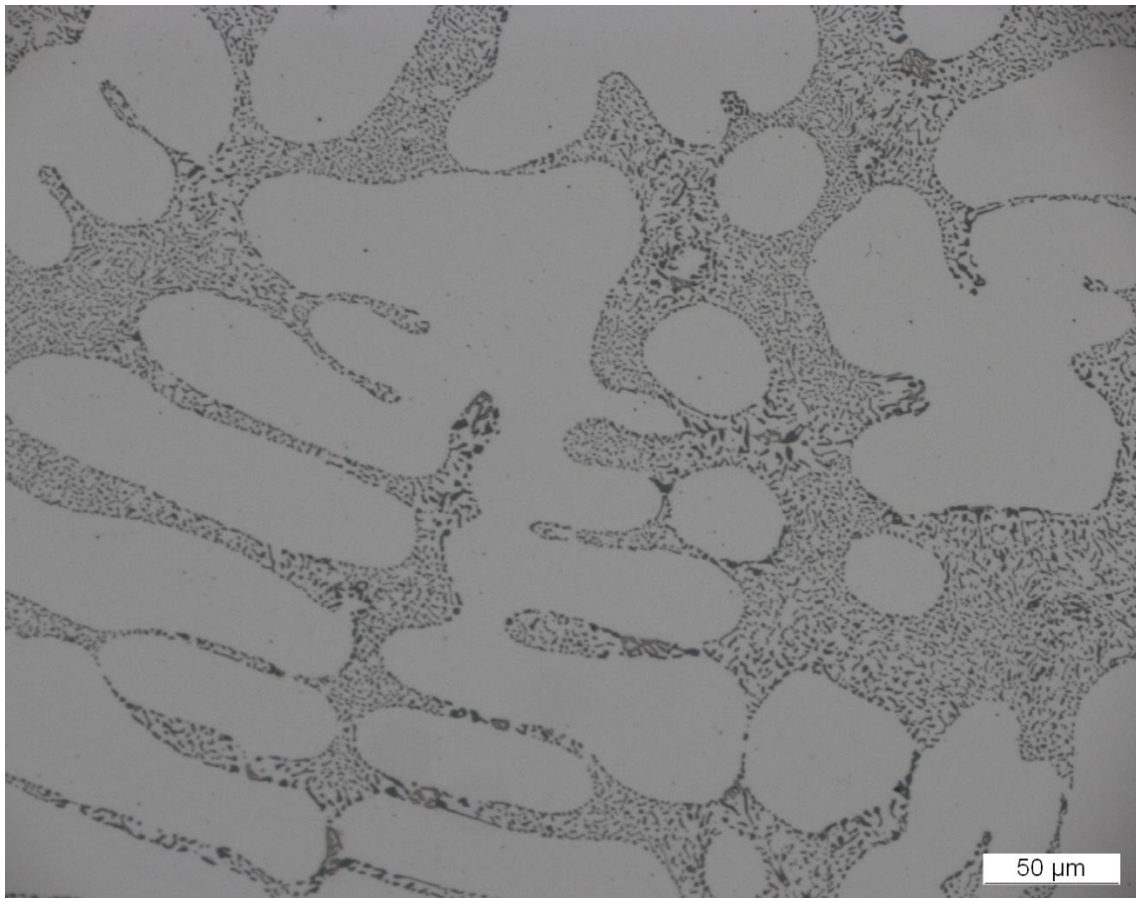
Casting process: **Triplex D30**

Subjective homogeneity: **(95 ± 7) %**

Objective classification, degree of mod. (*M*):

Modified, Homogeneous, *M* = 99 %

Micrograph No. 23:



Chemical composition:

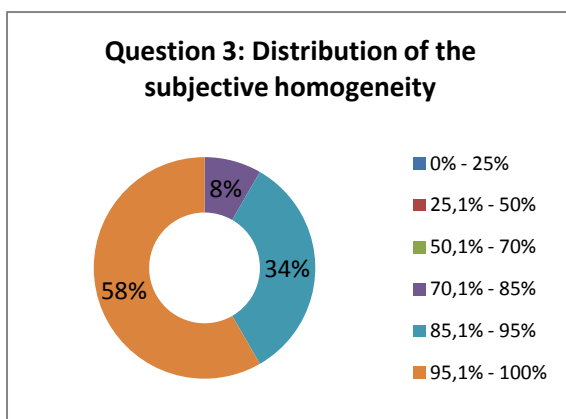
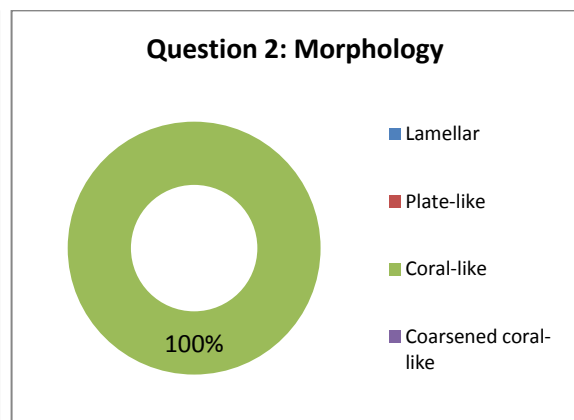
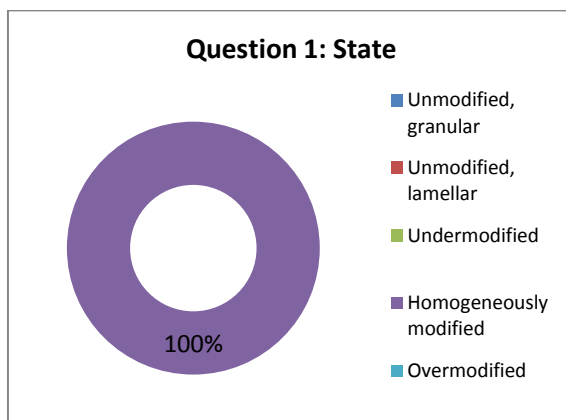
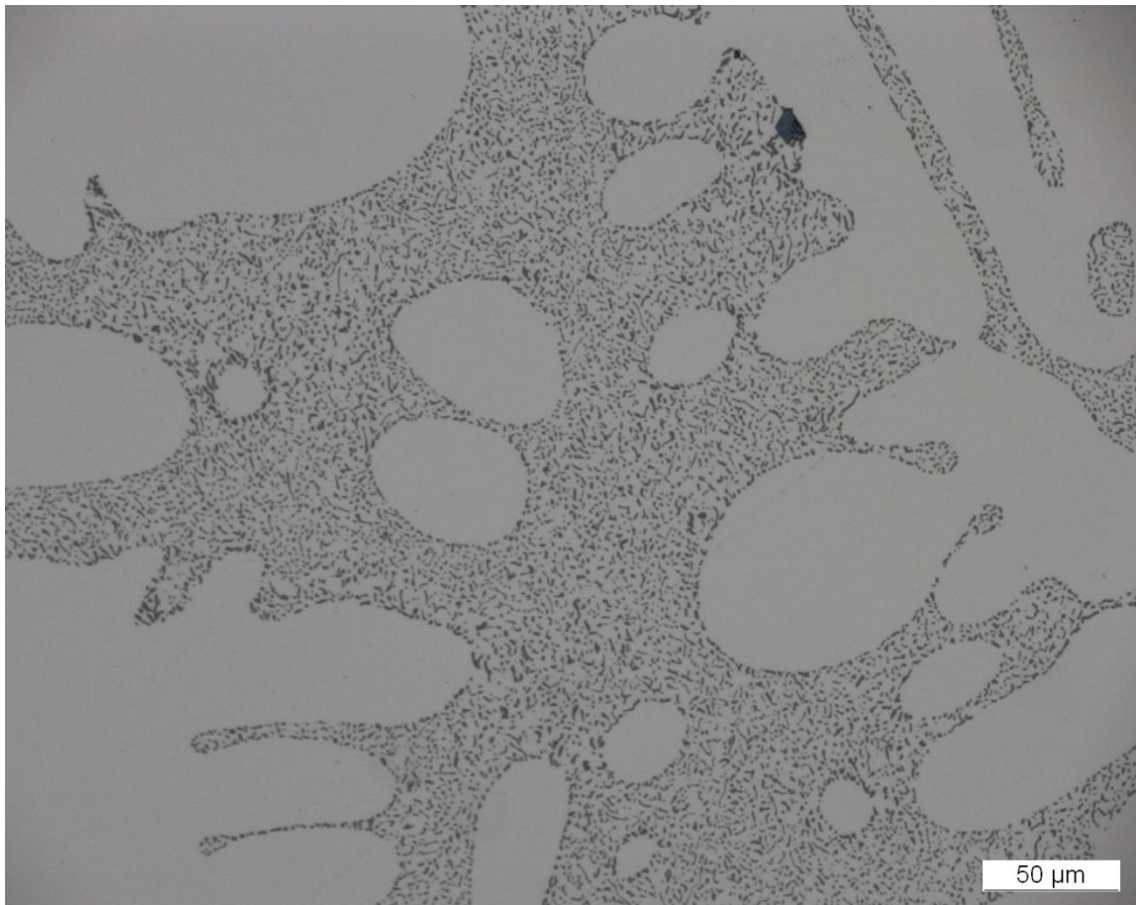
Al - 7 wt.% Si - 250 ppm Sr - 2.5 ppm P - 800 ppm Fe

Casting process: **Triplex D30**

Subjective homogeneity: **(91 ± 7) %**

Objective classification, degree of mod. (*M*):

Modified, Inhomogeneous, *M* = 94 %



Chemical composition:

Al - 7 wt.% Si – 250 ppm Sr

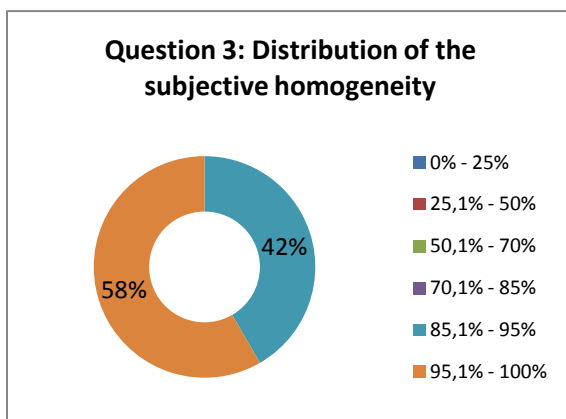
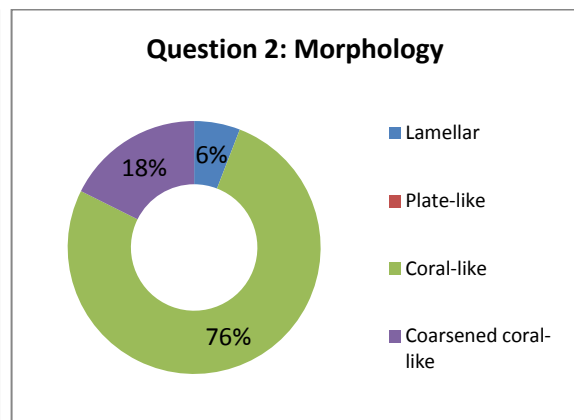
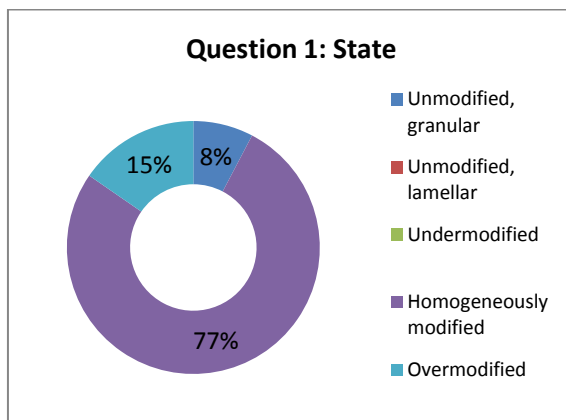
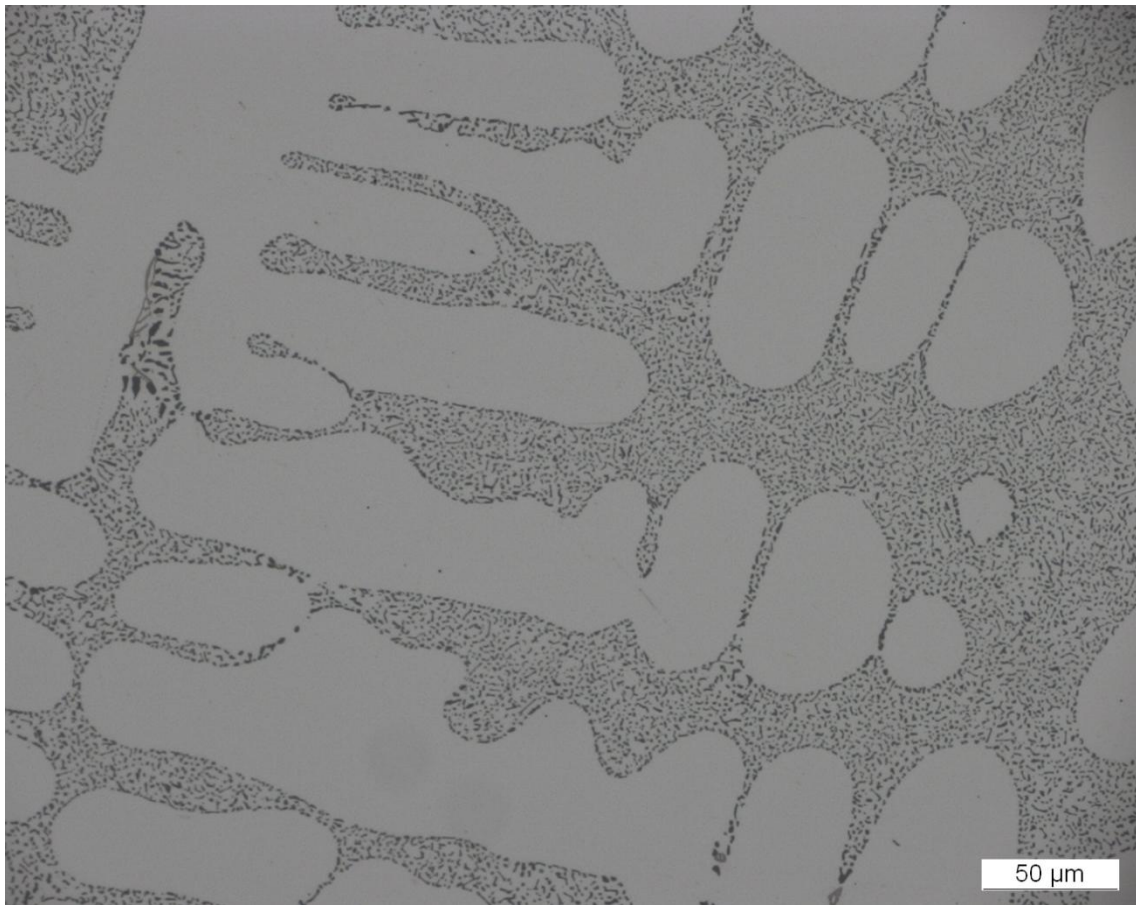
Casting process: **Triplex D30**

Subjective homogeneity: $(96 \pm 7) \%$

Objective classification, degree of mod. (*M*):

Modified, Homogeneous, $M = 100 \%$

Micrograph No. 25:



Chemical composition:

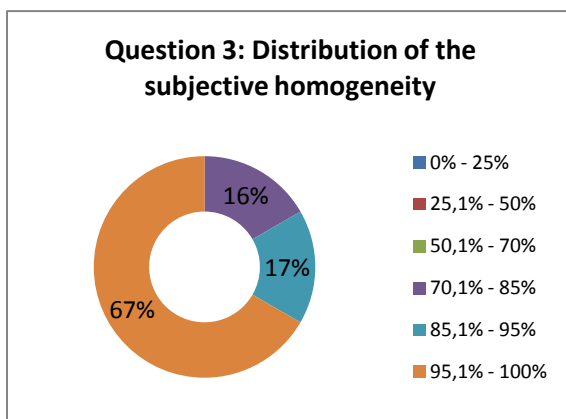
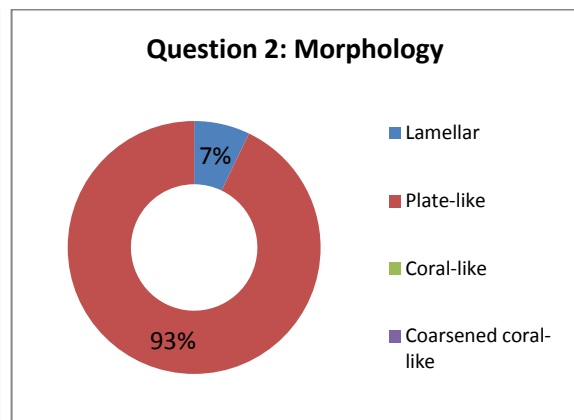
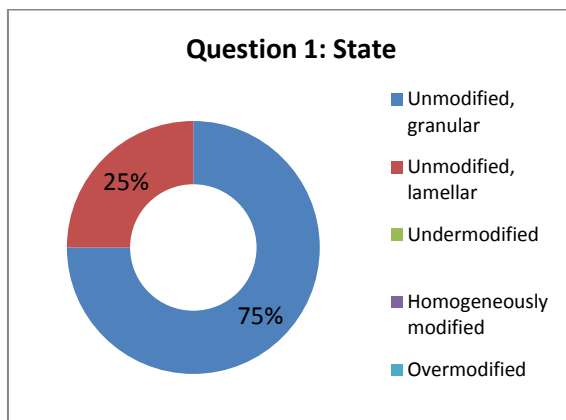
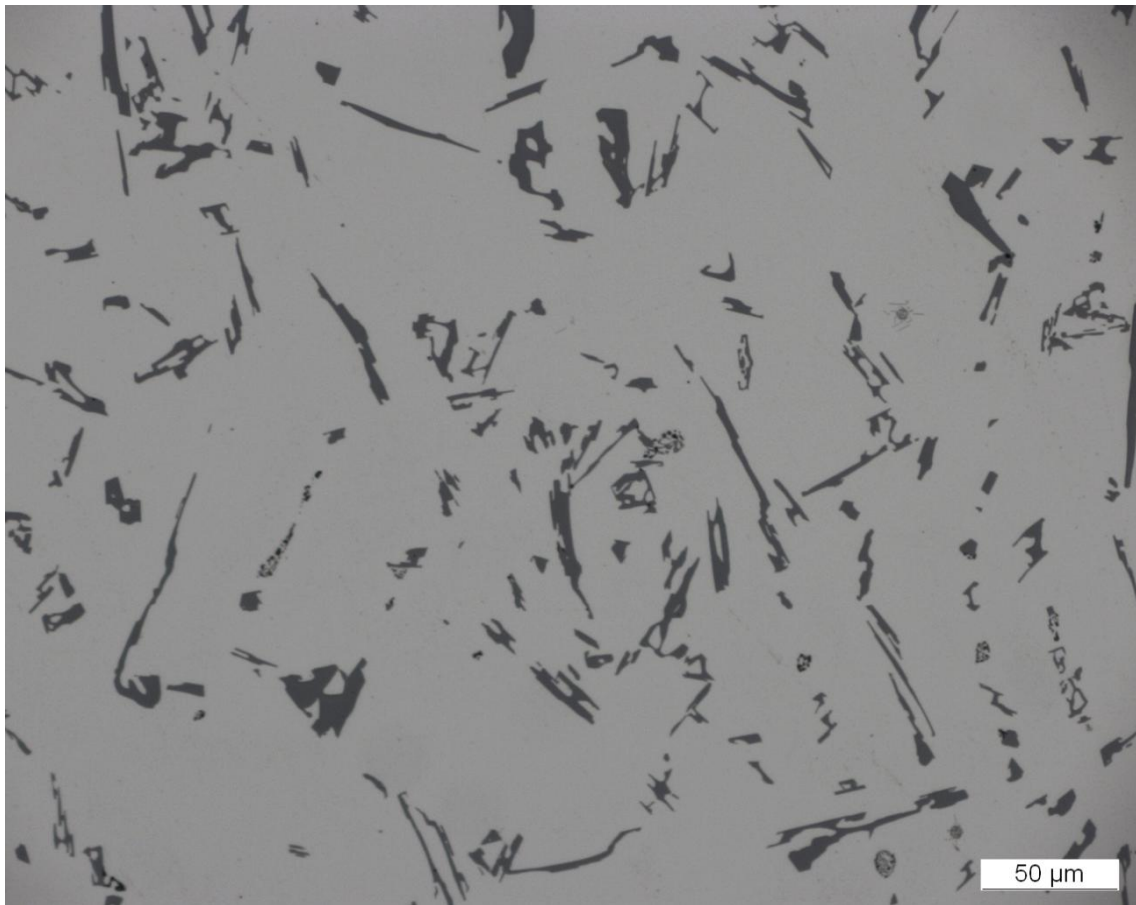
Al - 7 wt.% Si - 250 ppm Sr - 5 ppm P - 400 ppm Fe

Casting process: **Triplex D30**

Subjective homogeneity: **(97 ± 3) %**

Objective classification, degree of mod. (*M*):

Modified, Homogeneous, *M* = 100 %



Chemical composition:

Al - 7 wt.% Si - 0.3wt.% Mg - 5 ppm P

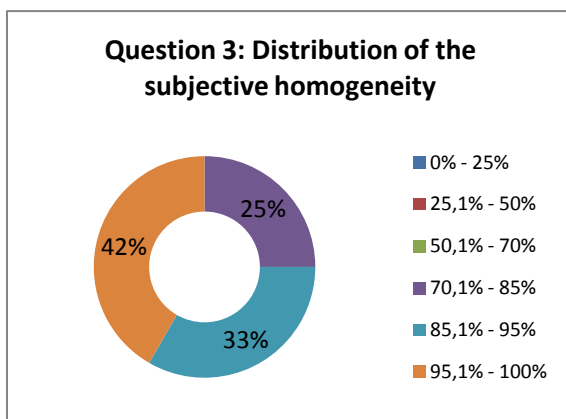
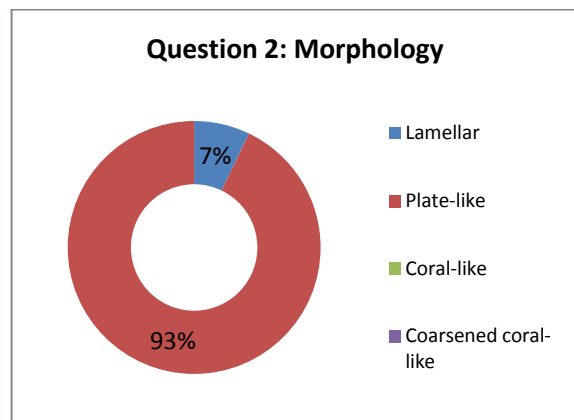
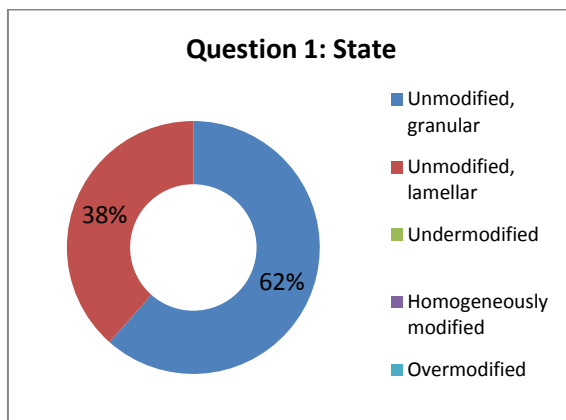
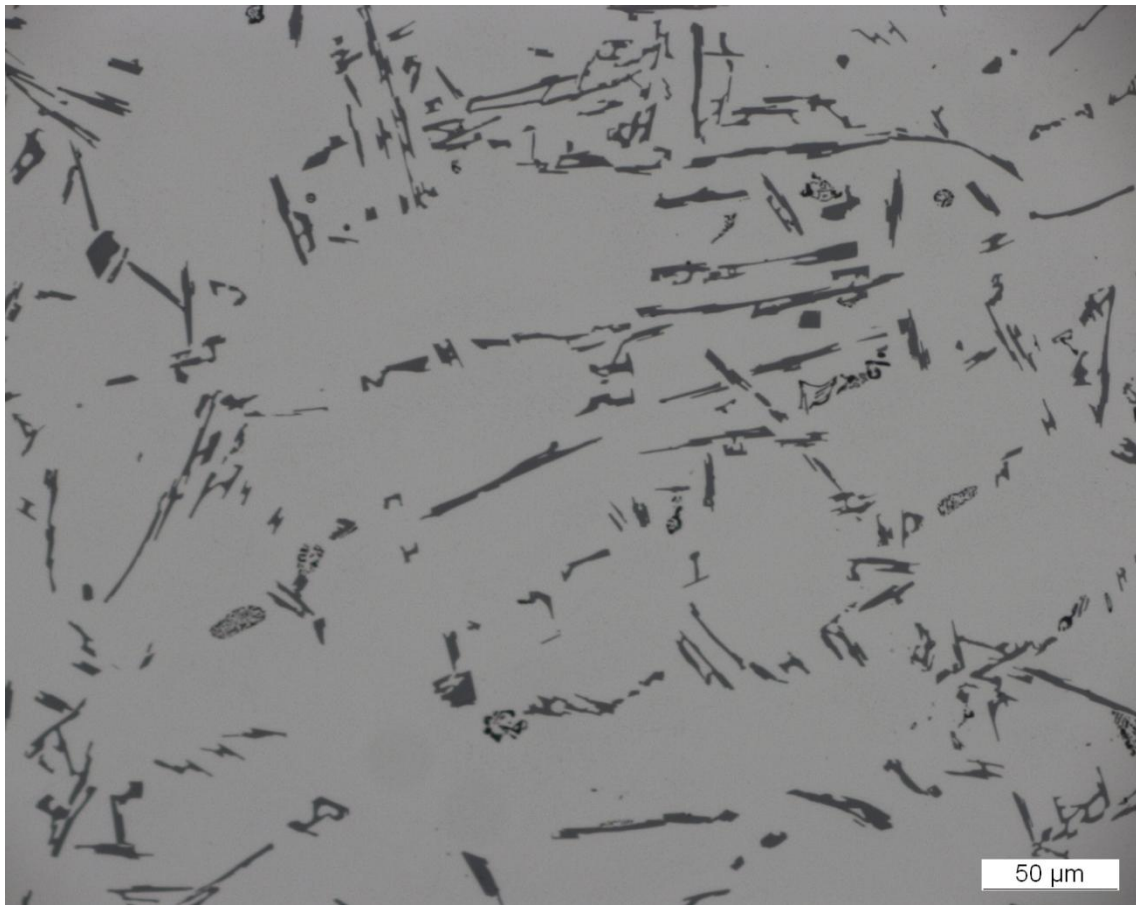
Casting process: **Triplex D30**

Subjective homogeneity: **(96 ± 7) %**

Objective classification, degree of mod. (*M*):

Unmodified, *M* = n.a.

Micrograph No. 27:



Chemical composition:

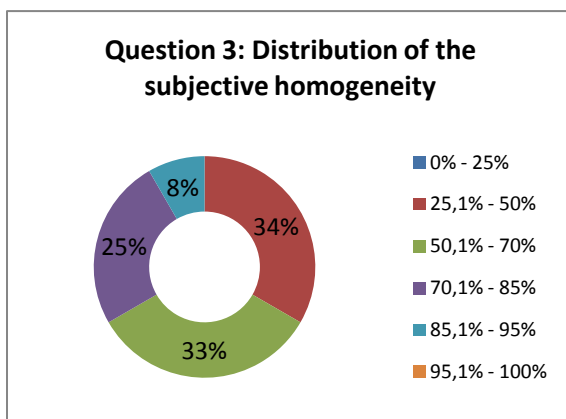
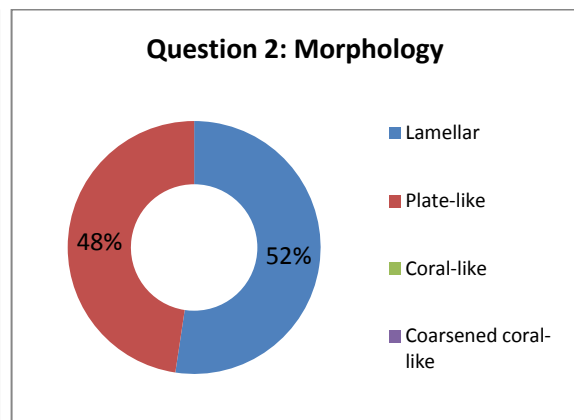
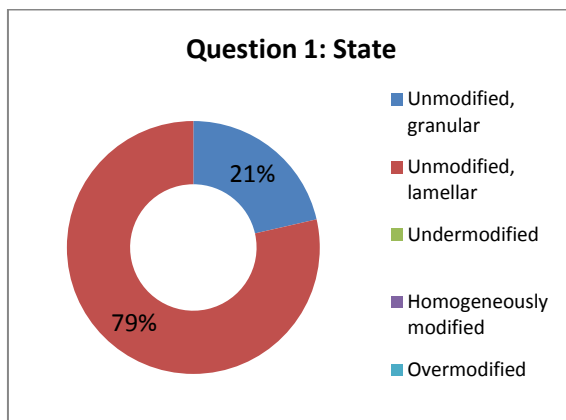
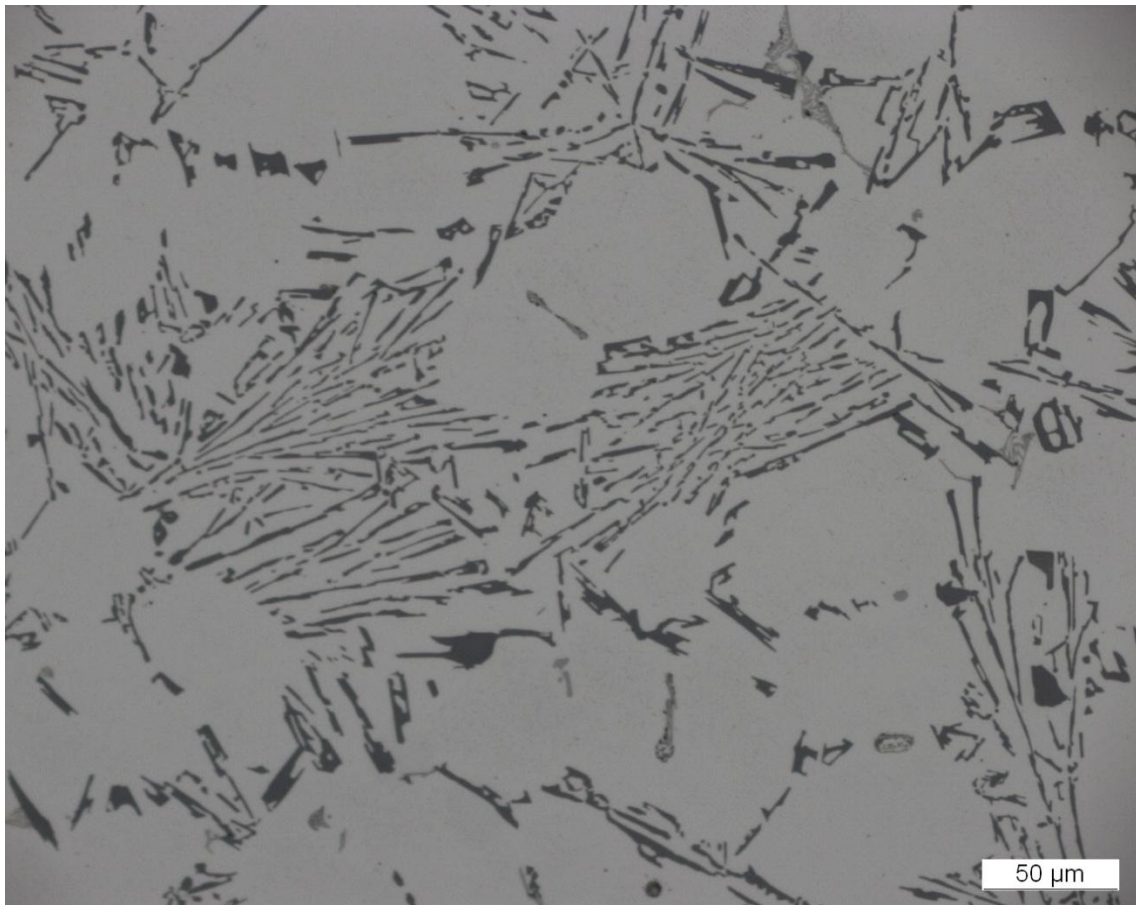
Al - 7 wt.% Si - 0.3wt.% Mg - 2.5 ppm P

Casting process: **Triplex D30**

Subjective homogeneity: **(93 ± 8) %**

Objective classification, degree of mod. (*M*):

Unmodified, *M* = n.a.



Chemical composition:

Al - 7 wt.% Si - 0.3wt.% Mg - 800 ppm Fe

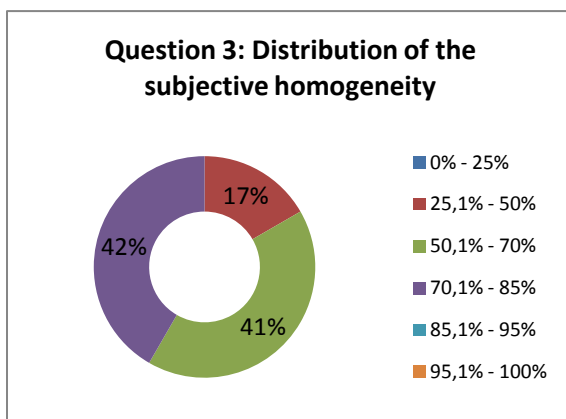
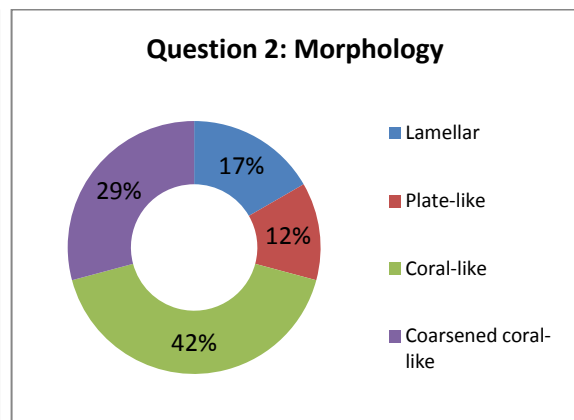
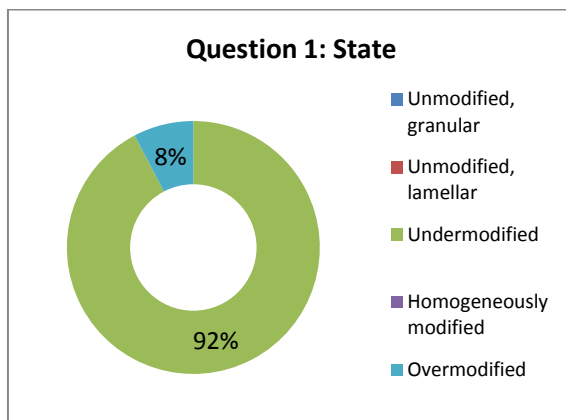
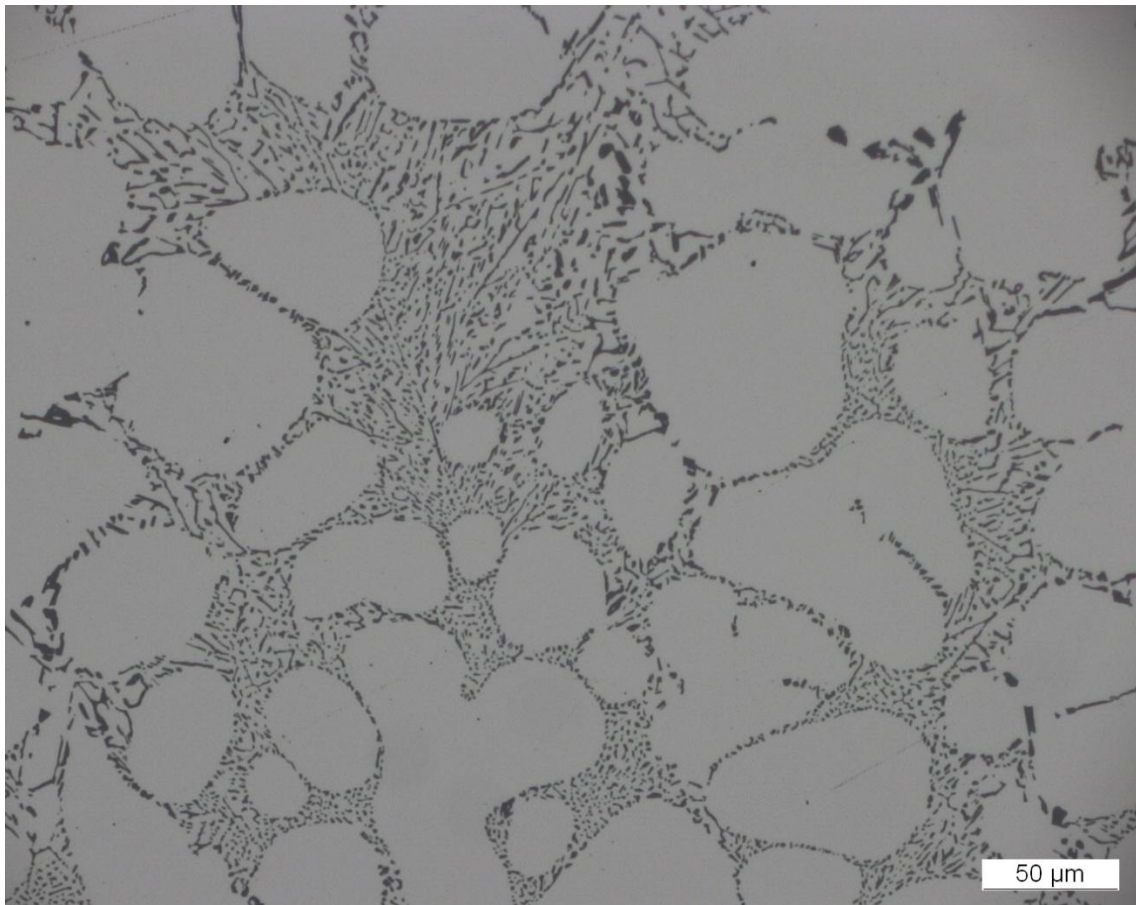
Casting process: **Triplex D30**

Subjective homogeneity: $(66 \pm 13) \%$

Objective classification, degree of mod. (*M*):

Unmodified, *M* = n.a.

Micrograph No. 29:



Chemical composition:

Al - 7 wt.% Si - 0.3wt.% Mg - 50 ppm Sr

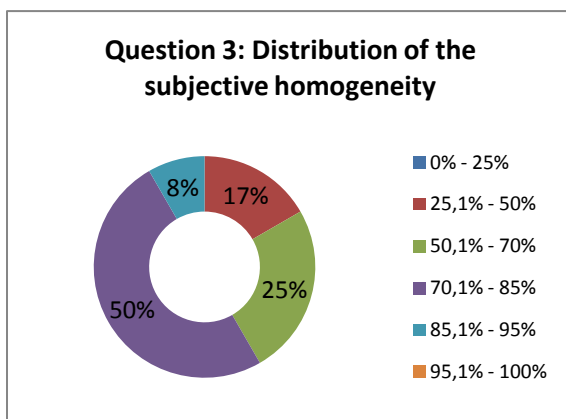
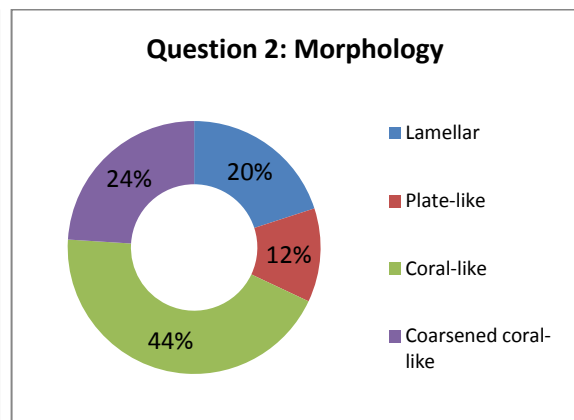
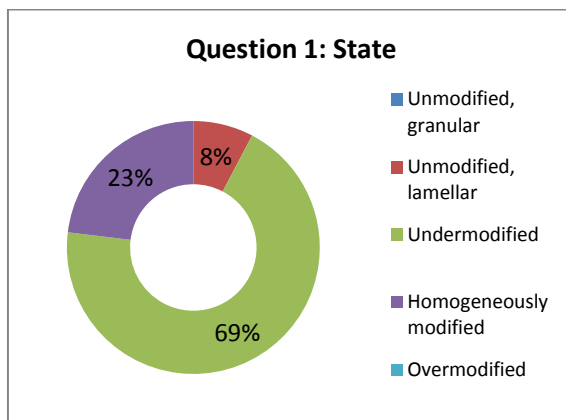
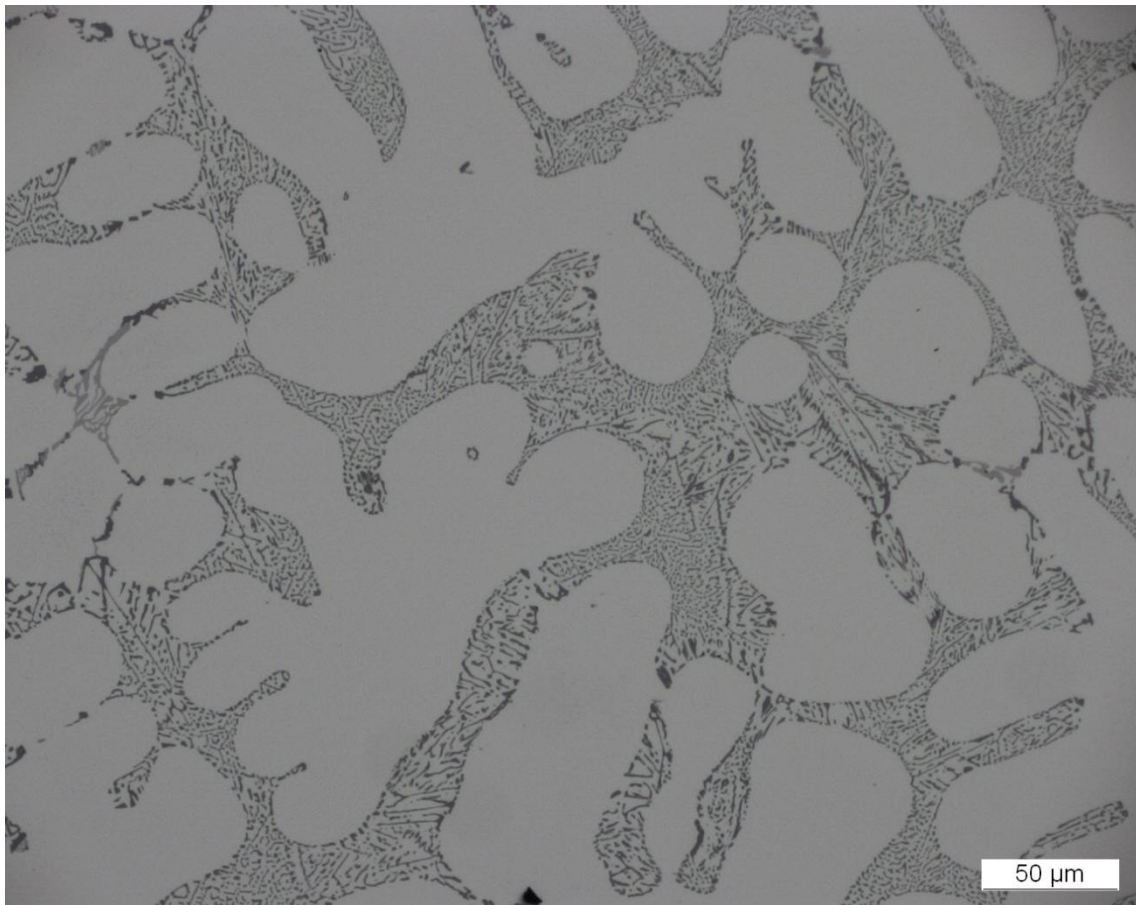
Casting process: **Triplex D30**

Subjective homogeneity: **(69 ± 11) %**

Objective classification, degree of mod. (*M*):

Modified, Inhomogeneous, *M* = 79 %

Micrograph No. 30:



Chemical composition:

Al - 7 wt.% Si - 0.3wt.% Mg - 50 ppm Sr - 5 ppm P - 800 ppm Fe

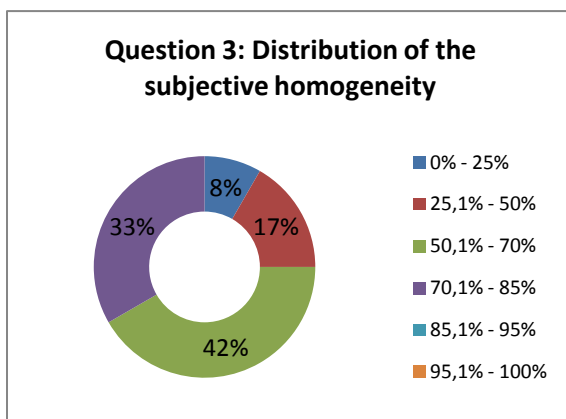
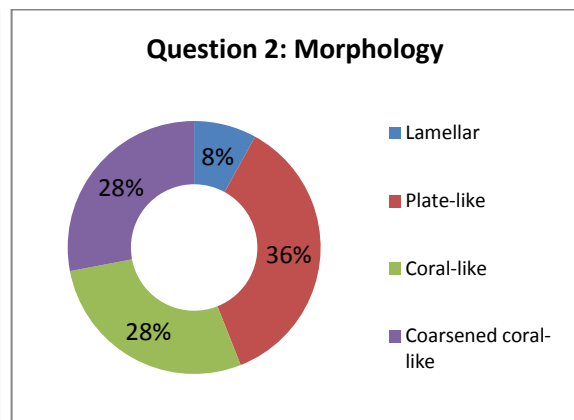
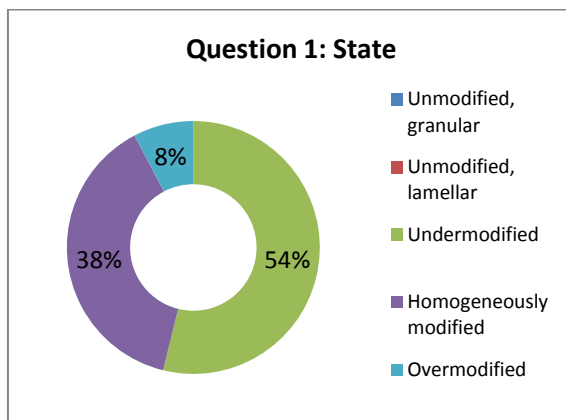
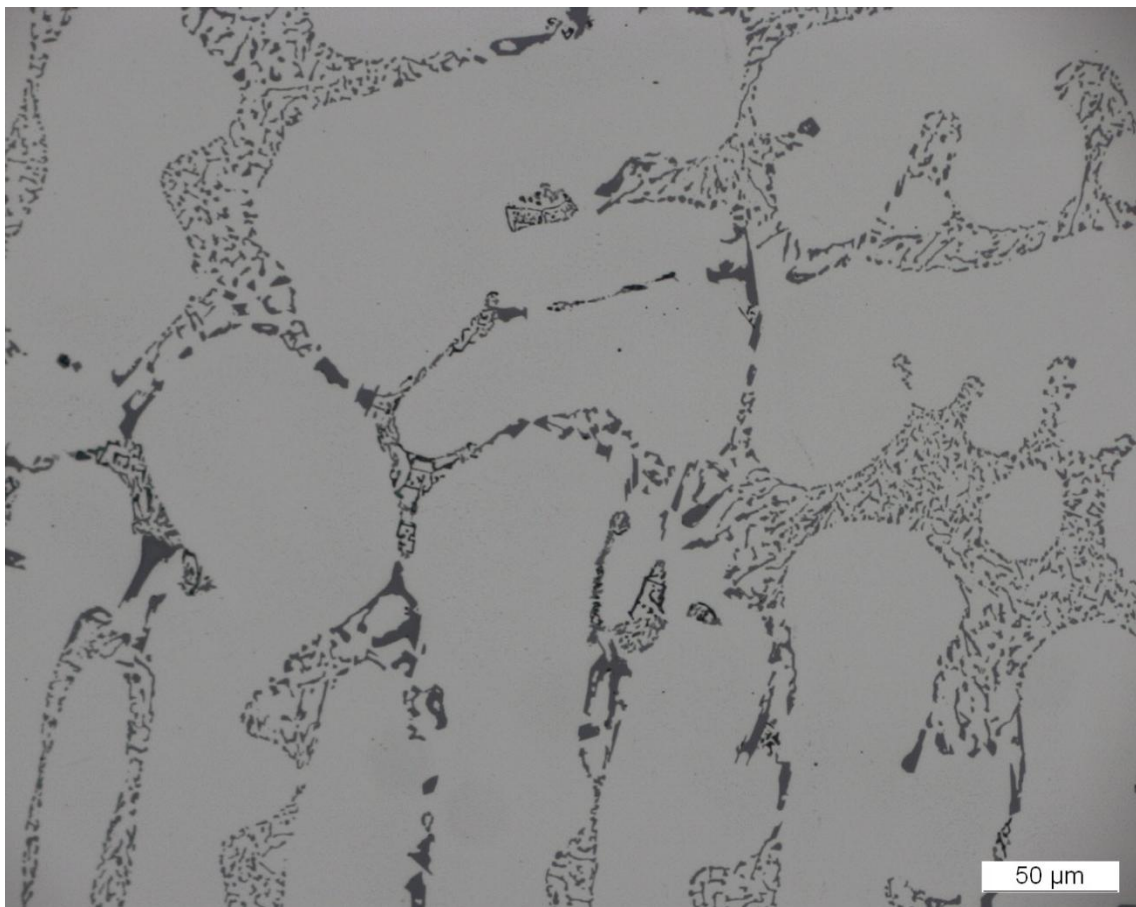
Casting process: **Triplex D30**

Subjective homogeneity: **(73 ± 13) %**

Objective classification, degree of mod. (*M*):

Modified, Inhomogeneous, *M* = 73 %

Micrograph No. 31:



Chemical composition:

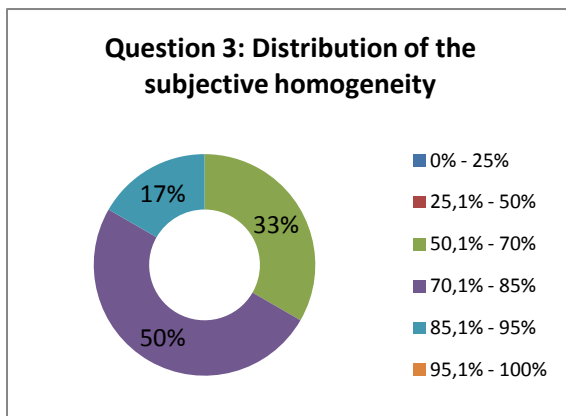
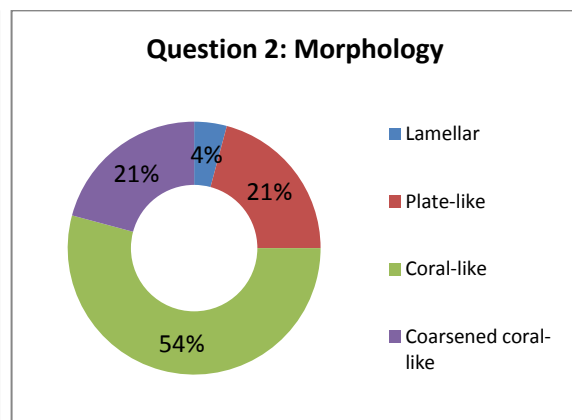
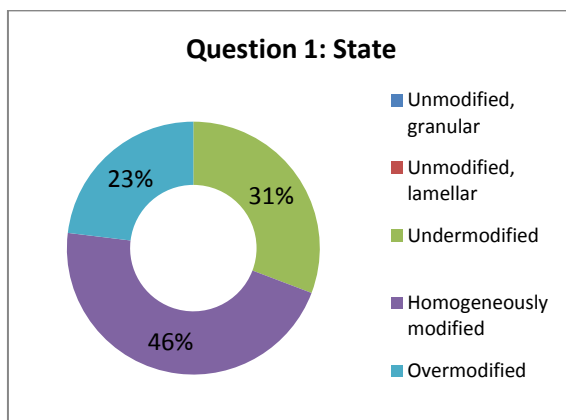
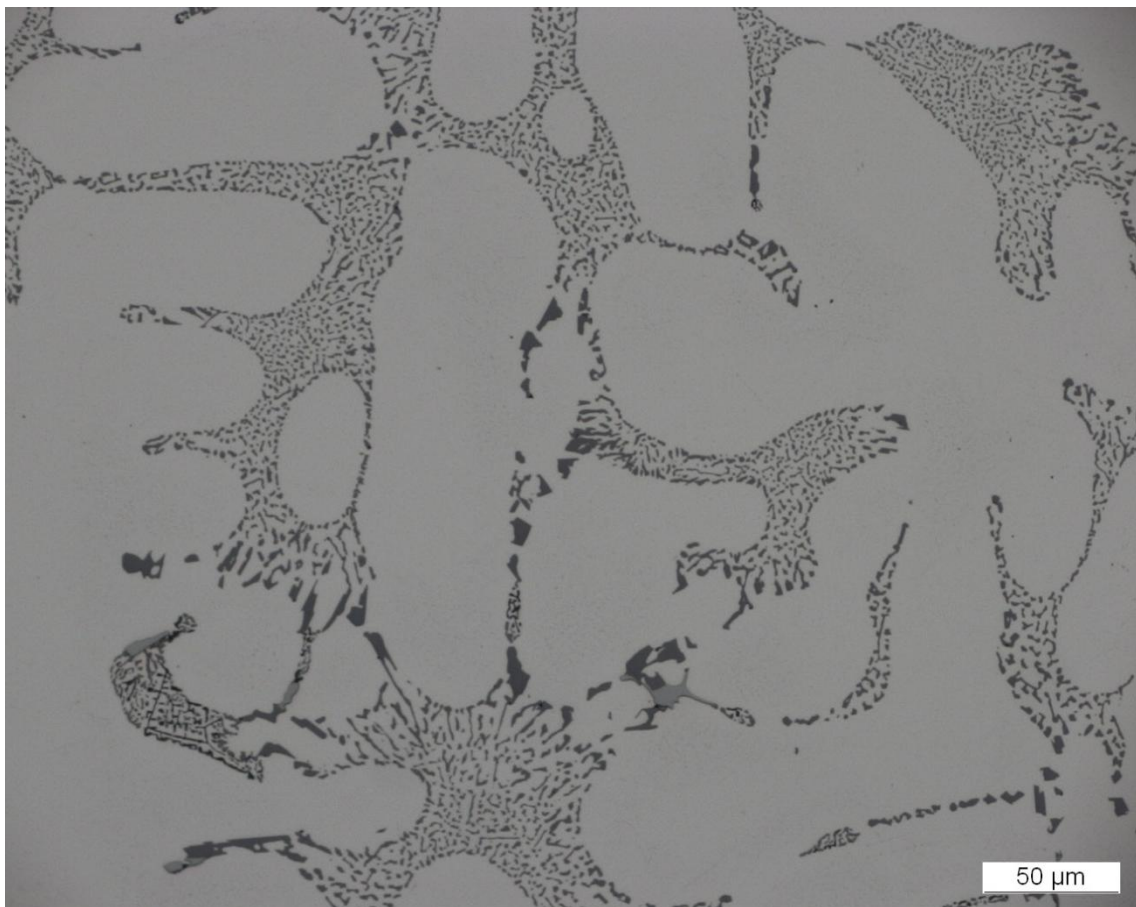
Al - 7 wt.% Si - 0.3wt.% Mg - 100 ppm Sr

Casting process: **Triplex D30**

Subjective homogeneity: **(62 ± 16) %**

Objective classification, degree of mod. (*M*):

Modified, Inhomogeneous, *M* = 39 %



Chemical composition:

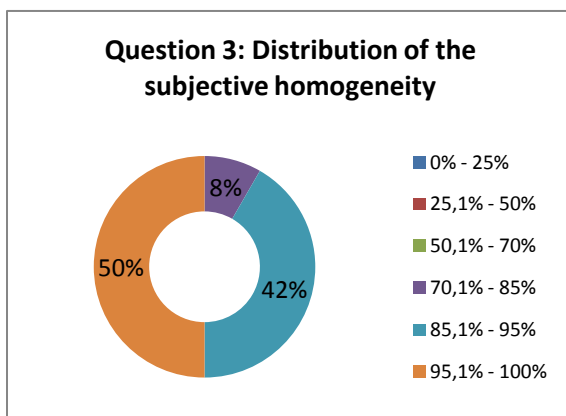
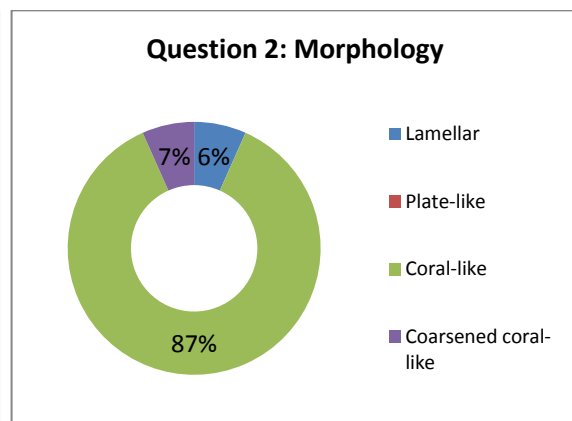
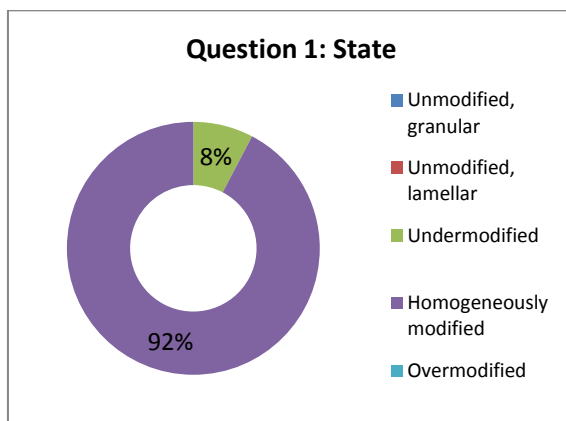
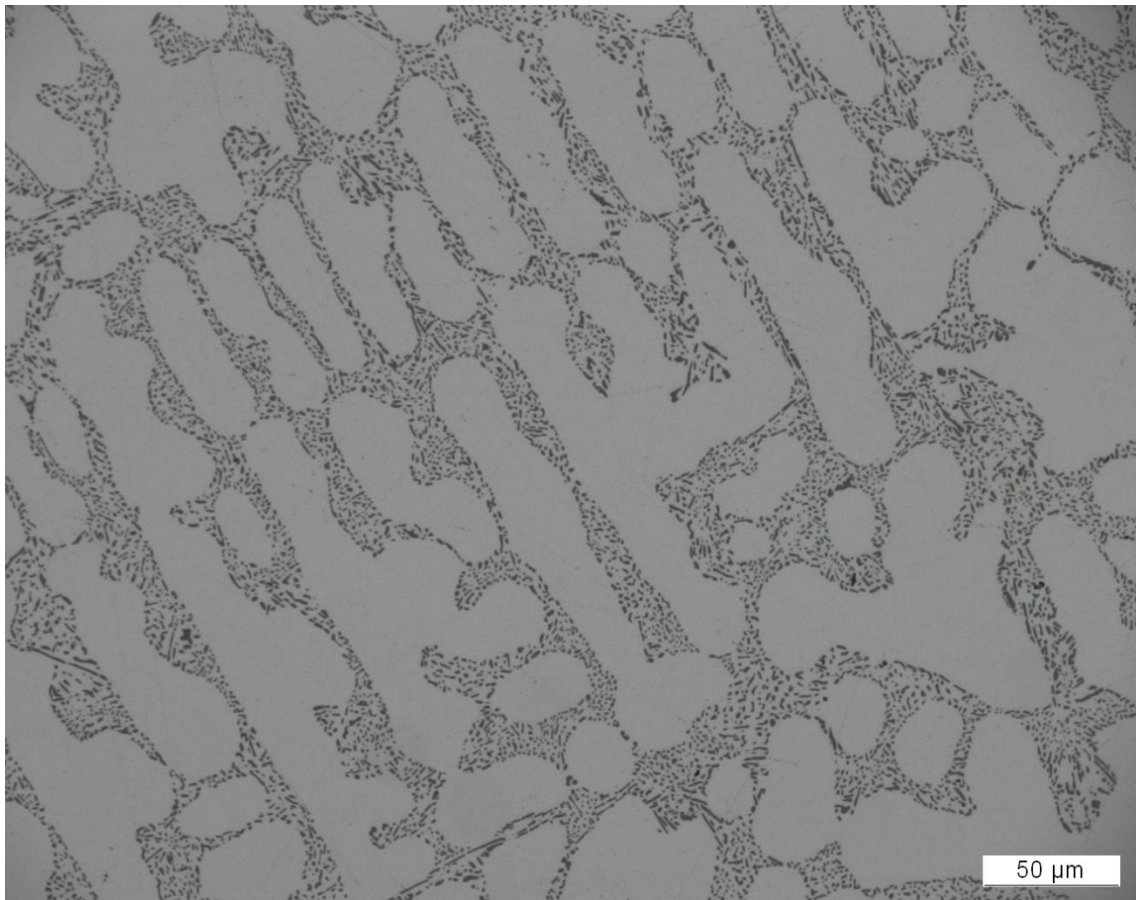
Al - 7 wt.% Si - 0.3wt.% Mg - 250 ppm Sr - 2.5 ppm P

Casting process: **Triplex D30**

Subjective homogeneity: **(76 ± 9) %**

Objective classification, degree of mod. (*M*):

Modified, Inhomogeneous, *M* = 61 %



Chemical composition:

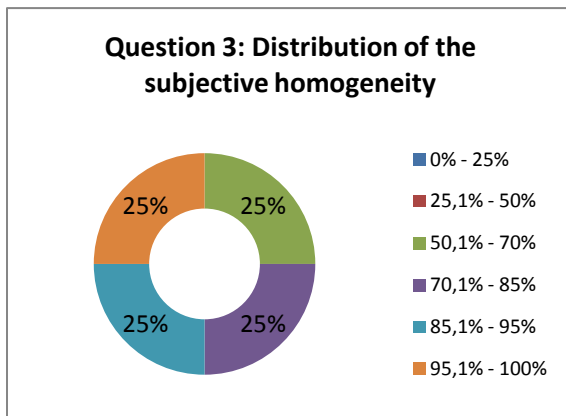
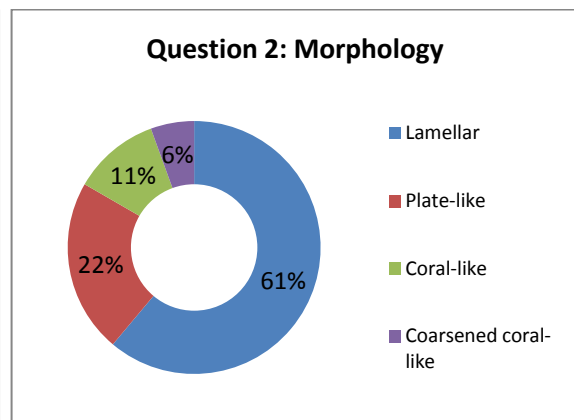
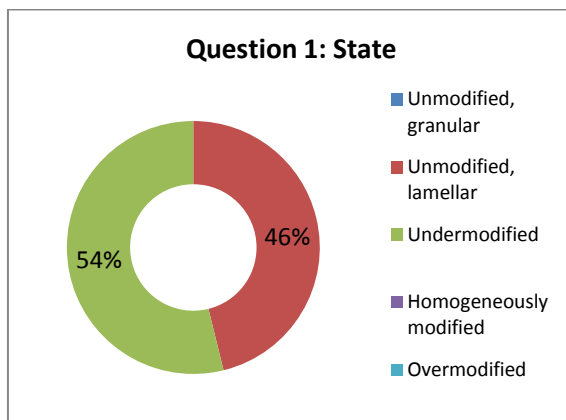
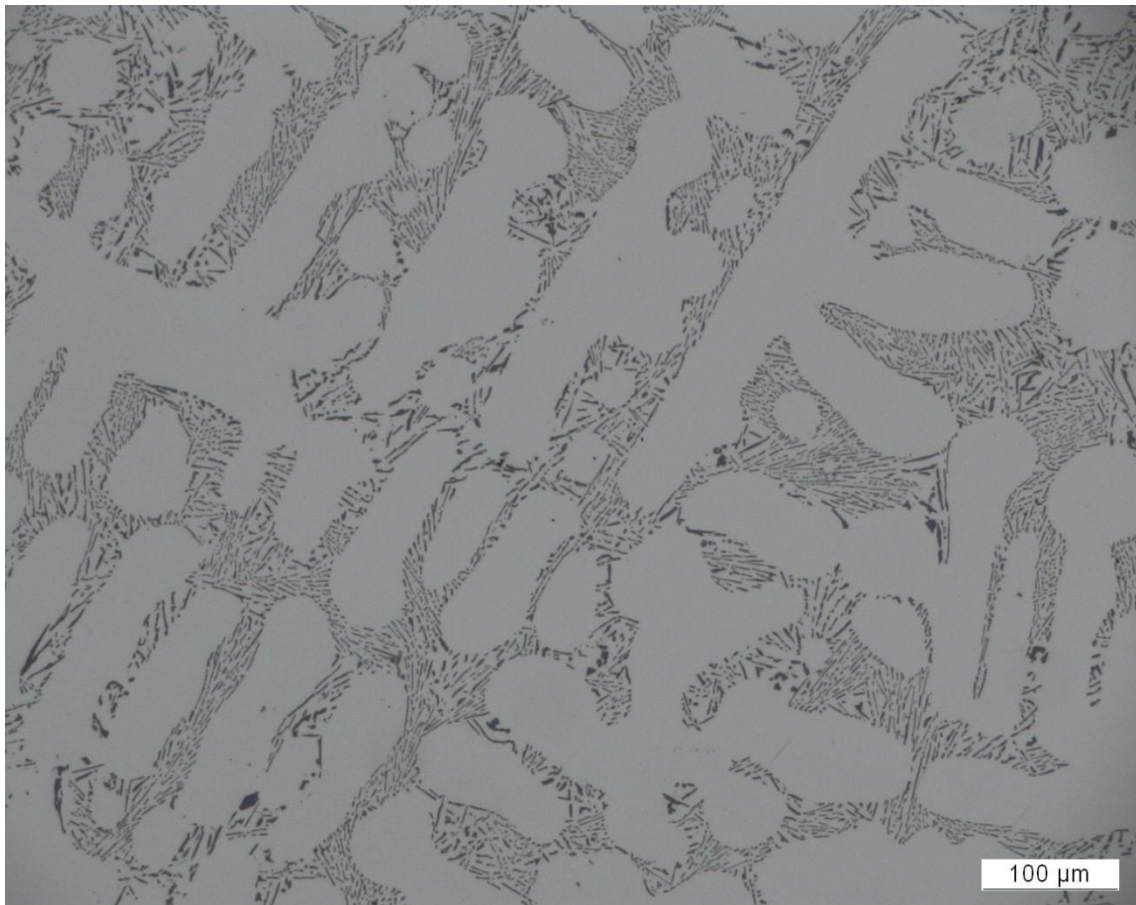
Al - 7wt.% Si

Casting process: **Ingot mould**

Subjective homogeneity: **(95 ± 7) %**

Objective classification, degree of mod. (*M*):

Modified, Homogeneous, *M* = 100 %



Chemical composition:

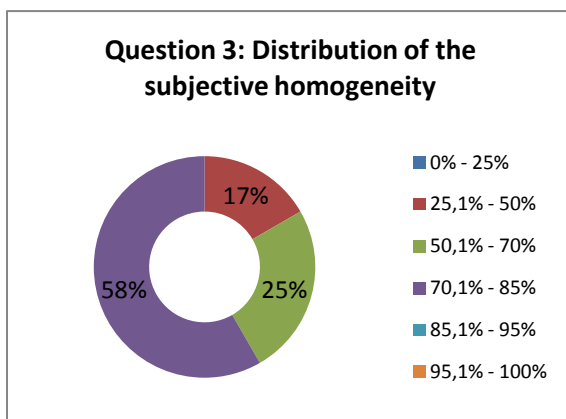
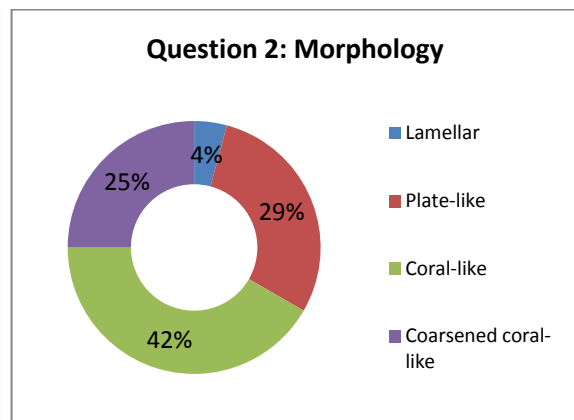
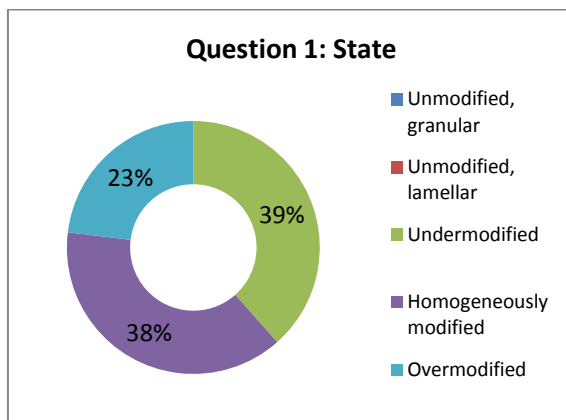
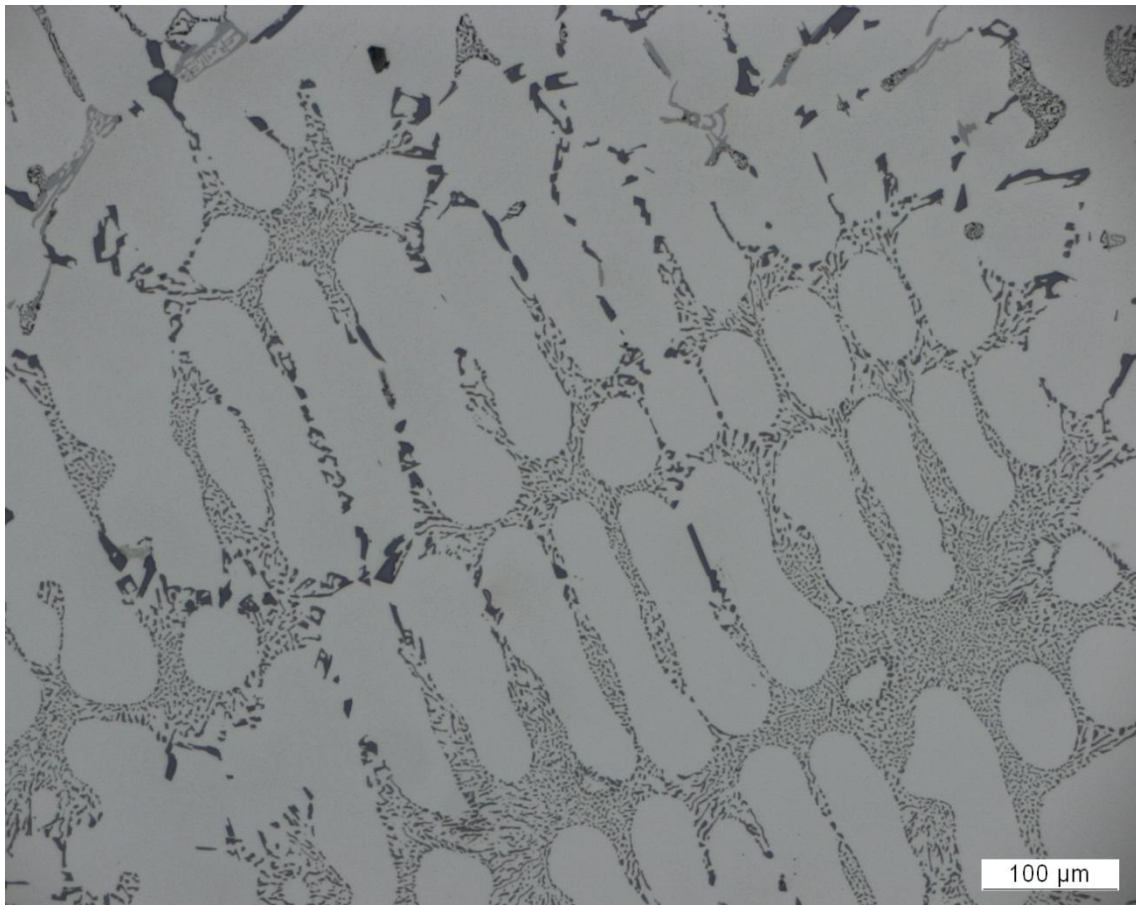
Al - 7wt. % Si

Casting process: **Sand mould**

Subjective homogeneity: **(85 ± 12) %**

Objective classification, degree of mod. (*M*):

Modified, Inhomogeneous, *M* = 90 %



Chemical composition:

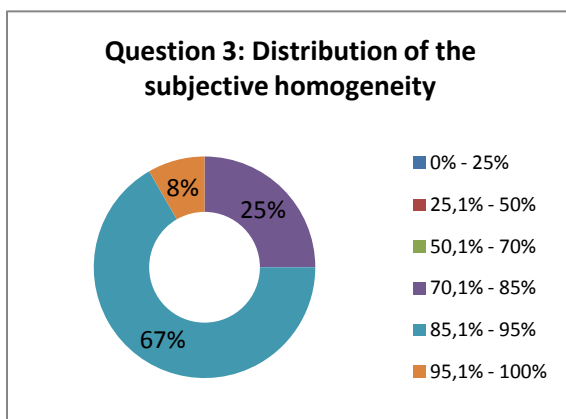
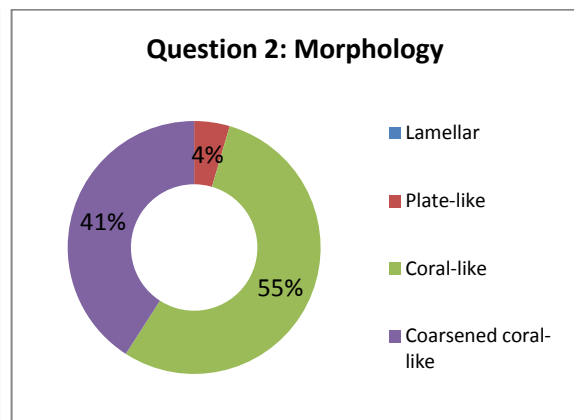
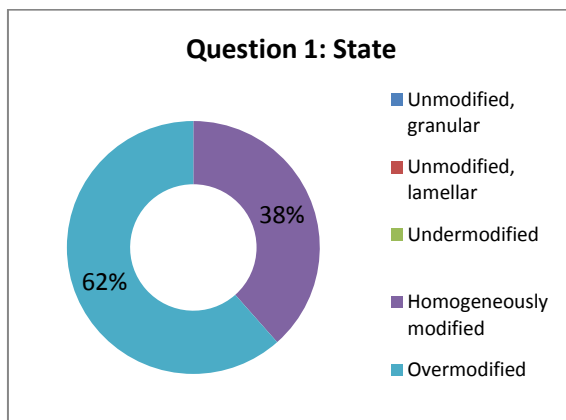
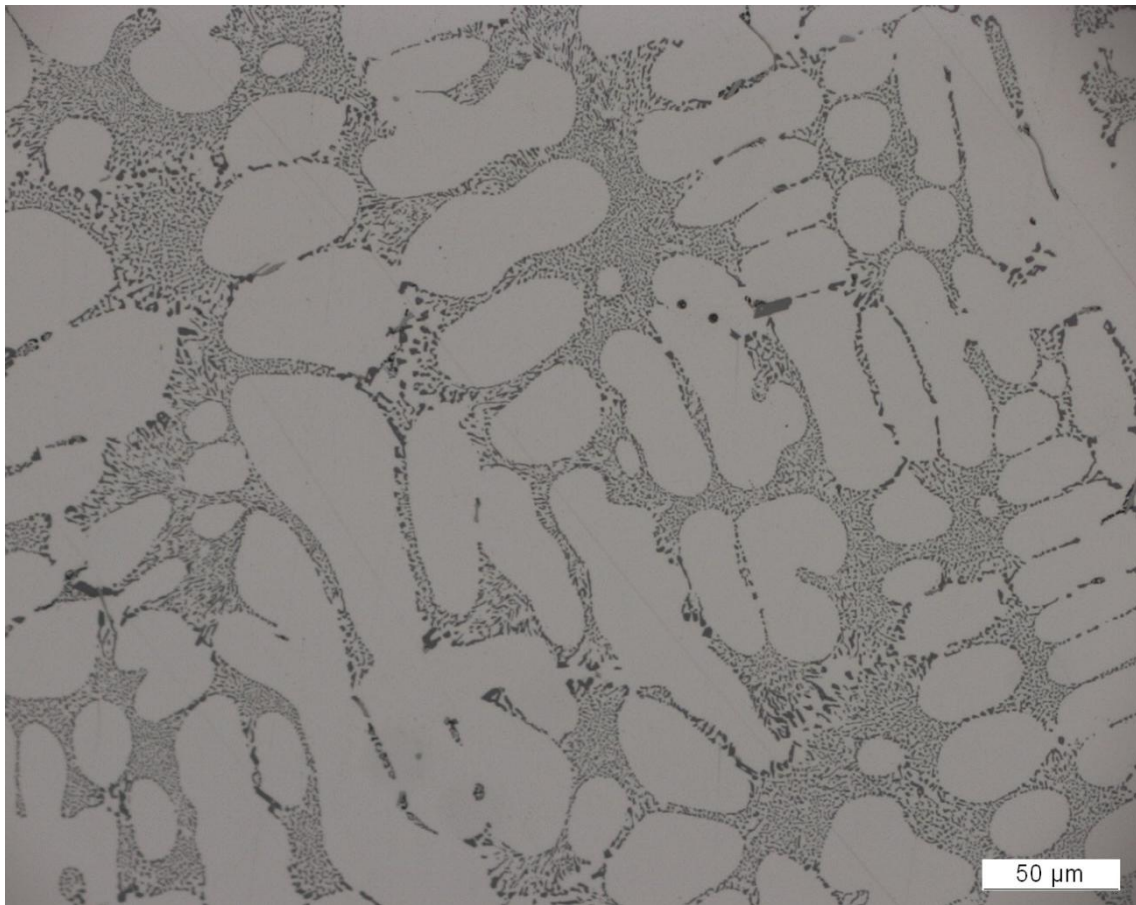
Al - 7 wt.% Si - 0.3wt.% Mg - 350 ppm Sr

Casting process: **Sand mould**

Subjective homogeneity: **(70 ± 12) %**

Objective classification, degree of mod. (*M*):

Modified, Inhomogeneous, *M* = 74 %



Chemical composition:

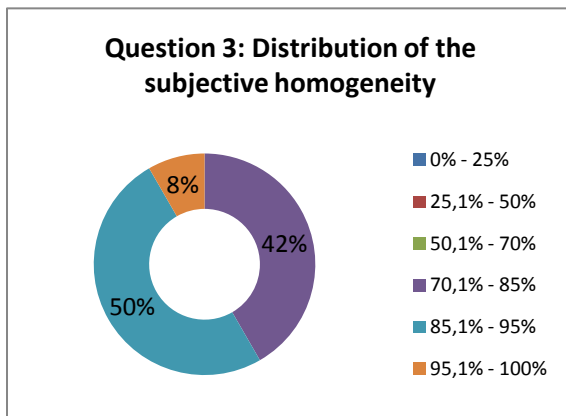
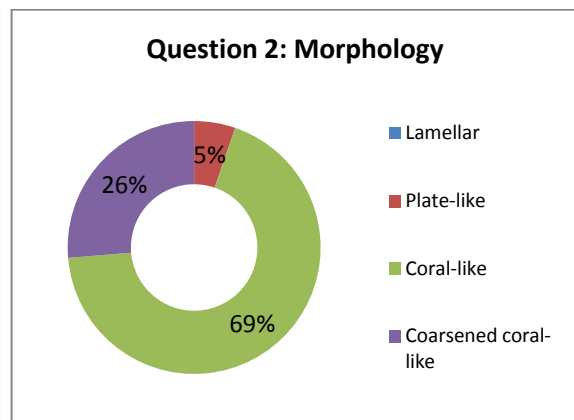
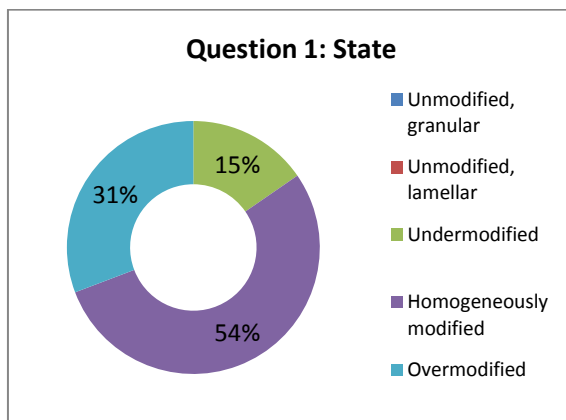
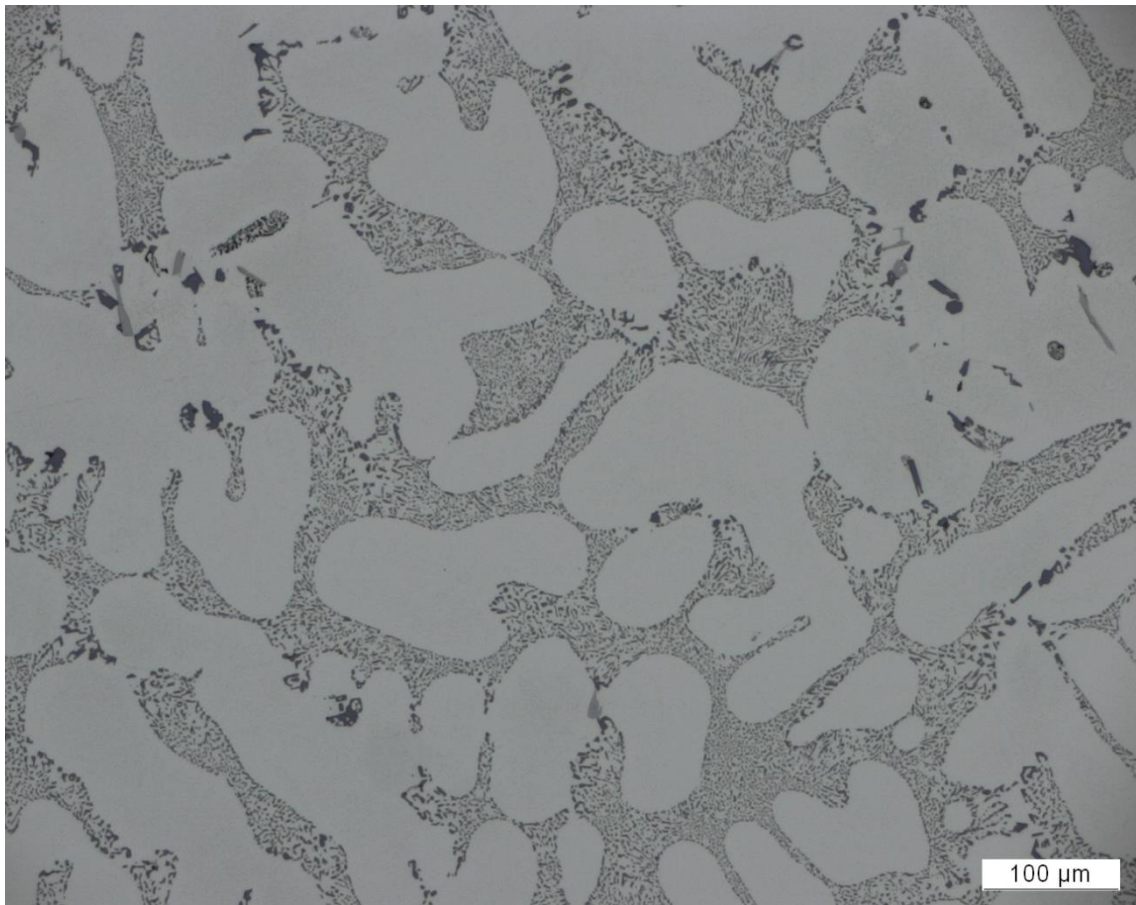
Al - 7 wt.% Si - 0.3wt.% Mg - 350 ppm Sr

Casting process: **Ingot mould**

Subjective homogeneity: **(89 ± 6) %**

Objective classification, degree of mod. (*M*):

Modified, Inhomogeneous, *M* = 90 %



Chemical composition:

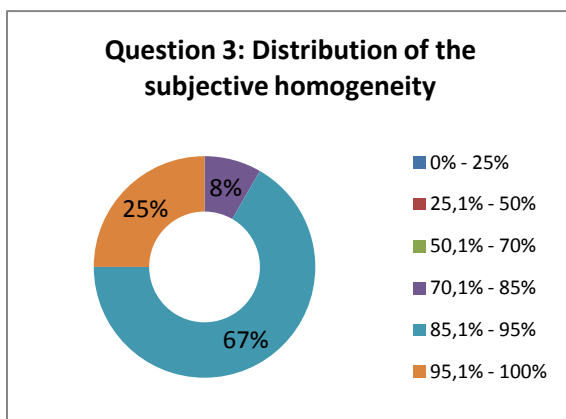
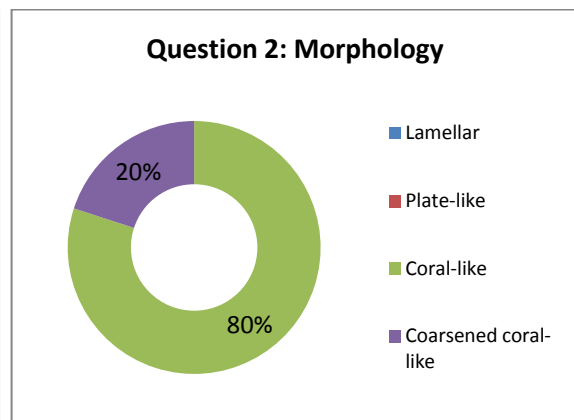
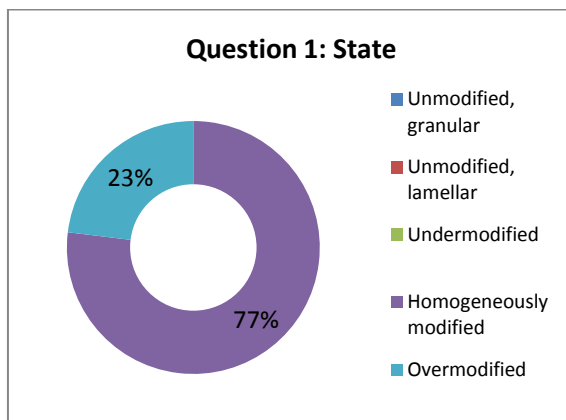
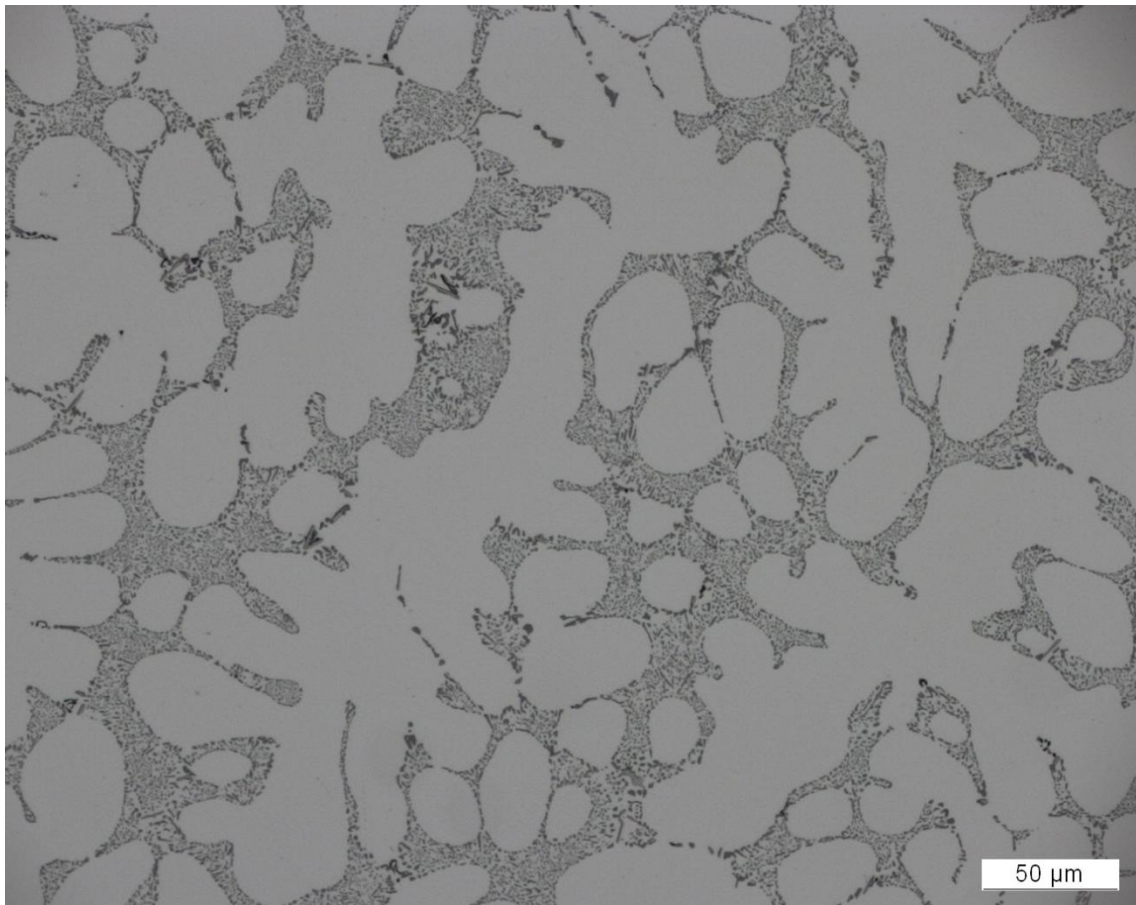
Al - 7 wt.% Si - 0.3wt.% Mg - 55 ppm Sr

Casting process: Sand mould

Subjective homogeneity: $(86 \pm 7) \%$

Objective classification, degree of mod. (*M*):

Modified, Inhomogeneous, *M* = 86 %



Chemical composition:

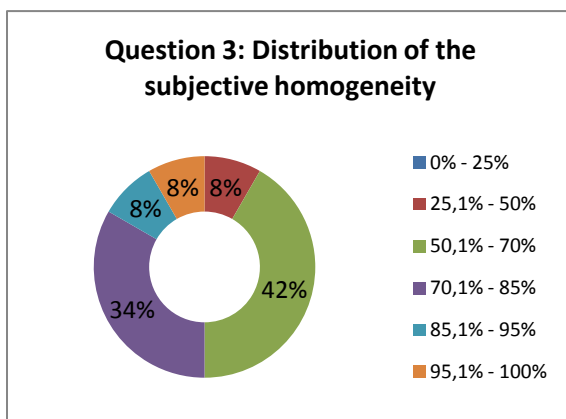
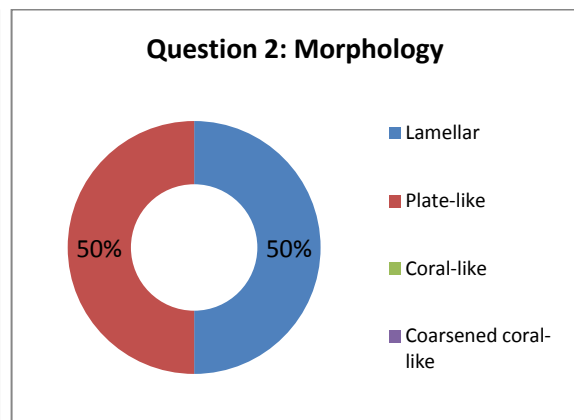
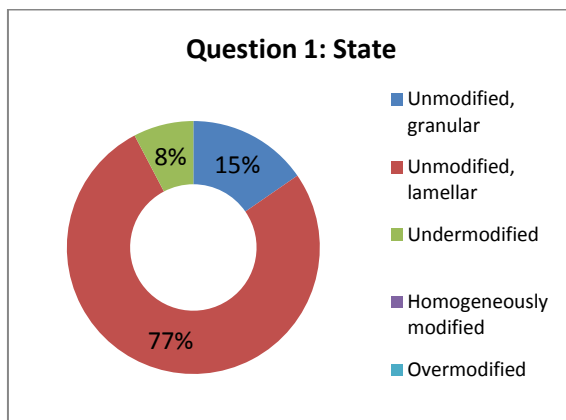
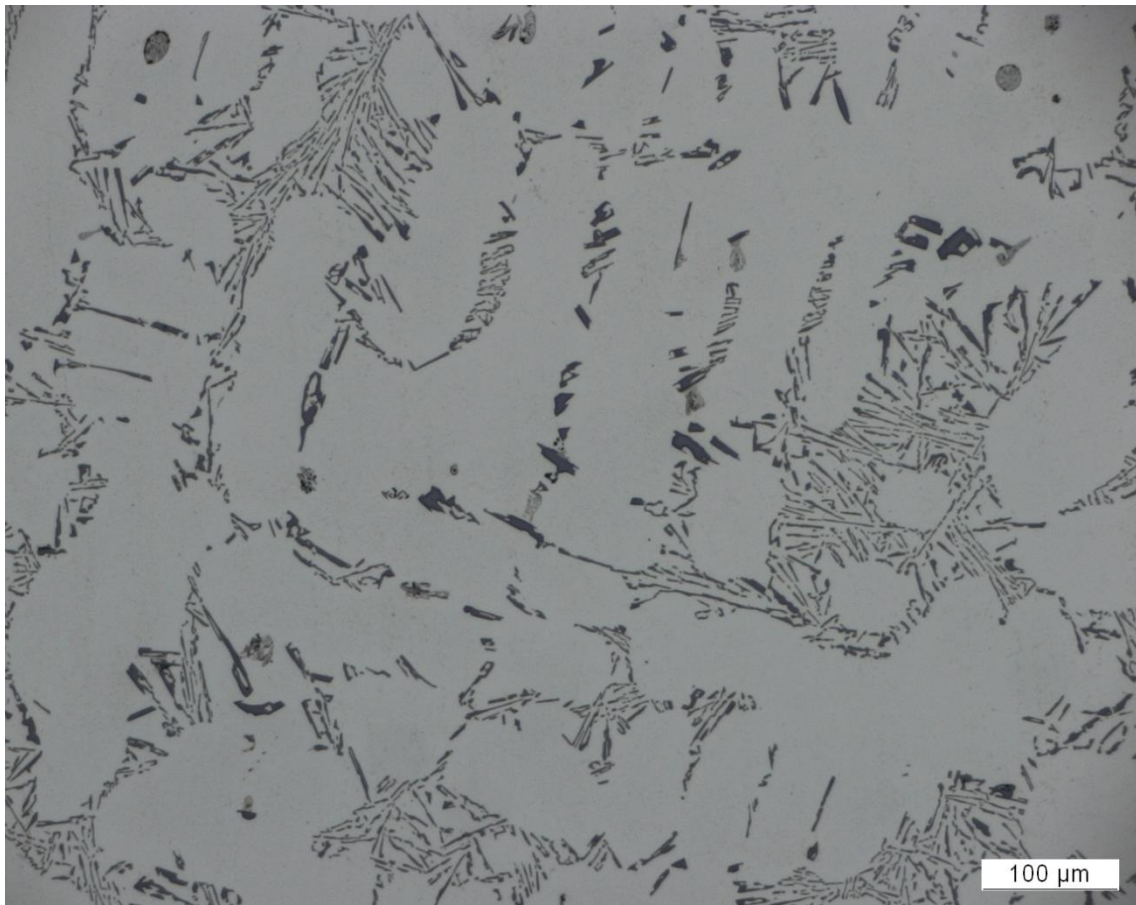
Al - 7 wt.% Si - 0.3wt.% Mg - 55 ppm Sr

Casting process: **Ingot mould**

Subjective homogeneity: **(93 ± 6) %**

Objective classification, degree of mod. (*M*):

Modified, Inhomogeneous, *M* = 83 %



Chemical composition:

Al - 7 wt.% Si - 0.3wt.% Mg

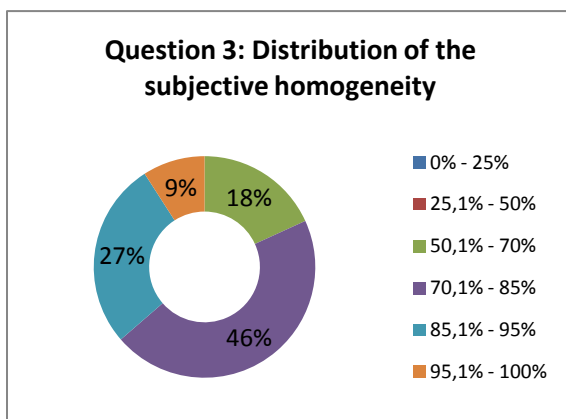
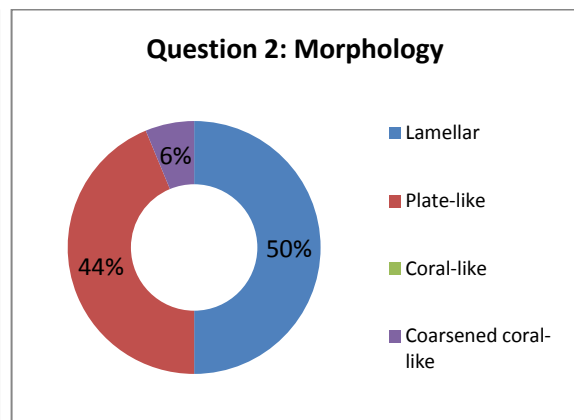
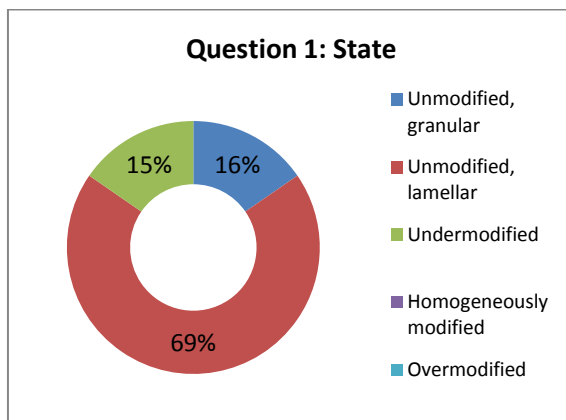
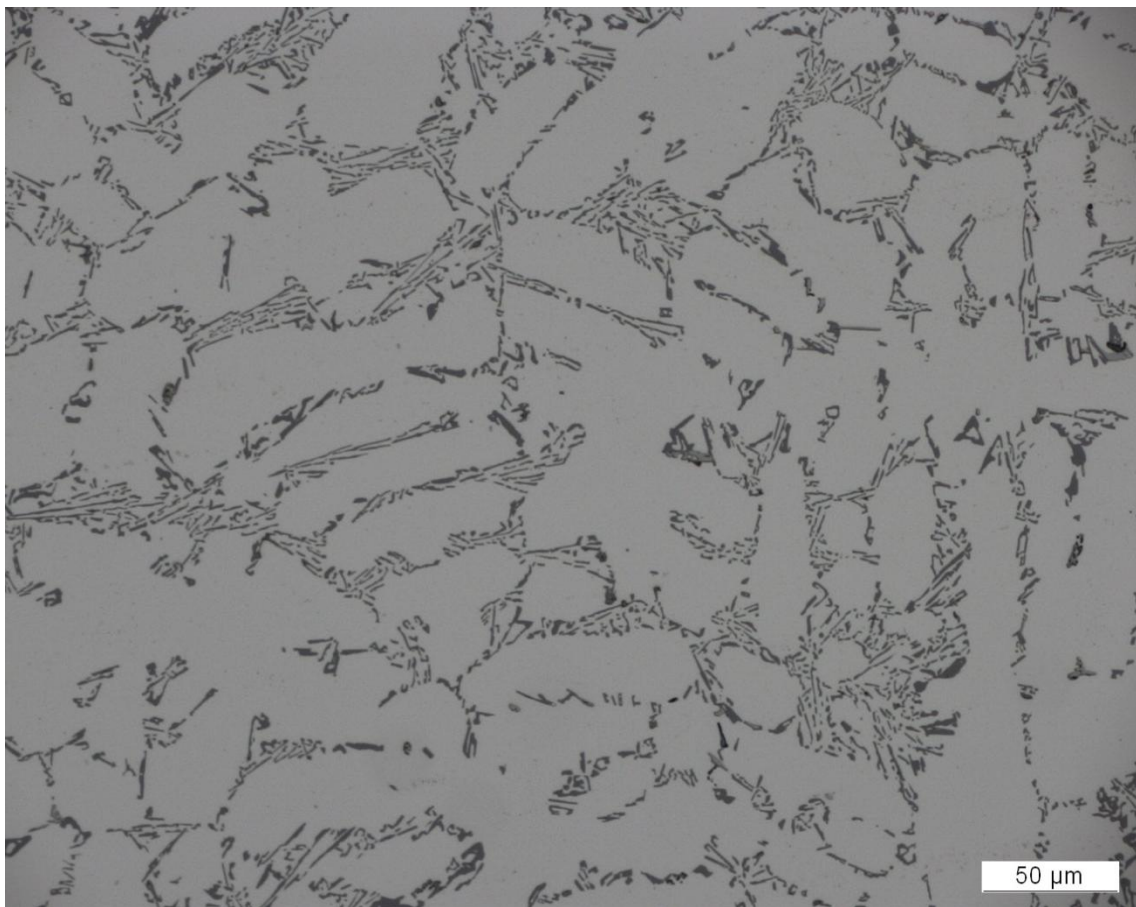
Casting process: **Sand mould**

Subjective homogeneity: **(73 ± 13) %**

Objective classification, degree of mod. (*M*):

Unmodified, *M* = n.a.

Micrograph No. 40:



Chemical composition:

Al - 7 wt.% Si - 0.3wt.% Mg

Casting process: **Ingot mould**

Subjective homogeneity: **(82 ± 11) %**

Objective classification, degree of mod. (*M*):

Unmodified, *M* = n.a.

References

- [1] P. Rossi, M. Engstler, F. Mücklich, Homogeneity Quantification Method and its Application to Microstructure Assessment, *Pract. Metallogr.* 51 (2014) 180–199. doi:10.3139/147.110287.
- [2] P. Rossi, M. Engstler, F. Mücklich, Quantitative Classification and Assessment of Sr Modification in hypoeutectic Al-Si and Al-Si-Mg alloys, *Pract. Metallogr.* 52 (2015). In press
- [3] P. Rossi, S. Suarez, F. Soldera, F. Mücklich, Quantitative Assessment of the Reinforcement Distribution Homogeneity in CNT/Metal Composites, *Adv. Eng. Mater.* (2014) 1–5. doi:10.1002/adem.201400352.
- [4] J.E. Gruzleski, B.M. Closset, *The Treatment of Liquid Aluminum-Silicon Alloys*, American Foundrymen's Society, USA, 1999.
- [5] J.L. Murray, A.J. McAlister, The Al-Si (Aluminum-Silicon) system, *Bull. Alloy Phase Diagrams.* 5 (1984) 74–84.
- [6] Q. Wang, C. Davidson, Solidification and precipitation behaviour of Al-Si-Mg casting alloys, *J. Mater. Sci.* 36 (2001) 739–750.
- [7] L. Wang, M. Makhlouf, D. Apelian, Aluminum die casting alloys: Alloy composition, microstructure, and properties-performance relationships, *Int. Mater. Rev.* 40 (1995) 221–238.
- [8] L. Lu, K. Nogita, S.D. McDonald, A.K. Dahle, L. Lu, A.K. Dahle, Eutectic solidification and its role in casting porosity formation, *JOM.* 56 (2004) 52–58. doi:10.1007/s11837-004-0254-8.
- [9] R. Frilley, Some Alloys of Metals with Silicon and the Density of Alloys, *Rev. Metall.* 8 (1911) 457–559.
- [10] A. Pacz, Specification of Letters Patent: Alloy, 1387900, 1921.
- [11] A. Pacz, Modification of aluminum, aluminum alloys, and alloys containing aluminum, 2013926, 1935.
- [12] F. Lasagni, A. Lasagni, C. Holzapfel, F. Mücklich, H.P. Degischer, Three Dimensional Characterization of Unmodified and Sr-Modified Al-Si Eutectics by FIB and FIB EDX Tomography, *Adv. Eng. Mater.* 8 (2006) 719–723. doi:10.1002/adem.200500276.
- [13] F. Lasagni, a. Lasagni, M. Engstler, H.P. Degischer, F. Mücklich, Nano-characterization of Cast Structures by FIB-Tomography, *Adv. Eng. Mater.* 10 (2008) 62–66. doi:10.1002/adem.200700249.

- [14] S. Shankar, Y.W. Riddle, M.M. Makhlof, Nucleation mechanism of the eutectic phases in aluminum–silicon hypoeutectic alloys, *Acta Mater.* 52 (2004) 4447–4460. doi:10.1016/j.actamat.2004.05.045.
- [15] M. Timpel, N. Wanderka, R. Schlesiger, T. Yamamoto, N. Lazarev, D. Isheim, et al., The role of strontium in modifying aluminium–silicon alloys, *Acta Mater.* 60 (2012) 3920–3928. doi:10.1016/j.actamat.2012.03.031.
- [16] S. Lu, A. Hellawell, Growth mechanisms of silicon in Al-Si alloys, *J. Cryst. Growth.* 73 (1985) 316–328.
- [17] W.R. Osório, N. Cheung, J.E. Spinelli, The effects of a eutectic modifier on microstructure and surface corrosion behavior of Al-Si hypoeutectic alloys, (2007) 1421–1427. doi:10.1007/s10008-007-0300-x.
- [18] S. Hegde, K.N. Prabhu, Modification of eutectic silicon in Al–Si alloys, *J. Mater. Sci.* 43 (2008) 3009–3027. doi:10.1007/s10853-008-2505-5.
- [19] M. Makhlof, H. Guthy, The aluminum–silicon eutectic reaction: mechanisms and crystallography, *J. Light Met.* 7 (2001) 199–218.
- [20] F. Lasagni, A. Lasagni, C. Holzapfel, F. Mücklich, H.P. Degischer, Three Dimensional Characterization of Unmodified and Sr- Modified Al- Si Eutectics by FIB and FIB EDX Tomography, *Adv. Eng. Mater.* 8 (2006) 719–723. doi:10.1002/adem.200500276.
- [21] H.A. Steent, A. Hellawell, Structure and properties of aluminium-silicon eutectic alloys, *Acta Metall.* 20 (1972) 363–370. doi:10.1016/0001-6160(72)90030-2.
- [22] D.C. Jenkinson, L.M. Hogan, The modification of aluminium-silicon alloys with strontium, *J. Cryst. Growth.* 28 (1975) 171–187. doi:10.1016/0022-0248(75)90233-X.
- [23] C.R. Ho, B. Cantor, Modification of hypoeutectic Al-Si alloys, *J. Mater. Sci.* 30 (1995) 1912–1920. doi:10.1007/BF00353013.
- [24] Y. Birol, Interaction of grain refinement with B and modification with Sr in aluminium foundry alloys, *Mater. Sci. Technol.* 28 (2012) 70–76. doi:10.1179/1743284711Y.0000000081.
- [25] G. Sigworth, Theoretical and practical aspects of the modification of Al-Si alloys, *AFS Trans.* 91 (1983) 7–16.
- [26] Z. Zhang, J. Li, H. Yue, J. Zhang, T. Li, Microstructure evolution of A356 alloy under compound field, *J. Alloys Compd.* 484 (2009) 458–462. doi:10.1016/j.jallcom.2009.04.125.
- [27] Y.H. Cho, H.-C. Lee, K.H. Oh, a. K. Dahle, Effect of Strontium and Phosphorus on Eutectic Al-Si Nucleation and Formation of β -Al₅FeSi in Hypoeutectic Al-Si Foundry Alloys, *Metall. Mater. Trans. A.* 39 (2008) 2435–2448. doi:10.1007/s11661-008-9580-8.

- [28] J.G. Kaufman, Elwin L. Rooy, *Aluminum Alloy Castings: Properties, Processes, and Applications*, ASM International, Ohio, USA, 2004.
- [29] Q. Li, T. Xia, Y. Lan, W. Zhao, L. Fan, P. Li, Effect of rare earth cerium addition on the microstructure and tensile properties of hypereutectic Al–20%Si alloy, *J. Alloys Compd.* 562 (2013) 25–32. doi:10.1016/j.jallcom.2013.02.016.
- [30] G.K. Sigworth, *Modification of Aluminum-Silicon Alloys*, 15 (2008) 240–254. doi:10.1361/asmhba0005301.
- [31] D. Apelian, G.K. Sigworth, K.R. Whaler, *Assessment of Grain Refinement and Modification Of A-Si Foundry Alloys By Thermal Analysis*, *AFS Trans.* 92 (1984) 297–307.
- [32] G. Chai, L. Bäckerud, *Einige Einflußgrößen auf die Veredelung von Aluminiumgußlegierungen bei Zusatz von strontiumhaltigen Vorlegierungen*, *Giesserei-Praxis.* 12 (1993) 206–213.
- [33] N. Tenekedjiev, H. Mulazimoglu, B. Closset, J. Gruzleski, *Microstructures and Thermal Analysis of Strontium-Treated Aluminum-Silicon Alloys*, American Foundry Society, USA, 1995.
- [34] K. Kuhnke, *Characterizing the Structure of Aluminium-Silicon Cast Alloys*, *Prakt. Met.* 46 (2009). doi:10.3139/147.110071.
- [35] G.K. Sigworth, *Determining grain size and eutectic modification in aluminum alloy castings*, *Mod. Cast.* 77 (1987) 23–25.
- [36] M. Farkašová, E. Tillová, *Modification of Al-Si-Cu cast alloy*, (2013) 210–215.
- [37] D.P. Kanicki, W.M. Rasmussen, *Processing molten aluminum - part 1: understanding silicon modification*, *Mod. Cast.* 80 (1990) 24–27. doi:ISSN: 00267562.
- [38] S. Bercovici, *Control of Solidification Structures and Properties of Al-Si Alloys*, *Congr. Int. Fonderie.* (1978).
- [39] A.K. Dahle, K. Nogita, S.D. McDonald, J.W. Zindel, L.M. Hogan, *Eutectic nucleation and growth in hypoeutectic Al-Si alloys at different strontium levels*, *Metall. Mater. Trans. A.* 32 (2001) 949–960. doi:10.1007/s11661-001-0352-y.
- [40] F. Lasagni, a. Lasagni, E. Marks, C. Holzapfel, F. Mücklich, H.P. Degischer, *Three-dimensional characterization of “as-cast” and solution-treated AlSi12(Sr) alloys by high-resolution FIB tomography*, *Acta Mater.* 55 (2007) 3875–3882. doi:10.1016/j.actamat.2007.03.004.
- [41] M. Timpel, N. Wanderka, B.S. Murty, J. Banhart, *Three-dimensional visualization of the microstructure development of Sr-modified Al–15Si casting alloy using FIB-EsB tomography*, *Acta Mater.* 58 (2010) 6600–6608. doi:10.1016/j.actamat.2010.08.021.

- [42] K. Nogita, J. Drennan, A.K. Dahle, Evaluation of Silicon Twinning in Hypo-Eutectic Al-Si Alloys, *Mater. Trans.* 44 (2003) 625–628. doi:10.2320/matertrans.44.625.
- [43] B. Closset, J.E. Gruzleski, Structure and properties of hypoeutectic Al-Si-Mg alloys modified with pure strontium, *Metall. Trans. A.* 13 (1982) 945–951. doi:10.1007/BF02643389.
- [44] S. Khan, R. Elliott, Effect of antimony on the growth kinetics of aluminium-silicon eutectic alloys, *J. Mater. Sci.* 29 (1994) 736–741.
- [45] K.G. Basavakumar, P.G. Mukunda, M. Chakraborty, Influence of grain refinement and modification on microstructure and mechanical properties of Al–7Si and Al–7Si–2.5Cu cast alloys, *Mater. Charact.* 59 (2008) 283–289. doi:10.1016/j.matchar.2007.01.011.
- [46] Y. Sun, S. Pang, X. Liu, Z. Yang, G. Sun, Nucleation and growth of eutectic cell in hypoeutectic Al-Si alloy, *Trans. Nonferrous Met. Soc. China.* 21 (2011) 2186–2191. doi:10.1016/S1003-6326(11)60993-X.
- [47] S. Nafisi, R. Ghomashchi, Effects of modification during conventional and semi-solid metal processing of A356 Al-Si alloy, *Mater. Sci. Eng. A.* 415 (2006) 273–285. doi:10.1016/j.msea.2005.09.108.
- [48] P. Liliu, Metallurgical parameters controlling the microstructural evolution in Al-Si-Mg and Al-Si-Cu casting alloys, Université du Québec à Chicoutimi, 2003.
- [49] M.F. Hafiz, T. Kobayashi, Mechanical properties of modified and nonmodified eutectic Al-Si alloys, *J. Japan Inst. Light Met.* 44 (1994) 28–34.
- [50] M. Shamsuzzoha, L.M. Hogan, The twinned growth of silicon in chill-modified Al–Si eutectic, *J. Cryst. Growth.* 82 (1987) 598–610. doi:10.1016/S0022-0248(87)80004-0.
- [51] L.A. Narayanan, F.H. Samuel, J.E. Gruzleski, Dissolution of Iron Intermetallics in Al-Si Alloys through Nonequilibrium Heat Treatment, 26 (1995).
- [52] K. Nogita, H. Yasuda, K. Yoshida, K. Uesugi, A. Takeuchi, Y. Suzuki, et al., Determination of strontium segregation in modified hypoeutectic Al – Si alloy by micro X-ray fluorescence analysis, 55 (2006) 787–790. doi:10.1016/j.scriptamat.2006.07.029.
- [53] H. Liao, Y. Sun, G. Sun, Correlation between mechanical properties and amount of dendritic α -Al phase in as-cast near-eutectic Al – 11 . 6 % Si alloys modified with strontium, 335 (2002) 62–66.
- [54] R. Dasgupta, C. Brown, S. Marek, Analysis of overmodified 356 aluminum alloy, *AFS Trans.* 96 (1988) 297–310.
- [55] H. Frederiksson, M. Hillert, N. Lange, The Modification of Aluminum-Silicon Alloys by Sodium, *J. Inst. Met.* 101 (1973) 285–299.

- [56] D.R. Hamilton, R.G. Seidensticker, Propagation Mechanism of Germanium Dendrites, *J. Appl. Phys.* 31 (1960) 1165. doi:10.1063/1.1735796.
- [57] K. Kobayashi, L. Hogan, The crystal growth of silicon in Al-Si alloys, *J. Mater. Sci.* 20 (1985) 1961–1975. doi:10.1007/BF01112278.
- [58] M. Shamsuzzoha, L.M. Hogan, The crystal morphology of fibrous silicon in strontium-modified Al-Si eutectic, *Philos. Mag. A.* 54 (1986) 459–477. doi:10.1080/01418618608243605.
- [59] A. Hellawell, The growth and structure of eutectics with silicon and germanium, *Prog. Mater. Sci.* 15 (1970) 3–78.
- [60] M. Kitamura, S. Hosoya, I. Sunagawa, Growth forms of twinned crystals, *J. Japanese Assoc. Cryst. Growth.* 6 (1979) 95–101.
- [61] H. Liao, S. Guoxiong, Massive Si Phase and Its Growth Mechanism in Al-Si Casting Alloy, *J. Mater. Sci. Technol.* 20 (2004) 589–591.
- [62] B.M. Thall, B. Chalmers, Modification in aluminum–silicon alloys, *J. Inst. Met.* 78 (1949) 79–97.
- [63] V. Davies, J. West, Influence of small additions of sodium on the surface tension of Al and Al-Si alloys, *J. Inst. Met.* 92 (1964) 208.
- [64] S.C. Flood, J.D. Hunt, Modification of Al-Si eutectic alloys with Na, 15 (1981) 287–294.
- [65] Y. Tsumara, On the Theory of Modification of Aluminium–Silicon Alloys, *Nippon Kinzoku Gakkaisi.* 21 (1957) 69–83.
- [66] V. Davies, J.M. West, Factors Affecting the Modification of the Aluminum-Silicon Eutectic, *J. Inst. Met.* 92 (1964) 175–180.
- [67] S. Lu, A. Hellawell, The mechanism of silicon modification in aluminum-silicon alloys: Impurity induced twinning, *October.* 18 (1987) 1721–1733. doi:10.1007/BF02646204.
- [68] M. Shamsuzzoha, L.M. Hogan, Crystal morphology of unmodified aluminium-silicon eutectic microstructures, 76 (1986) 429–439.
- [69] M. Shamsuzzoha, L.M. Hogan, D.J. Smith, P. a. Deymier, A transmission and high-resolution electron microscope study of cozonally twinned growth of eutectic silicon in unmodified Al-Si alloys, *J. Cryst. Growth.* 112 (1991) 635–643. doi:10.1016/0022-0248(91)90119-P.
- [70] J. Li, P. Schumacher, Effects of Yb Additions on Refinement of Eutectic Si in Al-5Si Alloys, *TMS Light Met.* (2013) 1017–1022.

- [71] J.H. Li, M. Albu, T.H. Ludwig, Y. Matsubara, F. Hofer, L. Arnberg, et al., Modification of eutectic Si in Al-Si based alloys, *Mater. Sci. Forum.* 796 (2014) 130–136. doi:10.4028/www.scientific.net/MSF.794-796.130.
- [72] P.D. Hess, E.V. Blackmun, Strontium as a modifying agent for hypoeutectic aluminum-silicon alloys, *Trans Am Foundrymen's Soc.* 83 (1975) 87–90.
- [73] A. Bayram, A. Uguz, The effect of spheroidising and Na-modification on the mechanical properties of Al-Si cast alloys, *Metall.* 53 (1999) 131–134.
- [74] N. Fatahalla, M. Hafiz, M. Abdulkhalek, Effect of microstructure on the mechanical properties and fracture of commercial hypoeutectic Al-Si alloy modified with Na, Sb and Sr, *J. Mater. Sci.* 34 (1999) 3555–3564. doi:10.1023/A:1004626425326.
- [75] A.M. Samuel, H.W. Doty, S. Valtierra, F.H. Samuel, Effect of grain refining and Sr-modification interactions on the impact toughness of Al-Si-Mg cast alloys, *Mater. Des.* 56 (2014) 264–273. doi:10.1016/j.matdes.2013.10.029.
- [76] M. Djurdjevic, H. Jiang, J. Sokolowski, On-line prediction of aluminum–silicon eutectic modification level using thermal analysis, *Mater. Charact.* 46 (2001) 31–38. doi:10.1016/S1044-5803(00)00090-5.
- [77] S. Heugenhauer, B. Stauder, M. Djurdjevic, P. Schumacher, Bildanalytische Methode zur Charakterisierung des Veredelungsgrades von Aluminium-Silizium Gusslegierungen, *Prakt. Met. Sonderband.* 44 (2012) 231–236.
- [78] I. Geltungsbereich, S.A.S. Legierungen, Bestimmung des Dendriten arm abstandes für Gussstücke aus Aluminium-Gusslegierungen, (2011).
- [79] H. Hadwiger, Vorlesungen über Inhalt Oberfläche und Isoperimetrie, Springer-Verlag, Berlin, 1957.
- [80] J.C. Russ, R.T. Dehoff, *Practical Stereology*, 2nd Editio, Kluwer Academic/Plenum Press, New York, 2000.
- [81] J.C. Russ, *Practical Stereology*, Premium Press, New York, 1986.
- [82] A. Velichko, C. Holzapfel, A. Siefers, K. Schladitz, F. Mücklich, Unambiguous classification of complex microstructures by their three-dimensional parameters applied to graphite in cast iron, *Acta Mater.* 56 (2008) 1981–1990. doi:10.1016/j.actamat.2007.12.033.
- [83] H. Oettel, H. Schumann, *Metallografie*, 15th. Ed., Wiley-VCH, Weinheim, 2011.
- [84] J.C. Russ, *The image processing handbook*, 5th ed., CRC Press, Boca Raton, USA, 2007.
- [85] J.J. Friel, *Practical Guide to Image Analysis*, ASM International, USA, 2000.

- [86] J. Ohser, F. Mücklich, *Statistical Analysis of Microstructures in Materials Science*, John Wiley & Sons, Chichester, NY, USA, 2000.
- [87] M.A. Delesse, Procédé mécanique pour déterminer la composition des roches, *Ann. Des Mines*. 13 (1848).
- [88] A. Rosiwal, Über geometrische Gesteinsanalysen, *Verh. KK Geol. Reichsanst. Wien*. 5 (1898) 143–175.
- [89] E. Thomson, Quantitative Microscopic Analysis, *J. Geol.* 38 (1930) 193–222.
- [90] A.A. Glagolev, On the geometrical methods of quantitative minerologic analysis of rocks, *Trans. Inst. Econ Min. Moskau*. 59 (1933) 1–47.
- [91] S.A. Saltykov, *Stereometrische Metallographie*, Dt. Verlag F. Grundstoffindustrie. (1974).
- [92] J. Ohser, K. Schladitz, *3D Images of Materials Structures: Processing and Analysis*, Wiley-VCH, Weinheim, 2009.
- [93] J. Li, L. Lu, M.O. Lai, Quantitative analysis of the irregularity of graphite nodules in cast iron, *Mater. Charact.* 45 (2000) 83–88. doi:10.1016/S1044-5803(00)00052-8.
- [94] S. Arasan, S. Akbulut, a. S. Hasiloglu, The relationship between the fractal dimension and shape properties of particles, *KSCE J. Civ. Eng.* 15 (2011) 1219–1225. doi:10.1007/s12205-011-1310-x.
- [95] A. Velichko, Quantitative 3D characterization of graphite morphologies in cast iron using FIB microstructure tomography, Saarland University (UdS), 2008.
- [96] A. Okabe, B. Boots, K. Sugihara, S.N. Chiu, *Spatial Tessellations: Concepts and Applications of Voronoi Diagrams*, Wiley and Sons, West Sussex, England, 2000.
- [97] M.G.H.M. Hendriks, M.J.G.W. Heijman, W.E. van Zyl, J.E. ten Elshof, Quantitative Analysis of Microstructural Homogeneity and Capacitance Correlations in Palladium/Yttria-Stabilized Zirconia Composites, *J. Am. Ceram. Soc.* 85 (2002) 2097–2101.
- [98] G. Trefalt, A. Benčan, M. Kamplet, B. Malič, Y. Seo, K.G. Webber, Evaluation of the homogeneity in Pb(Zr,Ti)O₃–zirconia composites prepared by the hetero-agglomeration of precursors using the Voronoi-diagram approach, *J. Eur. Ceram. Soc.* 34 (2014) 669–675. doi:10.1016/j.jeurceramsoc.2013.09.014.
- [99] M.J.G.. Heijman, N.. Benes, J.. ten Elshof, H. Verweij, Quantitative analysis of the microstructural homogeneity of zirconia-toughened alumina composites, *Mater. Res. Bull.* 37 (2002) 141–149. doi:10.1016/S0025-5408(01)00806-6.

- [100] N. Yang, J. Boselli, I. Sinclair, Simulation and quantitative assessment of homogeneous and inhomogeneous particle distributions in particulate metal matrix composites., *J. Microsc.* 201 (2001) 189–200.
- [101] N. Yang, J. Boselli, P.J. Gregson, I. Sinclair, Simulation and quantitative assessment of finitesize particle distributions in metal matrix composites, *Mater. Sci. Technol.* 16 (2000) 797–805. doi:http://dx.doi.org/10.1179/026708300101508469.
- [102] X. Wang, J. Zhang, S. Shahid, A. ElMahdi, R. He, X. Wang, et al., Gini coefficient to assess equity in domestic water supply in the Yellow River, *Mitig. Adapt. Strateg. Glob. Chang.* 17 (2011) 65–75. doi:10.1007/s11027-011-9309-7.
- [103] Y. Masaki, N. Hanasaki, K. Takahashi, Y. Hijioka, Global-scale analysis on future changes in flow regimes using Gini and Lorenz asymmetry coefficients, *Water Resour. Res.* 50 (2014) 4054–4078.
- [104] B. Chen, C. Gu, H. Wang, J. Tao, Y. Wu, Q. Liu, et al., Research on Gini coefficient application in the distribution of water pollution, *J. Food, Agric. Environ.* 10 (2012) 833–838.
- [105] G.R. Lopes, R. Da Silva, M.M. Moro, J.P.M. De Oliveira, Scientific collaboration in research networks: A quantification method by using Gini coefficient, *Int. J. Comput. Sci. Appl.* 9 (2012) 15–31.
- [106] K. Kiêu, K. Adamczyk-Chauvat, H. Monod, R.S. Stoica, A completely random - tessellation model and Gibbsian extensions, *Spat. Stat.* 6 (2013) 118–138. doi:10.1016/j.spasta.2013.09.003.
- [107] M.O. Lorenz., *Methods of Measuring the Concentration of Wealth*, *Publ. Am. Stat. Assoc.* 9 (1905) 209–219.
- [108] C. Gini, *Variabilità e Mutiabilità, Contributo allo Studio delle Distribuzioni e delle Relazioni Statistiche*, C. Cuppini, Bologna, Italy, 1912.
- [109] L. Ceriani, P. Verme, The origins of the Gini index: extracts from *Variabilità e Mutabilità* (1912) by Corrado Gini, *J. Econ. Inequal.* 10 (2011) 421–443. doi:10.1007/s10888-011-9188-x.
- [110] S. Yitzhaki, More than a dozen alternative ways of spelling Gini, *Res. Econ. Inequal.* 8 (1998) 13–30.
- [111] L.S. Temkin, *Inequality*, Oxford University Press, New York, 1993.
- [112] M. a. Smirnov, I.Y. Pyshmintsev, a. N. Boryakova, Classification of low-carbon pipe steel microstructures, *Metallurgist.* 54 (2010) 444–454. doi:10.1007/s11015-010-9321-2.
- [113] G. Thewlis, Classification and quantification of microstructures in steels, *Mater. Sci. Technol.* 20 (2004) 143–160. doi:10.1179/026708304225010325.

- [114] B. Yegnanarayana, *Artificial Neural Networks*, PHI Learning Pvt. Ltd., 2009.
- [115] D. Li, Y. Liu, Y. Zhang, F. Meng, Study on thermal analysis models used in gray cast iron quality prediction, *Int. J. Cast Met. Res.* 11 (1999) 391–394.
- [116] R. Song, Q. Zhang, M. Tseng, B. Zhang, The application of artificial neural networks to the investigation of aging dynamics in 7 175 aluminium alloys ‘ j, 3 (1995) 7–9.
- [117] S. Malinov, W. Sha, J.J. Mckeown, Modelling the correlation between processing parameters and properties in titanium alloys using arti ® cial neural network, 21 (2001).
- [118] T. Malinova, N. Pantev, S. Malinov, Prediction of surface hardness after ferritic nitrocarburising of steels using artificial neural networks, 17 (2001).
- [119] R. Francis, J. Sokolowski, Prediction of the aluminum silicon modification level in the AlSiCu alloys using artificial neural networks, *Metalurgija.* 14 (2008) 3–15.
- [120] V. Sundararaghavan, N. Zabaras, Classification and reconstruction of three-dimensional microstructures using support vector machines, *Comput. Mater. Sci.* 32 (2005) 223–239. doi:10.1016/j.commatsci.2004.07.004.
- [121] A. Gumula, T. Debiński, M. Głowacki, Automatic approach to microstructural image recognition and analysis, *Steel Res. Int, Spec. Ed.* (2012) 1331–1334.
- [122] K. Roberts, G. Weikum, F. Mücklich, Untersuchungen zur automatischen Klassifikation von Lamellengraphit mit Hilfe des Stützvektorverfahrens (Examinations on the Automatic Classification of Lamellar Graphite Using the Support Vector Machine), *Pract. Metallogr.* 42 (2003) 396–410.
- [123] T.M. Nunes, V.H.C. de Albuquerque, J.P. Papa, C.C. Silva, P.G. Normando, E.P. Moura, et al., Automatic microstructural characterization and classification using artificial intelligence techniques on ultrasound signals, *Expert Syst. Appl.* 40 (2013) 3096–3105. doi:10.1016/j.eswa.2012.12.025.
- [124] M.D. Uchic, L. Holzer, B.J. Inkson, E.L. Principe, P. Munroe, Three-Dimensional Microstructural Characterization Using Focused Ion Beam Tomography, *MRS Bull.* 32 (2007) 408–416.
- [125] J. Baruchel, J.-Y. Buffiere, E. Maire, P. Merle, G. Peix, *X-ray Tomography in Material Science*, Hermes Science, 2000.
- [126] D.C. Copley, J.W. Eberhard, G.A. Mohr, Computed tomography part I: Introduction and industrial applications, *J. Met.* 46 (1994) 14–26.
- [127] M. Defrise, F. Noo, H. Kudo, Rebinning-based algorithms for helical cone-beam CT, *Phys. Med. Biol.* 46 (2001) 2911–37.

- [128] L.A. Giannuzzi, F.A. Stevie, *Introduction to Focused Ion Beams: Instrumentation, Theory, Techniques and Practice*, Springer Science & Business Media, USA, 2005.
- [129] A. Elmoutaouakkil, G. Fuchs, P. Bergounhon, R. Péres, F. Peyrin, Three-dimensional quantitative analysis of polymer foams from synchrotron radiation x-ray microtomography, *J. Phys. D Appl. Phys.* 36 (2003) A37–A43.
- [130] G. Nicoletto, R. Konečná, S. Fintova, Characterization of microshrinkage casting defects of Al–Si alloys by X-ray computed tomography and metallography, *Int. J. Fatigue.* 41 (2012) 39–46. doi:10.1016/j.ijfatigue.2012.01.006.
- [131] N. Limodin, A. El Bartali, L. Wang, J. Lachambre, J.-Y. Buffiere, E. Charkaluk, Application of X-ray microtomography to study the influence of the casting microstructure upon the tensile behaviour of an Al–Si alloy, *Nucl. Instruments Methods Phys. Res. Sect. B.* 324 (2014) 57–62. doi:10.1016/j.nimb.2013.07.034.
- [132] L. Wei, C. Sinka, L. Che, Statistical analysis of pore structure and compression behaviour of Al-Si foams, *Int. J. Model. Identif. Control.* 20 (2013) 379 – 386. doi:10.1504/IJMIC.2013.057571.
- [133] L. Qian, H. Toda, K. Uesugi, T. Ohgaki, M. Kobayashi, T. Kobayashi, Three-dimensional visualization of ductile fracture in an Al–Si alloy by high-resolution synchrotron X-ray microtomography, *Mater. Sci. Eng. A.* 483-484 (2008) 293–296. doi:10.1016/j.msea.2006.10.201.
- [134] Joachim Frank, *Electron Tomography: Methods for Three-Dimensional Visualization of Structures in the Cell*, 2nd editio, Springer Science & Business Media, USA, 2008.
- [135] K. Thompson, D. Lawrence, D.J. Larson, J.D. Olson, T.F. Kelly, B. Gorman, In situ site-specific specimen preparation for atom probe tomography., *Ultramicroscopy.* 107 (2007) 131–139. doi:10.1016/j.ultramicro.2006.06.008.
- [136] M.K. Miller, *Atom Probe Tomography: Analysis at the Atomic Level*, Springer US, 2000.
- [137] B. Gault, M.P. Moody, J.M. Cairney, S.P. Ringer, *Atom Probe Microscopy*, Springer Science & Business Media, 2012.
- [138] J. Barrirero, M. Engstler, N. Ghafoor, N. de Jonge, M. Odén, F. Mücklich, Comparison of segregations formed in unmodified and Sr-modified Al-Si alloys studied by atom probe tomography and transmission electron microscopy, *J. Alloys Compd.* 611 (2014) 410–421. doi:10.1016/j.jallcom.2014.05.121.
- [139] A. Gurumurthy, A.M. Gokhale, A. Godha, M. Gonzales, *Montage Serial Sectioning: Some Finer Aspects of Practice*, *Metallogr. Microstruct. Anal.* 2 (2013) 364–371. doi:10.1007/s13632-013-0100-x.
- [140] S. Ghosh, D. Dimiduk, *Computational Methods for Microstructure-Property Relationships*, Springer Science & Business Media, 2010.

- [141] N. Chawla, V.V. Ganesh, B. Wunsch, Three-dimensional (3D) microstructure visualization and finite element modeling of the mechanical behavior of SiC particle reinforced aluminum composites, *Scr. Mater.* 51 (2004) 161–165. doi:10.1016/j.scriptamat.2004.03.043.
- [142] M. Li, S. Ghosh, T.N. Rouns, H. Weiland, O. Richmond, W. Hunt, *Serial Sectioning Method in the Construction of 3-D Microstructures for Particle-Reinforced MMCs*, (1998).
- [143] J. Alkemper, P.W. Voorhees, Quantitative serial sectioning analysis., *J. Microsc.* 201 (2001) 388–94.
- [144] P. Rossi, *Microstructure analysis using FIB tomography of Al-Si alloys manufactured by different processes*, Saarland University, 2009.
- [145] J. Konrad, S. Zaefferer, D. Raabe, Investigation of orientation gradients around a hard Laves particle in a warm-rolled Fe₃Al-based alloy using a 3D EBSD-FIB technique, *Acta Mater.* 54 (2006) 1369–1380. doi:10.1016/j.actamat.2005.11.015.
- [146] L. Holzer, Review of FIB-tomography, in: I. Utke, S. Moshkalev, P. Russell (Eds.), *Nanofabrication Using Focus. Ion Electron Beams Princ. Appl.*, Oxford University Press, 2011: pp. 410–435.
- [147] L. Holzer, F. Indutnyi, P.H. Gasser, B. Münch, M. Wegmann, Three-dimensional analysis of porous BaTiO₃ ceramics using FIB nanotomography., *J. Microsc.* 216 (2004) 84–95. doi:10.1111/j.0022-2720.2004.01397.x.
- [148] J. Chang, H. Ko, Twin probability of eutectic Si in rare earth modified Al-7wt% Si alloy, *J. Mater. Sci. Lett.* 19 (2000) 197–199. doi:10.1023/A:1006746321922.
- [149] B. Zhang, M. Garro, C. Tagliano, Dendrite arm spacing in aluminium alloy cylinder heads produced by gravity semi-permanent mold, *Metall. Sci. Technol.* 21 (2003).
- [150] D. Loyd, *Physics Lab Manual*, 3rd Editio, Thomson Books/Cole, Belmont, USA, 2008.
- [151] M. Manahan, A. Argon, O. Harling, The development of a miniaturized disk bend test for the determination of postirradiation mechanical properties, *J. Nucl. Mater.* 104 (1981) 1545–1550. doi:10.1016/0022-3115(82)90820-0.
- [152] J.M. Baik, J. Kameda, O. Buck, Development of Small Punch Tests for Ductile-Brittle Transition Temperature Measurement of Temper Embrittled Ni-Cr Steels, in: W.R. Corwin, G.E. Lucas (Eds.), *Use Small-Scale Specimens Test. Irradiat. Mater.*, ASTM International, Baltimore, USA, 1986: pp. 92–111. doi:10.1520/STP32997S.
- [153] Y.W. Ma, K.B. Yoon, Assessment of tensile strength using small punch test for transversely isotropic aluminum 2024 alloy produced by equal channel angular

pressing, Mater. Sci. Eng. A. 527 (2010) 3630–3638.
doi:10.1016/j.msea.2010.02.057.

- [154] X. Mao, H. Takahashi, Development of a further-miniaturized specimen of 3 mm diameter for tem disk (\varnothing 3 mm) small punch tests, J. Nucl. Mater. 150 (1987) 42–52. doi:10.1016/0022-3115(87)90092-4.
- [155] T. Kobayashi, I. Yamamoto, M. Niinomi, Introduction of a New Dynamic Fracture Toughness Evaluation System, J. Test. Eval. 21 (1993) 145–153. doi:10.1520/JTE11763J.
- [156] P. De Bièvre, H. Günzler, Validation in Chemical Measurement, Springer, Germany, 2004.
- [157] S.L.R. Ellison, V.J. Barwick, T.J.D. Farrant, Practical Statistics for the Analytical Scientist: A Bench Guide, Royal Society of Chemistry, 2009. doi:10.1039/9781847559555.
- [158] Q. Wang, J.W. Knight, Method For Automatic Quantification Of Dendrite Arm Spacing In Dendritic Microstructures, US20130272599 A1, 2013.

Curriculum Vitae

Paulo Eliseo Rossi

✉ St. Johanner Str. 56,
66115 Saarbrücken, Germany
@ paulopaulorossi@daad-alumni.de

-Born on April 20th 1984 in Neuquén, Argentina
-Very good level in **English** and **German**
-Mother tongue: **Spanish**



Since 09/2014

Product Development Engineer

Where: Nemak Dillingen, Dillingen, Germany.
Business Sector: Cast aluminum engine blocks for the automotive industry.
Responsibilities: Product development using virtual simulation.

Since 10/2010

Ph. D. in Material Sciences

Expected to graduate: 2015 as *Dr.-Ing.*
Where: Chair for Functional Materials, Saarland University, Germany.
Scholarships: *Roberto Rocca Education Program* and *Deutscher Akademischer Austauschdienst (DAAD)*.
Submitted Thesis: *Quantitative Classification and Assessment of Modification in Hypoeutectic Aluminum-Silicon Alloys*
Publications:
P. Rossi, M. Engstler, F. Mücklich, Quantitative Classification and Assessment of Sr Modification in Hypoeutectic Al-Si and Al-Si-Mg alloys, *Pract. Metallogr.* 52 (2015).
P. Rossi, S. Suarez, F. Soldera, F. Mücklich, Quantitative Assessment of the Reinforcement Distribution Homogeneity in CNT/Metal Composites, *Adv. Eng. Mater.* (2014) 1–5.
P. Rossi, M. Engstler, F. Mücklich, Homogeneity Quantification Method and its Application to Microstructure Assessment, *Pract. Metallogr.* 51 (2014) 180–199.

